UNIVERSITY OF SOUTHAMPTON

FACULTY OF PHYSICAL AND APPLIED SCIENCES

Quantified Evaluation of the Significance of Higher Order Effective Moments and Dielectrophoretic Forces

by

Hossein Nili

Thesis for the degree of Doctor of Philosophy

January 2012

UNIVERSITY OF SOUTHAMPTON

ABSTRACT

FACULTY OF PHYSICAL AND APPLIED SCIENCES

Electronics and Computer Science

Doctor of Philosophy

QUANTIFIED EVALUATION OF THE SIGNIFICANCE OF HIGHER ORDER EFFECTIVE MOMENTS AND DIELECTROPHORETIC FORCES

by Hossein Nili

In analysis of electric field interactions with dielectrics, higher order moments and dielectrophoretic force terms are commonly ignored in what has become known as the dipole approximation. The very few multipolar studies in the literature have either confined analysis to spherical particles or modelled non-spherical particles as spheres of similar dimensions. A major obstacle in analysing the significance of higher order moments has been the limitedness of multipole moment determination techniques. Analytic derivations for higher order moments are only available for spherical particles. This work addresses this roadblock and presents a hybrid numerical-analytical method for determination of the first three effective moments of particles of any shape subjected to electric fields of arbitrary geometry. Results of applying this method for determining higher order dielectrophoretic force terms have been verified by comparison against total force calculations using the Maxwell stress tensor method, known for its mathematical rigorousness in accounting for all interaction between an applied electric field and subject dielectric(s). It is shown that the dipole approximation is particularly unreliable for non-spherical particles, importantly comprising the vast majority of bioparticles. It is shown that higher order terms can constitute up to half the dielectrophoretic force on dielectric particles in suspension. With the current trend toward micro- and nano-electrode geometries used for single particle analysis, and a consequent increase in the number of instances where invoking the dipole approximation can be highly inaccurate, this work offers a computationally inexpensive and verifiably accurate means for determining higher order moments and dielectrophoretic forces.

Contents

Chapter One – Aims and Objectives……1

1.1. Research question……3
1.2. Problem solving approach……4
1.3. Statement of intent……5
1.4. Motivation: the big picture and why higher-order effects matter……6
1.5. Thesis outline……8

Chapter Two – Dielectrophoresis: An Introduction to the Phenomenon……11

2.1. Electrostatics……13
2.1.1. Electric fields……13
2.1.2. The electric dipole and multipoles……14
2.1.3. Dielectrics and polarisation……18
2.2. Dielectrophoresis……20
2.2.1. Polarisation of dielectric particles in suspension: the induced dipole……20
2.2.2. The dielectrophoretic force……21
2.2.3. Applications of dielectrophoresis……22
2.3. AC electrokinetics: variants of dielectrophoresis……26
2.3.1. AC electrokinetic force as dielectrophoresis……26
2.3.2. AC electrokinetic torque: electro-rotation……26
2.3.3. AC electrokinetic force as traveling-wave dielectrophoresis……28
2.4. Summary……29

Chapter Three – Calculation of the Dielectrophoretic Force: Background and Theory……33

3.1. Determining DEP force terms: the effective moment method……35
3.1.1. The effective moments: definition……35
3.1.2. The effective moment method: formulation……36
3.1.3. The dipole approximation: statement and criterion for reliability……37
3.1.4. Effective moment method calculations of the DEP force in the literature……38
3.1.5. Determination of the effective moments……43
3.2. Determining the total DEP force: the Maxwell stress tensor method……45
3.2.1. Maxwell stress tensor: definition……45
3.2.2. Maxwell stress tensor calculation of the dielectrophoretic force……46
3.3. Summary……47

Chapter Four - Effective Moments and Dielectrophoretic Force Terms in Axial Symmetry: Results and Discussion……51

4.1. Background and theory……53
4.1.1. Method for determination of linear effective moments……53
4.1.2. Physical problem specifications……53
4.1.3. Field derivative and effective moment calculation techniques……55
4.1.4. Dielectrophoretic force term calculation method……57
4.1.5. Summary……57
4.2. Electric field magnitude and derivatives……58
4.2.1. The disc-plane electrode geometry……58
4.2.2. The point-plane electrode geometry……60
4.3. The linear effective moments……63
4.3.1. Results……63
4.3.1.1. The disc-plane electrode geometry……63
4.3.1.2. The point-plane electrode geometry……64
4.3.2. Discussion……65
4.3.2.1. Effect of electrode geometry……65
4.3.2.2. Effect of particle shape……66
4.3.2.3. Effect of particle size……66
4.3.3. Summary and conclusions……73
4.4. Dielectrophoretic force terms in axial symmetry……75
4.4.1. Results and discussion……75
4.4.2. Summary and conclusions……78

Chapter Five - Maxwell Stress Tensor Calculation of the Total Dielectrophoretic Force in Axial Symmetry: Results and Discussion..83

5.1. Background and theory……85
5.1.1. The Maxwell stress tensor method in axial symmetry ……85
5.1.2. Physical problem specifications……85
5.1.3. Numerical implementation of the Maxwell stress tensor method ……86
5.2. Total dielectrophoretic force in axial symmetry ……88
5.2.1. Results and discussion……88
5.2.2. Summary and conclusions……90
5.3. Multipolar dielectrophoretic forces in axial symmetry……92
5.3.1. Results and discussion……92
5.3.1.1. The disc-plane electrode geometry……92
5.3.1.2. The point-plane electrode geometry……93
5.3.1.3. Effect of particle size……96
5.3.2. Summary and conclusions……97

Chapter Six – Effective Moments and Dielectrophoretic Forces in Non-axisymmetric Geometry: Results and Discussion……..103

6.1. Background and theory……..105
6.1.1. Method for determination of general effective moments ……105
6.1.2. Physical problem specifications……109
6.1.3. Dielectrophoretic force terms with general effective moments……112
6.2. Electric field magnitude and gradients……114
6.2.1. Results and discussion……114
6.2.1.1. The near-field region……114
6.2.1.2. The mid-field region……115
6.2.1.3. The far-field region……116
6.2.2. Summary and conclusions……117
6.3. The general effective moments……119
6.3.1. Results……119
6.3.1.1. The near-field region……119
6.3.1.2. The mid-field region……121
6.3.1.3. The far-field region……122
6.3.2. Discussion……123
6.3.2.1. Effect of electric field geometry……123
6.3.2.2. Effect of particle geometry……126
6.3.3. Summary and conclusions……129
6.4. The dielectrophoretic force terms……131
6.4.1. Results and discussion……131
6.4.1.1. The near-field region……131
6.4.1.2. The mid-field region……132
6.4.1.3. The far-field region……133
6.4.2. Summary and conclusions……135
6.5. The total dielectrophoretic force……136
6.5.1. Maxwell stress tensor calculation of the dielectrophoretic force……136
6.5.1.1. Results and discussion……136
6.5.1.2. Summary and conclusions……138
6.5.2. The significance of higher-order dielectrophoretic forces……139
6.5.2.1. Results and discussion……139
6.5.2.2. Summary and conclusions……143

Chapter Seven – Summary, Conclusions and Further Work……149

7.1. Summary……151
7.2. Conclusions……154
7.2.1. Higher-order moments……154
7.2.2. Higher-order dielectrophoretic forces……156
7.2.3. Relevance of key conclusions……158
7.3. Further work……161

DECLARATION OF AUTHORSHIP

I, Hossein Nili

declare that the thesis entitled

"Quantified Evaluation of the Significance of Higher Order Moments and Dielectrophoretic Forces"

and the work presented in the thesis are both my own, and have been generated by me as the result of my own original research. I confirm that:

- this work was done wholly or mainly while in candidature for a research degree at this University;
- where any part of this thesis has previously been submitted for a degree or any other qualification at this University or any other institution, this has been clearly stated;
- where I have consulted the published work of others, this is always clearly attributed;
- where I have quoted from the work of others, the source is always given. With the exception of such quotations, this thesis is entirely my own work;
- I have acknowledged all main sources of help;
- where the thesis is based on work done by myself jointly with others, I have made clear exactly what was done by others and what I have contributed myself;
- none of this work has been published before submission.

Signed:

Date: 28/01/2012

Acknowledgements

I would like to express gratitude towards Dr Nicolas Green for his supervision and companionship through the years of my PhD, and for introducing me to an exciting interface of mathematics and life sciences, unknown to me before enrolling for an MSc course on Lab-on-a-Chip. Extra and very important thanks go to Dr Green and the Nano Research Group at Southampton for providing me with a generous studentship for the PhD.

I am also thankful to the colleagues at the group who were encouraging during the ups and comforting during the downs of my PhD life; thank you Pejwaak Salimi, Sara Aghdaei, Mehdi Banakar, Ehsan Jaberansary, Nima Kalhor, Mario Alberto Garcia Ramirez, Asa Asadollahbaik, Barbara Cortese, Hamza Rouabah, Sun Kai, Ashwin Usgaocar and Tristan Temple. The full list would include all at the Nano Group for their share in providing a friendly working and living environment at the tiny Portakabins and the shiny Mountbatten. I would also like to express special thanks to Dr Tao Sun for his continued encouragements and helpful advice.

Thanking the special ones is far broader a matter to fit into the context of a PhD thesis. Yet it is more than appropriate that I express most heartfelt gratitude towards my loving and beloved family for their truly unwavering support in all senses of the matter.

Chapter One

Aims and Objectives

1.1. Research question

As the title of the thesis reflects, this body of work is aimed at quantifying the significance of higher-order effective moments and dielectrophoretic force terms. Dielectrics form a large portion of physical materials and dielectric particles, importantly including biological particles such as cells, viruses and bacteria, are the subject of increased attention. Applications involving dielectric particles in suspension require a force to be exerted on the particles so that the particles can be made to move for the purpose of characterisation and/or manipulation.

Conventional theory for the electrical force exerted on dielectrics ignores the effect of higher-order moments. The assumption that higher-order moments are negligible is referred to as the dipole approximation. In dielectric characterisation, the dipole approximation assumes that the electrical energy stored in dielectrics is sufficiently represented by the first-order effective moment, i.e. that higher-order terms in the electric potential due to a dielectric subjected to an electric field are negligible.

In dielectrophoresis (DEP), the phenomenon that describes the motion of dielectrics when subjected to a non-uniform electric field, the dipole approximation assumes that higher-order force terms, arising from the interaction of electric field gradients with higher-order moments, contribute negligibly to the electrical force experienced by the dielectric. In both versions of the dipole approximation, it is the interaction of electric field gradients with charges due to polarisation of the dielectric(s) that is being ignored due to deemed negligence.

It is commonly stated, as a qualitative measure, that the dipole approximation will be reliable for dielectric characterisation or determination of the dielectrophoretic force as long as particle dimensions are notably smaller than a characteristic scale of electric field non-uniformity. While it appears obvious, from the definition of the dipole approximation, that higher-order moments and DEP force terms will be insignificant if the electric field varies negligibly across particle dimensions, the criterion fails to provide any quantitative measure of the condition or the subject: it is not clear how insignificant field variations across particle dimensions need to be for the higher-order moments/forces to be negligible. As moments and force terms of ascending order arise from field gradients of ascending order, one would expect field *magnitude* variations across particle dimensions to be insufficient measure, even as qualitative as it stands, for the significance of multipolar effects. As regards the subject of the criterion, it is not clear how insignificant higher-order moments/forces will be once the requirements, however qualitative, are met.

The research question for this body of work is: how could we determine the significance of higher-order interactions between electric fields and dielectrics, and how significant can the higher-order moments and dielectrophoretic forces be, compared to the baseline first-order moment/force as predicted by the dipole approximation. Although the results of this work are applicable to dielectrics of arbitrary size, attention is focussed towards micro-metre dielectric particles in suspensions, which comprise the majority of biological particles involved in lab-on-a-chip applications where multiple (bio)chemical processes are integrated onto a single chip, bringing about several advantages over alternative conduction of the processes on actual laboratory scale.

1.2. Problem solving approach

Higher-order moments of and corresponding terms of the DEP force on dielectric particles in suspension result from interactions of electric field gradients and polarisation charges at the particle/electrolyte interface. To examine the circumstances under which higher-order effects find significance, electric fields with varying degrees of non-uniformity, with the definition of non-uniformity extended not only to include the first-order but also higher-order field gradients, need to be studied. Due to the shape-dependent nature of the polarisation mechanism, particles of different shapes need to be examined. The latter examination will allow investigation into the validity of common particle shape approximations. As effective moments of arbitrary order have only been derived analytically for spherical particles, it has been common practice to approximate ellipsoidal, cylindrical and more highly non-spherical particles such as erythrocytes as spheres of similar dimensions. Comparison of first- and higher-order moments of spherical and common non-spherical particles could provide the errors incurred upon typical approximations.

The approach taken in this work to find the solution to the research question posed in the previous section includes two major steps. In the first step, particle and electric field geometries that lend themselves to axial symmetry are examined. The assumption of axial symmetry serves as a good starting point since: (a) calculations, numerical and analytical, of the electric field gradients, effective moments of particles, and dielectrophoretic forces are greatly simplified; (b) the method for determining the effective moments up to any order of particles of arbitrary shape in axisymmetric geometries has already been developed. Two different electrode configurations, three different particle shapes (each with different dimensions) and different particle positions along the axis of electric field symmetry will be examined to encompass a wide range of circumstances regarding particle and electric field geometry. The novelty in the first batch of results lies in calculations of higher-order

dielectrophoretic force terms, comparison of the force term results with Maxwell stress tensor calculations of the total DEP force in each case, and hence deriving multipolar contributions to the dielectrophoretic force for electric fields and particles of different geometry.

The second step of the approach lifts the axisymmetric assumption and as such is novel in methodology and results. A method devised for calculation of first-, second- and third-order effective moments of particles of arbitrary shape subjected to electric fields of arbitrary geometry will be used in conjunction with the effective moment method to determine the significance of higher-order moments and DEP forces for particles of different shapes subjected to electric fields of varying degrees of curvature. The technique for determining higher-order contributions to the DEP force is similar to that used in axisymmetric circumstances: calculations of the total force using the Maxwell stress tensor method are compared with force term calculations using a completely different method: the effective moment method. In axial symmetry and otherwise, excellent agreement is observed between the two sets of results, importantly providing – as well as contributions from individual terms to the DEP force – verification for the numerical calculations.

1.3. Statement of intent: generality of analysis

In analysing the significance of higher order effective moments and dielectrophoretic forces, attention will be focussed on particle and electric field geometry as determining factors. Effects of other field/particle parameters, importantly including electric field frequency and particle orientation should be examined in a broader investigation but will not be considered in this work. It will also be assumed in this work that the dielectric particles in suspension and their suspending media re ideal dielectrics. As will be explained in Chapter Two, real dielectrics conduct electricity. Accordingly, they are characterised with a permittivity which is a complex quantity defined in terms of a real part, which is the real permittivity or the dielectric constant, and an imaginary part determined by electric field frequency and the dielectric's finite conductivity. In line with focussing attention on the effects of particle and electric field geometry on the significance of higher order effective moments and dielectrophoretic forces, this work shall assume that all dielectrics involved are non-conducting.

In analysis of higher order effective moments and dielectrophoretic forces, a stopping point needed to be decided upon as in theory, there are an infinite number of terms in the electric potential due to a dielectric particle subjected to an electric field and, accordingly, effective moments and dielectrophoretic forces up to any order can be considered. In three-

dimensional space and with general multipoles representing particle polarisation (case of Chapter Six), only the first three multipoles can be realised. In the special case of axial symmetry (case of Chapters Four and Five), where the multipoles are linear (constituent poles and displacement vectors aligned with the axis of field symmetry), there is no limit on the order of effective multipoles that can be considered. To be consistent with the case of non-axisymmetric settings, only the first three effective moments and, correspondingly, only the first three dielectrophoretic force terms will be examined in this work.

The method that shall be presented in Chapter Six for determination of higher order effective moments is applicable to any particle and electric field geometry. It importantly relies on an integration of the electric potential – as can be obtained by finite element method (FEM) solution of the Poisson equation – to determine each of the first three effective moments and as such does not involve (the highly error-prone) FEM differentiation.

To make effective moment method calculations of the DEP force terms, electric field derivatives need to be determined. This work studies electrode structures within which (or along the symmetry axes of which) the electric field has been derived analytically. All calculations of electric field gradients in this work are hence analytical. If the DEP force terms are to be determined in an electrode configuration for which analytic derivations of the electric field are not available, careful mesh strategies need to be incorporated for the successive numerical differentiation required for obtaining electric field gradients.

1.4. Motivation: the big picture and why higher-order effects matter

Dielectric particles in suspension are encountered in a variety of application areas. An important example is the rapidly emerging area of science and technology known as lab-on-a-chip where multiple bio/chemical processes are integrated onto a single chip of only millimetres (and smaller) in size, with the prospect of faster and more readily-available analysis. A typical lab-on-a-chip device consists of a network of micro- and nano-channels through which flow narrow streams of fluid suspending biological and/or synthetic particles. Most suspending fluids and suspended particles, including water and blood (as fluids) and cells, viruses and bacteria (as particles) exhibit dielectric properties.

The reactions that take place on a lab-on-a-chip device require motion of the suspensions. The motion will have two facets, most obviously not independent of one another: that of the suspending fluid, and that of the suspended particle. The motion of fluids in small (down to pico-litre) volumes through narrow channels, and how it differs from conventional fluid dynamics, is the subject of on-going research and falls beyond the scope of this work, and the

knowledge of the author. It is the motion of dielectric particles, not accounting for effects from motion of the suspending fluid, which will be tended to in this work.

There are a number of mechanisms with which dielectric particles in suspension can be made to move through the exertion of a force. An important set of techniques, used favourably in a wide range of lab-on-a-chip (among other) applications, utilises electric fields for imparting force on, and moving dielectric particles. In lab-on-a-chip, the techniques are collectively referred to as AC electrokinetics, the most widely used of which is dielectrophoresis. As mentioned previously, DEP is the phenomenon through which a non-uniform electric field interacts with charges due to polarisation of dielectrics, resulting in the exertion of a net electrical force. Since its advent, DEP has found widespread applications in lab-on-a-chip design for characterisation of biological particles, separation of particles based on morphological and internal properties, e.g. healthy from infected cells, and manipulation of particles in suspension for a controlled reaction to take place.

In almost all DEP-based design, the so-called dipole approximation, which ignores higher-order interaction between the electric field and polarisation charges, is invoked for determination of the electrical force. The conventional theory for dielectric spectroscopy measurements, where properties of dielectric particles in suspension are determined from their effective moments – representatives of the electrical energy stored in the dielectrics – accounts only for the first-order moment. Non-spherical particles, comprising the majority of biological particles, are commonly modelled as spheres for which the moments have been derived analytically.

While the first-order approximation serves well to model a variety of circumstances to the *required* accuracy – particularly in DEP separation applications where mostly the direction, rather than the magnitude, of the force is of importance – there is an increasing number of circumstances where modelling based on the dipole approximation can result in substantial error, and where accuracy in determination of the dielectric properties or the DEP force is of crucial importance. In such circumstances, accurate determination of the moments/force requires accounting for higher-order effects.

As effective moments up to an arbitrary order have only been derived analytically for particles of spherical shape, the effort required to calculate higher-order moments and incorporate them in DEP or dielectric spectroscopy studies of biological and synthetic particles, the vast majority of which are non-spherical, is assumed not worthy of their possible significance. However, with the current trend toward micro- and nano-electrode geometries fabricated for the analysis of single micron and sub-micron particles, giving rise

to large field curvatures across subject dielectrics, even the qualitative and far from definitive criterion commonly stated in the literature for the reliability of the dipole approximation – that particle dimensions are notably smaller than the scale of field non-uniformity – predicts higher-order moments and forces of increased significance.

What forms the major obstacle in not accounting for higher-order effects, i.e. the absence of analytic techniques for derivation of higher-order moments, has been addressed in this work by using numerical techniques. A method has been developed that enables calculation of the first three moments of particles of arbitrary shape subjected to electric fields of arbitrary geometry. Effective moment results are combined with analytic calculations of electric field gradients to derive first- and higher-order force terms. To ensure accuracy of the numerical calculations, force term derivations are compared against total force calculations using an alternative method, also implemented numerically.

The method developed in this work has been applied to specific particle-field geometries, but can be used to derive effective moments and dielectrophoretic forces in any situation. Comparison of force term results against total force calculations can be used for validation of the results, and accuracy in determining particle properties or electrical forces on particles in lab-on-a-chip and indeed any other application involving dielectric polarisation can be substantially improved as a result.

1.5. Thesis outline

This chapter is followed by an introduction to dielectric polarisation, the representative effective moments, the net electrical force resulting from the interaction of an applied electric field and the effective moments, i.e. dielectrophoresis, and its applications (Chapter Two). Chapter Three presents the two methods used in this work for calculation of the dielectrophoretic force: the effective moment method for derivation of DEP force terms, and the Maxwell stress tensor method for calculating the total DEP force and for validating force term results.

Chapters Four, Five and Six present and discuss the results obtained for the effective moments of, and dielectrophoretic forces on particles of different shapes subjected to electric fields of different geometry. Results obtained with the assumption of axial symmetry, and hence linear effective moments, are presented and discussed in Chapters Four and Five. Chapter Four presents the results of applying an available method for the determination of linear effective moments to spherical, ellipsoidal and cylindrical particles subjected to the axisymmetric fields of point-plane and disc-plane electrode configurations. Calculations of

the first three effective moments of the particles, as well as derivations of the significance of higher-order moments are presented and discussed. Errors incurred in values of first- and higher-order moments upon typical particle shape approximations – in axial symmetry – are evaluated. Chapter Four will also present calculations of the first three DEP force terms and discuss their dependency on particle and electric field parameters.

Chapter Five, the shortest of the results chapters, presents the application of the Maxwell stress tensor (MST) method for derivation of the total dielectrophoretic force on spherical and non-spherical particles in axial symmetry. The chapter also importantly evaluates the significance of multipolar contributions to the DEP force in different circumstances regarding particle and electric field geometry by comparing force term results obtained from the effective moment method against total force calculations using the MST method. The comparison also serves as validation for the numerical calculations.

In Chapter Six, the assumption of axial symmetry is lifted and a novel method is presented for derivation of the general effective moments of particles of arbitrary shape subjected to electric fields of arbitrary geometry. The method is applied to spherical, ellipsoidal and brick-shaped particles at different positions within an interdigitated electrode configuration to derive the first two effective moments and corresponding DEP force terms. As in the case of axial symmetry, total force calculations using the alternative Maxwell stress tensor method will be compared against force term results for validation of numerical calculations and analysis of the significance of multipolar contributions. The thesis will close with a summary of what has been presented, a list of key conclusions and suggestions for further work (Chapter Seven).

Chapter Two

Dielectrophoresis: An Introduction to the Phenomenon

2.1. Electrostatics

2.1.1. Electric fields

Electric charge is a fundamental, conserved property of matter that causes it to experience electrical force when near other electrically charged matter. The SI unit of electric charge is the coulomb (C). It has been demonstrated through experiments that electric charge is quantised, i.e. comes in multiples of individual units called the elementary charge e, equal to $1.6 \times 10^{-19} C$.

The electrical force is normally depicted through the notion of an electric field. The electric field is a vector field with SI units of Newtons per coulomb (N/C) or, equivalently, volts per metre (V/m). The electric field $\boldsymbol{E}$ is a vector field, with its magnitude at a given point defined as the force that would be exerted on a positive test charge of 1 coulomb placed at that point. The direction of the field is given by the direction of that force. The electrical force experienced by electric charge q subjected to an electric field $\boldsymbol{E}$ is given by:

$$\boldsymbol{F} = q\boldsymbol{E} \tag{2.1}$$

Figure 2.1 shows the electric field vectors around a negative point charge [1]. Also shown in the figure are the so-called equipotential surfaces, which represent contours of constant electric potential. The electric potential φ is defined to be the scalar function related to the electric field through the gradient operator ∇:

$$\boldsymbol{E} = -\nabla\varphi \tag{2.2}$$

The branch of physics that concerns the behaviour of stationary or slowly-moving electric charge is referred to as electrostatics. The fundamental equation of electrostatics is Coulomb's law, which gives the electrical force between two point charges Q_1 and Q_2:

$$\boldsymbol{F} = \frac{Q_1 Q_2}{4\pi\epsilon_0 r^2}\hat{\boldsymbol{r}}_{12} \tag{2.3}$$

In equation (2.3), r is the distance between the two charges, $\hat{\boldsymbol{r}}_{12}$ is the unit vector pointing from Q_1 to Q_2, and ϵ_0 is the permittivity of free space, a constant equal to 8.854×10^{-12}.

The distribution of electric charge is related to the resulting electric field by what is known as Gauss's law:

$$\nabla \cdot \boldsymbol{E} = \rho/\epsilon_0 \tag{2.4}$$

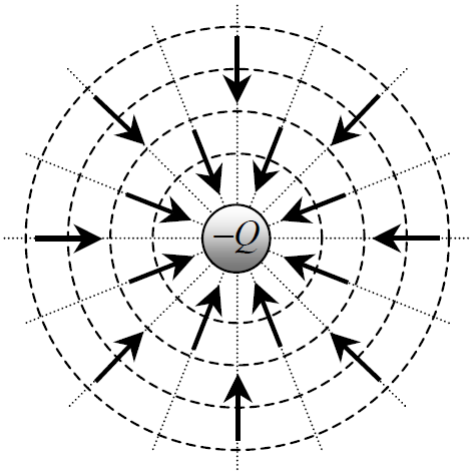

Figure 2.1. Electrostatic field and potential – The equipotential surfaces (dashed), electric field lines (dotted) and electric field vectors (arrows) around a negative point charge. Figure copied from [1].

where $\nabla \cdot \boldsymbol{E}$ is the divergence of the electric field and ρ denotes the volume charge density. Gauss's law is one of the four Maxwell equations which form the basis of classical electrodynamics. The law can be used to derive Coulomb's law (equation 2.3) and vice versa. Substituting for the electric potential, equation (2.4) gives:

$$\nabla^2 \varphi = -\rho/\epsilon_0 \tag{2.5}$$

The partial differential equation above is referred to as Poisson's equation, and is solved – analytically, if possible, and numerically, otherwise – to obtain the electrostatic potential or electric field in a physical system. In most cases, the charge density ρ is zero, and Poisson's equation reduces to what is known as Laplace's equation:

$$\nabla^2 \varphi = 0 \tag{2.6}$$

2.1.2. The electric dipole and multipoles

The electric dipole is a measure of the separation of positive and negative electric charges in a system of charges, and hence the overall polarity of the charge system. The equipotential surfaces and electric field lines and vectors arising from an electric dipole are shown in figure 2.2. As shown in the figure, a dipole simply consists of equal and oppositely-signed charges separated by a finite displacement vector $\boldsymbol{d}$. An electric dipole is characterised by its moment, given by:

$$\boldsymbol{p}^{(1)} = Q\boldsymbol{d} \tag{2.7}$$

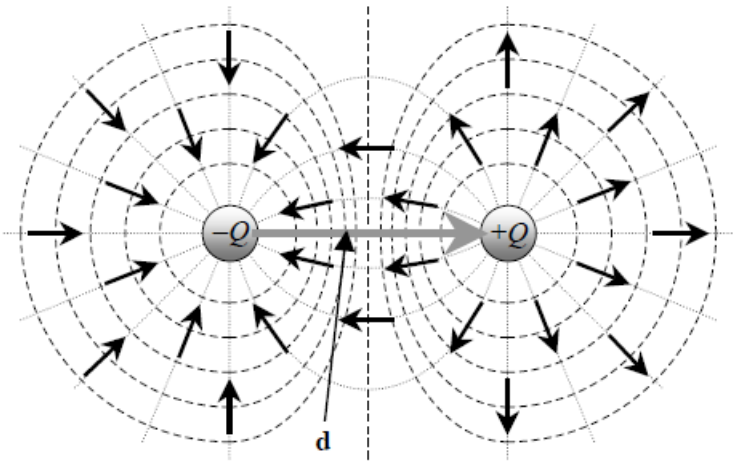

Figure 2.2. The electric dipole – The equipotential surfaces (dashed), electric field lines (dotted) and electric field vectors (black arrows) around a dipole formed from positive and negative point charges displaced by a vector d that shows the direction of the dipole moment. Figure copied from [1].

The superscript (1) denotes the order of the charge distribution, a reference that higher-order multipoles can be constructed in the same manner that a dipole is formed from displacement of equal and oppositely-charged monopoles, i.e. point charges (that can be regarded as multipoles of order 0).

Figure 2.3 shows how multipoles of second- and third-orders, known as the quadrupole and the octupole, respectively, can be constructed from those of the preceding order, equal but opposite in polarity, displaced by a finite vector $\boldsymbol{d}_n$ [2]. The multipole construction scheme is attributed to Stratton, who was among the first scientists to note the significance of higher-order multipoles in dielectric polarisation [3].

The moment of an n^{th}-order multipole is a dyadic tensor of rank n. For the monopole, dipole, quadrupole and octupole in figure 2.3, the moments are defined as [2]:

$$\boldsymbol{p}^{(0)} = q \tag{2.8a}$$

$$\boldsymbol{p}^{(1)} = q\boldsymbol{d}_1 \tag{2.8b}$$

$$\boldsymbol{p}^{(2)} = q(\boldsymbol{d}_1\boldsymbol{d}_2 + \boldsymbol{d}_2\boldsymbol{d}_1) \tag{2.8c}$$

$$\boldsymbol{p}^{(3)} = q(\boldsymbol{d}_1\boldsymbol{d}_2\boldsymbol{d}_3 + \boldsymbol{d}_1\boldsymbol{d}_3\boldsymbol{d}_2 + \boldsymbol{d}_2\boldsymbol{d}_1\boldsymbol{d}_3 + \boldsymbol{d}_2\boldsymbol{d}_3\boldsymbol{d}_1 + \boldsymbol{d}_3\boldsymbol{d}_1\boldsymbol{d}_2 + \boldsymbol{d}_3\boldsymbol{d}_2\boldsymbol{d}_1) \tag{2.8d}$$

where $\boldsymbol{d}_i\boldsymbol{d}_j$ denotes the dyadic product of vectors $\boldsymbol{d}_i$ and $\boldsymbol{d}_j$.

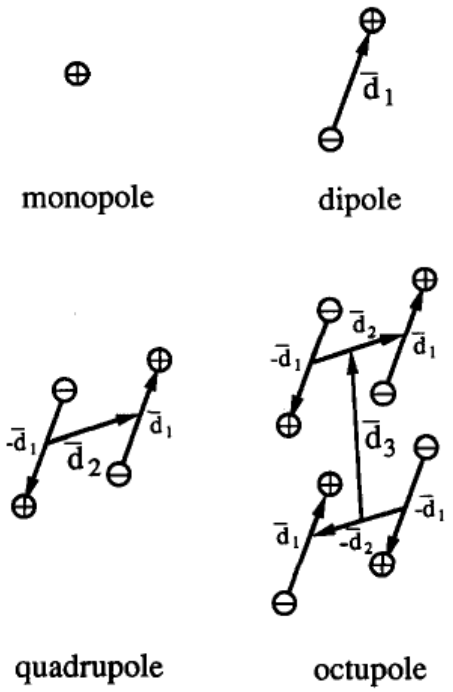

Figure 2.3. Electric multipoles – Structure of electric multipoles of first three orders generated, starting from a point charge, from two multipoles of the preceding order, equal in charge but opposite in polarity, displaced by a finite vector: the electric monopole (n=0), the electric dipole (n=1), the electric quadrupole (n=2), and the electric octupole (n=3). Figure copied from [2].

The electrostatic potentials due to the multipoles can be represented through shorthand formulae using the above definitions for their respective moments [2]:

$$\varphi^{(0)} = \frac{\boldsymbol{p}^{(0)}}{4\pi\epsilon_m} f(\boldsymbol{r}) \tag{2.9a}$$

$$\varphi^{(1)} = -\frac{\boldsymbol{p}^{(1)} \cdot \nabla f(\boldsymbol{r})}{4\pi\epsilon_m} \tag{2.9b}$$

$$\varphi^{(2)} = \frac{\boldsymbol{p}^{(2)} : \nabla\nabla f(\boldsymbol{r})}{8\pi\epsilon_m} \tag{2.9c}$$

$$\varphi^{(3)} = -\frac{\boldsymbol{p}^{(3)} \vdots \nabla\nabla\nabla f(\boldsymbol{r})}{24\pi\epsilon_m} \tag{2.9d}$$

where ϵ_m is the permittivity of the medium in which the multipoles sit, $f(\boldsymbol{r}) \equiv r^{-1}$, ∇ is the gradient operator, and [:] and [⋮] denote generalised second- and third-order dot products, respectively. A general multipole of order n gives rise to an electrostatic potential given by [2]:

$$\varphi^{(n)} = (-1)^n \frac{\boldsymbol{p}^{(n)} [\cdot]^{(n)} \nabla^{(n)} f(\boldsymbol{r})}{4\pi\epsilon_m n!} \tag{2.10}$$

where $[\cdot]^{(n)}$ denotes the n^{th}-order generalised dot product, $\nabla^{(n)}$ is the gradient operator applied n consecutive times, and $\boldsymbol{p}^{(n)}$, the moment of the n^{th}-order multipole is defined as [3]:

$$\boldsymbol{p}^{(n)} = q \sum \boldsymbol{d}_i \boldsymbol{d}_j \dots \boldsymbol{d}_k \tag{2.11}$$

where the summation Σ is taken over all permutations of $i \neq j \dots \neq k$ with $1 \leq i \leq n$, $1 \leq j \leq n$, ..., $1 \leq k \leq n$.

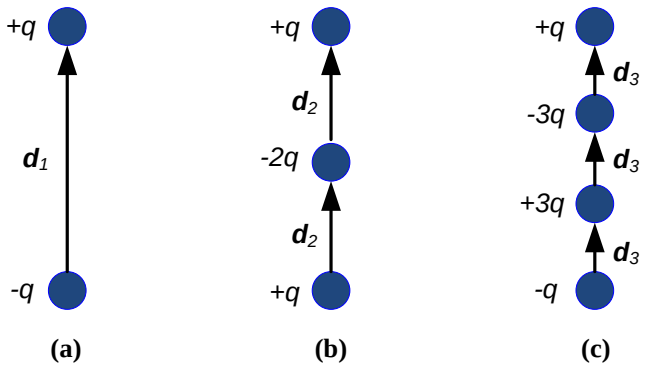

Figure 2.4. Linear multipoles – Structure of first three linear multipoles showing constituent charges and displacement vectors: (a) the linear dipole (n=1), (b) the linear quadrupole (n=2), and (c) the linear octupole (n=3).

An important special case is when the constituent vectors $\boldsymbol{d}_n$ of the n^{th}-order multipole are aligned with a single axis. The multipoles are then referred to as linear, and the moments take a much simpler form. Figure 2.4 shows the structure of the first three linear multipoles. As all point charges lie on the same axis, the moments of linear multipoles reduce to scalar, rather than tensor, quantities. For the n^{th}-order linear multipole, the moment is given by:

$$p^{(n)} = n!\, q d_n^n \tag{2.12}$$

where d_n denotes the magnitude of the (equal) displacement vectors constituting the n^{th}-order linear multipole. Linear multipoles are important in that it has been shown that the potential due to any axisymmetric distribution of charge can be represented with those due to linear multipoles of ascending order [4].

2.1.3. Dielectrics and polarisation

The interaction of electric fields with charged matter can be described through Coulomb's law. The force exerted by an applied electric field on a charged particle is simply expressed by equation (2.1). However, not all materials normally bear electric charge. An important group of materials known as dielectrics undergo a process known as polarisation when subjected to an electric field. The process involves slow motion of electric charges, originally bound within the dielectric material, from their equilibrium positions.

Polarisation of dielectrics is represented through polarisation density vector $\boldsymbol{P}$, which is related to the bound volume charge density ρ_b through the following equation:

$$\rho_b = -\nabla \cdot \boldsymbol{P} \tag{2.13}$$

Accounting for free and bound charge densities ρ_f and ρ_b, respectively, Gauss's law (equation 2.4) can be written as:

$$\nabla \cdot \boldsymbol{E} = (\rho_f + \rho_b)/\epsilon_0 \tag{2.14}$$

Using equation (2.13) for the bound charge density, this can be rewritten as:

$$\nabla \cdot (\epsilon_0 \boldsymbol{E} + \boldsymbol{P}) = \rho_f \tag{2.15}$$

The vector $\boldsymbol{D} = \epsilon_0 \boldsymbol{E} + \boldsymbol{P}$, whose divergence is equal to the volume charge density, is known as the electric flux density. For an ideal dielectric, i.e. one with zero conductivity, $\boldsymbol{D}$ is also written as:

$$\boldsymbol{D} = \epsilon_0 \epsilon_r \boldsymbol{E} \tag{2.16}$$

where ϵ_r is a dimensionless parameter, known as relative permittivity, which characterises the dielectric material. The permittivity of the dielectric $\epsilon = \epsilon_0 \epsilon_r$ is the constant of proportionality between the electric flux density $\boldsymbol{D}$ and electric field vector $\boldsymbol{E}$.

Real dielectrics, however, have a finite conductivity σ, as a result of which their permittivity takes a more complicated form. The example of a dielectric-filled parallel plate capacitor and its equivalent circuit serves to illustrate this complication in a straightforward manner. The equivalent circuit for a capacitor with plates of area A separated by a real dielectric of thickness d consists of the parallel combination of a capacitor C filled with an ideal dielectric and a resistor R of resistance $d/\sigma A$. The impedance of the parallel combination can be written as that of a capacitor of capacitance $\tilde{C} = \tilde{\epsilon} A/d$, where $\tilde{\epsilon}$, a complex variable representing the permittivity of the real dielectric, is given by:

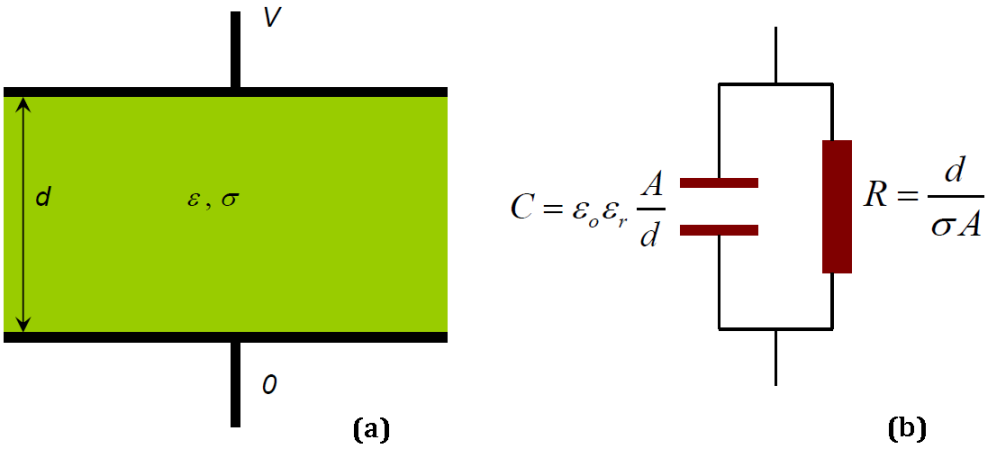

Figure 2.5. Non-ideal dielectrics – The example of (a) a parallel plate capacitor filled with a non-ideal dielectric of permittivity ϵ and conductivity σ with (b) its equivalent circuit consisting of the parallel combination of a capacitor *C* filled with an ideal dielectric and a resistor *R* modelling the conductivity of the non-ideal dielectric. The example is used to illustrate the notion of complex permittivity for real dielectrics. Figure courtesy of Dr Nicolas G. Green.

$$\tilde{\epsilon} = \epsilon - j\sigma/\omega \tag{2.17}$$

where $\boldsymbol{j} = \sqrt{-1}$. Equation (2.17) gives the relationship between the complex permittivity of a non-ideal, conducting dielectric to its conductivity and (real) permittivity. The important consequence of equation (2.17) is that the polarisation of dielectrics is a frequency-dependent phenomenon. The frequency of the electric field can be adjusted for the conductivity or permittivity of a dielectric material to dominate its polarisation behaviour.

2.2. Dielectrophoresis

2.2.1. Polarisation of dielectric particles in suspension: the induced dipole

When a dielectric particle suspended in a dielectric medium is subjected to an electric field, both dielectrics polarise. As a result of polarisation, electric charge builds up at the interface between the two dielectrics. Since the dielectric properties (ϵ, σ) of the two dielectrics would be different, there will be imbalance of, and hence net charge at the particle/medium interface. The process is referred to as interfacial or Maxwell-Wagner polarisation and forms the basis of a wide variety of applications involving electromechanics of particles.

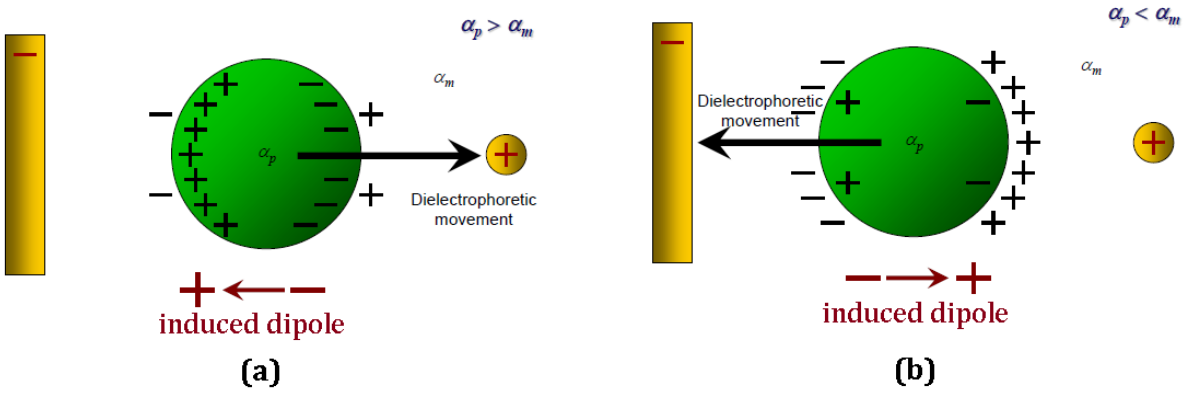

Figure 2.6. The induced dipole and dielectrophoretic movement – Application of a non-uniform electric field to a dielectric particle (green sphere) of polarisability α_p suspended in a dielectric medium of polarisability α_m will lead to build-up of net charge at the particle/medium interface, hence the formation of an induced dipole, the two poles of which experience unequal forces. The imbalance of force gives rise to particle motion through the dielectrophoretic force that tends to drive the particle (a) towards regions of high electric field intensity if $\alpha_p > \alpha_m$, or (b) away from regions of high electric field intensity if $\alpha_p < \alpha_m$. The two effects are referred to as positive and negative dielectrophoresis, respectively. Figure courtesy of Dr Nicolas G. Green.

The simplest, yet most illustrative, picture that can be presented for the polarisation of a dielectric particle in suspension is that involving the formation of an induced dipole, shown in figure 2.3. The figure shows two cases: one where the particle is more polarisable than its suspending medium and one where the medium is more polarisable than the particle. Polarisability of dielectrics, often denoted as α or complex $\tilde{\alpha}$, accounting for the complex nature of dielectric permittivity, is a measure of the amount of charge that is dislocated as a result of the application of an electric field. Unlike permittivity and conductivity, which are shape-independent properties of the dielectric material, polarisability accounts for the geometry of the body of dielectric and therefore reflects on the shape-dependent nature of

dielectric polarisation. It is indeed this dependency on morphology that complicates the picture of particle polarisation beyond that of a simple dipole.

Figure 2.3 shows that when particle polarisability is larger or smaller than that of the suspending medium, net charge will build up on either side of the particle, hence the formation of an induced dipole. The induced dipole will be aligned with or against the applied electric field depending on whether particle polarisability α_p is greater or smaller, respectively, than medium polarisability α_m. If the dielectric particle in suspension is subjected to an electric field which is non-uniform, and only then, the induced dipole, and hence the particle, will experience a net force that tends to drive the particle towards areas of higher or lower electric field intensity depending again on whether particle polarisability is greater or smaller than that of the medium, respectively. The force exerted by a non-uniform electric field on a suspended dielectric particle is known as the dielectrophoretic force and the phenomenon referred to as dielectrophoresis (DEP). Positive and negative DEP are the names given to dielectric particle movement towards high and low field intensity regions, respectively. The dependency of interfacial polarisation on electric field frequency, among other factors including particle and medium dielectric properties, has enabled the realisation of a wide variety of applications for dielectrophoresis.

Although first observations of the phenomenon date back to the late 19th century as an effect arising in the behaviour of soil samples, the term dielectrophoresis was coined by Herbert Pohl in 1951 to describe the motion of biological particles under the influence of non-uniform electric fields [5]. Pohl went on to study the effect in detail and published a seminal book on the subject in 1978 [6].

2.2.2. The dielectrophoretic force

The dielectrophoretic force on a dielectric particle can be calculated from the force exerted by the applied electric field on the induced dipole. Figure 2.7 shows the electric field vectors at the two poles of a dipole subjected to a non-uniform electric field $\boldsymbol{E}$. The net force on the dipole, from equation (2.1), is:

$$\boldsymbol{F} = q\boldsymbol{E}(\boldsymbol{r} + \boldsymbol{d}) - q\boldsymbol{E}(\boldsymbol{r}) \tag{2.18}$$

If $\boldsymbol{d} \to 0$, and only the first-order term in $\boldsymbol{d}$ is retained:

$$\boldsymbol{F} \cong q(\boldsymbol{d} \cdot \nabla \mathbf{E}) = \boldsymbol{p}^{(1)} \cdot \nabla \mathbf{E} \tag{2.19}$$

where $\boldsymbol{p}^{(1)}$ is the dipole moment.

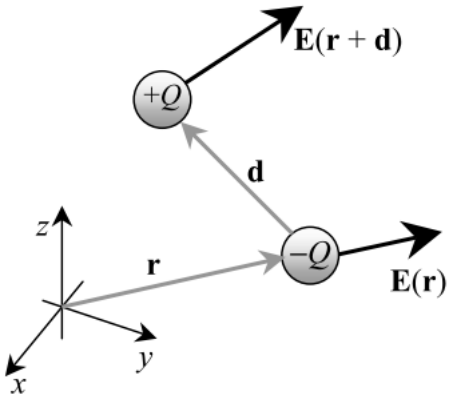

Figure 2.7. Electrical force on a dipole – The unequal electric field vectors experienced by the two poles of a dipole subjected to a non-uniform electric field, resulting in the exertion of a net dielectrophoretic force. Figure copied from [1].

Higher-order forces will include terms corresponding to multipoles of higher orders. The approximation in equation (2.19) that ignores multipolar terms is referred to as the dipole approximation and is used widely for determination of the dielectrophoretic force in different circumstances regarding particle and electric field geometry. The criterion stated in the literature for the dipole approximation to be reliable in predicting the dielectrophoretic force on a dielectric particle is that the induced dipole be small compared to the scale of non-uniformities of the imposed electric field, or rather the electric field vary negligibly across particle dimensions [2]. It is the principal goal of this work to present a quantitative measure of the significance of higher-order moments and corresponding DEP forces.

2.2.3. Applications of dielectrophoresis

The critical feature of dielectrophoresis is that it requires field non-uniformities in order to create movement. The rapid development of dielectrophoresis as a method was made capable by the production of micro-electrodes using semiconductor fabrication methods. Techniques borrowed from the electronics industry, as well as novel techniques and materials have allowed the realisation of a wide range of electrode geometry for exerting dielectrophoretic force on suspended particles.

The interdigitated (also called castellated) electrode structure accommodates well-defined regions of electric field maxima and minima and has hence found widespread use, particularly for DEP separation applications [7-11]. In an important example, depicted in figure 2.8 [10] the balance of DEP against gravitational force at different heights above an interdigitated array of electrodes has been exploited to separate breast cancer cells from normal blood cells [10, 11]. Cancerous and healthy cells have been seen to levitate at different

heights above the electrode array and therefore subject to different flow velocities, given the parabolic flow profile within the channel above the electrodes. The difference in elution times of the two groups of cells has enabled separation in what has been termed a DEP/G-FFF (gravitational field flow fractionation) device.

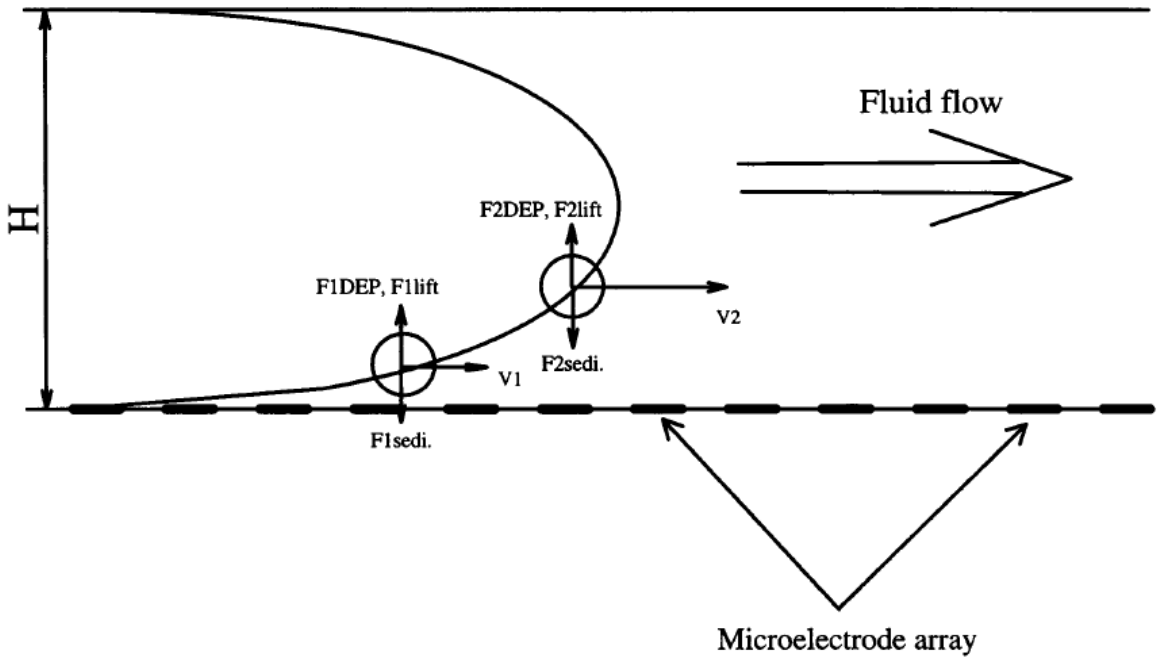

Figure 2.8. Interdigitated electrode structure used for dielectrophoretic separation based on the field flow fractionation principle – A fluid flow is established in a thin chamber whose bottom plane supports an interdigitated microelectrode array. Two particles of different dielectric properties equilibrate at different heights under the balance of DEP levitation, hydrodynamic lift, and sedimentation forces. Particle 2, being levitated further away from the chamber bottom wall, exhibits a larger velocity under the influence of fluid drag than particle 1. Figure copied from [10].

Another widely used electrode configuration is the polynomial or parabolic arrangement. When the electrodes are energised by applying voltages, particles of greater polarisability than their suspending media can be made to move towards electrode edges where the electric field is maximum, while particles with polarisabilities smaller than that of the suspending fluid at the applied field frequency can be trapped at the field null at the centre of the electrode arrangement. The electrode structure has been extensively for separation [12-14] and trapping [15] purposes. Figure 2.9 shows an example where two different types of bacteria have been separated by applying a sinusoidal voltage to the polynomial electrode configuration [14].

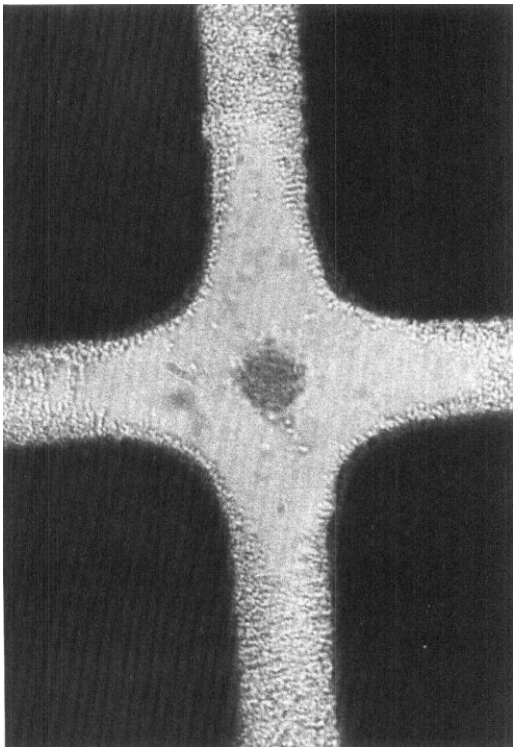

Figure 2.9. Dielectrophoretic separation using the polynomial electrode configuration – DEP separation of E. coli (of polarisability smaller than the suspending medium) and M. lysodeikticus (of polarisability greater than the suspending medium) in a polynomial electrode system after application of a 4V peak-to-peak sinusoidal 100kHz signal. The suspending medium is 280 mM mannitol. Figure copied from [14]

As most biological particles are dielectrics, dielectrophoresis is particularly fitted to lab-on-a-chip applications where multiple processes involving characterisation, manipulation and separation of bioparticles are integrated onto a single chip. Dielectrophoresis is advantageous over other means of inducing particle motion in its non-invasive nature and easy integration onto micro-devices, not relying on any moving parts. Early biomedical applications of dielectrophoresis were limited to studying the response of cells to electric fields for characterization purposes. Nowadays, the technique has found widespread use for a variety of biotechnological and diagnostic applications [16]. Examples include separation of human breast cancer cells from blood [17], trapping [18] and manipulation of DNA [19, 20] – of importance to the development of point-of-care devices for detection and identification of pathogenic micro-organisms, aggregation of hemispherical cells as a first step toward the creation of artificial stem cell microniches *in vitro*, and creating engineered skin with artificial placodes of different sizes and shapes in different spatial patterns [21].

Dielectrophoresis has established its status as a versatile technique for separation of dielectric – biological and otherwise – particles in suspension. Through the frequency-dependent characteristics of dielectric particles, DEP has access to a wide range of particle properties, and can be modified by the choice of suspending medium. Factors relating to fluid

behaviour can complicate DEP separation of dielectric particles [22]. Yet it has been shown that once these phenomena are correctly identified and incorporated in the design process, they can take their part in the toolbox of electrokinetic techniques for separation applications [23].

Advances in fabrication technology have broadened the applicability of dielectrophoresis through realization of micro- and nano-electrode geometries that are capable of generating electric fields strong enough to move nanoparticles [12, 24] such as viruses [25, 26] and chromosomes [27]. At the nano-scale, effects such as thermal and hydrodynamic forces find increased significance. Yet it has been shown that the 'nuisances' are controllable and not significant enough to hinder nanoparticle motion due to dielectrophoresis [28].

Applications of dielectrophoresis are not limited to the realm of diagnostics involving biological particles. As early as 1924, Hatfield achieved separation of minerals using DEP [29]; interestingly, the work has been pursued by other research groups up until very recently [30]. Other examples where dielectrophoresis has been used for industrial applications include construction of a current-limiting fuse using DEP collection of conductive particles between two electrodes [31], depositing a patterned coating of a nano-structured material onto a substrate using positive DEP [32], and the fabrication of nano-scale devices, composed of movable components brought together in a fluid medium by exertion of the dielectrophoretic force – among other interactions [33].

With further developments in the design of suitable electrode geometry and in the modelling of phenomena that occur alongside dielectrophoretic motion of particles, DEP applications are expected to advance further, enabling manipulation and characterization of a yet wider range of particles.

2.3. AC electrokinetics: variants of dielectrophoresis

2.3.1. AC electrokinetic force as dielectrophoresis

AC electrokinetics is the name given to a group of techniques that utilise alternating (AC) electric fields to move dielectric particles in suspension. The most widely used of AC electrokinetic techniques is dielectrophoresis. While DC electric fields can be used to exert electrical force on charged or dielectric particles, the use of AC electric fields for moving particles is specific to dielectrics. Reversing the direction of an applied electric field will reverse the direction of motion of a charged particle (based on equation 2.1), whereas in dielectrophoresis, the direction of motion is independent of that of the applied electric field. For a spherical particle of radius a, the time-averaged DEP force by an electric field $\boldsymbol{E}$ is given by the following expression, in which higher-order moments have been neglected:

$$\langle \boldsymbol{F}_{DEP} \rangle = \pi \epsilon_m a^3 Re\left[\widetilde{K}(\omega)\right] \nabla |\boldsymbol{E}|^2 \tag{2.20}$$

where ϵ_m is (the real part of) the permittivity of the suspending medium, and $\widetilde{K}(\omega)$, termed the Clausius-Mossotti factor, represents the dependency of the dielectrophoretic force on electric field angular frequency ω, and is given by:

$$\widetilde{K}(\omega) = \left(\tilde{\epsilon}_p - \tilde{\epsilon}_m\right) / \left(\tilde{\epsilon}_p + 2\tilde{\epsilon}_m\right) \tag{2.21}$$

where $\tilde{\epsilon}_p$ and $\tilde{\epsilon}_m$ are the (in general) complex permittivities of the particle and its suspending medium, respectively.

It is evident from equation (2.20) that the DEP force is independent of the direction of the applied electric field. The feasibility of using AC electric fields for exerting force on dielectrics brings an important advantage to applications involving dielectric particles as the electric field frequency can be used as a control parameter for the dielectrophoretic force.

2.3.2. AC electrokinetic torque: electro-rotation

While an electric field of non-uniform magnitude exerts force on a dielectric particle in suspension, a field of non-uniform phase will exert torque, and hence result in the rotation of a subject dielectric. The phenomenon is referred to as electro-rotation (ROT) and is another important AC electrokinetic technique, used for dielectric characterisation studies [34].

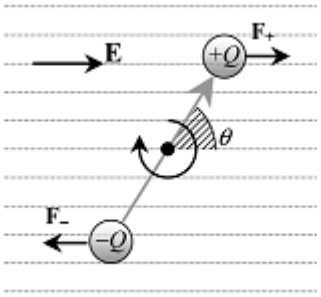

Figure 2.10. Torque by a uniform electric field on a dipole – In a uniform field E (indicated by the vector and dotted field lines), the two point charges constituting a dipole experience equal and opposite forces resulting in a torque about the centre point of the dipole. Figure copied from [1].

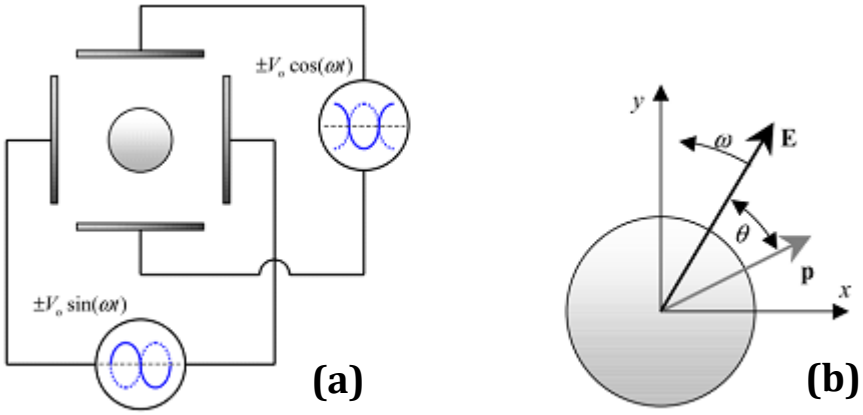

Figure 2.11. AC electrokinetic torque (electro-rotation) - (a) A schematic diagram of an electro-rotation setup. Four signals, successively 90° out of phase are applied to four electrodes encircling the particle. (b) Schematic diagram showing how the induced dipole moment of a particle lags behind a rotating applied electric field. Figure copied from [1].

As shown in figure 2.8, a dipole sitting in a uniform electric field $\boldsymbol{E}$ will be subject to a torque that tends to align the dipole with the applied electric field. Assuming that the dipole in the figure represents polarisation charges at the interface of a dielectric particle and its suspending medium, the particle will be subject to no net force but will experience a torque given by:

$$\Gamma = \boldsymbol{p}^{(1)} \times \boldsymbol{E} \tag{2.22}$$

Alignment of the dipole with the electric field vector will not be immediate as it takes a finite amount of time for polarisation charges to move towards the particle/electrolyte interface and form a dipole.

In a field of non-uniform phase, i.e. a rotating electric field, where the field vector changes direction, this time delay gives rise to a net electro-rotational torque, as shown in figure 2.9. The figure also shows an example electro-rotation setup, where voltages of 90° phase difference re applied to successive electrodes encircling the particle to generate a rotating electric field.

The first-order electro-rotational torque on a spherical particle of radius a is given by [35]:

$$\Gamma_{ROT} = -4\pi\epsilon_m a^3 Im\left[\tilde{K}(\omega)\right]|\boldsymbol{E}|^2 \tag{2.23}$$

Differences with the expression for the dielectrophoretic force on the same particle (given by equation 2.20) can be readily observed: Firstly, the ROT torque is proportional to the square of the electric field magnitude while the DEP force is a function of the gradient of the square of the field magnitude – and is therefore zero in uniform electric fields. Secondly, the electro-rotational torque depends on the imaginary rather than the real part of the Clausius-Mossotti factor. As a result, particles may experience both dielectrophoresis and electro-rotation with the relationship between the two determined by the dielectric properties of the particles and their suspending media.

2.3.3. AC electrokinetic force as traveling-wave dielectrophoresis

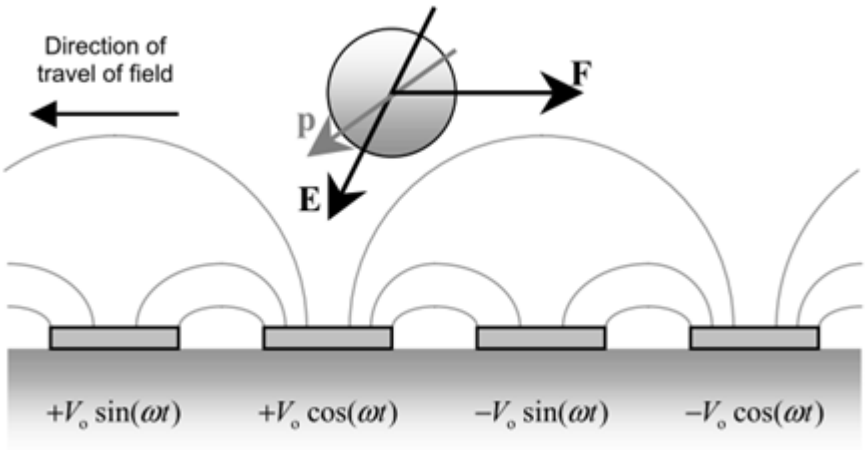

Figure 2.12. Traveling-wave dielectrophoresis – Schematic diagram of a linear traveling wave dielectrophoresis array and the consecutive phase-shifted signals required to generate the traveling electric field. Also shown are the approximate field lines for time *t*=0, the electric field and the dipole moment induced in the particle together with the force on the particle. Figure copied from [1].

Traveling-wave DEP can be considered as the linear analog of electro-rotation where voltages of 90° phase difference are applied to successive electrodes that are laid out as tracks, rather

than being arranged in a circle. This generates an electric field wave which travels along the electrodes. The dipole induced in the particle moves with the electric field but lags behind the field, as in electro-rotation. As shown in figure 6, the result is the induction of a force, rather than a torque, given – for a spherical particle of radius a – by [36]:

$$\boldsymbol{F}_{twDEP} = -\frac{4\pi\epsilon_m a^3 Im[K(\omega)]|\boldsymbol{E}|^2}{\lambda} \tag{2.24}$$

where λ is the wavelength of the traveling wave.

The negative sign in equation (5) indicates that, as shown in figure 2.10, the twDEP force propels particles in the opposite direction to the moving field vector. For a finite twDEP force to be exerted on a particle, two criteria need to be met: (a) the particle must experience a DEP force that levitates it above the electrode array, and (b) some loss mechanism needs to be present for the imaginary part of the Clausius-Mossotti factor to be non-zero. Since its advent, twDEP has been used for characterising and separating cells and micro-organisms [37, 38].

2.4. Summary

An introduction has been presented to the underlying principle of dielectrophoresis: motion of dielectric particles in suspension as a result of electric field interactions with polarisation charges at the particle/electrolyte interface. The established status of DEP together with examples of its wide-ranging applications, particularly in the realm of biochemical analysis has been touched upon, and variants of the technique that use electric field non-uniformities for exerting force or torque on dielectrics have been briefly described.

It has been shown that in the simplest of field-particle geometries, polarisation charge at a particle/electrolyte interface can be represented as an induced dipole. It was also mentioned that, in principle, the dielectrophoretic force may be calculated from the electrical force experienced by the induced dipole. The next chapter will embark on more realistic geometries where higher order multipoles, also introduced in this chapter, are of importance, and will present the notion of *effective* multipoles that serve to circumvent ambiguity regarding the constitution of *induced* multipoles from an unknown mixture of bound and free charge.

References

[1] Morgan, H., Green, N.G.: AC Electrokinetics of Colloids and Nanoparticles. Research Studies Press (2003).

[2] Jones, T. B., Washizu, M.: Multipolar dielectrophoretic and electrorotation theory. J. Electrostat. 37, 121-134 (1996).

[3] Stratton, J. A.: Electromagnetic Theory. McGraw-Hill, New York (1941).

[4] Becker, R.: Electromagnetic fields and interactions. Blaisdell, London (1964).

[5] Pohl, H. A.: The Motion and Precipitation of Suspensoids in Divergent Electric Fields. J. Appl. Phys. 22, 869-871 (1951).

[6] Pohl, H. A.: Dielectrophoresis: the behavior of neutral matter in nonuniform electric fields. Cambridge University Press, Cambridge (1978).

[7] Alazzam, A., Stiharu, I., Bhat, R., Meguerditchian, A. N.: Interdigitated comb-like electrodes for continuous separation of malignant cells from blood using dielectrophoresis. Electrophoresis 32, 1327-1336 (2011).

[8] Li, H. B., Bashir, R.: Dielectrophoretic separation and manipulation of live and heat-treated cells of Listeria on microfabricated devices with interdigitated electrodes. Sensor Actuat B-Chem. 86, 215-221 (2002).

[9] Zhu, K., Kaprelyants, A. S., Salina, E. G., Markx, G. H.: Separation by dielectrophoresis of dormant and nondormant bacterial cells of Mycobacterium smegmatis. Biomicrofluidics 4, 022809 (2010).

[10] Huang, Y., Wang, X.-B., Becker, F. F., Gascoyne, P. R. C.: Introducing dielectrophoresis as a new force field for field-flow fractionation. Biophys. J. 73, 1118-1129 (1997).

[11] Yang, J., Huang, Y., Wang, X.-B., Becker, F. F., Gascoyne, P. R. C.: Cell separation on microfabricated electrodes using dielectrophoretic/gravitational field-flow fractionation. Anal. Chem. 71, 911-918 (1999).

[12] Morgan, H., Hughes, M. P., Green, N. G.: Separation of Submicron Bioparticles by Dielectrophoresis. Biophys. J. 77, 516-525 (1999).

[13] Green, N. G., Morgan, H.: Dielectrophoresis of Submicrometer Latex Spheres. 1. Experimental Results. J. Phys. Chem. B 103, 41-50 (1999).

[14] markx, G. H., Huang, Y., Zhou, X.-F., Pethig, R.: Dielectrophoretic characterization and separation of micro-organisms. Microbiology 140, 585-591 (1994).

[15] Green, N. G., Morgan, H., Milner, J. L.: Manipulation and trapping of sub-micron bioparticles using dielectrophoresis. J. Biochem. Biophys. Methods 35, 89-102 (1997).

[16] Pethig, R., Markx, G. H.: Applications of dielectrophoresis in biotechnology. Trends Biotechnol. 15, 426-432 (1997).

[17] Becker, F. F., Wang, X. B., Huang, Y., Pethig, R., Vykoukal, J., Gascoyne, P. R. C.: Separation of human breast cancer cells from blood by differential dielectric affinity. Proc. Natl. Acad. Sci. USA 92, 860-864 (1995).

[18] Asbury, C. L., van den Engh, G.: Trapping of DNA in nonuniform oscillating electric fields. Biophys. J. 74, 1024-1030 (1998).

[19] Zheng, L., Brody, J. P., Burke, P. J.: Electronic manipulation of DNA, proteins, and nanoparticles for potential circuit assembly. Biosens. Bioelectron. 20, 606-619 (2004).

[20] Washizu, M., Kurosawa, O.: Electrostatic manipulation of DNA in microfabricated structures. IEEE Trans. Ind. Appl. 26, 1165-1172 (1990).

[21] Pethig, R.: Review Article – Dielectrophoresis: Status of the theory, technology, and applications. Biomicrofluidics 4, 022811 (2010).

[22] Ramos, A., Morgan, H., Green, N. G., Castellanos, A.: AC Electric-Field-Induced Fluid Flow in Microelectrodes. J. Colloid Interface Sci. 217, 420-422 (1999).

[23] Gascoyne, P. R. C., Vykoukal, J.: Particle separation by dielectrophoresis. Electrophoresis 23, 1973-1983 (2002).

[24] Hughes, M. P.: AC electrokinetics: applications for nanotechnology. Nanotechnology 11, 124-132 (2000).

[25] Morgan, H., Green, N. G.: Dielectrophoretic manipulation of rod-shaped viral particles. J. Electrostat. 42, 279-293 (1997).

[26] Hughes, M. P., Morgan, H.: Dielectrophoretic trapping of single sub-micrometre scale bioparticles. J. Phys. D: Appl. Phys. 31, 2205-2210 (1998).

[27] Prinz, C., Tegenfeldt, J. O., Austin, R. H., Cox, E. C., Sturm, J.C.: Bacterial chromosome extraction and isolation. Lab Chip 2, 207–212 (2002).

[28] Ramos, A., Morgan, H., Green, N. G., Castellanos, A.: AC electrokinetics: a review of forces in microelectrode structures. J. Phys. D: Appl. Phys. 31, 2338-2353 (1998).

[29] Hatfield, H.: Dielectric separation: a new method for treatment of ores. Trans. Inst. Mining Metallurgy 33, 335-370 (1924).

[30] Ballantyne, G. R., Holtham, P. N.: Application of dielectrophoresis for the separation of minerals. Miner. Eng. 23, 350-358 (2010).

[31] Ohtsuka, S., Hikita, M.: Self-recovering current limiting fuse using dielectrophoretic force. U.S. Patent 7,626,483. Aug. 10, 2005.

[32] Oh, S., Zhou, O.: Deposition method for nanostructure materials. U.S. Patent 7,455,757, Nov. 25, 2008.

[33] Tupper, M. M., Cima, M. J., Chopinaud, M. E.: Manipulating micron scale items. U.S. Patent 7,338,636, Mar. 4, 2008.

[34] Jones, T. B.: Electromechanics of Particles. Cambridge University Press, Cambridge (1995).

[35] Arnold, W. M., Zimmermann, U.: Electro-rotation – development of a technique for dielectric measurements on individual cells and particles. J. Electrostat. 21, 151-91 (1988).

[36] Huang, Y., Wang, X.-B., Tame, J., Pethig, R.: Electrokinetic behaviour of colloidal particles in traveling electric fields: studies using yeast cells. J. Phys. D: Appl. Phys. 26, 312-322 (1993).

[37] Hagedorn, R., Fuhr, G., Muller, T., Gimsa, J.: Traveling-wave dielectrophoresis of microparticles. Electrophoresis 13, 49-54 (1992).

[38] Morgan, H., Green, N. G., Hughes, M. P., Monaghan, W., Tan, T. C.: Large area traveling-wave dielectrophoresis particle separator. J. Micromech. Microeng. 7, 65-70 (1997).

Chapter Three

Calculation of the Dielectrophoretic Force: Background and Theory

3.1. Determining DEP force terms: the effective moment method

3.1.1. The effective moments: definition

As mentioned in Chapter Two, polarisation of dielectric particles in suspension gives rise to, in the simplest case regarding particle and electric field geometry, the induction of a dipole. In more sophisticated circumstances, the arrangement of charge at the particle/electrolyte interface may not be sufficiently represented by a dipole alone. Higher-order multipoles may be required to represent particle polarisation. Yet even in the simplistic case of an induced dipole sufficiently representing polarisation, quantified definition of the dipole and calculation of the dielectrophoretic force as the force exerted by the applied electric field on the dipole is subject to ambiguity as polarisation charge consists of an unknown mixture of bound and free charge, very difficult (due to the rather complicated mechanism of polarisation), if not impossible, to calculate.

The effective moment method cleverly circumvents this ambiguity through the definition of *effective* (as compared to actual, induced) multipoles as those *free-charge* multipoles (constructed using the scheme presented in figure 2.3) that when positioned at the particle location within the electric field and the suspending medium, would give rise to the same electrostatic potential as that arising from the particle in suspension itself. Terms of ascending order in the expression for the potential due to a dielectric particle are attributed to effective multipoles of ascending order and the moments of the effective multipoles are determined by equalling the n^{th}-order term of the potential due to the particle with the potential due to the n^{th}-order multipole [1].

The effective moments of a dielectric particle can be regarded as representatives of the energy stored by the applied electric field in the particle. The effective moment of order n represents the n^{th}-order term of the electrical energy stored in the particle, or rather the energy stored by the $(n-1)^{th}$-order field gradient in the particle. In three dimensions, only the first three multipoles (as shown in figure 2.3) can be realised, with the effective dipole, quadrupole and octupole moments representing the energy stored by the electric field magnitude and its first- and second-order gradients, respectively, in the dielectric particle. It is on the fact that effective moments represent electrical energy stored in dielectric particles that dielectric spectroscopy measurements are based. The studies are aimed at determining dielectric properties of particles, singly or en masse in a suspension, based on measurements of their effective moments.

In axial symmetry, polarisation of dielectric particles in suspension can be represented by linear multipoles [2]. As the name implies, and as depicted in figure 2.4, the poles and displacement vectors constituting the linear multipoles are aligned with the axis of charge symmetry and the limitation to only the first three multipoles is lifted. Linear effective moments up to any order can be considered and could contribute to the potential due to particle-field geometries that are axially symmetric.

Determining the effective moments of dielectric particles is a complicated task, due to the heavy mathematics involved. Testimony to the difficulty in deriving the effective moments of particles in a general case is the fact that only for spherical particles have the moments of an arbitrary order n been analytically calculated [3]. Among non-spherical shapes, only the effective dipole moment of an ellipsoidal particle has been derived analytically [4]. In the absence of analytical methods for determining the higher-order moments of non-spherical particles, modelling is often made with a sphere of similar dimensions. The literature is abundant with examples of highly non-spherical particles such as carbon nanotubes [5], erythrocytes [6-9], viruses [10, 11] and protein [12, 13] approximated as spheres, or at best spheroids, for simplicity of modelling. One goal of this work is to assess the validity of common particle shape approximations by comparing first- and higher-order moments of spherical and non-spherical particles in axial symmetry and otherwise.

3.1.2. The effective moment method: formulation

The notion of effective moments not only facilitates unambiguous moment-based characterisation of dielectric properties, but also enables calculation of the individual terms of the dielectrophoretic force on particles. The n^{th}-order term of the DEP force on a dielectric particle in suspension possessing effective moments $\boldsymbol{p}^{(n)}$ when subjected to an electric field $\boldsymbol{E}$ is given by [3]:

$$\boldsymbol{F}^{(n)} = \frac{1}{n!}\boldsymbol{p}^{(n)}[\cdot]^{(n)}\nabla^{(n)}\boldsymbol{E} \tag{3.1}$$

where $\nabla^{(n)}\boldsymbol{E}$ denotes the n^{th}-order gradient of the applied electric field. The n^{th}-order term of the DEP force by an electric field on a dielectric particle in suspension represents the interaction between the $(n-1)^{th}$-order field gradient and the representative for the electrical energy it stores in the particle, i.e. the n^{th}-order effective moment. It is important to note that as a result of the shape-dependent nature of polarisation, $\boldsymbol{p}^{(n)}$, and therefore $\boldsymbol{F}^{(n)}$, would encompass the effect of particle as well as electric field geometry.

3.1.3. The dipole approximation: statement and criterion for reliability

The dipole approximation ignores the effect of higher-order moments in polarisation of dielectric particles. In dielectric spectroscopic measurements, the dipole approximation posits negligible contribution from higher-order effective moments to the electrical energy stored in dielectrics. In calculation of the dielectrophoretic force, multipolar force terms given by equation (3.1) are assumed by the dipole approximation to contribute negligibly to the electrical force experienced by a dielectric particle subjected to a non-uniform electric field.

The dipole approximation greatly simplifies calculations of the DEP force and dielectric characterisation of particles. It has therefore been used extensively for both purposes in a wide variety of circumstances regarding particle and electric field specifications. The general criterion for higher-order moments to have insignificant effect has been stated to be particle dimensions being notably smaller than a characteristic length scale of electric field non-uniformity, i.e. the electric field varying negligibly across particle dimensions. In older dielectric spectroscopic measurements and dielectrophoretic applications, which often involved suspensions of a large number of micro-metre and sub-micron particles subjected to the electric fields generated by electrodes of considerably larger dimensions than those of the particles, the stated criterion was easily satisfied, and higher-order moments were not found worthy of consideration. With the current trend toward micro- and nano-electrode geometries used for analysis of single particles comparable in size to the electrodes, the stated criterion for the reliability of the dipole approximation is far from satisfied.

An example work where single particles have been manipulated and characterized within electrode gaps comparable in size to particle dimensions is the ‘opposite field’ dielectrophoresis structure used by Holzel [14] to generate two AC electric fields exhibiting antiparallel field gradients to shift micro-particles back and forth. It can be expected that the discrepancy observed between experimental results and the first-order theoretical model are due to the significance of higher order effective moments, particularly near electrode edges.

The quadrupole trap designed by Rosenthal and Voldman for patterning arrays of single cells is another example where large field gradients at particle positions can be expected to give rise to added significance for higher order effective moments and dielectrophoretic forces and may be responsible for the difference between experimental observations and the dipole approximation-based model. An example of the discrepancy and a schematic of the design are shown in figure 3.1, from which the effect of particle size on the discrepancy can be clearly noticed [15].

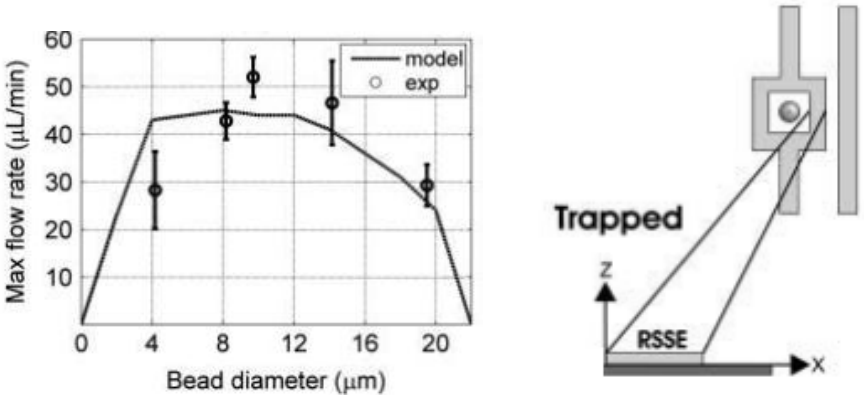

Figure 3.1. Discrepancy between experimental results and theoretical model based on the dipole approximation in a quadrupole trap – Dielectrophoretic trap design for patterning arrays of single cells (right). The trap strength has been validated by measuring the maximum flow rate that polystyrene beads could withstand while remaining trapped. Plot shows dependency of maximum flow rate on bead diameter. Discrepancy between the experimental results (solid line) and the model (circle) may be due to the significance of higher order effective moments in the large field gradient within the DEP trap. Figure copied from [16].

Another example where micro-metre particles are subjected to high-gradient electric fields generated by microelectrode geometry is the impedance analysis chip of Morgan and co-workers, shown in figure 3.2. The accuracy required for accomplishing particle focussing may be satisfied by a first-order prediction of the DEP force, but it can be expected that particle characterisation should involve accounting for higher order moments at certain positions within the electrode structure [16].

In the aforementioned and other examples, the circumstances regarding particle and electric field geometry are such that it can only be *expected* that higher order moments and/or forces will be of significance. It is very important to note, as it is an intended aim of this work that no conclusive judgement regarding the reliability of the dipole approximation can be made before calculations are made of the higher order moments/forces.

3.1.4. Effective moment method calculations of the DEP force in the literature

It was the observation by Jones and co-workers of the DEP levitation of particles against gravity at a field null [17] – where the first-order force is identical to zero – that brought the significance of higher-order moments to attention. The condition for the reliability of the dipole approximation was accordingly extended to include positions of field null. Thomas Jones and Masao Washizu have developed the theory of higher-order moments and multipolar dielectrophoretic forces using tensor notation. Few other research groups have also paid attention to the possible significance of higher-order interactions between electric fields and subject dielectrics. Most notably, Clague and co-workers have observed second-

order contributions up to 10% to the total DEP force on spherical particles positioned within an interdigitated electrode configuration [18].

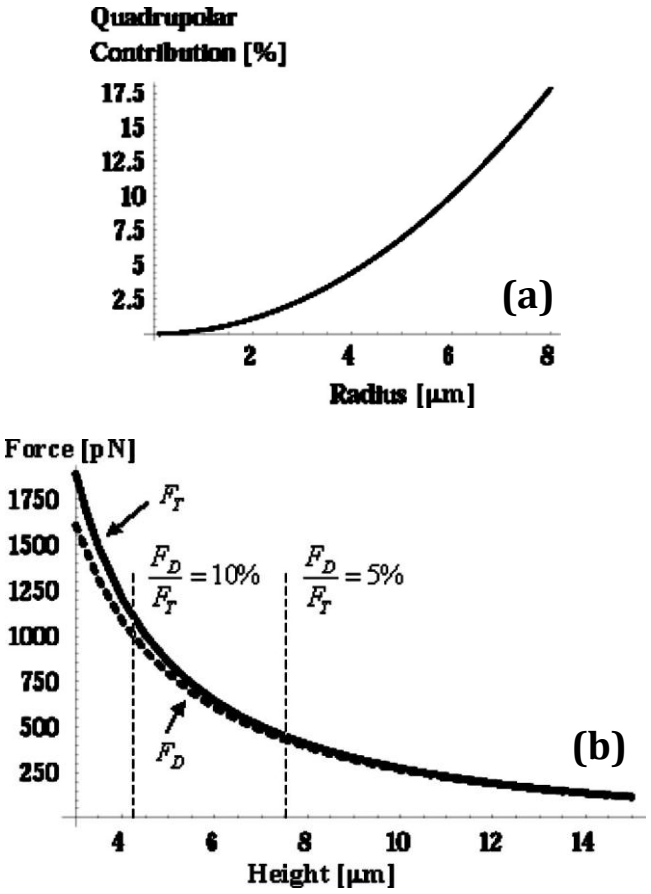

Figure 3.2. Significance of the second-order dielectrophoretic force on a spherical particle – (a) Plot of the quadrupolar contribution to the total DEP force as a function of the latex bead radius. The bead is fixed in position within an interdigitated electrode configuration; (b) DEP forces acting on the 6μm latex bead at different heights above the interdigitated electrode array. F_T represents the sum of first- and second-order force terms calculated using the effective moment method, while F_D represents the DEP force, as predicted by the dipole approximation. Figure copied from [18].

The authors have made note of the rise in significance of the higher-order contribution upon increasing particle size, as shown in figure 3.1. They have also observed the increase in second-order contribution to the total force as the particle nears the interdigitated electrode array, where electric field curvature is largest. This is shown through the growing difference between the total force F_T (calculated by summing first- and second-order terms) and the force predicted by the dipole approximation F_D as particle height above the electrode array is reduced (figure 3.1b). The work by the Clague group is significant in its use of an analytical technique for derivation of the second-order force term. However, analysis is inevitably

confined to spherical particles for which the multipole moments can be determined analytically.

The increase in significance of higher-order moments as particle size is increased has also been noted by Zhu et al [19] in their analysis of light-induced dielectrophoresis of spherical and ellipsoidal particles. As shown in figure 3.2, they have observed an increase in the gap between the DEP force predicted by the dipole approximation, and that determined by accounting for the second-order term as particle radius is increased. The authors have used numerical calculations of the electric field and its gradients to obtain the first- and second-order term of the DEP force on spherical particles from analytic expressions. They have extended analysis to include ellipsoidal particles, but analysis has been confined to the first-order term, for which the effective moment of corresponding order can be derived analytically.

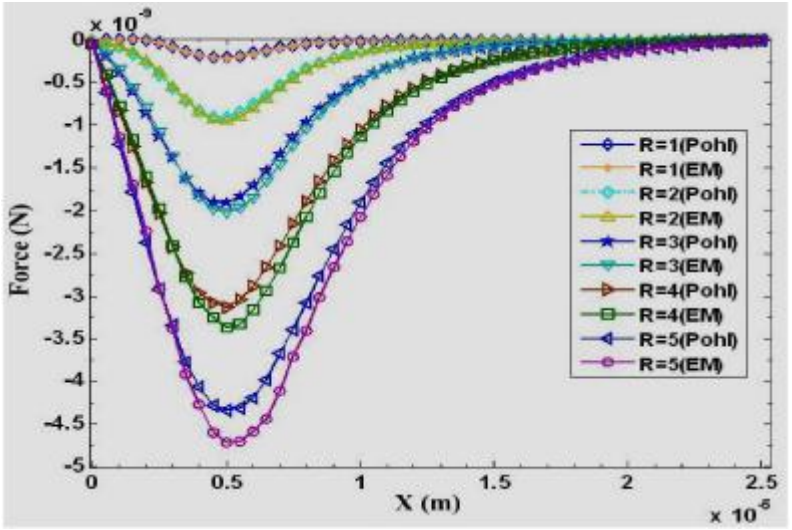

Figure 3.3. Increase in significance of higher-order dielectrophoresis with increasing particle size – DEP forces acting on a spherical cell subjected to a light-induced nonuniform electric field for different cell radii R. (Pohl) represents the dielectrophoretic force as originally derived, i.e. the dipole approximation, and (EM) represents the force as calculated from the effective moment method by summing first- and second-order terms. Figure copied from [19].

Confinement of analysis to the first-order term of the DEP force on non-spherical particles is also seen in the work by Rosales and Lim [20] on the significance of multipolar forces in an octupole trap comprising of eight planar electrodes (figure 3.3). The authors have calculated first-, second- and third-order terms of the DEP force on a spherical particle using the effective moment method, but have stopped at the first-order term for the case of an

ellipsoidal particle as "unfortunately, only a dipolar approximation is available for ellipsoids in the literature". To 'compensate', the authors have derived the total electrical force experienced by the ellipsoid using the mathematically rigorous Maxwell stress tensor method (to be introduced in the next section) to yield higher-order contribution to the DEP force.

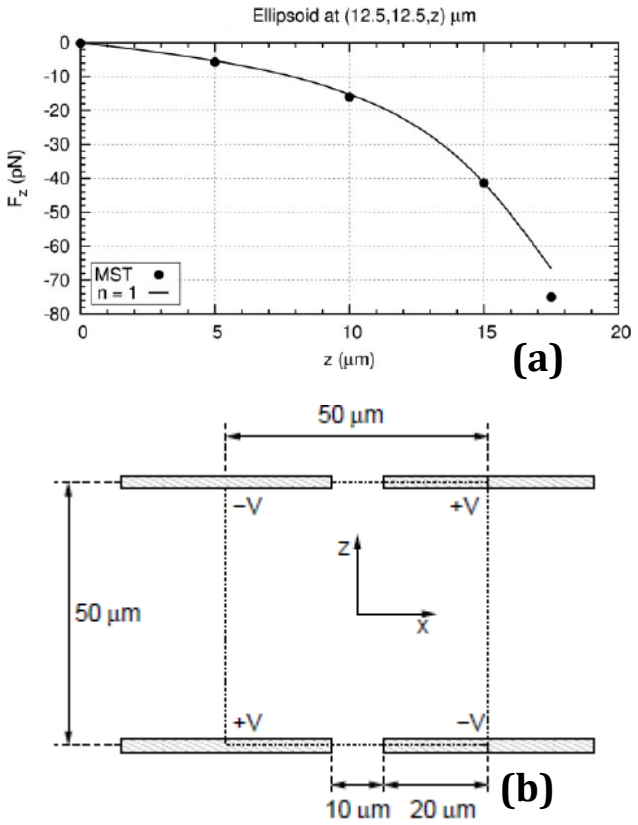

Figure 3.4. Significance of higher-order terms in the DEP force on an ellipsoidal particle – (a) DEP force on an ellipsoid with semi-major axes of dimensions 10µm, 10µm and 2.5µm as a function of distance from the centre of an octupole trap with eight planar electrodes, a frontal view of which is shown in (b). MST denotes the total DEP force on the particle as calculated from the Maxwell stress tensor method, and n=1 denotes the DEP force predicted by the dipole approximation, i.e. the first-order DEP force term. Figure copied from [20].

Another work on the significance of higher-order DEP force terms in that by Kim et al, where analytic expressions for the effective moments of a dielectric sphere have been used in conjunction with analytic derivations of the electric field and its gradients in a 'moving dielectrophoresis' electrode structure (figure 3.4a) to obtain the first three terms of the DEP force on spherical particles of different radii [21]. The authors state that numerical methods "are not suitable for the calculation of the higher-order dielectrophoretic forces" as "their accuracy is typically limited to first-order dielectrophoretic force". The results of the analytical calculations by the group suggest that second- and third-order forces, individually and combined, contribute negligibly to the DEP force on spherical particles. As shown in

figure 3.4, there is almost an order-of-magnitude difference between the magnitudes of first- and higher-order DEP forces on a 5μm sphere. It can be expected that higher-order forces would become comparable to the first-order term is the radius of the spherical particle attains values closer to electrode dimensions. It may also be the case that the electric field curvatures in the electrode structure are insignificant along the direction of particle motion: the x −axis in figure 3.4.

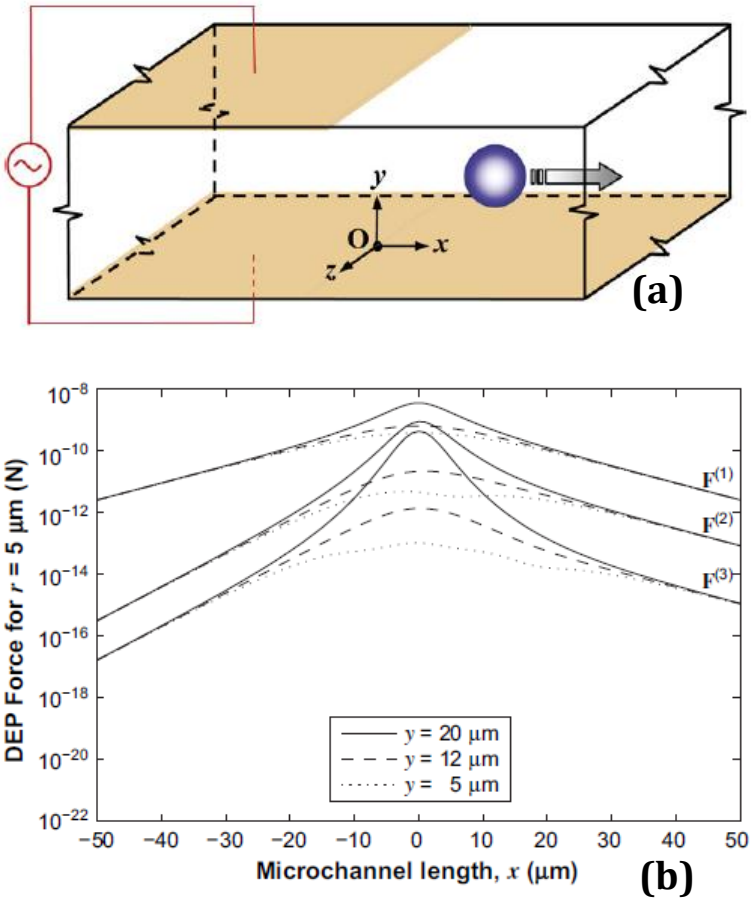

Figure 3.5. Significance of second- and third-order terms of the DEP force on a spherical particle – (a) Structure of the 'moving dielectrophoresis' electrode geometry used by Kua et al for analytical derivation of higher-order contributions to DEP forces on spherical particles, (b) Variations with positions within the electrode geometry of first- ($F^{(1)}$), second- ($F^{(2)}$) and third-order ($F^{(3)}$) terms of the DEP force on a spherical particle of radius 5μm. Figure copied from [21].

The work presented through figures 3.1 to 3.4 is about all that has been done towards investigating the significance of higher-order DEP forces. Although the formulation of the effective moment method has been fully developed, no attempt has been made to determine multipolar DEP forces on non-spherical particles. The biggest roadblock appears to be the lack of analytic derivations for the higher-order moments of non-spherical particles. This

work will demonstrate how numerical methods can be used as an alternative to determine the effective moments of particles of arbitrary shape. The credibility of numerical calculations of DEP force terms will be verified by comparison of results against total force calculations using the Maxwell stress tensor method.

3.1.5. Determination of the effective moments

Although the effective moment method presents a straightforward formulation for multipolar dielectrophoretic forces that identifies closely with the conventional formulae for calculation of the DEP force, it still requires the effective moments to be calculated for derivation of dielectrophoretic force terms. Calculation of the effective moments is also the essential requirement for dielectric spectroscopic measurements of particle properties.

As mentioned previously, only for spherical particles have the effective moments of arbitrary order been analytically derived and the only equivalent analytic expression for non-spherical particles is that for the effective dipole moment of an ellipsoid. In the absence of analytical techniques, resort can made to numerical means of determining the higher-order moments of non-spherical particles.

An important advance in the field has been made by Green and Jones who have devised a hybrid numerical-analytical method for determining the effective moments, up to any order, of particles of arbitrary shape subjected to axially symmetric electric fields [22]. The assumption of axial symmetry, rendering the effective multipoles linear, has greatly simplified the process of deriving the effective moments. The method, which shall be presented in Chapter Four, uses the analytic expression for the potential due to a particle subjected to an axisymmetric electric field to derive the linear effective moments by numerical weighted integration of the potential over a spherical Gaussian surface that encloses the particle. By basing derivations on an integration of the electric potential, the error-prone process of differentiation in numerical solvers is circumvented.

This work will present results of applying the aforementioned method to spherical, ellipsoidal and cylindrical particles of different dimensions subjected to the axisymmetric electric fields of two different electrode geometries. The effective moments are calculated using the method, and the results combined with analytical derivations of the electric field magnitude and its gradients to obtain the first three terms of the DEP force experienced by the particles.

In non-axisymmetric geometries, the electrostatic potential due to a dielectric particle, represented through the sum of potentials due to general, rather than linear, effective

multipoles, takes a more complicated form. This work will present a novel method with which the first three effective moments of particles of arbitrary shape subjected to electric fields of arbitrary geometry can be determined. The method will be applied to determine the effective moments of spherical, ellipsoidal and brick-shaped particles at different positions within an interdigitated electrode configuration – widely used in dielectrophoretic applications, particularly for separation of particles based on dielectric properties. As in the axisymmetric case, effective moment calculations will be combined with analytic derivations of the electric field magnitude and its gradients to derive the first three terms of the DEP force on particles.

3.2. Determining the total DEP force: the Maxwell stress tensor method

3.2.1. Maxwell stress tensor: definition

Stress, a measure of force per unit area, is normally represented through a tensor. When an excitation is applied to a body sitting in a medium resulting in exertion of force on the body, the stress tensor at each surface area element of the body can be regarded as an operator that takes the vector normal to the area element and yields the force acting on that area element through the following expression:

$$F_i = \sum_{j=1}^{3} A_j T_{ji}^{(2)} \qquad i = 1,2,3 \tag{3.2}$$

where F_i and A_j are elements of the force and normal vectors, respectively, with i and j indexing the axes in a chosen coordinate system. $T_{ji}^{(2)}$ are the elements of the rank-2 stress tensor $\boldsymbol{T}^{(2)}$. Based on equation (3.2), integration of the stress tensor over any enclosing surface A yields the force exerted by the excitation on the subjected body:

$$\boldsymbol{F} = \oint (\boldsymbol{T}^{(2)} \cdot \boldsymbol{n}) dA \tag{3.3}$$

where $\boldsymbol{n}$ is the unit vector normal to A.

Where the excitation is an electric field, the stress tensor is called the Maxwell stress tensor and integration over a surface enclosing a body of dielectric subjected to an electric field gives the total electrical force experienced by the dielectric, encompassing all interaction between the electric field and the dielectric. The components of the Maxwell stress tensor due to an electric field $\boldsymbol{E}$ are given by:

$$\boldsymbol{T}^{(2)} = \epsilon_m (\boldsymbol{EE} - \frac{1}{2} E^2 \boldsymbol{U}^{(2)}) \tag{3.4}$$

where ϵ_m is the (real part of the) permittivity of the medium in which the dielectric body sits, $\boldsymbol{EE}$ denotes the dyadic product of the electric field vector with itself, E is the electric field magnitude, and $\boldsymbol{U}^{(2)}$ is the unit tensor of rank 2.

There are other elements in the expression for Maxwell stress tensor components that include the magnetic field vector. In most DEP applications, the frequency of the applied electric field falls below 100 MHz. This corresponds to a wavelength of a few metres which is several orders of magnitude larger than the dimensions of a typical DEP device. As a result, the requirements of the so-called near-field approximation are satisfied and the effects due to magnetic fields can be neglected.

3.2.2. Maxwell stress tensor calculation of the dielectrophoretic force

Gascoyne and co-workers have derived the expression for the total DEP force on a dielectric particle suspended in a dielectric medium, from integration of the Maxwell stress tensor over an enclosing surface A [23]:

$$\boldsymbol{F}_{DEP}^{MST} = \frac{1}{2}\epsilon_m \oint (2\boldsymbol{E}_m\boldsymbol{E}_m - E_m^2\boldsymbol{U}) \cdot \boldsymbol{n}dA \tag{3.5}$$

where $\boldsymbol{E}_m$ denotes the electric field vector inside the suspending medium, $\boldsymbol{E}_m\boldsymbol{E}_m$ being the dyadic product of the vector with itself, and E_m the vector magnitude.

Equation (3.5) presents the formulation for Maxwell stress tensor derivation of the dielectrophoretic force. The method is known for its mathematical rigorousness in that it accounts for all interaction between an applied electric field and a dielectric particle in suspension that result in electrical force on the particle. The DEP force calculated from the Maxwell stress tensor (MST) method is therefore referred to as the 'total' dielectrophoretic force. MST-method calculation of the dielectrophoretic force will encompass the effects of first- and higher-order moments, and therefore comparison with effective moment method calculation of the DEP force terms can yield contributions from dipolar and multipolar terms to the total dielectrophoretic force.

In this work, the Maxwell stress tensor method will be incorporated to calculate the total DEP force on spherical and non-spherical particles in axial symmetry, and otherwise. The Maxwell stress tensor will be numerically integrated over multiple enclosing surfaces – to ensure minimal error is imparted by the numerical solver on the results obtained. MST calculation of the total DEP force not only helps derive first- and higher-order contributions to the dielectrophoretic force, but also importantly serves as verification for numerical force term calculations.

3.3. Summary

Two methods for calculation of the dielectrophoretic force on dielectric particles in suspension have been introduced: the effective moment method relies on the determination of effective moments and field gradients to yield DEP force terms of ascending order, and the Maxwell stress tensor method relies on integration of the Maxwell stress tensor over a surface enclosing the particle to yield the total DEP force. The two methods can be regarded as complimentary: the Maxwell stress tensor method is known for its mathematical rigorousness in encompassing all interactions between an applied electric field and subject dielectrics, but does not distinguish between first- and higher-order contributions to the DEP force. The effective moment method fills this void by providing formulae for calculating individual DEP force terms.

The next three chapters will present calculations, based on the effective moment method, of the first three terms of the dielectrophoretic force on particles of different shapes subjected to electric fields of different geometry. The multipole moments are calculated using an available numerical method for axisymmetric geometries and a novel method applicable to particles and fields of arbitrary geometry in a non-axisymmetric setting. To determine the significance of higher-order contributions to the DEP force and for verification of the numerical results, effective moment method calculations of the dielectrophoretic force terms will be compared against total force calculations using the Maxwell stress tensor method.

References

[1] Jones, T.B.: Multipole corrections to Dielectrophoretic Force. IEEE Trans. Ind. Appl. IA-21, 930-934 (1985).

[2] Becker, R.: Electromagnetic fields and interactions. Blaisdell, London (1964).

[3] Washizu, M., Jones, T. B.: Multipolar dielectrophoretic force calculation. J. Electrostat. 33, 187-198 (1994).

[4] Stratton, J. A.: Electromagnetic Theory. McGraw-Hill, New York (1941).

[5] Krupke, R., Hennrich, F., Weber, H. B., Kappes, M. M., von Lohneysen, H.: Simultaneous deposition of metallic bundles of single-walled carbon nanotubes using ac-dielectrophoresis. Nano Lett. 3, 1019-1023 (2003).

[6] Becker, F. F., Wang, X. B., Huang, Y., Pethig, R., Vykoukal, J., Gascoyne, P. R. C.: Separation of human breast cancer cells from blood by differential dielectric affinity. Proc. Natl. Acad. Sci. USA 92, 860-864 (1995).

[7] Gascoyne, P. R. C., Mahidol, C., Ruchirawat, M., Satayavivad, J., Watcharasit, P., Becker, F. F.: Microsample preparation by dielectrophoresis: isolation of malaria. Lab Chip 2, 70-75 (2002).

[8] Sukhorukov, V. L., Mussauer, H., Zimmermann, U.: The effect of electrical deformation forces on the electropermeabilization of erythrocyte membranes in low- and high-conductivity media. JMB 163, 235-245 (1998).

[9] Minerick, A. R., Zhou, R. H., Takhistov, P., Chang, H. C.: Manipulation and characterization of red blood cells with alternating current fields in microdevices. Electrophoresis 24, 3703-3717 (2003).

[10] Morgan, H., Green, N. G.: Dielectrophoretic manipulation of rod-shaped viral particles. J. Electrostat. 42, 279-293 (1997).

[11] Park, K., Akin, D., Bashir, R.: Electrical capture and lysis of vaccinia virus particles using silicon nano-scale probe array. Biomed Microdevices 9, 877-883 (2007).

[12] Lapizco-Encinas, B. H., Ozuna-Chacón, S., Rito-Palomares, M.: Protein manipulation with insulator-based dielectrophoresis and direct current electric fields. J. Chromatogr. A 1206, 45-51.

[13] Hölzel, R., Calander, N., Chiragwandi, Z., Willander, M., Bier, F. F.: Trapping single molecules by dielectrophoresis. Phys. Rev. Lett. 95, 128102 (2005).

[14] Holzel, R.: Single particle characterization and manipulation by opposite field dielectrophoresis. J. Electrostat. 56, 435-447 (2002).

[15] Rosenthal, A., Voldman, J.: Dielectrophoretic traps for single-particle patterning. Biophys. J. 88, 2193-2205 (2005).

[16] Morgan, H., Holmes, D., Green, N. G.: High speed simultaneous single particle impedance and fluorescence analysis on a chip. Curr. Appl. Phys. 6, 367-370 (2006).

[17] Washizu, M., Jones, T. B., Kaler, K. V. I. S.: Higher-order dielectrophoretic effects: levitation at a field null. Biochim. Biophys. Acta 1108, 215-223 (1992).

[18] Liang, E., Smith, R. L., Clague, D. S.: Dielectrophoretic manipulation of finite sized species and the importance of the quadrupolar contribution. Phys. Rev. E 70, 066617 (2004).

[19] Zhu, S., Hong, Y., Ni, Z., Song, C., Analysis of the influence of the cell geometry and cell proximity effects on the single-cell trapping using light-induced dielectrophoresis. IEEE/ICME Intl. Conf. on Comp. Med. Eng. 1720-1725 (2007).

[20] Rosales, C., Lim, K. M.: Numerical comparison between Maxwell stress method and equivalent multipole approach for calculation of the dielectrophoretic force in single-cell traps. Electrophoresis 26, 2057-2065 (2005).

[21] Kua, C. H., Lam, Y. C., Yang, C., Youcef-Toumi, K., Rodriguez, I.: Modeling of dielectrophoretic force for moving dielectrophoresis electrodes. J. Electrostat. 66, 514-525 (2008).

[22] Green, N. G., Jones, T. B.: Numerical determination of the effective moments of non-spherical particles. J. Phys. D: Appl. Phys. 40, 78-85 (2007).

[23] Wang, X., Wang, X-B., Gascoyne, P. R. C.: General expressions for dielectrophoretic force and electrorotational torque derived using the Maxwell stress tensor method. J. Electrostat. 39, 277-295 (1997).

Chapter Four

Effective Moments and Dielectrophoretic Force Terms in Axial Symmetry: Results and Discussion

Abstract

Calculations are presented for the first three effective moments of, and first three terms of the dielectrophoretic (DEP) force on spherical, ellipsoidal and cylindrical particles subjected to axisymmetric electric fields generated by point-plane and disc-plane electrode geometries. The effective moments are calculated using a hybrid numerical-analytical method that involves numerical integration of the potential due to the particles represented, through an analytic expression, by linear multipoles of ascending order in axial symmetry. Analytic calculations are also presented for the electric field magnitude and its first three derivatives along the symmetry axes of the two electrode geometries. The effective moment method is then invoked to derive the first three terms of the DEP force on the particles from calculations of the effective moments and field derivatives of corresponding order. The effects of particle and field geometry on the linear moments and dielectrophoretic force terms are discussed. The assumption of axial symmetry serves as a good starting point towards the goal of quantifying the significance of higher-order moments and DEP force terms, in that the effective moments representing particle polarisation become linear and calculations are greatly simplified as a result.

Overview

Section 4.1 presents the methods used for calculating the effective moments and dielectrophoretic force terms in axial symmetry and illustrates the physical problem to which the methods will be applied. Section 4.2 presents analytical calculations of the electric field magnitude and its first three derivatives along the symmetry axes of the two axisymmetric electrode configurations. Section 4.3 presents and discusses calculations of the first three effective moments of spherical, ellipsoidal and cylindrical particles positioned on the symmetry axes of point-plane and disc-plane electrode geometries. Effects of particle and field geometry on the significance of higher-order effective moments and particle characterisation errors incurred upon approximating non-spherical shapes with spheres of similar dimensions are also discussed. Section 4.4 presents and discusses DEP force term results obtained using the effective moment method. Discussions on the significance of higher-order DEP forces are reserved for Chapter Five where total force calculations using the Maxwell stress tensor method will be compared against force term results to derive higher-order contributions to the dielectrophoretic force in different circumstances regarding particle and field geometry.

4.1. Background and theory

4.1.1. Method for determination of linear effective moments

It has been shown that any axisymmetric distribution of charge can be represented by linear multipoles of ascending order [1]. Accordingly, the electrostatic potential due to a dielectric particle in suspension subjected to an axially symmetric electric field can be expressed as [2]:

$$\varphi_{particle} = \sum_{n=1}^{\infty} \frac{p^{(n)}}{4\pi\epsilon_m r^{n+1}} P_n(\cos\theta) \tag{4.1}$$

where the term being summed is the potential due to an n^{th}-order linear multipole. The multipoles representing particle polarisation are known as *effective* multipoles and their moments $p^{(n)}$ referred to as effective moments. Originally tensors of rank n, the effective moments are reduced to scalar quantities in axial symmetry. In equation (4.1), ϵ_m is permittivity of the suspending medium, r is radial distance from centre of effective multipoles, i.e. centre of particle, and $P_n(\cos\theta)$ are the Legendre polynomials, θ being the azimuthal angle in spherical coordinates. As the Legendre polynomials are mutually orthogonal, the linear effective moments can be derived from the potential due to the particle they represent [3]:

$$p^{(n)} = 4\pi\epsilon_m R_{int}^{n+1} \frac{2n+1}{2} \int_0^{\pi} \varphi_{particle} P_n(\cos\theta) \sin\theta \, d\theta \tag{4.2}$$

The integral in equation (4.2) can be performed over any spherical surface of radius R_{int} that fully encloses the particle and as such, the method is applicable to particles of arbitrary shape.

4.1.2. Physical problem specifications

Figure 4.1 shows the structures of the two electrode geometries studied in this chapter for the generation of axially symmetric electric fields, namely the point-plane and the disc-plane configurations. ±1V is applied to point/disc and plane electrodes to generate axially symmetric electric fields. The examination of two different electrode arrangements and different radii for the point/disc electrodes is for investigating the effect of electrode (and hence electric field) geometry on the linear moments and dielectrophoretic force terms. The plane electrode has been taken to be excessively large for the Neumann boundary condition imposed by vertical simulation domain walls to have minimal effect on the electric fields along the axes of symmetry.

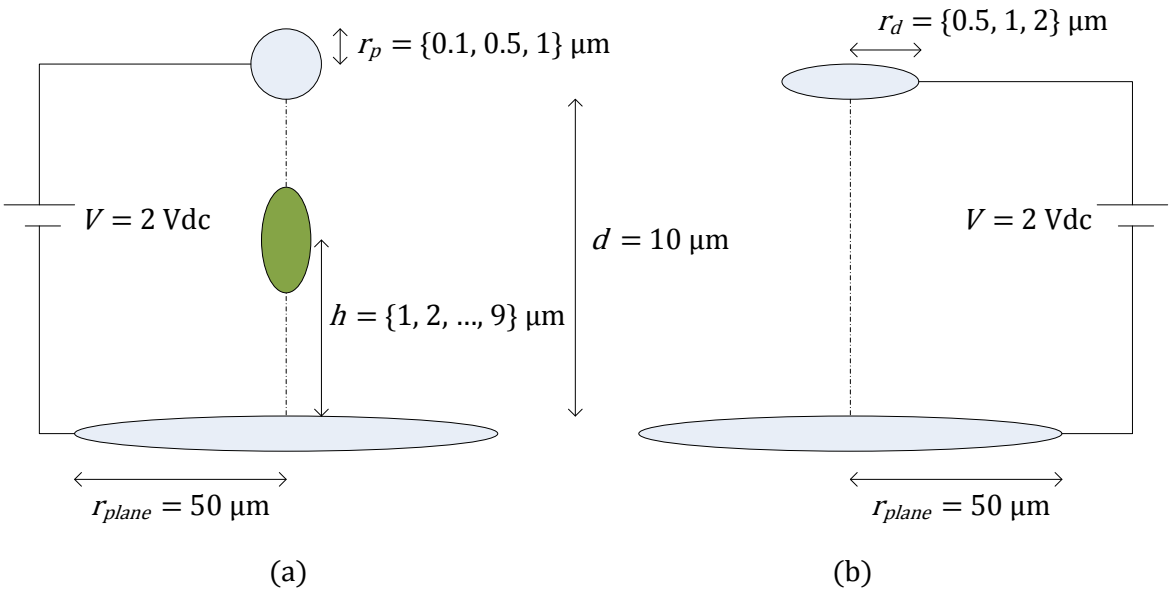

Figure 4.1. The axisymmetric electrode geometries – Specifications of the (a) point-plane and (b) disc-plane electrode arrangements studied in this chapter for the analysis of effective moments and dielectrophoretic force terms in axial symmetry. ±1V is applied to point/disc and plane electrodes to generate axially symmetric electric fields. The use of two different electrode configurations and different radii for the point/disc electrodes is for investigating the effect of electrode geometry on the linear effective moments and DEP force terms. The range of particle positions *h* along the symmetry axes of the two electrode geometries, which translates into a corresponding range of electric field magnitude and curvature strengths, is also shown in the figure.

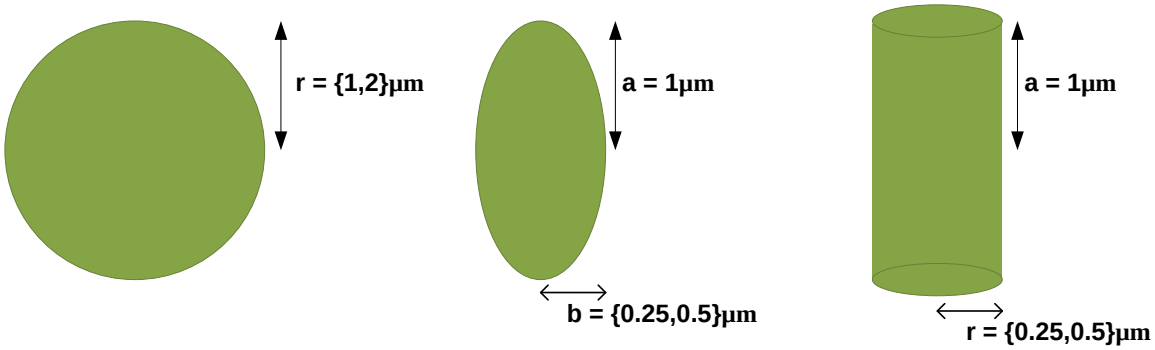

Figure 4.2. The axisymmetric particles – Shapes and dimensions of the dielectric particles subjected to axisymmetric electric fields by being positioned on the symmetry axes of point-plane and disc-plane electrode configurations (of specifications given in figure 4.1). The third (out-of-plane) dimension of the ellipsoidal particle is assumed to equal *b*. The use of different particle shapes and dimensions is for investigating the effect of particle geometry on the linear effective moments and dielectrophoretic force terms. It is assumed that the particles and their suspending media are ideal dielectrics with relative permittivities of 3 and 80 (pertaining to SU-8 and water), respectively.

As mentioned in Chapter One (Section 1.3) this work examines electrode structures within which (or, in the axisymmetric considered in this chapter, along the symmetry axes of which) an analytic derivation for the electric field is available, so that the successive differentiation required to obtain electric field gradients can be done analytically, without resorting to error-prone numerical differentiation. For the disc-plane electrode geometry, the electric field along the axis of field symmetry has been derived by Sloggett and co-workers using the Schwarz-Christoffel mapping method [5]. The derivation is presented in Appendix B. For the point-plane electrode geometry, the analytic derivation by Coelho and Debeau – based on a hyperbolic approximation for the point electrode – has been used for the electric field along the axis of field symmetry [6]. The derivation is presented in Appendix C.

The effect of particle geometry is investigated by considering three different particle shapes, as shown in figure 4.2. It is important to note that, due to axial symmetry, the ellipsoidal particles are in fact spheroids with their third (out-of-plane) half-dimension equal to b. Two sets of dimensions for each of the three particle shapes are analysed in this chapter. For the spherical particle, two different radii are considered to observe the effect of particle size on the moments and DEP force terms. For ellipsoidal and cylindrical particles, two different aspect ratios λ (defined as a/b and a/r for ellipsoidal and cylindrical particles, respectively) are examined to observe the effect of 'thinning' particles on the linear moments and dielectrophoretic force terms.

Different particle positions along the symmetry axes of either of the two electrode geometries correspond to electric field magnitude and curvatures of different strengths. It is assumed throughout this chapter that the particles and their suspending media are ideal dielectrics with relative permittivities of 3 and 80 (pertaining to SU-8 and water), respectively. As such, the particles are less polarisable than their suspending media and therefore subject to negative DEP, tending to move the particles away from the point/disc electrodes where the electric field is strongest. In accordance, the positive direction is taken to be that towards the plane electrode in both electrode configurations.

4.1.3. Field derivative and effective moment calculation techniques

The electric field magnitude and its first three derivatives along the symmetry axis of the point-plane electrode geometry are calculated using an analytic method based on a hyperbolic approximation of the point electrode [6] (derivation presented in Appendix C). For the disc-plane geometry, electric field magnitude and curvatures are calculated using a Schwarz-Christoffel mapping (SCM)-based analytical method [5] (derivation presented in Appendix B). Analytical calculation of electric field magnitude and derivatives is

advantageous over numerical means as the finite element method is highly unreliable in successive differentiation of functions, due to its discretisation of data.

The linear effective moments of the particles are calculated by numerically performing the integral in equation (4.2) over three different spherical surfaces: those of radii equal to, 0.5μm larger than, and 0.9μm larger than the longest half-dimension of the particle. The largest of integration surface radii has been chosen such that a marginal distance of at least 0.1μm is kept between the integration surface and the electrodes. The use of three different integration surfaces is to assure minimal error is imparted by the numerical solver to effective moment calculations. The standard numerical solver used to obtain the results of this work has been FlexPDE. However, due to issues with numerical implementation of the Maxwell stress tensor method in FlexPDE (to be reported on in Chapter Five), effective moment calculations of this chapter were cross-checked against those obtained with an alternative software – FEniCS. Results obtained with three different integration surfaces in FlexPDE agreed with each other and with those obtained in FEniCS to within an error margin of no more than 0.5%.

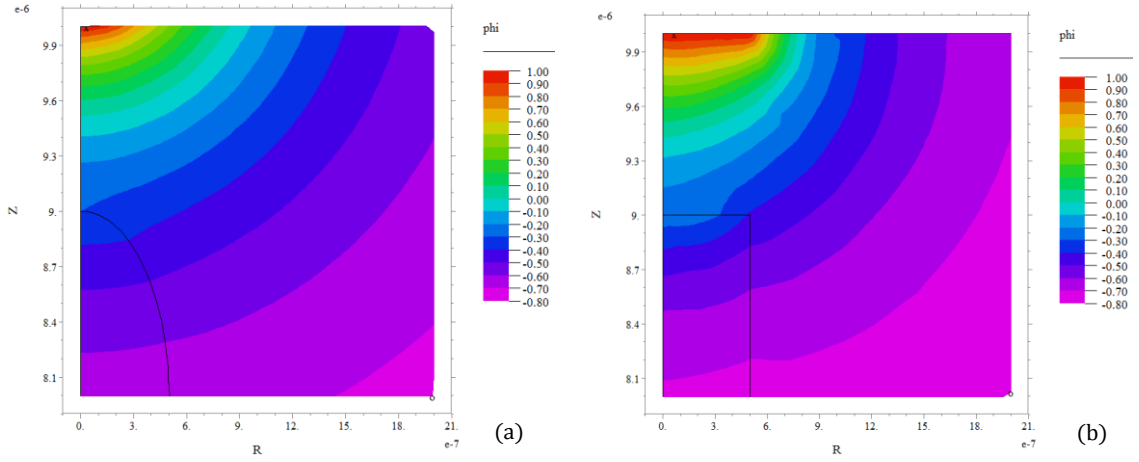

Figure 4.3. The axisymmetric simulation domains – Portions of simulation domains in FlexPDE for calculation of the effective moments of (a) an ellipsoidal (a=1μm, b=0.5μm) particle positioned at h=8μm on the symmetry axis of the point-plane electrode geometry with point electrode radius r_p=0.5μm, and (b) a cylindrical (a=1μm, r=0.5μm) particle positioned at h=8μm on the symmetry axis of the disc-plane electrode geometry with disc electrode radius r_d=0.5μm. The effect of particle polarisation is observed through distortions to background equipotential surfaces.

As can be seen from equation (4.2), calculation of the linear effective moments requires derivation of the potential due to the particle they represent. In this work the potential

$\varphi_{particle}$ due to each given particle positioned on the symmetry axis of the point-/disc-plane electrode geometry has been calculated from:

$$\varphi_{particle} = \varphi_{with\ particle} - \varphi_{background} \tag{4.3}$$

In equation (4.3), the 'background' potential $\varphi_{background}$ is the electric potential distribution within the electrode geometry in the *absence* of the particle. The $\varphi_{with\ particle}$ potential is the electric potential distribution in the *presence* of the particle at its given position along the symmetry axis of the electrode geometry. The subtraction of the background potential from the potential in the presence of the particle yields the perturbation caused by the particle to the potential distribution within the electrode structure, i.e. the potential due to the particle.

Figure 4.3 shows a zoom-in of the simulation domain in FlexPDE for determination of the electric potential due to ellipsoidal and cylindrical particles positioned at $h = 8\mu m$ on the symmetry axes of point-plane and disc-plane electrode structures, respectively with point/disc electrode radii of 0.5μm. Due to axial symmetry, only half the original domain, as portrayed in figure 4.1, needs to be simulated. Figure 4.3 shows the simulation domain for $h \geq 8\mu m$, so that the perturbation caused by the placement of the particles can be more clearly visualised. The particles are seen to give rise to distortions to 'background' equipotential surfaces. It is the difference between the background potential and that with the particles inserted on the symmetry axes that yields $\varphi_{particle}$, as given in equation (4.3).

4.1.4. Dielectrophoretic force term calculation method

The first three terms of the dielectrophoretic force on particles are calculated using the effective moment method. The n^{th}-order term of the DEP force exerted by an electric field $\boldsymbol{E}$ on a particle of effective moments $\boldsymbol{p}^{(n)}$ is given by [2]:

$$\boldsymbol{F}^{(n)} = \frac{1}{n!}\boldsymbol{p}^{(n)}[\cdot]^{(n)}\nabla^{(n)}\boldsymbol{E} \tag{4.4}$$

where $[\cdot]^{(n)}$ denotes the generalised dot product and $\nabla^{(n)}\boldsymbol{E}$ is the n^{th}-order gradient of the electric field. In axial symmetry, the effective moments are linear and only the component of electric field magnitude and gradients that are aligned with the axis of symmetry contribute to the DEP force exerted on the particles. As a result, equation (4.4) reduces to:

$$F^{(n)} = \frac{1}{n!}p^{(n)}\frac{d^nE}{dz^n} \tag{4.5}$$

where, with no loss of generality, the axis of symmetry has been assumed to be aligned with the z-axis in the cylindrical coordinate system. As expressed through equation (4.5), axial

symmetry reduces dielectrophoretic force terms to scalar quantities representing their magnitude.

4.1.5. Summary

The method for determination of the effective moments of particles in axial symmetry has been introduced. Specifications of the physical problem to which the method will be applied have also been presented. Spherical, ellipsoidal and cylindrical particles of different dimensions subjected to the axisymmetric electric fields of point-plane and disc-plane electrode geometries will be analysed to investigate the effects of electrode and particle geometry on the linear effective moments and DEP force terms. Simulation techniques for obtaining the effective moments of the dielectric particles, the bases of the analytical methods for determining the electric field magnitude and its derivatives, and the formulation of the effective moment method for obtaining the DEP force terms have also been presented.

4.2. Electric field magnitude and derivatives

This section presents and discusses analytical calculations of the electric field magnitude and its first three derivatives along the symmetry axes of point-plane and disc-plane electrode geometries. Electric field curvatures determine the energy stored in dielectric particles in the form of effective moments. Field magnitude and derivative results are also important in that they are required for the calculation of dielectrophoretic force terms from the effective moment method. In the results to be presented, units for electric field magnitude and first-, second- and third-order derivatives are V.(μm)$^{-1}$, V.(μm)$^{-2}$, V.(μm)$^{-3}$ and V.(μm)$^{-4}$, respectively.

4.2.1. The disc-plane electrode geometry

The electric field magnitude at a point of height h above the plane electrode on the symmetry axis of the disc-plane geometry has been calculated analytically using the Schwarz-Christoffel mapping method [5] (see Appendix B):

$$E(h) = \frac{V}{d}\left[1 - \frac{\pi}{d}\cos\left(\frac{\pi h}{d}\right)\right] \tag{4.6}$$

where d is the separation between the disc and plane electrodes and V is the voltage applied across the electrodes, 2V in this work. It can be noticed that the radius r_d of the disc electrode does not appear in the expression for the electric field magnitude along the symmetry axis of the disc-plane geometry. This is because it has been found that, as a rule of thumb, the disc electrode needs to be at least 20 times smaller than the separation between disc and plane electrodes for r_d to affect the electric field along the axis of symmetry [5]. In fact, it is only when the disc electrode converges in shape towards a point electrode that field magnitude along the axis of symmetry shows dependency on disc electrode radius. As the smallest of disc electrode radii examined in this work, $r_d = 0.5\mu m$, is large enough not to disturb the electric field magnitude along the symmetry axis, equation (4.6) can be safely applied to the intents and purposes of this chapter.

Figure 4.4 shows the results obtained for the electric field magnitude and its first three derivatives along the symmetry axis of the disc-plane geometry (of specifications given in figure 4.1). The field derivatives have been calculated by analytical differentiation of equation (4.6) in MATLAB. The results show that the electric field strengthens towards the disc electrode whereas electric field derivatives bear (odd or even) symmetry around the midpoint h = 5μm. It can be noticed that values of the electric field magnitude and first three derivatives do not undergo significant change along the symmetry axis of the disc-plane

geometry; all values are seen to remain within the same order of magnitude as height *h* above the plane electrode is increased from 0 to 10μm.

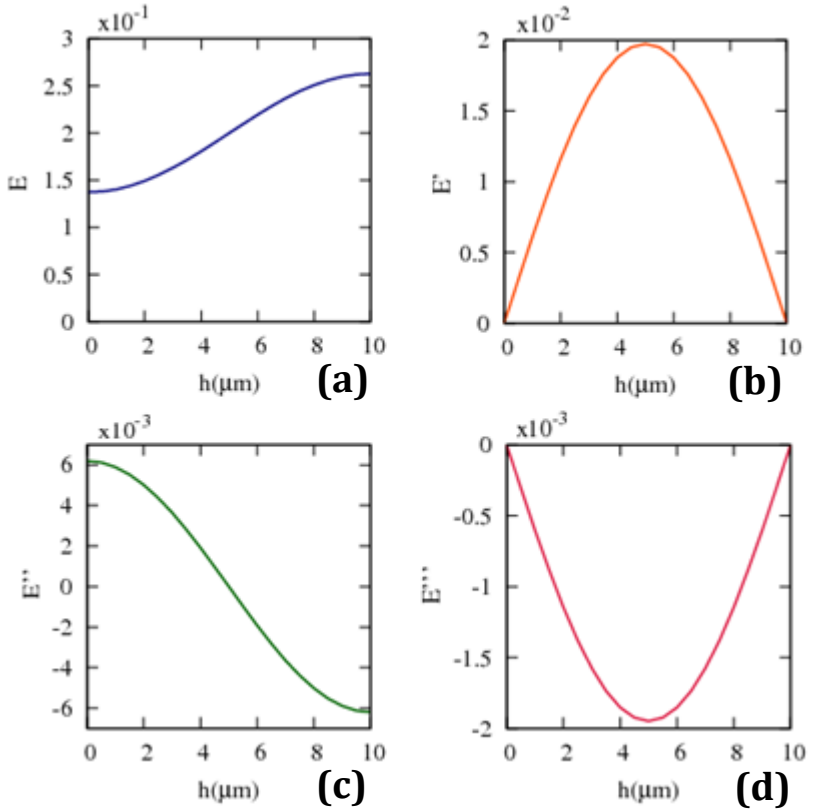

Figure 4.4. Electric field magnitude and derivatives along symmetry axis of disc-plane geometry – Variations with height *h* above the plane electrode of the (a) electric field magnitude, and its (b) first-, (c) second-, and (d) third-order derivatives along the symmetry axis of the disc-plane electrode geometry (of specifications given in figure 4.1). Identical results are obtained with disc electrode radii in the range {0.5,1,2}μm. The electric field magnitude has been calculated analytically using equation 4.6 (derivation presented in Appendix B) and the field gradients are obtained by analytic differentiation of equation 4.6 in MATLAB.

The first derivative of the electric field is seen to attain positive values at all positions along the symmetry axis of the electrode geometry while second- and third-order derivatives are seen to be negative-valued for $h > 5\mu m$ and at all h, respectively. As the field magnitude and its first- and second-order derivatives determine the energy stored in particles in the form of effective dipole, quadrupole and octupole moments, respectively, negative values for the second-order field derivative imply that at $h > 5\mu m$, the effective octupole moment should attain negative values, acting to reduce the energy stored in the particles in the form of effective dipole and quadrupole moments. Values of the third-order field derivative have no implications regarding the first three effective moments, but influence the third-order DEP force term in accordance with equation (4.5).

4.2.2. The point-plane electrode geometry

The electric field magnitude at a point of height h above the plane electrode on the symmetry axis of the point-plane electrode geometry has been derived analytically using the Schwarz-Christoffel mapping method [6]:

$$E(h) = \frac{aC}{(d-h)(2a-d+h)+(a-d+h)r_p} \tag{4.7}$$

where r_p is the radius of the point electrode, d is the separation between the two electrodes, i.e. the length of the axis of symmetry, $a = d + r_p$ and C is given by:

$$C = \frac{V}{\ln[2\left(\frac{a}{r_p}\right)^{\frac{1}{2}}]} \tag{4.8}$$

where V is the voltage across the electrodes, 2V in this work. It can be seen that unlike the case of the disc-plane geometry, the radius of the point electrode affects the electric field magnitude along the symmetry axis of the point-plane geometry.

Results obtained for the electric field magnitude and its first three derivatives along the symmetry axis of the point-plane geometry with r_p=0.5μm are shown in figure 4.5. The electric field derivatives have been calculated by analytical differentiation of equation (4.7) in MATLAB. Notable contrasts between the plots in figure 4.5 for the point-plane geometry with those of figure 4.4 for the disc-plane geometry can be easily identified. Firstly, the radius of the point electrode is seen to affect values of the electric field magnitude and its first three derivatives along the symmetry axis of the point-plane geometry. At all but the closest of positions to the point electrode, larger point electrodes are seen to give rise to stronger electric field magnitudes and curvatures. It is only at positions very close to the point electrode that an opposite effect is observed; near smaller point electrodes, which more closely resemble an electric field singularity, electric field magnitudes and curvatures attain increased strength. Trends with which the electric field magnitude and its derivatives vary with position along the axis of symmetry are seen *not* to vary with changing point electrode radius.

Another important difference with the case of the disc-plane geometry is in variation patterns with h of the electric field magnitude and its derivatives. In both axisymmetric electrode geometries, the electric field magnitude increases away from the plane electrode. However, the rate of increase is notably sharper in the case of the point-plane geometry. The electric field magnitude was shown to remain within the same order of magnitude along the symmetry axis of the disc-plane geometry, while the field at the point electrode is seen to be

stronger than that at the plane electrode of the point-plane geometry by two orders of magnitude. Electric field derivatives at point and plane electrodes are also seen to differ by multiple orders of magnitude while field derivatives along the symmetry axis of the disc-plane geometry were seen to attain values within the same order of magnitude and symmetrical around the midpoint. The resemblance of an electric field singularity by the point electrode gives rise to a high concentration of electric field magnitude and curvature strength around the point electrode and, consequently, very sharp decreases in electric field magnitude and curvature towards the plane electrode.

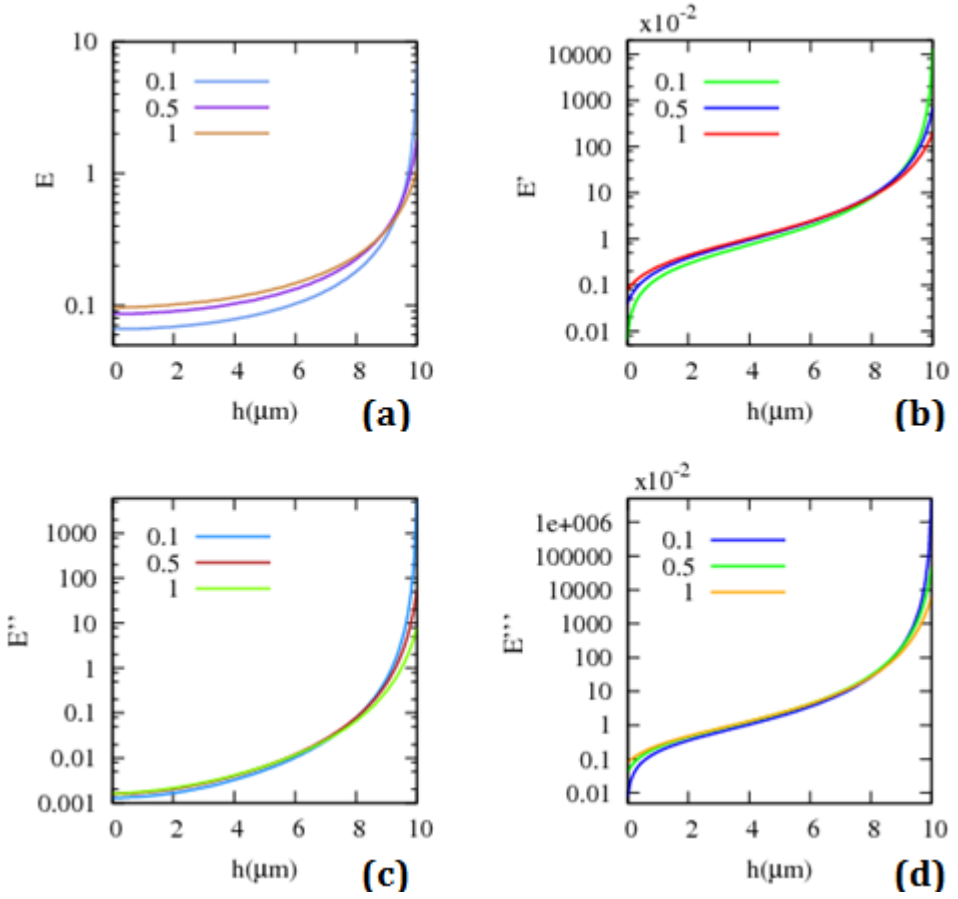

Figure 4.5. Electric field magnitude and derivatives along symmetry axis of point-plane geometry – Variations with height *h* above the plane electrode of (a) the electric field magnitude, and its (b) first-, (c) second-, and (d) third-order derivatives along the symmetry axis of the point-plane electrode geometry (of specifications given in figure 4.1) with point electrode radius r_p=0.5μm. The electric field magnitude has been calculated analytically using equation 4.7 (derivation presented in Appendix C) and the field gradients have been obtained by analytic differentiation of equation 4.7 in MATLAB.

Another difference between the two axisymmetric electrode geometries lies in the signs of the electric field derivatives. Values of the second-order field derivative along the symmetry axis of the disc-plane geometry were seen to be negative for $h > 5\mu m$, and the third-order

field derivative was seen to be negative-valued for all h. In the point-plane geometry, all of the first three electric field derivatives are seen to be positive-valued at all positions along the axis of symmetry. Positive-valued field derivatives act to add to the energy stored in particles in the form of the effective dipole moment, through positive-valued higher-order moments.

The significant difference between the field magnitude and gradient profiles of the two different electrode geometries can be regarded as an important design consideration when it comes to choice of electrode geometry for dielectrophoretic applications. It is important to note that the field magnitude and gradient profiles for a disc-plane electrode geometry of disc electrode radius $r_d = 0.5\mu m$ is vastly different from those of a point-plane electrode geometry of $r_p = 0.5\mu m$. The trends with which the field magnitude and gradients vary with position along the symmetry axes of the two electrode structures as well as the signs and magnitudes of the field gradients are notably different, with direct implications regarding the effective moments and dielectrophoretic forces – as will be seen in future sections.

4.3. The linear effective moments

This section presents and discusses calculations of the first three effective moments of spherical, ellipsoidal and cylindrical particles at different positions along the symmetry axes of point-plane and disc-plane electrode configurations. The effective moments, linear in axial symmetry, are calculated using the hybrid numerical-analytical method presented in Section 4.1. The effective moments are representative of the energy stored by the electric field in dielectric particles and are used extensively as bases for dielectric characterisation studies [7]. In most analyses, higher-order moments are ignored due to their deemed negligence. This section is aimed at quantifying the significance of higher-order moments in different circumstances regarding particle and electric field geometry to provide assessment of the commonly-invoked dipole approximation. In the results to be presented, units for the dipole, quadrupole and octupole moments are C.m, C.m^2 and C.m^3, respectively.

4.3.1. Results

4.3.1.1. The disc-plane electrode geometry

Results obtained for the first three effective moments of spherical (r=1μm), ellipsoidal (a=1μm, b=0.5μm) and cylindrical (a=1μm, r=0.5μm) particles positioned on the symmetry axis of the disc-plane electrode geometry are shown in figure 4.6.

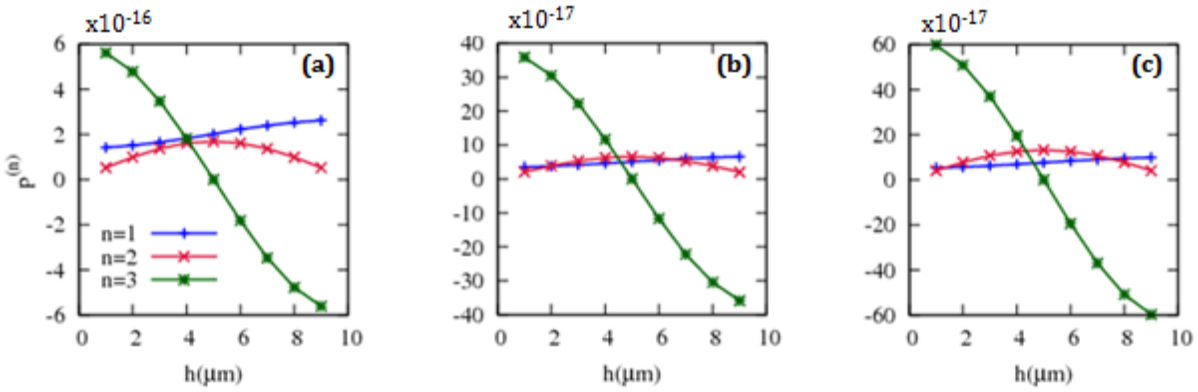

Figure 4.6. Linear effective moments in disc-plane electrode geometry – Variations with particle centre height *h* above the plane electrode of the effective dipole (n=1), quadrupole (n=2) and octupole (n=3) moments of (a) spherical (r=1μm), (b) ellipsoidal (a=1μm, b=0.5μm), and (c) cylindrical (a=1μm, r=0.5μm) particles positioned on the symmetry axis of the disc-plane electrode geometry (of specifications given in figure 4.1). Identical results are obtained with disc electrode radii r_d={0.5,1,2}μm.

As expected from electric field curvatures of n^{th} order determining the energy stored in particles in the form of $(n+1)^{th}$-order effective moments, the trends with which the effective moments vary with position along the axis of symmetry are seen to be identical to

those of field curvatures of preceding order and independent of particle shape. As with the electric field magnitude, the effective dipole moment is seen to increase with height above the plane electrode. As with the first derivative of the electric field along the axis of symmetry, the effective quadrupole moment attains values symmetrical around a maximum at midpoint $h = 5\mu m$. As with the second-order field derivative, values of the effective octupole moment are seen to bear odd symmetry around a null at the midpoint, becoming negative for $h > 5\mu m$.

As expected from field curvature results, changing disc electrode radius within the range {0.5, 1, 2}μm does not affect values of the linear moments. The effect of particle geometry on the effective moments and, importantly, the significance of higher-order moments will be discussed in Section 4.3.2.

4.3.1.2. The point-plane electrode geometry

Figure 4.7 shows variations with particle centre height above the plane electrode of the first three effective moments of spherical (r=1μm), ellipsoidal (a=1μm, b=0.5μm) and cylindrical (a=1μm, r=0.5μm) particles positioned on the symmetry axis of the point-plane electrode geometry with point electrode radius r_p=0.5μm.

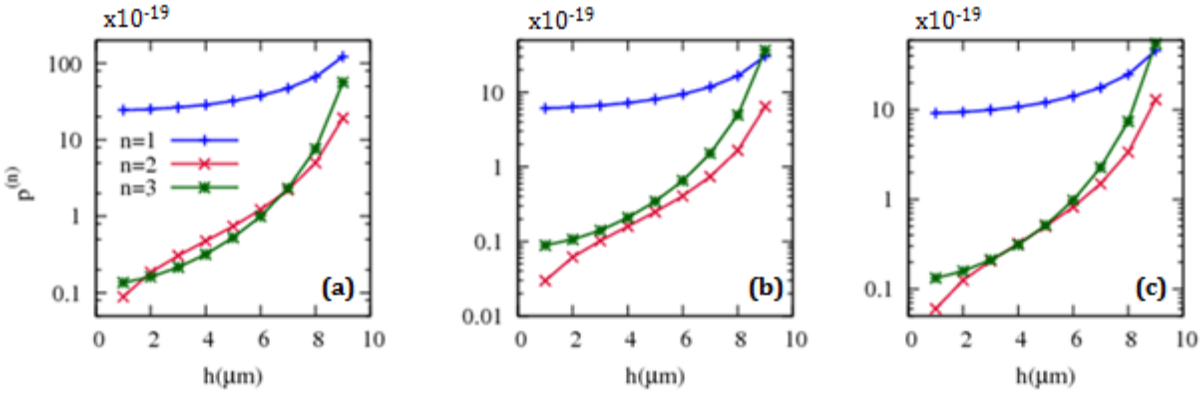

Figure 4.7. Linear effective moments in point-plane electrode geometry – Variations with particle centre height *h* above the plane electrode of the effective dipole (n=1), quadrupole (n=2) and octupole (n=3) moments of (a) spherical (r=1μm), (b) ellipsoidal (a=1μm, b=0.5μm), and (c) cylindrical (a=1μm, r=0.5μm) particles positioned on the symmetry axis of the point-plane electrode geometry (of specifications given in figure 4.1) with r_p=0.5μm.

As with the disc-plane geometry, variations patterns with *h* of the effective moments are identical to those of field curvatures of preceding order. All of the first three effective moments are seen to sharply increase with particle height above the plane electrode. For all

three particle shapes, higher-order moments are seen to be negligible, compared to the dipole moment, at all but the nearest of positions to the point electrode.

4.3.2. Discussion

4.3.2.1. Effect of electrode geometry

It may be understood from a comparison of the plots in figures 4.6 and 4.7 that electrode shape can significantly impact the effective moments of particles subjected to axisymmetric electric fields. Variation patterns with position along the axis of symmetry as well as the values of the effective moments of spherical and non-spherical particles were seen to differ notably among the two electrode geometries. In consistency with electric field curvature results presented in the previous section, the effective moments of particles positioned on the symmetry axis of the disc-plane geometry were seen to attain values within the same order of magnitude, whereas in the point-plane geometry, values sharply decreased towards the plane electrode, spanning multiple orders of magnitude. In the point-plane geometry, higher-order moments were seen to be comparable to the effective dipole moment only at positions closest to the point electrode. With the disc-plane geometry, higher-order moments were seen to be of much added significance: For all three particle shapes, the effective octupole moment was seen to attain values larger than lower-order moments, regardless of position along the axis of symmetry. For non-spherical particles near the midpoint $h = 5\mu m$, values attained by the effective quadrupole moment were seen to exceed those of the dipole moment.

While varying disc electrode radius within the range {0.5,1,2}μm was seen to have no impact on the effective moments, increasing point electrode radius gives rise to larger effective dipole, quadrupole and octupole moments for spherical, ellipsoidal and cylindrical particles – as shown in figure 4.8. The effect observed in the previous section of increased field magnitude and curvature strength near smaller point electrodes is not reflected in effective moment results due to the naturally-imposed constraint on particle centre proximity with the point electrode: at $h = 9\mu m$, the particle edge would reach the point electrode and higher positions could not be examined.

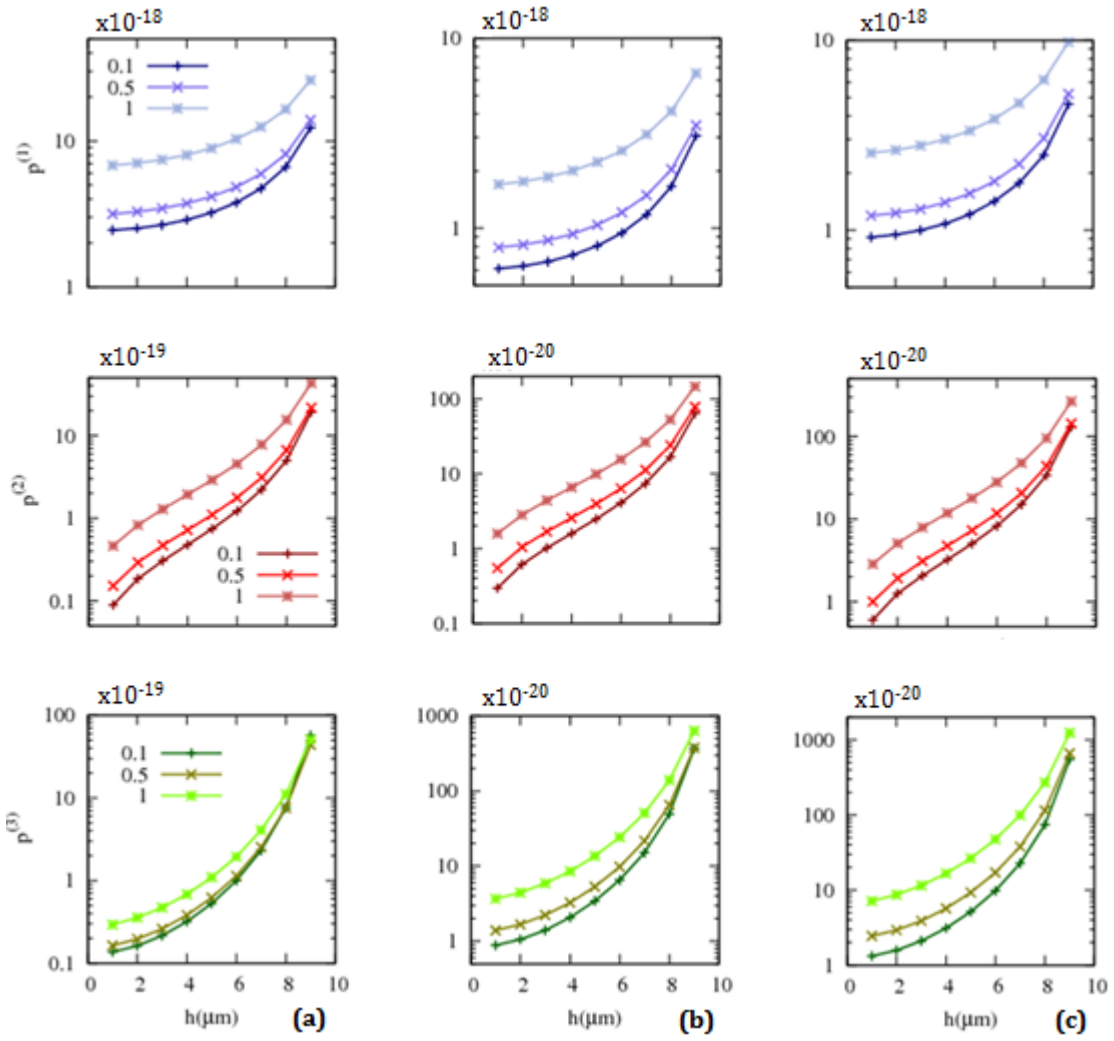

Figure 4.8. Effect of point electrode radius on linear effective moments in point-plane geometry – Variations with particle centre height *h* above the plane electrode of the first three effective moments of (a) spherical (r=1µm), (b) ellipsoidal (a=1µm, b=0.5µm), and (c) cylindrical (a=1µm, r=0.5µm) particles positioned on the symmetry axis of the point-plane electrode geometry (of specifications given in figure 4.1) with r_p={0.1,0.5,1}µm.

4.3.2.2. Effect of particle shape

It was shown in the previous section that particle geometry does not impact the trends with which the effective moments vary with particle position. However, values of the effective moments were seen to differ among different particle geometries. Figure 4.9 compares the first three effective moments of spherical, ellipsoidal and cylindrical particles positioned on the symmetry axes of point-plane and disc-plane electrode configurations. To broaden the investigation, two different aspect ratios, λ, have been considered for the non-spherical shapes.

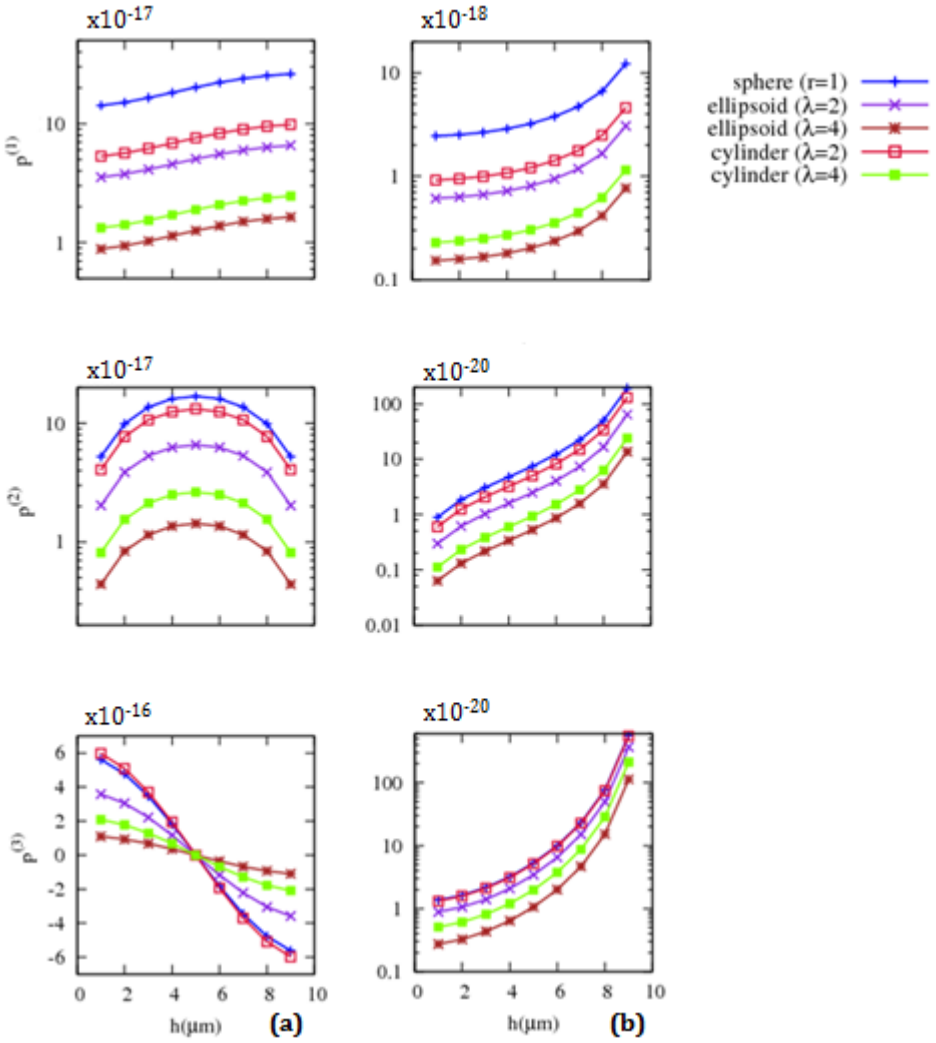

Figure 4.9. Effect of particle shape on linear effective moments – Variations with particle centre height *h* above the plane electrode of the first three effective moments of spherical (r=1μm), ellipsoidal (a=1μm,b={0.5,0.25}μm) and cylindrical (a=1μm,r={0.5,0.25}μm) particles positioned on the symmetry axes of (a) disc-plane and (b) point-plane electrode geometries (of specifications given in figure 4.1) when the point electrode radius is 0.5μm. Identical results are obtained with disc electrode radii in the range {0.5,1,2}μm. *λ* denotes the aspect ratio of non-spherical particles, defined as *a/b* for ellipsoidal and *a/r* for cylindrical particles.

It can be seen that with thinner ellipsoidal and cylindrical particles included, the effective moments are larger for particles of larger volume. The only exception posed to the pattern is the cylindrical (λ=2) particle possessing larger effective octupole moments (at all positions along the symmetry axis of either of the two electrode geometries) than the (larger in volume) spherical particle. It is inferred from the data in figure 4.9 that the effective dipole moment, and not higher-order moments, is directly proportional to particle volume. As a result, if dielectric particles subjected to axisymmetric fields were to be characterised based on their effective dipole moment only, approximation with a sphere of equal volume will incur no error. Whether or not the dipole moment would suffice for representation of the

energy stored by an applied electric field in dielectric particles would depend on the significance of higher-order moments.

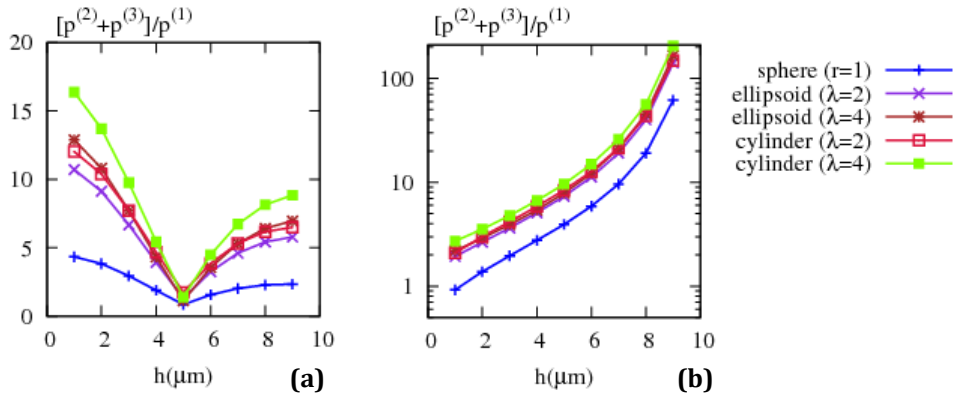

Figure 4.10. Significance of higher-order effective moments in axial symmetry – Variations with particle centre height *h* above the plane electrode of the ratio over the effective dipole moment of the sum of effective quadrupole and octupole moments of spherical (r=1μm), ellipsoidal (a=1μm,b={0.5,0.25}μm) and cylindrical (a=1μm,r={0.5,0.25}μm) particles positioned on the symmetry axes of (a) disc-plane and (b) point-plane electrode geometries (of specifications given in figure 4.1). λ denotes the aspect ratio of non-spherical particles, defined as a/b for ellipsoidal and a/r for cylindrical particles. The radius of the point electrode is taken to be 0.5μm. Similar results are obtained with point electrode radii 0.1μm and 1μm, and identical results are obtained for disc electrode radii in the range {0.5,1,2}μm.

The significance of higher-order moments can be defined as the ratio of the sum of effective quadrupole and octupole moments over the effective dipole moment, $\left[p^{(2)} + p^{(3)}\right]/p^{(1)}$. With this definition, the significance of higher-order moments of spherical, ellipsoidal and cylindrical particles at different positions along the symmetry axes of point-plane and disc-plane electrode geometries is plotted in figure 4.10. It can be seen that higher-order moments are considerably more significant in the point-plane geometry: Effective quadrupole and octupole moments of spherical and non-spherical particles are seen to sum up to values larger than that of the effective dipole moment by up to two orders of magnitude. In the disc-plane geometry, the ratio of higher-order moments over the effective dipole moment is seen to attain values between 0.5 (for all particle shapes at midpoint $h = 5\mu m$) and 16.5 (for the thinner cylindrical particle at $h = 1\mu m$). In general, higher-order moments are found to be of increased significance for non-spherical particles. It may be concluded from the data presented in figure 4.10 that using the dipole approximation for characterisation of particles subjected to axisymmetric fields will be subject to significant error, regardless of particle shape and position along the axis of symmetry. The error incurred will be 50% minimum, and – depending on electrode geometry, particle shape and position – may go well beyond 100%.

Table 4.1. Errors incurred in values of first three effective moments of non-spherical particles upon approximation with simpler shapes of similar dimensions – List of ratios of the first three effective moments of model particles (spheres or ellipsoids) over those of original particles (ellipsoids or cylinders) positioned on the symmetry axes of disc-plane (dsc-pln) and point-plane (pnt-pln) electrode geometries (of specifications given in figure 4.1). Different ratios are obtained at different positions along the symmetry axes of either of the two electrode geometries. Values in the table represent averages of ratios at different particle heights above the plane electrode in the two axisymmetric electrode configurations. The radius of the point electrode is taken to be 0.5μm. Similar results are obtained with point electrode radii 0.1μm and 1μm, and identical results are obtained for disc electrode radii in the range {0.5,1,2}μm.

Original particle	**Model particle**	**$p^{(1)}$ ratio**		**$p^{(2)}$ ratio**		**$p^{(3)}$ ratio**	
		dsc-pln	**pnt-pln**	**dsc-pln**	**pnt-pln**	**dsc-pln**	**pnt-pln**
Ellipsoid (a=1μm,b=0.5μm)	Sphere (r=1μm)	4.0	4.0	2.6	3.0	1.6	1.5
Ellipsoid (a=1μm,b=0.25μm)	Sphere (r=1μm)	16.7	16.7	12.5	14.3	5.0	5.0
Cylinder (a=1μm,r=0.5μm)	Sphere (r=1μm)	2.7	2.7	1.3	1.5	0.94	1.03
Cylinder (a=1μm,b=0.25μm)	Sphere (r=1μm)	11.1	11.1	6.3	8.3	2.7	2.7
Cylinder (a=1μm,r=0.5μm)	Ellipsoid (a=1μm,b=0.5μm)	0.7	0.7	0.5	0.5	0.6	0.7
Cylinder (a=1μm,b=0.25μm)	Ellipsoid (a=1μm,b=0.25μm)	0.7	0.7	0.5	0.6	0.5	0.5

Often in the literature on dielectric characterisation, non-spherical particles (comprising the vast majority of biological particles) are approximated as spheres, for which the effective moments have been derived analytically. On a number of other occasions, highly non-spherical particles such as erythrocytes have been approximated as ellipsoids, for which the effective dipole moment has been calculated analytically. As the effective dipole moment shows direct proportionality with particle volume, approximating particles of arbitrary shape with spheres of equal volume would incur no error in values of the effective dipole moment. No direct proportionality between higher-order moments and particle volume is observed. As a result, modelling non-spherical particles with simpler-to-model shapes, albeit of equal volume, will be subject to inevitable error in values of higher-order moments, shown to be comparable, and in most circumstances larger than, the effective dipole moment in axial symmetry (figure 4.10).

For quantitative assessment of the errors incurred in the values of linear effective moments upon approximating non-spherical particles with simpler shapes, a summary is presented in

Table 4.1. The table shows ratios of the effective dipole, quadrupole and octupole moments of model particles (spheres/ellipsoids) over those of original particles (ellipsoids/cylinders) in point-plane and disc-plane electrode configurations. The ratios differ depending on particle position along the axes of symmetry; values in the table represent the average of ratios at different particle positions along the symmetry axes of either of the two electrode geometries. It can be seen that in all cases, there is significant difference between the effective moments of original and model particles.

Table 4.2. Errors incurred in values of higher order effective moments of non-spherical particles upon approximation with simpler shapes of equal volume – List of ratios of the second- and third-order effective moments of model particles (spheres or ellipsoids) over those of original particles (ellipsoids or cylinders) positioned on the symmetry axes of disc-plane (dsc-pln) and point-plane (pnt-pln) electrode geometries (of specifications given in figure 4.1), when dimensions of the model particle are adjusted for volumes to equate. Different ratios are obtained at different positions along the symmetry axes of either of the two electrode geometries. Values in the table represent averages of ratios at different particle heights above the plane electrode in the two axisymmetric electrode configurations. The radius of the point electrode is taken to be 0.5µm. Similar results are obtained with point electrode radii 0.1µm and 1µm, and identical results are obtained for disc electrode radii in the range {0.5,1,2}µm.

Original particle	**Model particle**	**$p^{(2)}$ ratio**		**$p^{(3)}$ ratio**	
		dsc-pln	**pnt-pln**	**dsc-pln**	**pnt-pln**
Ellipsoid (a=1µm,b=0.5µm)	Sphere (equal volume)	1.4	1.9	1.4	1.4
Ellipsoid (a=1µm,b=0.25µm)	Sphere (equal volume)	10.5	12.8	3.2	3.3
Cylinder (a=1µm,r=0.5µm)	Sphere (equal volume)	1.9	2.2	1.2	1.7
Cylinder (a=1µm,b=0.25µm)	Sphere (equal volume)	8.5	9.0	3.4	3.4
Cylinder (a=1µm,r=0.5µm)	Ellipsoid (equal volume)	0.9	0.9	0.9	0.9
Cylinder (a=1µm,b=0.25µm)	Ellipsoid (equal volume)	0.9	0.8	0.9	0.8

For the effective dipole moment, ratios of the effective moments of model and original particles are representative of the volume ratio of the two particles. If the dimensions of the model particle are adjusted for volumes to equate, the error is reduced to zero. With higher-order moments, the ratios appear to include factors other than particle volume and as a result, error is not reduced to negligible values when volumes of model and original particles are equal. In fact, as shown in Table 4.2, effective moment ratios of model and original

particles are at times increased, implying larger approximation errors, when volumes are equated by adjusting model particle dimensions. It may be concluded that, given the increased significance of higher-order moments for non-spherical particles (figure 4.10), approximation with simpler shapes – albeit of equal volume – will incur considerable error in characterisation of particle dielectric properties based on values of the effective moments.

4.3.2.3. Effect of particle size

Particle size, and how it compares to a characteristic length scale of electric field non-uniformity, is often cited as an important factor in the reliability of the dipole approximation. This section analyses the effect of particle size on linear effective moments and, importantly, the significance of higher-order moments by comparing the effective dipole, quadrupole and octupole moments of spherical particles of two different radii, 1μm and 2μm, positioned along the symmetry axes of point-plane and disc-plane electrode geometries. As shown in figure 4.11, all of the first three effective moments increase by about an order of magnitude as the radius of the spherical particle is doubled. As expected from earlier results, the effective dipole moment (and not higher-order moments) increases by a factor equal to the volume ratio. Trends with which the effective moments vary with position along the axes of symmetry are seen to be retained upon doubling particle dimensions.

As shown in figure 4.12, the significance of higher-order moments also increases notably upon doubling particle dimensions. Effective quadrupole and octupole moments of the larger spherical particle are seen to add up to values up to 12 and 50 times larger than that of the effective dipole moment in disc-plane and point-plane geometries, respectively. Maximum higher-order to effective dipole moment ratios for the smaller sphere are 4 and 20 in disc-plane and point-plane geometries, respectively. The increased significance of higher-order moments for the larger sphere can be attributed to larger electric field magnitude and curvature variations across particles of longer dimensions along the axis of electric field symmetry.

It is important to note that particle positions at which the increase in significance of higher-order moments is more pronounced are not necessarily those at which the particle experiences the largest variation in electric field magnitude across its dimensions. It is the combined effect of electric field magnitude *and* curvature variations, as well as particle geometry (including size and shape), that determines the reliability of the dipole approximation. In the point-plane geometry, electric field magnitude and curvature profiles are similar; thereby the higher-order moments are most significant near the point electrode.

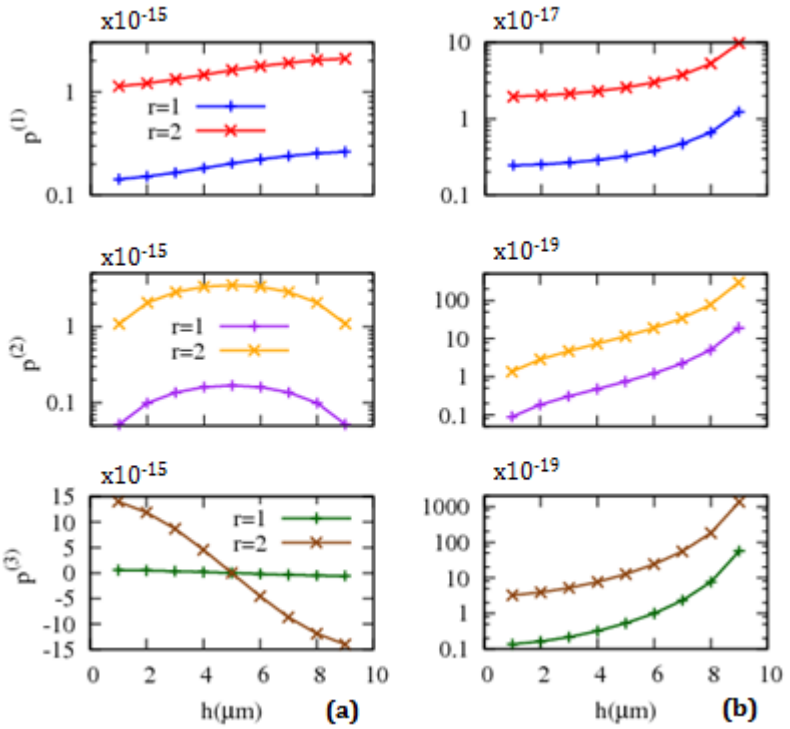

Figure 4.11. Effect of particle size on linear effective moments – Variations with particle centre height *h* above the plane electrode of the first three effective moments of spherical particles of radii 1μm (r=1) and 2μm (r=2) positioned on the symmetry axes of (a) disc-plane and (b) point-plane electrode configurations (of specifications given in figure 4.1). The point electrode radius is r_p=0.5μm and identical results are obtained with disc electrode radii in the range r_d={0.5,1,2}μm. Legend in part (a) applies to both figure parts.

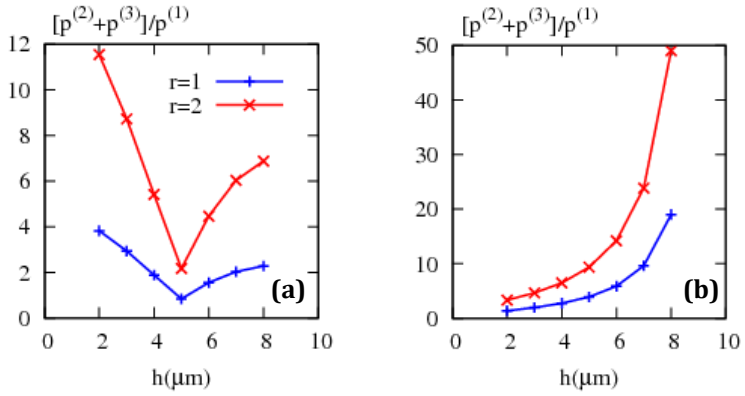

Figure 4.12. Effect of particle size on significance of higher-order moments in axial symmetry – Variations with particle centre height *h* above the plane electrode of the ratio over the effective dipole moment of the sum of effective quadrupole and octupole moments of spherical particles of two different radii (r={1,2}μm) positioned on the symmetry axes of (a) disc-plane, and (b) point-plane electrode geometries (of specifications given in figure 4.1). The radius of the point electrode is taken to be 0.5μm. Similar results are obtained with point electrode radii 0.1μm and 1μm, and identical results are obtained for disc electrode radii in the range {0.5,1,2}μm. Legend in part (a) applies to both figure parts.

In the disc-plane geometry, there is notable difference between field magnitude and curvature profiles. The resultant effect is higher-order moments that are most significant near either of the two electrodes where, incidentally, field magnitude variations across particle dimensions are *not* maximal.

4.3.3. Summary and conclusions

Results have been presented of applying a numerical-analytical method presented in Section 4.1 for determination of the effective dipole, quadrupole and octupole moments of spherical, ellipsoidal and cylindrical particles of different dimensions subjected to axisymmetric electric fields generated by point-plane and disc-plane electrode geometries. It has been shown that the trends with which first- and higher-order moments vary with particle position along the axis of electric field symmetry are determined solely by electric field gradients of preceding order. The effect of particle geometry – shape and size – is reflected in the values of the effective moments. The effective dipole moment has been shown to be directly proportional to particle volume. As a result, non-spherical particles can be approximated as spheres of equal volume if particle characterisation is to be made based on the dipole approximation.

Whether or not the effective dipole moment suffices for representation of the energy stored by the electric field in dielectric particles has been determined by analysing the significance of higher-order moments. It has been shown that effective quadrupole and octupole moments add up to values comparable to, and in most cases larger than that of the effective dipole moment. As a result, particle characterisation based on the effective dipole moment alone will be subject to significant error even where the electric field is almost uniform. Higher-order moments have been shown to be of added significance for non-spherical particles. In agreement with qualitative predictions, it has been shown that particles of longer dimensions along the axis of electric field symmetry possess more significant higher-order moments. However, it has been observed that 'by inspection' judgements on the reliability of the dipole approximation, based on electric field magnitude variations across particle dimensions or extent of electric field non-uniformity can be erroneous. As an example, higher-order moments of spherical and non-spherical particles positioned on the symmetry axis of the disc-plane electrode geometry have been shown to be *least* significant when the electric field is most highly non-uniform, with non-uniformity defined conventionally as the magnitude of the first-order electric field derivative. The reliability of the dipole approximation, or the significance of higher-order moments, has been shown to be determined from the combined effect of electric field magnitude and curvature variations as well as particle geometry (including shape and size).

4.4. Dielectrophoretic force terms in axial symmetry

This section presents calculations of the first three terms of the dielectrophoretic force on spherical, ellipsoidal and cylindrical particles of different dimensions subjected to axisymmetric electric fields generated by point-plane and disc-plane electrode geometries. The DEP force terms are calculated based on the effective moment method, by combining the field gradient and effective moment results of the previous two sections. Effects of variations in particle and field parameters on the DEP force terms will be discussed. The significance of higher-order forces shall be analysed in Chapter 5 where force term calculations using the effective moment method will be compared against total force calculations using the Maxwell stress tensor method to derive higher-order contributions to the DEP force on spherical and non-spherical particles. In the results to be presented, units for dielectrophoretic force terms will be pico-Newtons (pN).

4.4.1. Results and discussion

Results obtained for the first three terms of the DEP force on spherical, ellipsoidal and cylindrical particles positioned on the symmetry axis of the disc-plane electrode geometry are shown in figure 4.13, where two different aspect ratios are considered for the non-spherical shapes. The DEP force terms are calculated by weighted multiplication of effective moments and field gradients of corresponding order. Symmetrical variation patterns for electric field derivatives along the symmetry axis of the disc-plane geometry (figure 4.4) have resulted in higher-order force terms bearing odd symmetry around a null at the midpoint $h = 5\mu m$. Values of the dipolar DEP force are seen to be almost symmetrical around a maximum near the midpoint.

As expected from field gradient and effective moment results, the DEP force terms are not affected by variations in the disc electrode radius within the examined range of {0.5,1,2}μm. As with the effective moments, the DEP force terms are seen to be stronger on particles of larger volume – with the only exception posed by the cylindrical (a=1μm, r=0.5μm) particle being subject to stronger octupolar forces than the (larger in volume) spherical particle. The dipolar force (and not higher-order forces) is seen to be directly proportional to particle volume. Consequently, if higher-order DEP forces are to be ignored in accordance with the dipole approximation, the dielectrophoretic force on a particle of arbitrary shape can be calculated from that on a sphere of equal volume. The significance of higher-order DEP force terms in different circumstances regarding particle and field geometry will be discussed in Chapter 5.

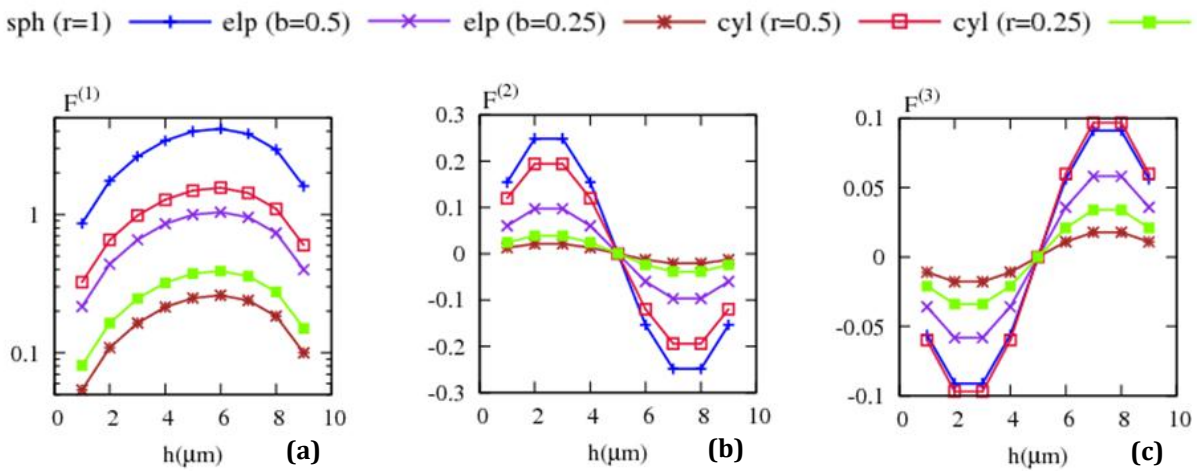

Figure 4.13. Dielectrophoretic force terms in disc-plane geometry – Variations with particle centre height *h* above the plane electrode of the (a) first-, (b) second-, and (c) third-order terms of the dielectrophoretic force on spherical (r=1μm), ellipsoidal (a=1μm,b={0.5,0.25}μm) and cylindrical (a=1μm,r={0.5,0.25}μm) particles positioned on the symmetry axis of the disc-plane electrode geometry (of specifications given in figure 4.1). Identical results are obtained with disc electrode radii in the range {0.5,1,2}μm. The unit for DEP force terms is pico-Newtons (pN).

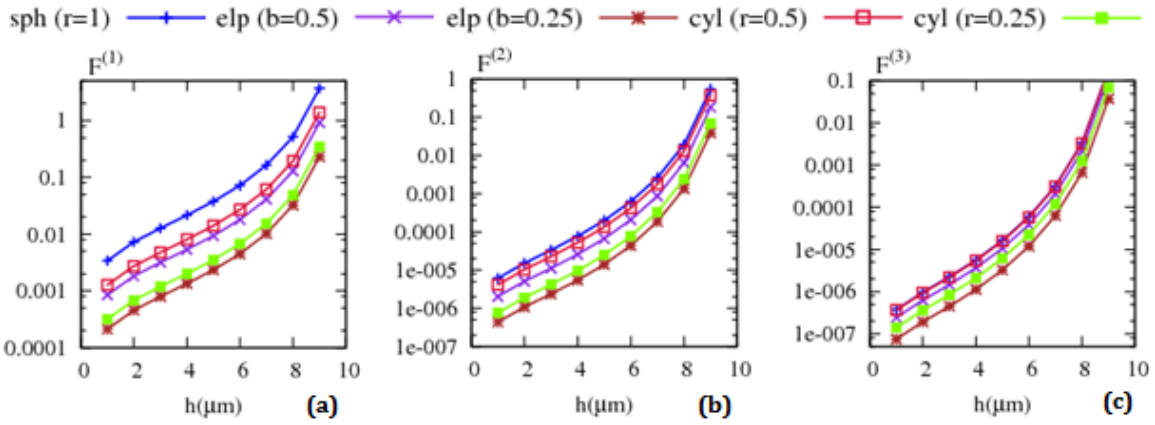

Figure 4.14. Dielectrophoretic force terms in point-plane geometry – Variations with particle centre height *h* above the plane electrode of the (a) first-, (b) second-, and (c) third-order terms of the dielectrophoretic force on spherical (r=1μm), ellipsoidal (a=1μm,b={0.5,0.25}μm) and cylindrical (a=1μm,r={0.5,0.25}μm) particles positioned on the symmetry axis of the point-plane electrode geometry (of specifications given in figure 4.1) of point electrode radius r_p=0.5μm. The unit for DEP force terms in pico-Newtons (pN).

Figure 4.14 shows the results obtained for the first three terms of the DEP force on spherical, ellipsoidal and cylindrical particles positioned on the symmetry axis of the point-plane electrode geometry with a 0.5μm-radius point electrode. It can be seen that as with electric field curvature and effective moment profiles, the trend for first- and higher-order forces on particles positioned on the symmetry axis of the point-plane geometry is that of sharply increasing strength towards the point electrode. As with the effective moments, DEP force

terms are seen to be stronger on particles of larger volume with the dipolar force (only) showing direct proportionality with particle volume.

The effect of point electrode radius on terms of the DEP force along the symmetry axis of the point-plane geometry is shown in figure 4.14 through plots of dipolar, quadrupolar and octupolar DEP forces on a spherical (r=1μm) particle positioned on the symmetry axes of point-plane electrode geometries with three different point electrode radii; {0.1,0.5,1}μm. It can be seen that all of the first three DEP force terms are stronger with larger point electrodes. The increase in strength is seen to be more pronounced on particles positioned further away from the point electrode.

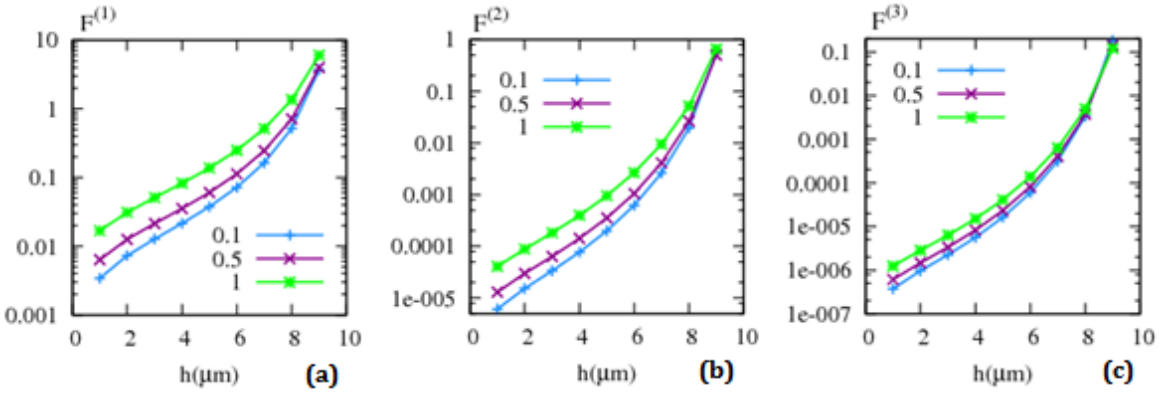

Figure 4.15. Effect of point electrode radius on dielectrophoretic force terms in point-plane geometry – Variations with particle centre height *h* above the plane electrode of the (a) first-, (b) second-, and (c) third-order terms of the dielectrophoretic force on a spherical (r=1μm) particle positioned on the symmetry axis of the point-plane electrode geometry (of specifications given in figure 4.1) with point electrode radii r_p={0.1,0.5,1}μm. The unit for DEP force terms in pico-Newtons (pN).

The effect of particle size on terms of the dielectrophoretic force in axial symmetry is shown in figure 4.16 through comparison of the first three terms of the DEP force on spherical particles of two different radii (1μm and 2μm) positioned on the symmetry axes of disc-plane and point-plane electrode geometries. It can be seen that, as expected from effective moment results (figure 4.11), doubling particle radius gives rise to a strengthening of all of the first three DEP force terms by about an order of magnitude. In both electrode geometries, particle size is seen not to affect the trends with which DEP force terms vary with particle position along the axis of electric field symmetry.

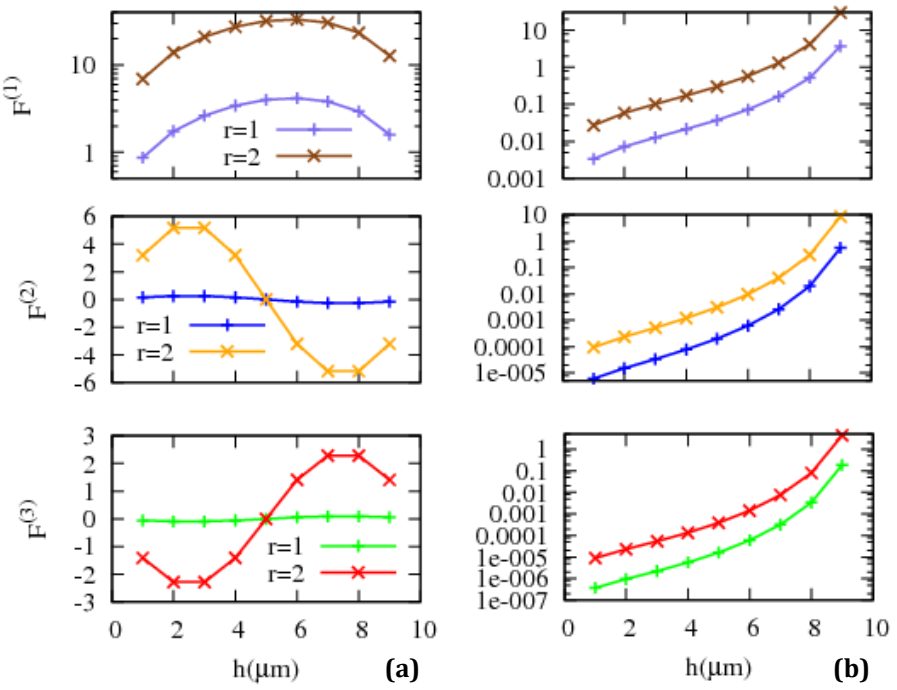

Figure 4.16. Effect of particle size on dielectrophoretic force terms in axial symmetry – Variations with particle centre height *h* above the plane electrode of the first three terms of the DEP force on spherical particles of radii 1μm (r=1) and 2μm (r=2) positioned on the symmetry axes of (a) disc-plane and (b) point-plane electrode geometries (of specifications given in figure 4.1). Identical results are obtained with disc electrode radii in the range {0.5,1,2}μm, and the radius of the point electrode is taken to be 0.5μm. Legend in part (a) applies to both figure parts. The unit for DEP force terms in pico-Newtons (pN).

4.4.2. Summary and conclusions

Results have been presented for the first three terms of the dielectrophoretic force on spherical, ellipsoidal and cylindrical particles subjected to axisymmetric electric fields generated by point-plane and disc-plane electrode geometries. The DEP force terms have been calculated using the effective moment method which involves weighted multiplication of effective moments and field derivatives of corresponding order. As such, trends with which the DEP force terms of a given order vary with particle position along the axis of electric field symmetry have been found not to depend on particle geometry and to be determined solely by those of electric field derivatives of the same and preceding order. Electrode geometry has been shown to have a significant effect on the DEP force terms as results obtained with point-plane and disc-plane geometries using the same dielectric particles have been found to be vastly different. It has been shown that the dipolar DEP force (and not multipolar terms) is directly proportional to particle volume. Therefore if the dipole approximation is to be invoked for calculation of the DEP force on particles of arbitrary shape, error-free approximation can be made with spheres of equal volume. The reliability of the dipole

approximation in predicting the dielectrophoretic force on spherical and non-spherical particles subjected to electric fields of varying magnitude and curvature strengths will be discussed in the next chapter.

Conclusions

- Trends with which the linear effective moments of dielectric particles subjected to axisymmetric electric fields vary with position along the axis of electric field symmetry are identical to those of electric field gradients of preceding order and independent of particle geometry.
- Particle geometry has notable effect on the values of the linear effective moments. First- and higher-order effective moments are generally larger for particles of larger volume. However, only the effective dipole moment is directly proportional to particle volume. As a result, approximating non-spherical particles with simpler shapes of equal volume will incur zero error only if higher-order moments are ignored in accordance with the dipole approximation.
- Effective quadrupole and octupole moments of spherical and non-spherical particles add up to values comparable to, and in many circumstances larger than, that of the effective dipole moment. For non-spherical particles, higher-order moments are of added significance, making the dipole approximation highly unreliable for dielectric characterisation purposes.
- Increasing particle size gives rise to more significant higher-order moments. However, electric field magnitude variation across particle dimensions does not set a general criterion for the reliability of the dipole approximation.
- As with effective moments, particle geometry impacts the values of dielectrophoretic force terms, but not the trends with which they vary with particle position along the axis of electric field symmetry. The trend with particle position of the DEP force term of a given order is determined by those of field greadients of the same and preceding order.

References

[1] Becker, R.: Electromagnetic fields and interaction. Blaisdell, London (1964).

[2] Jones, T. B.: Electromechanics of Particles. Cambridge University Press, Cambridge (1995).

[3] Green, N. G., Jones, T. B.: Numerical determination of the effective moments of non-spherical particles. J. Phys. D: Appl. Phys., 40, 78-85 (2007).

[4] Jones, T. B.: Basic theory of dielectrophoresis and electrorotation. IEEE Eng. Med. Biol. Mag., 22, 33-42 (2003).

[5] Sloggett, G. J., Barton, N. G., Spencer, S. J.: Fringing fields in disc capacitors. J. Phys. A: Math. Gen., 19, 2725-2736 (1986).

[6] Coelho, R., Debeau, J.: Properties of the tip-plane configuration. J. Phys. D: Appl. Phys. 4, 1266-1280 (1971).

[7] Asami, K.: Characterization of heterogeneous systems by dielectric spectroscopy. Prog. Polym. Sci. 27, 1617-1659 (2002).

Chapter Five

Maxwell Stress Tensor Calculation of the Total Dielectrophoretic Force in Axial Symmetry: Results and Discussion

Abstract

Calculations are presented of the total dielectrophoretic force on spherical, ellipsoidal and cylindrical particles subjected to axisymmetric electric fields generated by point-plane and disc-plane electrode configurations. Particle and electric field geometries are those for which the first three effective moments and DEP force terms were calculated in the previous chapter. In this chapter, the total DEP force is calculated using the mathematically rigorous Maxwell stress tensor method to (a) provide verification for the results presented previously for the DEP force terms, and (b) to determine contributions from higher-order terms to the dielectrophoretic force in different circumstances regarding particle and electric field geometry. By analysis of second- and third-order contributions to DEP forces in axial symmetry, the reliability of the dipole approximation is assessed. The assumption of axial symmetry serves as a good starting point as the problem domain becomes essentially two-dimensional, and calculations are greatly simplified as a result. The axisymmetric assumption will be dropped in the next chapter, where force term calculations based on general, rather than linear, effective moments will be compared against Maxwell stress tensor calculations of the total force in 3D to examine the significance of higher-order force terms in a broader context.

Overview

Section 5.1 presents the formulation of the Maxwell stress tensor (MST) method, used for total DEP force calculations in this chapter. The section also recaps the specifications of the physical problem to which the method will be applied and demonstrates issues with regard to numerical implementation of the MST method. Section 5.2 presents and discusses calculations of the total dielectrophoretic force on spherical and non-spherical particles in axial symmetry. Analysis is offered on the effects of particle and electrode geometry on the DEP force experienced by the particles. Section 5.3 compares DEP force term results of the previous chapter to total force calculations using the MST method to derive second- and third-order contributions to DEP forces in axial symmetry. The reliability of the dipole approximation in different circumstances regarding particle and electric field geometry is thoroughly investigated.

5.1. Background and theory

5.1.1. The Maxwell stress tensor method in axial symmetry

The total dielectrophoretic force exerted by a non-uniform electric field on a dielectric particle suspended in a dielectric medium can be obtained by integration of the Maxwell stress tensor over a surface enclosing the particle [1]:

$$\boldsymbol{F}^{MST} = \frac{1}{2}\oint(2\boldsymbol{E}_m\boldsymbol{E}_m - E_m^2\boldsymbol{U})\cdot\boldsymbol{n}dA \tag{5.1}$$

where $\boldsymbol{E}_m$ is the electric field vector inside the suspending medium, with E_m its magnitude and $\boldsymbol{E}_m\boldsymbol{E}_m$ denoting the dyadic product of the field vector with itself, $\boldsymbol{U}$ is the unit tensor of rank 2, and $\boldsymbol{n}$ is the unit vector normal to integration surface A. A brief introduction to tensor notation, including the definition of the unit tensor and the dyadic product of two (or more) vectors is presented in Appendix A.

The term 'total' corresponds to the method used for calculation of the dielectrophoretic force. The mathematically rigorous Maxwell stress tensor (MST) method encompasses all interaction between electric fields and subject dielectric particles (and media) that result in exertion of electrical force. It also marks distinction with the results presented in the previous chapter of individual 'terms' of the DEP force. In axial symmetry, equation (5.1) can be expressed in a much simpler form [2]:

$$\boldsymbol{F}^{MST} = \frac{1}{2}(\epsilon_p - \epsilon_m)\oint[E_{tm}^2 + E_{nm}^2\left(\frac{\epsilon_m}{\epsilon_p}\right)]\cdot\boldsymbol{n}dA \tag{5.2}$$

In equation (5.2), E_{tm} and E_{nm} are the tangential and normal components, respectively, of the electric field vector inside the suspending medium and ϵ_p and ϵ_m are the dielectric constants of the particle and its suspending medium, respectively.

5.1.2. Physical problem specifications

In this chapter, equation (5.2) will be used to derive the total dielectrophoretic force on spherical, ellipsoidal and cylindrical particles subjected to the axisymmetric electric fields generated by point-plane and disc-plane electrode geometries. Particle dimensions and specifications of the two electrode geometries are those used in the previous chapter for analysis of linear effective moments and dielectrophoretic force terms. Considering different particle and electrode geometries allows for examination of the circumstances under which higher-order DEP forces are significant and cannot be neglected in accordance with the dipole approximation. As in Chapter Four, it is assumed that the particles and their

suspending media are lossless dielectrics with relative permittivities of 3 and 80 (pertaining to SU-8 and water), respectively.

5.1.3. Numerical implementation of the Maxwell stress tensor method

According to Gauss' Law, integration of the Maxwell stress tensor over any surface enclosing a particle must yield the dielectrophoretic force on the particle. The integration surfaces used for deriving the total DEP force in this chapter are taken to be those used in the previous chapter for derivation of the effective moments, i.e. spherical surfaces of radii equal to, 0.5μm larger than, and 0.9μm larger than the longest half-dimension of the particles. The integrations were performed in the standard solver initially used to obtain the results reported on in this work, namely FlexPDE. The software, although not as user-friendly as other well-established packages such as COMSOL and ANSYS, allows easy control over all mesh parameters – crucial to obtaining reproducibly accurate results, particularly near the singularity-resembling point electrode.

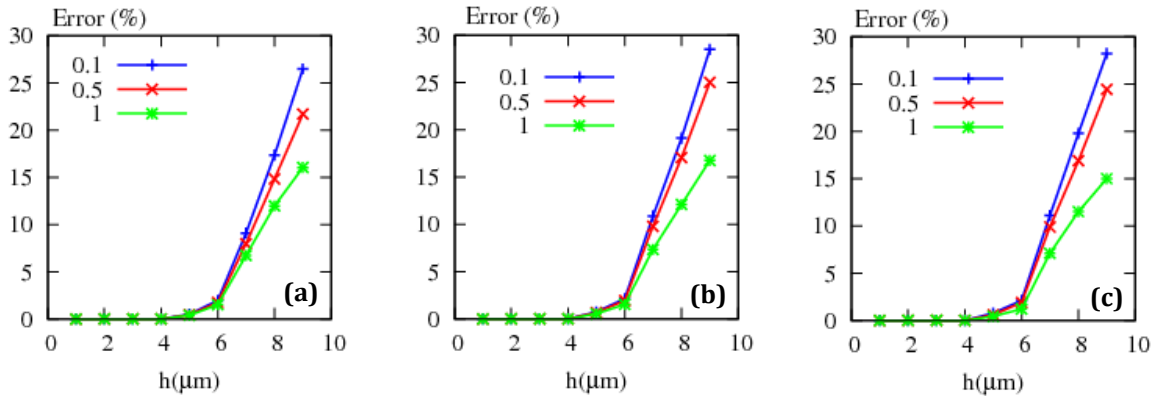

Figure 5.1. FlexPDE deficiency in numerical implementation of the Maxwell stress tensor method – Variations with particle centre height *h* above the plane electrode of the difference (in percentage) between largest and smallest values of the total dielectrophoretic force on (a) spherical (r=1μm), (b) ellipsoidal (a=1μm,b=0.5μm) and (c) cylindrical (a=1μm,r=0.5μm) particles positioned on the symmetry axis of the point-plane electrode configuration (of specifications given in figure 4.1) with three different point electrode radii: r_p={0.1,0.5,1}μm, obtained by numerical integration – in FlexPDE – of the Maxwell stress tensor over three different surfaces of integration: spheres of radii equal to, 0.5μm larger than, and 0.9μm larger than the longest half-dimension of particles.

Results obtained using the three different integration surfaces were found to be in excellent agreement (with error margins not exceeding 0.05%) for particles positioned on the symmetry axis of the disc-plane geometry. In the point-plane geometry, results only agreed favourably for particles closer to the plane electrode. Figure 5.1 shows the difference (in percentage) between largest and smallest values obtained for the DEP force on spherical,

ellipsoidal and cylindrical particles positioned on the symmetry axis of the point-plane electrode geometry. It can be seen that FlexPDE integration of the Maxwell stress tensor over different surfaces of integration yields values that are different by as much as nearly 30%. Refining the mesh grid around the point electrode did not prove effective in reducing the differences to insignificant values. Integration over particle surface was seen to generate a fourth set of values for the dielectrophoretic force which agreed to within an accuracy of more than 99% with the sum of dipolar, quadrupolar and octupolar force terms derived in the previous chapter. Performing integration of the Maxwell stress tensor in two alternative packages, FEniCS and COMSOL, produced results that were in excellent agreement with FlexPDE results obtained using integration over particle surface. This initiated a redo of effective moment calculations in FEniCS, in which case excellent agreement was observed – even at the nearest of positions to the point electrode – with FlexPDE results. The reason for the discrepancy between FlexPDE calculations of the dielectrophoretic force upon integration of the Maxwell stress tensor over different integration surfaces could not be verified, but it is understood that MST integration over particle surface *only* produces reliable results in FlexPDE.

5.2. Total dielectrophoretic force in axial symmetry

This section presents and discusses calculations of the total dielectrophoretic force on spherical, ellipsoidal and cylindrical particles of different dimensions subjected to the axisymmetric electric fields of point-plane and disc-plane electrode geometries. The DEP forces on the particles have been calculated by numerical integration of the Maxwell stress tensor over four different enclosing surfaces, that of the particle itself, and spheres of radii equal to, 0.5μm larger than, and 0.9μm larger than the longest half-dimension of the particles. The use of different integration surfaces is to ensure minimal error is imparted by the numerical solver on DEP force results. In all cases, the results agreed to within an error margin of no more than 1%. In the results to be presented, units for the dielectrophoretic force will be pico-Newtons (pN).

5.2.1. Results and discussion

Results obtained for the total dielectrophoretic force on spherical, ellipsoidal and cylindrical particles positioned on the symmetry axes of disc-plane and point-plane electrode configurations are shown in figure 5.2, where two different aspect ratios have been considered for the non-spherical shapes. For the point-plane geometry, the radius of the point electrode is taken to be 0.5μm. For the disc-plane configuration, changing disc electrode radius within the examined range of {0.5,1,2}μm is seen not to affect the DEP force experienced by particles positioned on the symmetry axis of the disc-plane geometry. This is in agreement with earlier observations of changing disc electrode radius within the same range not affecting field curvatures, effective moments and DEP force terms along the symmetry axis of the disc-plane geometry.

It appears from figure 5.2 that there are variation patterns with particle position along the axis of electric field symmetry specific to each electrode configuration and unaffected by particle geometry. In the disc-plane geometry, the DEP force is seen to attain values that are almost symmetrical around a maximum near the midpoint $h = 5\mu m$. As a given particle moves along the symmetry axis of the disc-plane geometry, the DEP force it experiences is seen to remain within the same order of magnitude. This is in clear contrast with the case of the point-plane geometry, where the DEP force on a particle spans multiple orders of magnitude as the particle is moved from the vicinity of the plane electrode towards the point electrode.

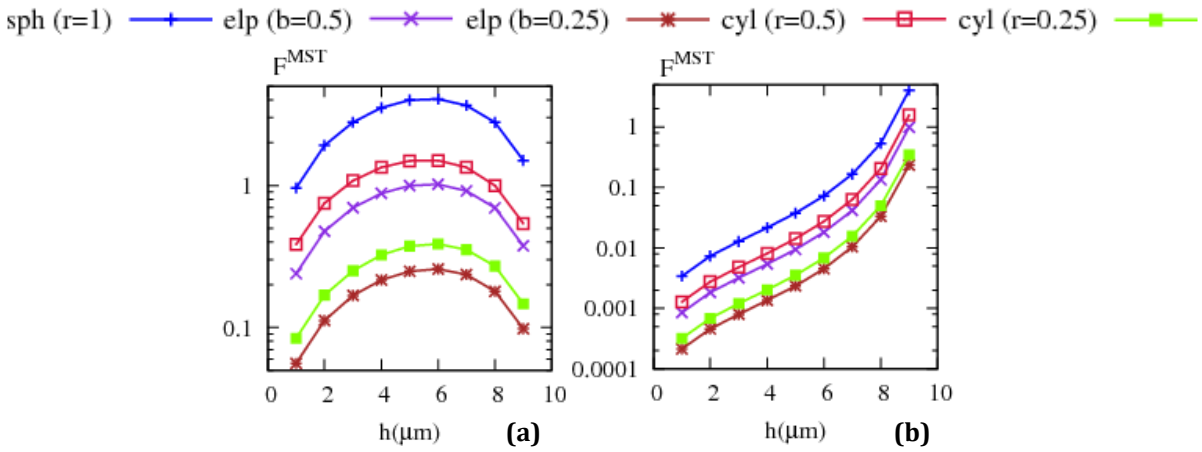

Figure 5.2. Total dielectrophoretic force in axial symmetry – Variations with particle centre height *h* above the plane electrode of the total DEP force on spherical (r=1μm), ellipsoidal (a=1μm,b={0.5,0.25}μm), and cylindrical (a=1μm,r={0.5,0.25}μm) particles positioned on the symmetry axes of (a) disc-plane and (b) point-plane electrode configurations (of specifications given in figure 4.1). The radius of the point electrode is taken to be 0.5μm, and identical results are obtained with disc electrode radii in the range {0.5,1,2}μm. Units for DEP force are pico-Newtons (pN).

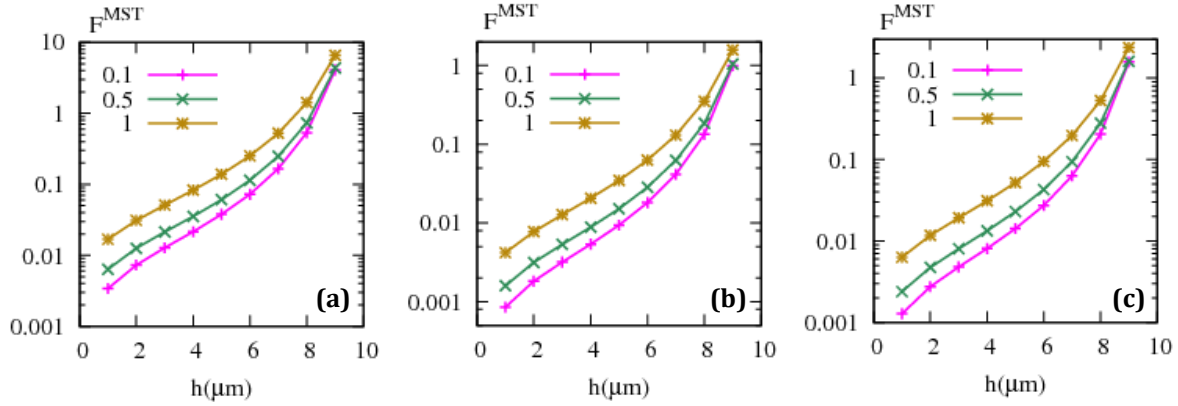

Figure 5.3. Effect of point electrode size on total dielectrophoretic force in point-plane geometry – Variations with particle centre height *h* above the plane electrode of the total DEP force on (a) spherical (r=1μm), (b) ellipsoidal (a=1μm,b=0.5μm) and (c) cylindrical (a=1μm,r=0.5μm) particles positioned on the symmetry axes of point-plane electrode configurations (of specifications given in figure 4.1) with three different point electrode radii: 0.1μm, 0.5 μm and 1 μm. Units for dielectrophoretic force are pico-Newtons (pN).

Particle geometry, of no effect on the trend with which the DEP force varies with position along the axis of electric field symmetry, is seen to have significant effect on the strength of the dielectrophoretic force at a given *h*. Particles of larger volume are seen to be subject to stronger DEP forces at all positions along the symmetry axes of either of the two electrode geometries, although no direct proportionality with particle volume (as with the dipolar force term) is observed. Among the five particles analysed, the spherical particle has largest

volume and is seen to be subject to DEP forces that are stronger than those on the ellipsoidal particles by about an order of magnitude.

The effect of point electrode radius on the DEP force experienced by particles positioned on the symmetry axis of the point-plane geometry is shown in figure 5.3, where DEP forces on spherical, ellipsoidal and cylindrical particle subjected to the axisymmetric electric fields of point-plane electrode geometries of point electrode radii {0.1,0.5,1}μm are compared. It can be seen that larger point electrodes give rise to stronger dielectrophoretic forces at all positions along the symmetry axis of the point-plane geometry, although the effect is found to be more pronounced at positions closer to the plane electrode. DEP forces are seen to remain within the same order of magnitude upon a tenfold increase in point electrode radius.

Figure 5.4 shows the effect of particle size on the total dielectrophoretic force in axial symmetry by comparing the DEP forces on spherical particles of radii 1μm and 2μm positioned on the symmetry axes of disc-plane and point-plane electrode configurations. In both electrode geometries, the DEP force is seen to increase by about an order of magnitude upon doubling particle radius, while trends with which the DEP forces vary with particle position along the axis of electric field symmetry are seen to be retained.

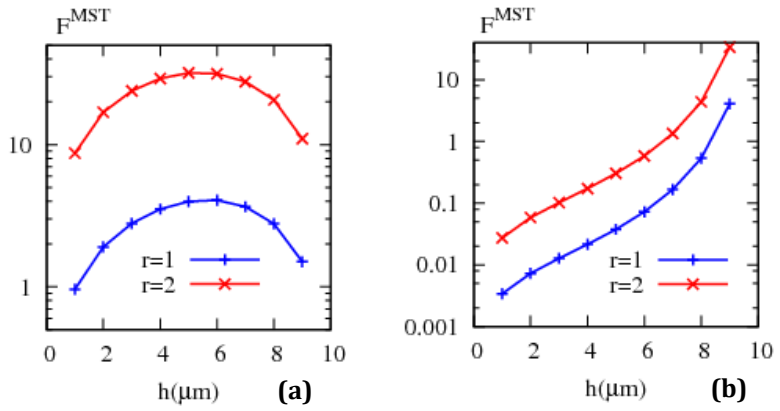

Figure 5.4. Effect of particle size on total dielectrophoretic force in axial symmetry – Variations with particle centre height *h* above the plane electrode of the total DEP force on spherical particles of radii 1μm (r=1) and 2μm (r=2) positioned on the symmetry axes of (a) disc-plane and (b) point-plane electrode geometries (of specifications given in figure 4.1). The radius of the point electrode is taken to be 0.5μm, and identical results are obtained with disc electrode radii in the range {0.5,1,2}μm. Units for DEP force are pico-Newtons (pN).

5.2.2. Summary and conclusions

Results have been presented for the total dielectrophoretic force on spherical, ellipsoidal and cylindrical particles of different dimensions subjected to the axisymmetric electric fields of

point-plane and disc-plane electrode geometries. The DEP forces have been calculated by numerical implementation of the Maxwell stress tensor (MST) method, known for its mathematical rigorousness for determining electrical force.

It has been shown that the trends with which DEP forces in axial symmetry vary with particle position can vary notably between different electrode arrangements, but are independent of particle geometry (including shape and size). The effect of particle geometry is reflected in the strength of exerted dielectrophoretic force. Although no direct proportionality with particle volume has been observed, it has been shown that particles of larger volume are subject to stronger DEP forces, regardless of electric field geometry or particle shape.

5.3. Multipolar dielectrophoretic forces in axial symmetry

This section analyses the significance of higher-order dielectrophoretic force terms in different circumstances regarding particle and electric field geometry in axial symmetry. Total DEP force calculations using the Maxwell stress tensor method are compared against calculations of first three DEP force terms based on the effective moment method to derive quadrupolar and octupolar contributions to the DEP force on spherical, ellipsoidal and cylindrical particles subjected to the axisymmetric electric fields of point-plane and disc-plane electrode geometries. At all positions along the symmetry axes of both electrode geometries and for all examined particle shapes and dimensions, the first three terms of the DEP force have been observed to add up to a value that differs from that of the total DEP force, as calculated from the MST method, by no more than 0.5%. The observation can be regarded as verification for DEP force term results, given the total force has been calculated using a completely different method – one known for its mathematical rigorousness for determining electrical force.

5.3.1. Results and discussion

5.3.1.1. The disc-plane electrode geometry

Figure 5.5 shows contributions (in percentage) from second- and third-order terms to the DEP force on spherical, ellipsoidal and cylindrical particles positioned on the symmetry axis of the disc-plane electrode geometry. The figure also shows the overall higher-order contribution to DEP forces on particles, obtained by summing second- and third-order contributions.

It can be seen that like higher-order effective moments, higher-order DEP forces are more significant for non-spherical particles. For all particle shapes, largest contribution from higher-order terms is for when particles are positioned near either of the two (disc or plane) electrodes. As particles move towards the midpoint $h = 5\mu m$, the DEP force they experience becomes increasingly dipolar. In fact, it is only at positions very close to the midpoint that higher-order DEP forces on spherical and non-spherical particles constitute less than 10% of the total force. Near disc and plane electrodes, higher-order terms are seen to contribute to ~40% and ~30%, respectively, of the DEP force on cylindrical particles.

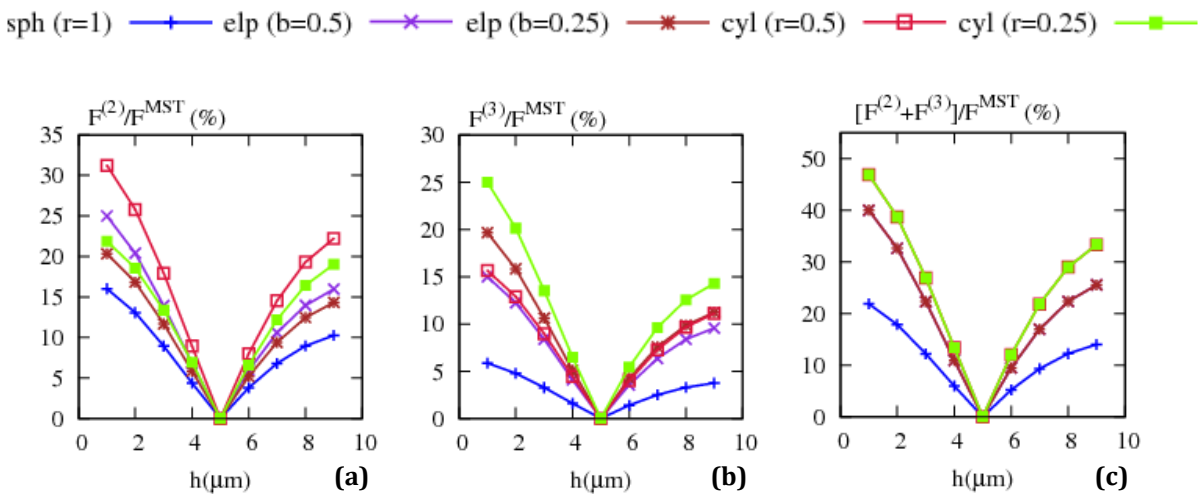

Figure 5.5. Higher-order contributions to the dielectrophoretic force in disc-plane electrode geometry – Variations with particle centre height *h* above the plane electrode of contributions (in percentage) from (a) second-order, (b) third-order, and (c) sum of second- and third-order terms to the total dielectrophoretic force on spherical (r=1μm), ellipsoidal (a=1μm,b={0.5,0.25}μm), and cylindrical (a=1μm,r={0.5,0.25}μm) particles positioned on the symmetry axis of the disc-plane electrode geometry (of specifications given in figure 4.1). Identical results obtained are for disc electrode radii in the range {0.5,1,2}μm.

An important observation made from the plots in figure 5.5 is that of particles of similar shapes, albeit of different aspect ratios, being subject to higher-order forces of equal significance. It is inferred from the data in figure 5.5 that although individual contributions from second- and third-order terms to the DEP force are different for ellipsoidal or cylindrical particles of different aspect ratios, but they add up to values that are equal, at a given position along the axis of electric field symmetry, for a given particle shape. Shape-dependent polarisation appears to give rise to 'set' values for higher-order contributions to the DEP force on a given particle shape. The values are clearly different for particles of different shapes, but for a given shape, changing aspect ratio (keeping the dimension along the axis of electric field symmetry intact) is seen to alter individual multipolar contributions to the total force, but not the overall contribution. For ellipsoidal and cylindrical particles, increasing aspect ratio is seen to give rise to more significant octupolar and less significant octupolar contributions to the dielectrophoretic force.

5.3.1.2. The point-plane electrode geometry

Results obtained for higher-order contributions to DEP forces on spherical, ellipsoidal and cylindrical particles positioned on the symmetry axis of the point-plane electrode geometry (of point electrode radius 0.5μm) are shown in figure 5.6.

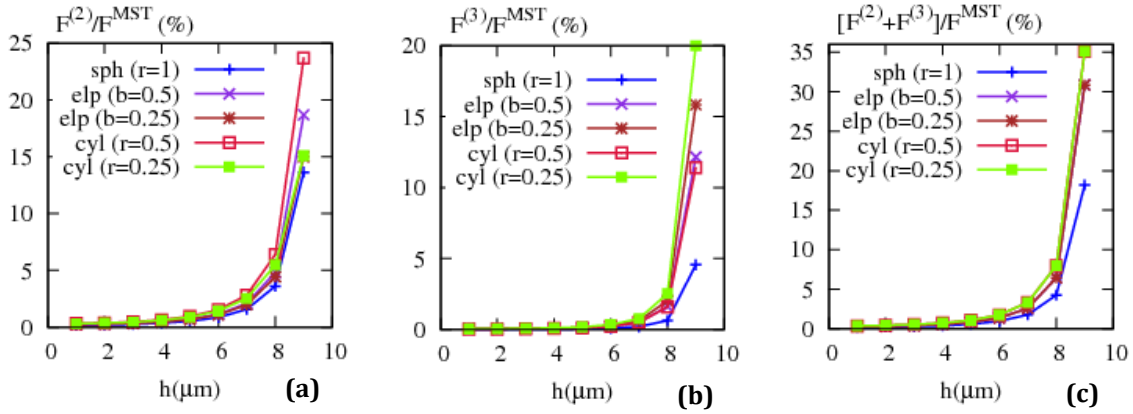

Figure 5.6. Higher-order contributions to the dielectrophoretic force in point-plane geometry – Variations with particle centre height *h* above the plane electrode of contributions (in percentage) from (a) second-order, (b) third-order, and (c) sum of second- and third-order terms to the total dielectrophoretic force on spherical (r=1μm), ellipsoidal (a=1μm,b={0.5,0.25}μm), and cylindrical (a=1μm,r={0.5,0.25}μm) particles positioned on the symmetry axis of the point-plane electrode geometry (of specifications given in figure 4.1) with point electrode radius 0.5μm.

It can be seen that in clear contrast with the disc-plane geometry, higher-order forces contribute negligibly to the DEP force on spherical and non-spherical particles, unless the particles are positioned near the point electrode. At $h = 9\mu m$, multipolar forces are seen to constitute ~35%, ~30% and ~20% of the DEP force on cylindrical, ellipsoidal and spherical particles, respectively. At $h = 7\mu m$, the DEP force on spherical, ellipsoidal and cylindrical particles is seen to be predominantly (>95%) dipolar. In similarity with the disc-plane geometry, higher-order forces are found to be more significant for non-spherical particles.

It can be seen from the plots in figure 5.6 that, as with the disc-plane geometry, non-spherical particles of the same shape but different aspect ratio are subject to higher-order DEP forces of equal significance. Individual contributions from each of the higher-order force terms are seen to be affected by changes in particle aspect ratio in a manner similar to that observed with the disc-plane geometry: increasing particle aspect ratio gives rise to smaller quadrupolar and larger octupolar contributions to the DEP force.

The effect of point electrode size on individual and overall contributions from higher-order terms to DEP forces on spherical, ellipsoidal and cylindrical particles positioned on the symmetry axis of the point-plane electrode geometry is shown in figure 5.7. It can be seen that reducing point electrode radius gives rise to increased contributions from second- and third-order terms to the DEP force on spherical and non-spherical particles. It was shown previously that first- and higher-order DEP force terms are weaker with smaller point electrodes. It is understood from the data in figure 5.7 that the rates of change of first- and

higher-order DEP force terms upon variations in point electrode radius are different, such that as the point electrode converges toward a field singularity, higher-order force terms find added significance.

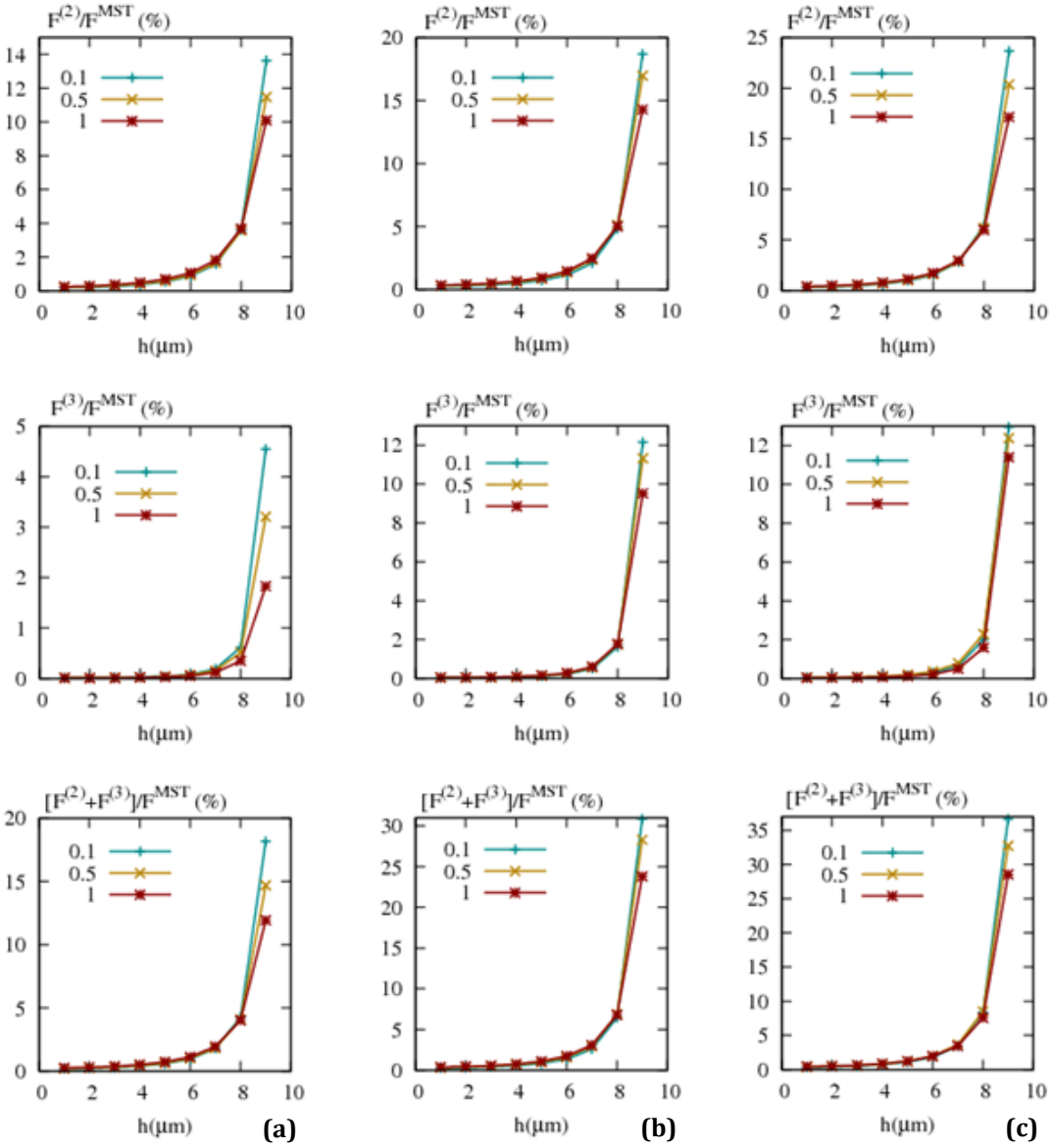

Figure 5.7. Effect of point electrode radius on higher-order contributions to the dielectrophoretic force in point-plane geometry – Variations with particle centre height *h* above the plane electrode of second-order (top row), third-order (middle row), and sum of second- and third-order (bottom row) contributions to the DEP force on (a) spherical (r=1µm), (b) ellipsoidal (a=1µm,b=0.5µm) and (c) cylindrical (a=1µm,r=0.5µm) particles positioned on the symmetry axes of point-plane electrode configurations (of specifications given in figure 4.1) with three different point electrode radii: 0.1µm, 0.5 µm and 1 µm.

The effect of point electrode radius on higher-order contributions to the DEP force is found to be modest compared to that of particle geometry. Reducing point electrode radius from 1μm to 0.1μm is seen to give rise to a ∼5% increase in multipolar contributions to the DEP force on spherical and non-spherical particles. For a given point electrode radius, higher-order contributions to DEP forces on spherical and cylindrical particles are seen to differ by ∼15%. It is important to note that regardless of particle geometry and electrode dimensions, higher-order DEP forces in the point-plane geometry can be considered negligible (<5% contribution to the total force) at all but the nearest of positions to the point electrode.

5.3.1.3. Effect of particle size

The effect of particle size on the significance of higher-order DEP force terms has been analysed by comparing contributions from second- and third-order terms to the dielectrophoretic forces experienced by spherical particles of two different radii, 1μm and 2μm, positioned on the symmetry axes of disc-plane and point-plane electrode geometries. As shown in figure 5.8, quadrupolar and octupolar contributions increase notably upon doubling particle radius. In the disc-plane geometry, maximum second- and third-order contributions to the DEP force are increased from ∼15% and ∼5%, respectively, for the 1μm-radius sphere to ∼35% and ∼15%, respectively, for the 2μm-radius particle. In the point-plane geometry, higher-order force terms are seen to constitute a maximum ∼40% of the DEP force on the larger spherical particle, up from ∼20% maximum for the 1μm-radius sphere.

Particle size is often cited as a criterion for the reliability of the dipole approximation. It has been said that higher-order DEP forces should find significance when particle dimensions become comparable to a characteristic length scale of electric field non-uniformity, i.e. when the electric field magnitude varies notably across particle dimensions. It can be concluded from the data in figure 5.8 that the criterion is by no means general. Although the increased significance of higher-order force terms for larger particles complies with the statement, it may be noticed that particle positions along the axes of electric field symmetry where higher-order forces are most significant are not necessarily those at which electric field magnitude variations across particle dimensions are maximal. As an example, higher-order forces on particles positioned on the symmetry axis of the disc-plane geometry are found to be *least* significant at the midpoint $h = 5\mu m$, where electric field variations across particle dimensions are largest.

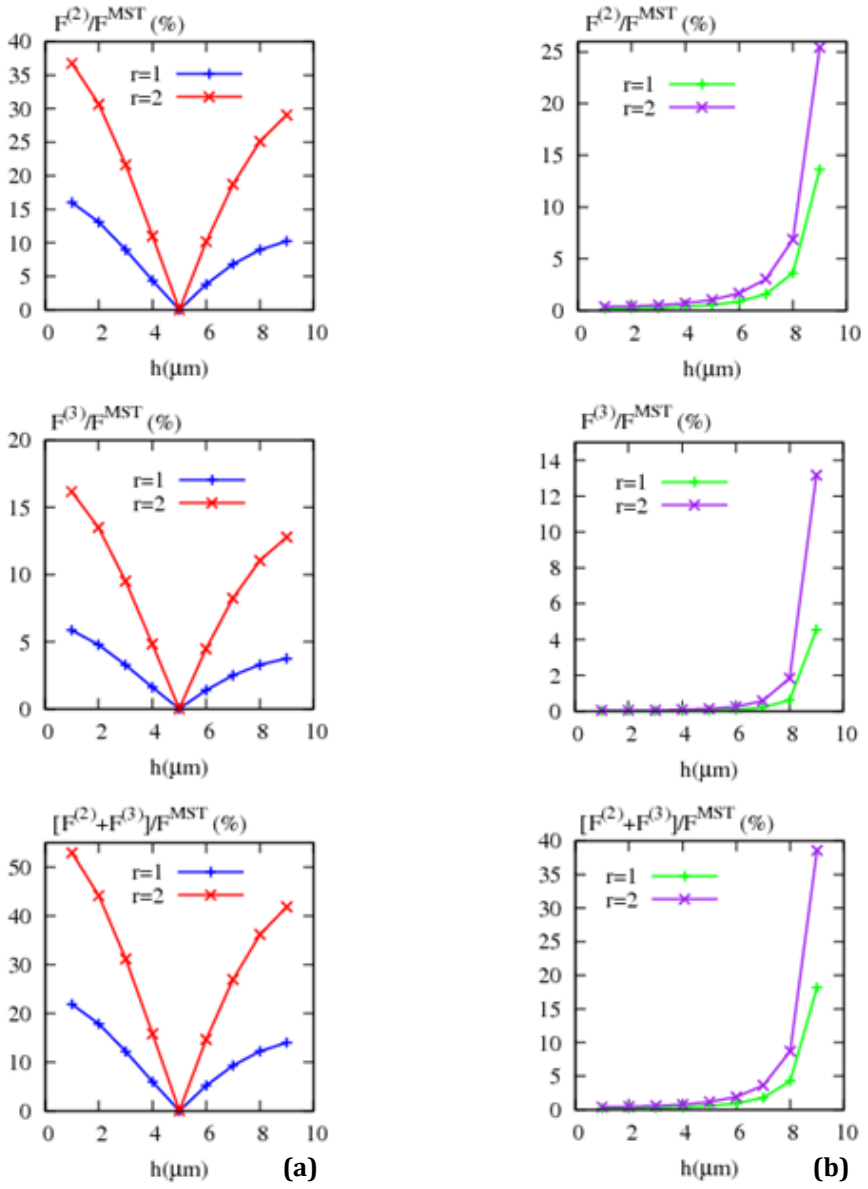

Figure 5.8. Effect of particle size on higher-order contributions to the dielectrophoretic force in axial symmetry – Variations with particle centre height *h* above the plane electrode of second-order (top row), third-order (middle row) and sum of second- and third-order contributions to the DEP force on spherical particles of radii 1μm (r=1) and 2μm (r=2) positioned on the symmetry axes of (a) disc-plane and (b) point-plane electrode geometries (of specifications given in figure 4.1). The radius of the point electrode is taken to be 0.5μm and identical results are obtained with disc electrode radii {0.5,1,2}μm.

5.3.2. Summary and conclusions

Results have been presented for individual and overall contributions from second- and third-order terms to the dielectrophoretic force on spherical, ellipsoidal and cylindrical particles of different dimensions subjected to the axisymmetric electric fields of point-plane and disc-plane electrode geometries. It has been shown that depending on particle and electrode

geometry and position along the axis of electric field symmetry, contributions from higher-order terms to the DEP force can range from negligible (<5%) to very significant (>50%).

The significance of higher-order DEP force terms has been shown to differ notably between the two axisymmetric electrode configurations. In the point-plane geometry, the DEP force has been found to be predominantly (>90%) dipolar at all but the nearest of positions to the point electrode. Using the dipole approximation for predicting the DEP force on spherical and non-spherical particles positioned on the symmetry axis of the point-plane geometry is therefore subject to insignificant (<10%) error, unless the particles are very close to the point electrode. It is important to distinguish between this and an earlier observation regarding the reliability of the dipole approximation. As illustrated previously, using the dipole approximation for particle characterisation based on the effective moments will be subject to significant error at all positions along the symmetry axis of the point-plane geometry. In fact, while higher-order *moments* add up to a value comparable to that of the dipole moment for particles positioned along the symmetry axis of the point-plane electrode geometry, higher-order *forces* are notably smaller than the dipolar DEP force on the particles.

In the disc-plane geometry, higher-order force terms have been shown to be most significant on particles positioned near either of the two (disc or plane) electrodes. Higher-order contributions to the DEP force are seen to be larger than those in the point-plane geometry. Smaller point electrodes, more closely resembling an electric field singularity, have been shown to give rise to greater contribution from higher-order DEP force terms along the symmetry axis of the point-plane geometry.

Particle geometry has been shown to have a notable effect on the significance of higher-order DEP force terms. As with the effective moments, higher-order force terms have been found to be more significant for non-spherical particles. The observations make the dipole approximation highly unreliable for particle characterisation based on the effective moments or the dielectrophoretic force, or indeed any DEP-based design involving non-spherical particles. Particles of a certain shape with equally long dimensions along the axis of electric field symmetry have been shown to be subject to higher-order forces of equal overall significance. Individual contributions from second- and third-order force terms have been shown to vary, for a given particle shape, depending on aspect ratio. Increasing the aspect ratio of, i.e. 'thinning' ellipsoidal or cylindrical particles has been shown to give rise to larger octupolar and smaller quadrupolar contributions to the DEP force, in a manner that the sum of second- and third-order contributions remains unchanged. In both axisymmetric electrode

geometries, higher-order forces have been shown to most significant for cylindrical, then ellipsoidal, then spherical particles.

Increasing the length of particle dimensions along the axis of electric field symmetry has been shown to notably increase the significance of higher-order DEP forces. Doubling the radius of a spherical particle has been shown to increase maximum higher-order contributions to the DEP force from ~20% to more than 50% in the disc-plane, and from ~20% to ~40% in the point-plane electrode geometry.

Conclusions

- Maxwell stress tensor calculations of the dielectrophoretic force on spherical, ellipsoidal and cylindrical particles of different dimensions subjected to the axisymmetric electric fields of point-plane and disc-plane electrode geometries are in excellent agreement with the sum of first three DEP force terms calculated using the effective moment method.
- Dielectrophoretic forces on the same particles at same positions along the axis of electric field symmetry can differ notably between different electrode configurations. Along the symmetry axis of a given electrode arrangement, trends with which dielectrophoretic forces vary with particle position are independent of particle geometry.
- Particles of larger volume experience stronger dielectrophoretic forces, but no direct proportionality with particle volume (as was observed with the DEP force predicted by the dipole approximation) is observed.
- Higher-order contributions to the DEP force can differ notably, in variation patterns with particle position along the axis of electric field symmetry and in value, between different electrode configurations. Higher-order forces are of little significance along the symmetry axis of the point-plane geometry, except for particles positioned very close to the point electrode. Second- and third-order contributions to the DEP force are considerably greater in the disc-plane geometry, comprising up to half the total force, depending on particle geometry and position along the axis of symmetry.
- Significant higher-order moments do not automatically result in significant higher-order DEP force terms. At most positions along the symmetry axis of the point-plane geometry, the dipole approximation – ignoring higher-order force terms – can be safely applied for prediction of the DEP force on spherical and non-spherical particles, but will be subject to significant error if invoked for particle characterisation based on the effective moments.
- Higher-order contributions to the DEP force are considerably larger for non-spherical particle shapes. The observation, alongside a similar one made previously with regard to higher-order moments, makes the dipole approximation highly unreliable in DEP force predictions or effective moment-based characterisation applications involving non-spherical particles.
- Overall contributions from second- and third-order terms to the DEP force are equal for particles of a given shape, albeit of different aspect ratio. Increasing the aspect ratio of ellipsoidal or cylindrical particles gives rise to larger octupolar and smaller quadrupolar contributions to the DEP force on the particles, in a manner that the sum of second- and third-order contributions remains independent of particle thinness and dependent only on particle shape and dimension along the axis of electric field symmetry.

- Increasing particle dimension along the axis of electric field symmetry notably increases quadrupolar and octupolar contributions to the DEP force exerted on the particle. However, electric field magnitude variation across particle dimensions has been found insufficient criterion for the reliability of the dipole approximation, as a counter-example has been demonstrated.

References

[1] Wang, X., Wang, X-B., Gascoyne, P. R. C.: General expressions for dielectrophoretic force and electrorotational torque derived using the Maxwell stress tensor method. J. Electrostat., 39, 277-295 (1997).

[2] Cheng, D. K., Field and Wave Electromagnetics, Addison-Wesley (1989).

Chapter Six

Effective Moments and Dielectrophoretic Forces in Non-axisymmetric Geometry: Results and Discussion

Abstract

A novel method is presented with which the general effective moments of dielectric particles in suspension subjected to electric fields of arbitrary geometry can be determined. The method is novel in that it does not make any assumptions regarding particle or electric field geometry. The method is applied to a physical problem involving spherical, ellipsoidal and brick-shaped particles at different positions within an interdigitated electrode configuration. By analysis of first- and higher-order moments of the differently-shaped particles subjected to electric fields of varying magnitude and curvature, the reliability of the dipole approximation in predicting the electrical energy stored in particles is assessed. Also, errors associated with approximating non-spherical particles with spheres of similar dimensions – for simplicity of modelling – are evaluated.

Effective moment calculations are combined with derivations of the electric field and its gradients to obtain the dielectrophoretic force terms. DEP force term calculations using the effective moment method are compared against Maxwell stress tensor calculations of the total DEP force to determine the significance of higher-order forces in different circumstances regarding particle and field geometry.

Overview

The chapter opens with a section on the theory of the method devised for the determination of general effective moments, the specifications of the physical problem to which the method will be applied, and the formulation of the effective moment method for determining dielectrophoretic force terms. This is followed by Section 6.2 where analytical calculations of the electric field and its gradients in different regions within the interdigitated electrode geometry are presented. Section 6.3 presents calculations of the effective moments of spherical and non-spherical particles at different positions within the interdigitated geometry and discusses the significance of the quadrupole moment in different conditions regarding particle and electric field geometry. The section also provides analysis on the errors incurred upon common particle shape approximations. In Section 6.4, field curvature and effective moment results are combined to derive first- and higher-order terms of the dielectrophoretic force on the particles. In Section 6.5, the significance of the quadrupolar force is evaluated by comparing DEP force term results against total force calculations using the mathematically rigorous Maxwell stress tensor method.

6.1. Background and theory

6.1.1. Method for determination of general effective moments

This section presents a novel method for determining the general effective moments of dielectric particles in suspension subjected to electric fields of arbitrary geometry. The assumption of axial symmetry, which greatly simplifies calculations and was the basis of the results obtained in previous chapters, is lifted so that no constraints are imposed on particle or electric field geometry.

As mentioned previously, the electric potential due to a dielectric particle subjected to an electric field can be expressed as the sum of those due to effective moments of ascending order. In three-dimensional space, analysis has to be confined to the first three effective moments. The scheme for construction of general multipoles was illustrated in Chapter Two. For derivation of the general effective moments, it is assumed that the displacement vectors constituting the first three general multipoles are aligned with the x-, y- and z-axes of the Cartesian coordinate system as shown in figure 6.1.

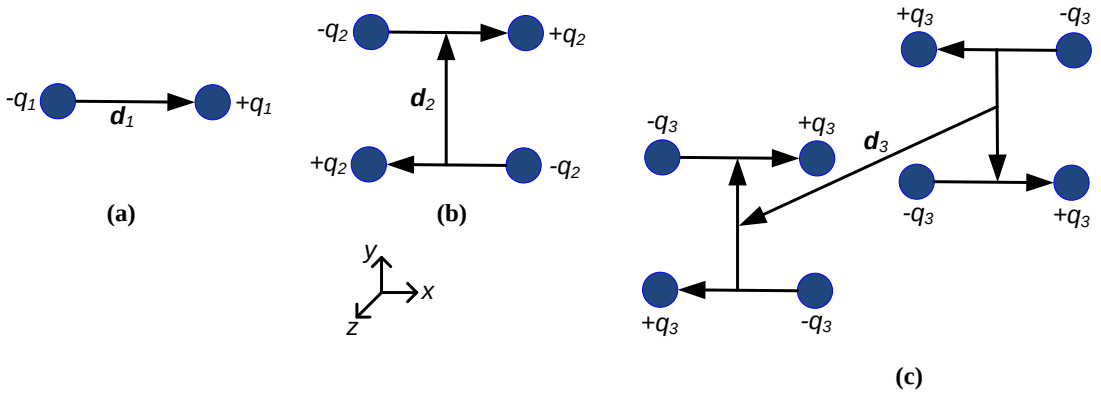

Figure 6.1. The general effective multipoles – Systematic generation of the first three general multipoles, according to Stratton's scheme [1]: (a) the dipole $(n = 1)$, (b) the quadrupole $(n = 2)$, and (c) the octupole $(n = 3)$. As shown in the figure, is assumed that d_1, d_2 and d_3 – constituent vectors of the effective dipole, quadrupole and octupole moments, respectively – are aligned with the $x-$, $y-$ and $z-$ axes of the Cartesian coordinate system, respectively.

6.1.1.1. Formulation of the method

Based on this assumption and using the equations in Chapter Two for the potential due to general multipoles (equations 2.9), the first three terms of the electrostatic potential due to a

dielectric particle in suspension subjected to an electric field, can be written in spherical coordinates (R, θ, ϕ) as:

$$\varphi^{(1)} = \frac{\boldsymbol{p}^{(1)}}{4\pi\epsilon_m R^2} G_1(\theta, \phi) \tag{6.1a}$$

$$\varphi^{(2)} = \frac{-3}{2} \cdot \frac{\boldsymbol{p}^{(2)}}{4\pi\epsilon_m R^3} G_2(\theta, \phi) \tag{6.1b}$$

$$\varphi^{(3)} = \frac{5}{3} \cdot \frac{\boldsymbol{p}^{(3)}}{4\pi\epsilon_m R^4} G_3(\theta, \phi) \tag{6.1c}$$

where $\boldsymbol{p}^{(1)}$, $\boldsymbol{p}^{(2)}$ and $\boldsymbol{p}^{(3)}$ are the effective dipole, quadrupole and octupole moments, respectively, representing polarisation at the particle/electrolyte interface, and the functions $G_n(\theta, \phi)$ are defined as:

$$G_1(\theta, \phi) = \sin\phi \cos\theta \tag{6.2a}$$

$$G_2(\theta, \phi) = \sin^2\phi \sin\theta \cos\theta \tag{6.2b}$$

$$G_3(\theta, \phi) = \sin^2\theta \cos\phi \sin\theta \cos\theta \tag{6.2c}$$

The functions $G_n(\theta, \phi)$ are found to be mutually orthogonal by the following definition:

$$\int_0^{\pi} \int_0^{2\pi} G_n(\phi, \theta) G_m(\phi, \theta)\, d\phi d\theta = 0, \ m \neq n \tag{6.3a}$$

$$\int_0^{\pi} \int_0^{2\pi} G_1(\phi, \theta) G_1(\phi, \theta) d\phi d\theta = \pi^2/9 \tag{6.3b}$$

$$\int_0^{\pi} \int_0^{2\pi} G_2(\phi, \theta) G_2(\phi, \theta) d\phi d\theta = 3\pi^2/128 \tag{6.3c}$$

$$\int_0^{\pi} \int_0^{2\pi} G_3(\phi, \theta) G_3(\phi, \theta) d\phi d\theta = \pi^2/256 \tag{6.3d}$$

Using the orthogonality defined by equations (6.3), the effective moments can be derived from the potential $\varphi_{particle}$ due to the particle they represent, from the following equations:

$$p^{(1)} = 4\pi\epsilon_m R^2 \cdot \frac{2}{\pi^2} \int_0^{\pi} \int_0^{2\pi} \varphi_{particle}\, G_1(\phi, \theta) d\phi d\theta \tag{6.4a}$$

$$p^{(2)} = -4\pi\epsilon_m R^3 \cdot \frac{64}{9\pi^2} \int_0^{\pi} \int_0^{2\pi} \varphi_{particle}\, G_2(\phi, \theta) d\phi d\theta \tag{6.4b}$$

$$p^{(3)} = 4\pi\epsilon_m R^4 \cdot \frac{192}{5\pi^2} \int_0^{\pi} \int_0^{2\pi} \varphi_{particle}\, G_3(\phi, \theta) d\phi d\theta \tag{6.4c}$$

6.1.1.2. Implementation of the method

Equations (6.4) form the foundation of the hybrid numerical-analytical method used in this chapter for the derivation of first-, second- and third-order effective moments of particles of arbitrary shape subjected to electric fields of arbitrary geometry. The general effective moments can be obtained from weighted integration of the potentials due to the particles they represent over an enclosing sphere. The potential due to a given particle at a given position within an electrode structure can be obtained, as in Chapter Four, from $\varphi_{particle} = \varphi_{with\ particle} - \varphi_{background}$, where $\varphi_{background}$ is the 'background' potential distribution within the electrode geometry in the absence of the particle, and $\varphi_{with\ particle}$ is the potential distribution with the particle inserted within the electrode geometry. Subtraction of the background potential from the 'with particle' potential gives the perturbation caused by the particle to the field lines/equipotential surfaces of the electrode geometry, i.e. the potential due to the particle.

The potentials $\varphi_{with\ particle}$ and $\varphi_{background}$ can be obtained numerically using finite element method-based packages. A subtraction yields the potential due to the particle of interest, and numerical integration of the functions given in equation (6.4) over a spherical surface that fully encloses the particle yields the effective moment of desired order. An important feature of the method used in this work is that it relies on integration of the potential – which is the original variable obtained from FEM simulation – for obtaining the effective moments, and thus no (error-prone) numerical differentiation is involved.

The electrode structure studied in this work is the interdigitated configuration, the particles are spherical, ellipsoidal or brick-shaped, and the standard FEM solver used for numerical implementation of the method defined through equations (6.4) is FlexPDE. Due to issues with regard to numerical implementation of the Maxwell stress tensor method in FlexPDE (discussed in Chapter Five), results have been checked against those obtained with an alternative package FEniCS with excellent agreement observed between the two sets of results (differences in no case exceeding 1%).

6.1.2.3. Magnitudes of the effective moments

As it has been assumed that the constituent vectors of the effective moments are aligned with the axes of the Cartesian coordinate system, only certain elements of the tensors $\boldsymbol{p}^{(1)}$, $\boldsymbol{p}^{(2)}$ and $\boldsymbol{p}^{(3)}$ are non-zero. The parameters $p^{(1)}$, $p^{(2)}$ and $p^{(3)}$ in equations (6.4) are representatives of the magnitudes of the tensors, defined in each case as the magnitude of the vector sum of non-zero elements.

The magnitude $p^{(1)}$ of the effective dipole moment is obtained as:

$$p^{(1)} = |q\boldsymbol{d}_1| = qd_{1x} = qd_1 \tag{6.5a}$$

as $d_{1y} = d_{1z} = 0$, due to $\boldsymbol{d}_1$ being aligned with the x −axis of the Cartesian coordinate system.

The magnitude $p^{(2)}$ of the effective quadrupole moment can be written as:

$$p^{(2)} = |q(\boldsymbol{d}_1\boldsymbol{d}_2 + \boldsymbol{d}_2\boldsymbol{d}_1)| = q(d_{1x}d_{2y} + d_{2y}d_{1x}) = 2qd_1d_2 \tag{6.5b}$$

since $d_{2x} = d_{2z} = 0$, due to $\boldsymbol{d}_2$ being aligned with the y −axis in the Cartesian coordinate system.

The magnitude $p^{(3)}$ of the effective octupole moment is obtained as:

$$\begin{aligned} p^{(3)} &= |q(\boldsymbol{d}_1\boldsymbol{d}_2\boldsymbol{d}_3 + \boldsymbol{d}_1\boldsymbol{d}_3\boldsymbol{d}_2 + \boldsymbol{d}_2\boldsymbol{d}_1\boldsymbol{d}_3 + \boldsymbol{d}_2\boldsymbol{d}_3\boldsymbol{d}_1 + \boldsymbol{d}_3\boldsymbol{d}_1\boldsymbol{d}_2 + \boldsymbol{d}_3\boldsymbol{d}_2\boldsymbol{d}_1)| \\ &= 6qd_{1x}d_{2y}d_{3z} = 6qd_1d_2d_3 \end{aligned} \tag{6.5c}$$

since $d_{3x} = d_{3y} = 0$, due to $\boldsymbol{d}_3$ being aligned with the z −axis.

6.1.1.4. Formulation for obtaining dielectrophoretic force terms

Once the effective moments representing particle/medium polarisation have been derived, the effective moment method can be invoked to derive dielectrophoretic force terms. The first three terms of the DEP force by a non-uniform electric field $\boldsymbol{E}$ on a dielectric particle of effective moments $\boldsymbol{p}^{(1)}$, $\boldsymbol{p}^{(2)}$ and $\boldsymbol{p}^{(3)}$ are given by:

$$\boldsymbol{F}^{(1)} = \boldsymbol{p}^{(1)} \cdot \nabla\boldsymbol{E} \tag{6.6a}$$

$$\boldsymbol{F}^{(2)} = \frac{1}{2}\boldsymbol{p}^{(2)} : \nabla\nabla\boldsymbol{E} \tag{6.6b}$$

$$\boldsymbol{F}^{(3)} = \frac{1}{6}\boldsymbol{p}^{(3)} \vdots \nabla\nabla\nabla\boldsymbol{E} \tag{6.6c}$$

where $\nabla\boldsymbol{E}$, $\nabla\nabla\boldsymbol{E}$, and $\nabla\nabla\nabla\boldsymbol{E}$ are first-, second- and third-order gradients of the electric field, respectively. A definition of vector gradients, within the context of tensor notation is presented in Appendix A.

6.1.2. Physical problem specifications

This section outlines the physical problem that will be used to illustrate the method presented in the previous section for determining the general effective moments and dielectrophoretic forces.

$h = 60\mu m$

$V = 1V$

$w + g = 40\mu m$

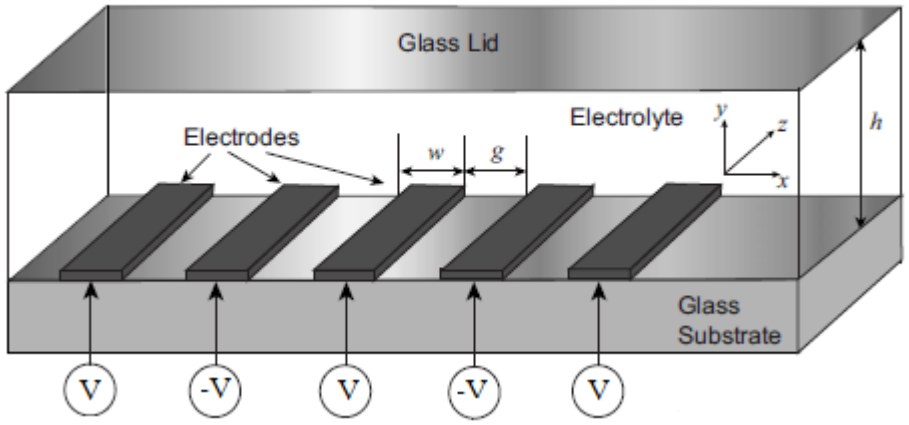

Figure 6.2. The interdigitated electrode geometry – Configuration and structural parameters of the interdigitated electrode geometry used for analysis of general effective moments and dielectrophoretic forces on spherical and non-spherical particles in suspension flowing through the channel above the interdigitated array of electrodes. The non-uniform electric field that exerts dielectrophoretic force on the particles is generated by applying voltages of equal magnitude (1V) and opposing polarity to successive electrodes. Drawing of the electrode structure layout courtesy of Dr Tao Sun.

The electrode geometry used for analysis of the effective moments and DEP forces is the interdigitated electrode configuration shown in figure 6.2. The structural parameters are chosen to be consistent with experimental conditions. The interdigitated array of electrodes lies on a glass substrate. Above the electrodes is a channel, capped by an insulating lid, through which the dielectric particles in suspension flow. The non-uniform electric field required for exertion of a dielectrophoretic force on the particles is generated by applying voltages of equal magnitude (1V) and alternating polarity to successive electrodes. To observe the effect of electrode geometry on the moments and DEP forces, three different combinations are considered for electrode width w and inter-electrode spacing g: $w < g$ $(w = 10\mu m, g = 30\mu m), w = g$ $(w = 20\mu m, g = 20\mu m), w > g$ $(w = 30\mu m, g = 10\mu m)$.

An important reason for choosing the interdigitated electrode geometry for analysis of general effective moments and corresponding DEP force terms, alongside its widespread use in dielectrophoretic applications (a review of related literature presented in Chapter Two), is that an analytic derivation is available for the electric field vector within the interdigitated

electrode geometry. Sun et al [2] have derived an expression, using the Schwarz-Christoffel mapping method, for the electric field vector at any given position within an interdigitated electrode configuration. The derivation is presented in Appendix D. Using this analytic expression, the field magnitude and its gradients – required for obtaining the DEP force terms in accordance with the effective moment method (equation 6.6) have all been derived analytically without resorting to highly error-prone numerical means of successive differentiation.

The particle geometries studied for the analysis of general effective moments and DEP forces are shown in figure 6.3. The third (out-of-plane) dimension of the non-spherical particles is assumed to equal b. Spherical, ellipsoidal and brick-shaped particles of similar dimensions are studied, to observe the effect of particle geometry on the moments and DEP forces. Comparing the effective moments of the differently-shaped particles allows for an assessment of the errors incurred in effective moment-based particle characterisation when non-spherical particles are approximated as spheres for simplicity of modelling. It will be assumed that the particles and their suspending media are lossless dielectrics with relative permittivities of 3 and 80 (pertaining to SU-8 and water), respectively.

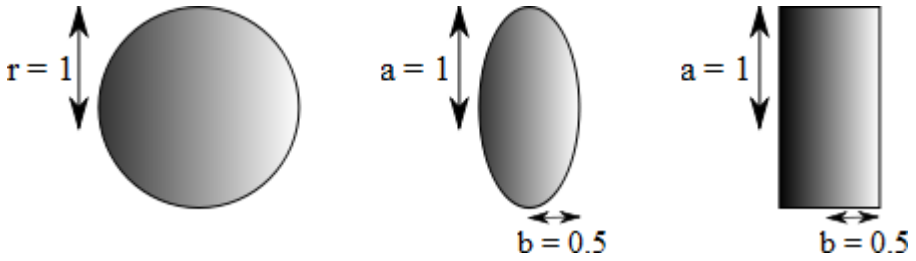

Figure 6.3. Particle geometries for analysis of general effective moments and dielectrophoretic forces – Shapes and dimensions of the dielectric particles in suspension studied for the analysis of general effective moments and DEP forces for when the particles are positioned within an interdigitated electrode configuration (of specifications given in figure 6.2). The third (out-of-plane) dimension of the non-spherical particles is assumed to equal b. Particles of different shapes but similar dimensions are studied to investigate the effect of particle geometry on the moments and DEP forces. It will be assumed that the particles and their suspending media are lossless dielectrics with relative permittivities of 3 and 80 (pertaining to SU-8 and water), respectively.

The effective moments and dielectrophoretic forces on the particles in figure 6.3 are calculated for when the particles are at three different heights within the insulator-capped channel above the interdigitated array of electrodes. Ignoring the effect of channel walls, and according to the axis labelling in figure 6.2, the electric field does not vary along the z −axis. As a result, it suffices to analyse the effective moments and dielectrophoretic forces in the $x - y$ plane, ignoring the z coordinates. It was assumed in the method for determination of

the general effective moments that the constituent vector $\boldsymbol{d}_3$ of the effective octupole is aligned with the z −axis of the Cartesian coordinate system. Based on this assumption, the electric field not varying along the z −axis gives rise to effective octupole moments identical to zero. Accordingly, the first *two*, rather than three, effective moments of the particles in figure 6.3 will be calculated in this chapter.

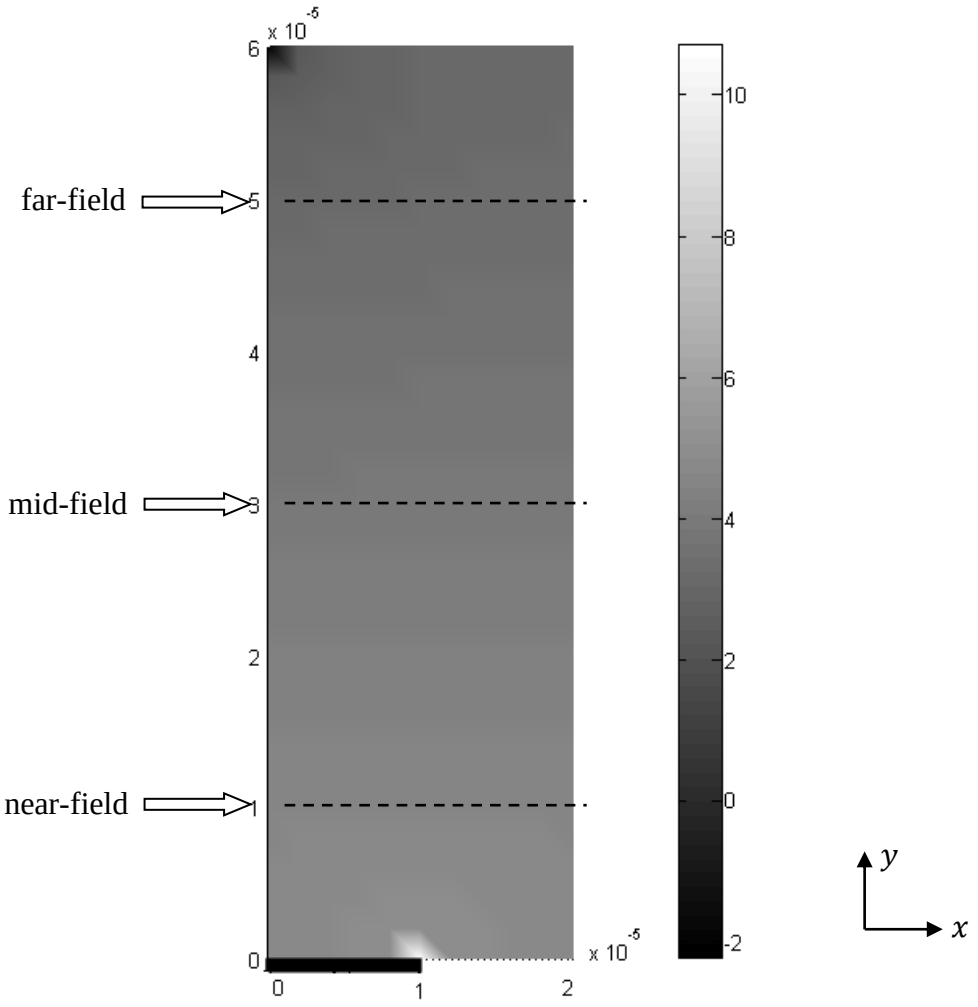

Figure 6.4. Simulation domain in interdigitated electrode geometry – A sample simulation domain in the interdigitated electrode geometry (of specifications given in figure 6.2), showing distribution of the electric field magnitude within the $x-y$ plane. Ignoring the effect of channel walls, the electric field magnitude does not vary along the z −axis of the Cartesian coordinate system, and analysis can therefore be confined to the $x-y$ plane. The domain shows the three regions, corresponding to different heights above the electrode surface, at which the general effective moments and dielectrophoretic forces will be calculated.

Figure 6.4 shows a sample simulation domain (along the $x-y$ plane) with the distribution of the electric field magnitude. The domain shows the three regions in which the effective moments and DEP forces will be calculated. As shown in the figure, the three regions correspond to different particle heights h above the array of interdigitated electrodes. Near-,

mid- and far-field regions correspond to particle centre heights 10μm, 30μm and 50μm above the electrode surface, within the 60μm-high channel, capped by an insulating lid. Results in the near-field region are expected to be most significantly affected by the large curvature due to the electric field maximum at the electrode tip. It is also important to note that results in the far-field region will be affected by the Neumann boundary condition imposed by the nearby insulating lid. The effect of the insulating lid is evident in the field magnitude distribution shown in figure 6.4 through the electric field minimum at the top-left corner of the simulation domain.

6.1.3. Dielectrophoretic force terms with general effective moments

As the effective octupole moment is identical to zero in the interdigitated electrode geometry of figure 6.2 (having ignored the effect of channel walls), the octupolar term of the DEP force on the particles will also be equal to zero, according to equation (6.6). Therefore the first *two*, rather than three, dielectrophoretic force terms will be calculated in this chapter. As the particles move within the $x-y$ plane, the dipolar and quadrupolar forces they experience bear $x-$ and $y-$components which may be calculated from equations (6.6) by applying tensor properties. In the results that will be presented later in the chapter, the *magnitudes* of dielectrophoretic force terms will be plotted, and their dependency on particle and field parameters discussed.

The $x-$ and $y-$components of the dipolar force $\boldsymbol{F}^{(1)}$ can be expressed as:

$$F_x^{(1)} = p_x^{(1)} \nabla_x E_x = p^{(1)} \frac{dE_x}{dx} \tag{6.7a}$$

$$F_y^{(1)} = p_x^{(1)} \nabla_x E_y = p^{(1)} \frac{dE_y}{dx} \tag{6.7b}$$

The magnitude of the dipolar force is therefore given by:

$$F^{(1)} = p^{(1)} \frac{dE}{dx} \tag{6.8}$$

where dE/dx is defined as:

$$\frac{dE}{dx} = \left[\left(\frac{dE_x}{dx} \right)^2 + \left(\frac{dE_y}{dy} \right)^2 \right]^{1/2} \tag{6.9}$$

For the quadrupolar force $\boldsymbol{F}^{(2)}$, the $x-$ and $y-$components can be written as:

$$F_x^{(2)} = \frac{1}{2} [p_{xy}^{(2)} \nabla_x \nabla_y E_x + p_{yx}^{(2)} \nabla_y \nabla_x E_x] = \frac{1}{4} p^{(2)} \frac{d^2 E_x}{dxdy} \tag{6.10a}$$

$$F_y^{(2)} = \frac{1}{2}[p_{xy}^{(2)}\nabla_x\nabla_y E_y + p_{yx}^{(2)}\nabla_y\nabla_x E_y] = \frac{1}{4}p^{(2)}\frac{d^2E_y}{dxdy} \tag{6.10b}$$

The magnitude of the quadrupolar force is therefore given by:

$$F^{(2)} = \frac{1}{4}p^{(2)}\frac{d^2E}{dxdy} \tag{6.11}$$

with $d^2E/dxdy$ defined as:

$$\frac{d^2E}{dxdy} = \left[\left(\frac{d^2E_x}{dxdy}\right)^2 + \left(\frac{d^2E_y}{dxdy}\right)^2\right]^{1/2} \tag{6.12}$$

This chapter will present analytical calculations of the electric field magnitude and its first- and second-order gradients (as defined by equations (6.9) and (6.12)). The field gradient calculations will be combined with calculations of the effective dipole and quadrupole moments of the particles in figure 6.3 to derive the first two terms of the DEP force on the particles from equations (6.8) and (6.11). Force term calculations will then be compared against total force calculations using the Maxwell stress tensor method to determine the significance of higher-order contributions in different circumstances regarding particle and electric field geometry.

6.2. Electric field magnitude and gradients

This section presents analytical calculations of the electric field magnitude and gradients at different positions within an interdigitated electrode configuration. Specifications of the electrode geometry, and the three regions at which the effective moments and dielectrophoretic forces are to be analysed were given in the previous section. The electric field magnitude and its first- and second-order gradients are calculated at near-, mid- and far-field regions of the interdigitated geometry, consisting of a channel, capped by an insulating lid, above an interdigitated array of electrodes. The field curvature results are important in that (a) they determine the energy stored in particles in the form of effective moments of succeeding order (with the electric field magnitude regarded as the field curvature of order $n = 0$), and (b) they are required for derivation of dielectrophoretic force terms from the effective moment method.

The electric field magnitude and gradients are calculated for three different combinations of electrode width w and inter-electrode spacing g: $w < g$ $(w = 10\mu m, g = 30\mu m), w = g$ $(w = 20\mu m, g = 20\mu m), w > g$ $(w = 30\mu m, g = 10\mu m)$. The calculations are based on a conformal mapping method-based derivation of the electric field vector at different positions within an interdigitated electrode configuration [2]. In the results to be presented, units for the electric field magnitude and its first- and second-order gradients will be V/m, V/m^2, and V/m^3, respectively.

6.2.1. Results and discussion

Electric field magnitude and gradient results will be presented in three sections, one for each of the three regions within the interdigitated electrode geometry (as specified in figure 6.4).

6.2.1.1. The near-field region

Variations with position along the x −axis of the electric field magnitude and its first- and second-order gradients in the near-field region of the interdigitated electrode geometry are shown in figure 6.5. It can be seen that, as expected from proximity with the electrode array, electric field curvatures are notably affected by variations in electrode width and spacing. When $w = g$, the electrode tip, and hence the field maximum, lies at the midpoint $x = 10\mu m$. In attribution, the field curvature profiles are seen to be symmetrical around a maximum at the midpoint. With electrode width larger than inter-electrode spacing ($w > g$), the position of the electric field maximum is shifted towards larger x, and the field curvatures are seen to generally become stronger with increasing x. The opposite situation occurs for $w < g$, with the field maximum shifted towards smaller x, and field magnitude and gradients decreasing

with increasing x. Values of the electric field magnitude and its gradients are seen to remain within the same order of magnitude as x is varied within the range $[0,20\mu m]$.

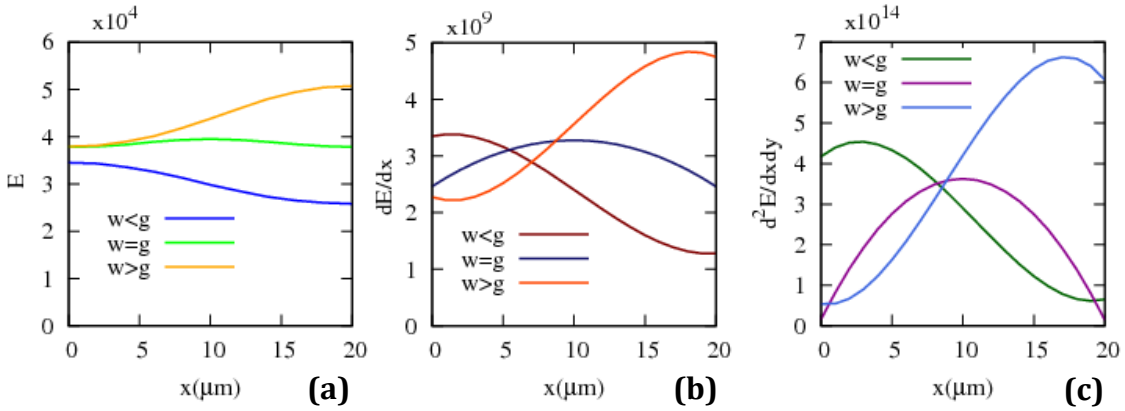

Figure 6.5. Electric field curvatures in the near-field region of the interdigitated electrode geometry – Variations with position x along the horizontal axis of (a) the electric field magnitude, and its (b) first- and (c) second-order gradients in the near-field $(y = 10\mu m)$ region of the interdigitated electrode geometry (of specifications given in figure 6.2). The results have been obtained with three different combinations of electrode width w and inter-electrode spacing g: $w < g$ $(w = 10\mu m, g = 30\mu m), w = g$ $(w = 20\mu m, g = 20\mu m), w > g$ $(w = 30\mu m, g = 10\mu m)$.

6.2.1.2. The mid-field region

Results obtained for the electric field magnitude and gradients in the mid-field region of the interdigitated electrode geometry are shown in figure 6.6. It can be seen that the electric field varies only negligibly as position x along the horizontal axis is varied within the range $[0,10\mu m]$. The effect of increasing the width/spacing ratio of the interdigitated electrodes is seen to be a strengthening of the electric field, at all positions within the mid-field region. First- and second-order field gradients are also seen not to change in large proportions as x is increased from 0 to 10μm. Among the field curvatures, the second-order gradient is seen to be more considerably affected by variations in position within the mid-field region. Depending on whether the width of the interdigitated electrodes is larger than, smaller than or equal to inter-electrode spacing, the second-order field gradient is seen to increase, decrease or remain almost constant with increasing x, respectively. Electric field curvatures are all seen to be stronger with wider electrodes.

The electric field magnitude remaining almost constant upon variations in position within the mid-field region, regardless of the position of the electric field maximum at the electrode tip, indicates that the mid-field region is distant enough from the electrode array for variations in

electrode width and spacing not to considerably affect the trend with which the field magnitude varies with x. This, as expected, is in clear contrast with the results presented previously for the near-field region of the interdigitated geometry where proximity with the electrode array was shown to result in notable dependency of field magnitude profiles on electrode geometry. The mid-field region appears to be also distant enough from the insulating lid for the field curvature imposed by the Neumann boundary condition not to affect electric field magnitude profiles.

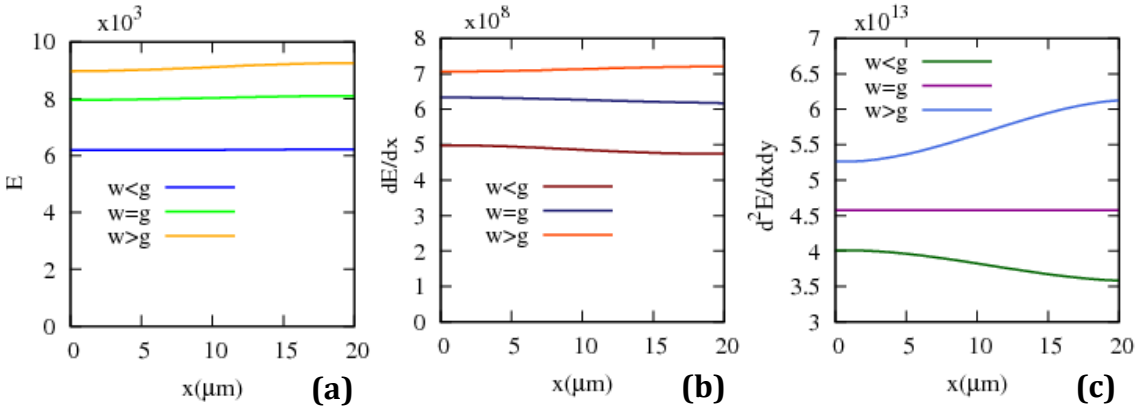

Figure 6.6. Electric field curvatures in the mid-field region of the interdigitated electrode geometry – Variations with position x along the horizontal axis of (a) the electric field magnitude, and its (b) first- and (c) second-order gradients in the mid-field ($y = 30\mu m$) region of the interdigitated electrode geometry (of specifications given in figure 6.2). The results have been obtained with three different combinations of electrode width w and inter-electrode spacing g: $w < g$ ($w = 10\mu m, g = 30\mu m$), $w = g$ ($w = 20\mu m, g = 20\mu m$), $w > g$ ($w = 30\mu m, g = 10\mu m$).

6.2.1.3. The far-field region

Results obtained for the electric field magnitude and its first- and second-order gradients in the far-field region of the interdigitated electrode geometry, near the insulating lid, are shown in figure 6.7. It can be seen that the field curvature due to the Neumann boundary condition imposed by the glass lid results in field magnitude profiles that are not constant with x, as was shown to be the case in the mid-field region of the electrode geometry. For all three combinations of electrode width and spacing, the electric field is seen to strengthen with increasing x. At a given position within the far-field region, stronger electric fields are seen to result from wider electrodes (and smaller inter-electrode spacing). First- and second-order gradients of the electric field are also seen to be larger with wider electrodes, although they are seen to follow opposing trends with position x along the horizontal axis: the first-order field gradient is seen to decrease, and the second-order gradient increase with

increasing x. Electrode geometry (through width and spacing) is seen to affect values, but not variation patterns with x, of electric field curvatures in the far-field region of the interdigitated electrode geometry.

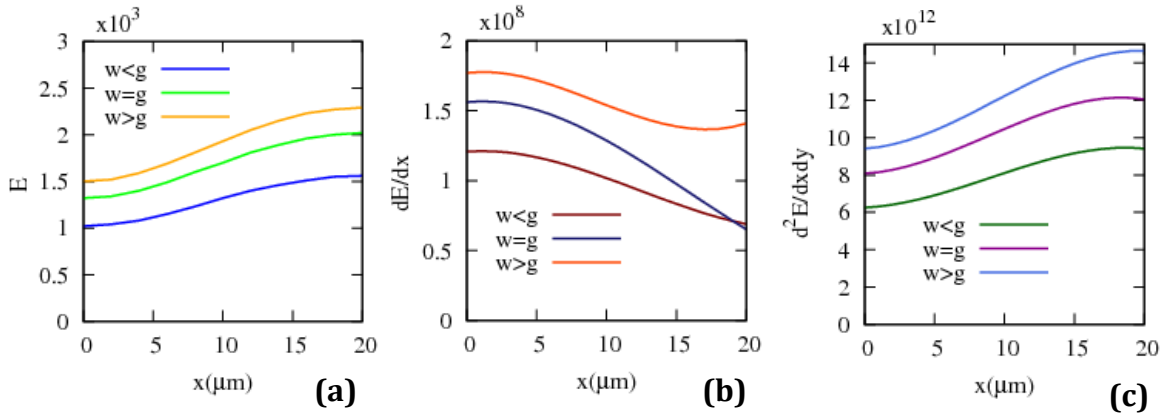

Figure 6.7. Electric field curvatures in the far-field region of the interdigitated electrode geometry – Variations with position x along the horizontal axis of (a) the electric field magnitude, and its (b) first- and (c) second-order gradients in the far-field ($y = 50\mu m$) region of the interdigitated electrode geometry (of specifications given in figure 6.2). The results have been obtained with three different combinations of electrode width w and inter-electrode spacing g: $w < g$ ($w = 10\mu m, g = 30\mu m$), $w = g$ ($w = 20\mu m, g = 20\mu m$), $w > g$ ($w = 30\mu m, g = 10\mu m$).

6.2.2. Summary and conclusions

Analytical calculations have been presented for the electric field magnitude and its first- and second-order gradients in near-, mid- and far-field regions of the interdigitated electrode geometry. It has been shown that field curvatures differ notably, in value and variation patterns with position along the horizontal axis, depending on height above the electrode array.

In the near-field region, closest to the electrode surface, changing electrode width (and inter-electrode spacing) has been seen to have a notable effect on the field magnitude and gradients; the position of the electric field maximum has been shown to be determined by electrode width, and field curvature profiles have been seen to differ depending on how the width and spacing of the interdigitated electrodes relate to one another. In the mid-field region of the electrode geometry, halfway between the electrode array and the insulating lid, little effect has been observed from field curvatures at either end of the channel on field magnitude and gradient profiles: as position x within the mid-field region spans the whole

$[0,20\mu m]$ range, the electric field magnitude and its gradients have been shown to remain almost unchanged.

The effect of the Neumann boundary condition imposed by the insulating lid capping the channel above the interdigitated array of electrodes has been seen to be electric field curvature profiles that do vary with position within the far-field region, in contrast to the observation made in the mid-field region of the electrode geometry. Electrode width and spacing has been shown to give rise to stronger field magnitudes and gradients in the far-field region, while variation patterns with position along the horizontal axis have been shown to remain almost independent of electrode dimensions. Field magnitude and gradients in the far-field region have been shown to be of the same order of magnitude of those of corresponding order in the mid-field region of the interdigitated geometry, and smaller than those in the near-field region by about an order of magnitude.

The electric field magnitude and its first- and second-order gradients determine the electrical energy stored in dielectric particles in the form of effective dipole, quadrupole and octupole moments, respectively – calculations of which will be presented in the next section. Effective moment calculations will be combined with field curvature results to determine the terms of the dielectrophoretic force on particles.

6.3. The general effective moments

This section presents and discusses calculations of the effective dipole and quadrupole moments of spherical, ellipsoidal and brick-shaped particles at different positions within an interdigitated electrode configuration. The effective moments are determined using the novel hybrid numerical-analytical method presented in Section 6.1. By comparing the results obtained for different particle shapes, the errors incurred in effective moment-based particle characterisation upon approximating non-spherical particles with spheres of similar dimensions will be assessed. Also, the significance of the effective quadrupole moment, and hence the reliability of the dipole approximation, in different circumstances regarding particle and electric field geometry will be examined.

6.3.1. Results

Effective moment calculations are presented in three different sections, one for each of the three regions within the interdigitated electrode geometry, as specified in figure 6.4. The moments are calculated by numerically performing the integrals in equations (6.3) over three different enclosing surfaces – to ensure minimal error is imparted by the numerical solver on the results obtained. The integration surfaces for deriving the effective moments of a particle are spheres, centred at the particle centre, of radii 1μm, 1.5μm and 1.9μm. The integration surfaces are chosen to be consistent with those used previously for the determination of linear effective moments in axial symmetry. The smallest enclosing surface is that most closely fitting the particle, and the radius of the largest integration surface is chosen such that a marginal distance of 0.1μm minimum is kept from domain walls.

Results have been originally obtained in the standard solver used in this work, namely FlexPDE. Due to issues reported on in Chapter Five regarding numerical implementation of the Maxwell stress tensor method in FlexPDE, all effective moment calculations in FlexPDE have been checked against those obtained in an alternative solver: FEniCS. In all cases, results obtained with the three different integration surfaces in FlexPDE agreed with each other and with those obtained in FEniCS to within an error margin of no more than 1%. In the results to be presented, units for the effective dipole and quadrupole moments will be C.m and $C.m^2$, respectively.

6.3.1.1. The near-field region

Results obtained for the first two effective moments of spherical, ellipsoidal and brick-shaped particles positioned in the near-field region of the interdigitated electrode geometry are shown in figure 6.8 for three different combinations of electrode width and spacing:

$w < g$ $(w = 10\mu m, g = 30\mu m), w = g$ $(w = 20\mu m, g = 20\mu m), w > g$ $(w = 30\mu m, g = 10\mu m)$.

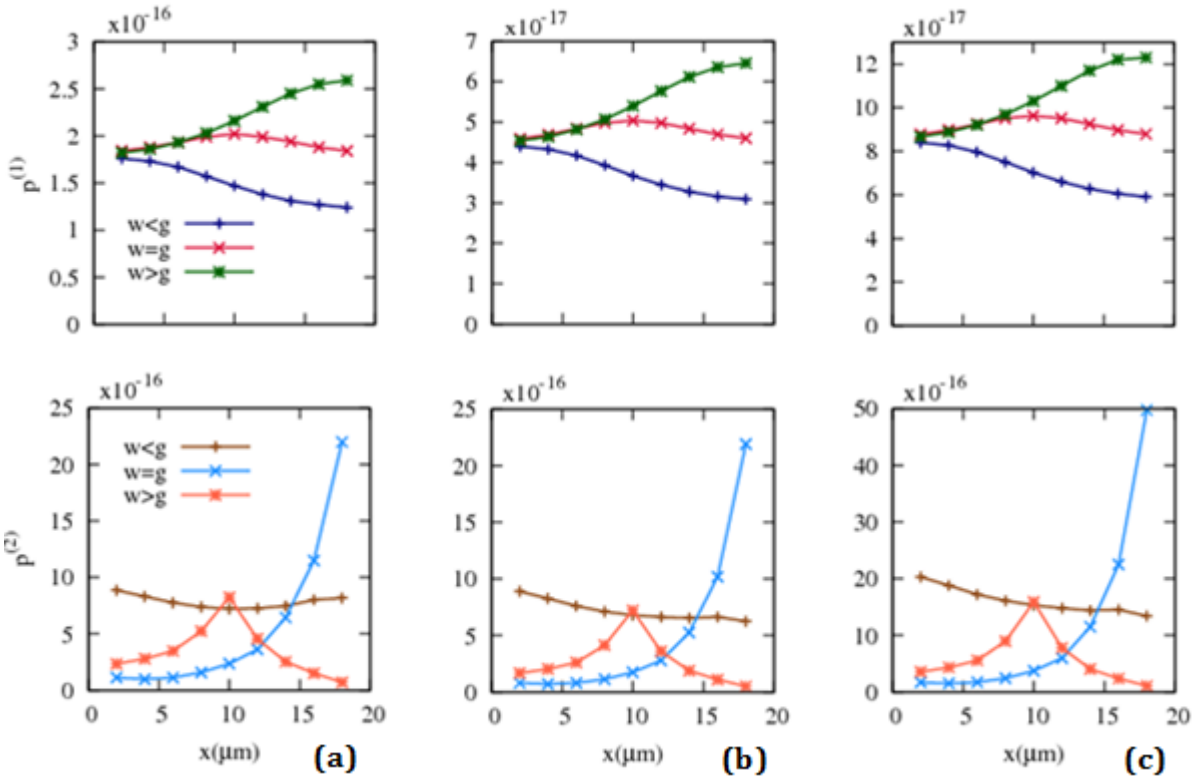

Figure 6.8. General effective moments in the near-field region of the interdigitated electrode geometry – Variations with particle position x along the horizontal axis of the effective dipole ($p^{(1)}$) and quadrupole ($p^{(2)}$) moments of (a) spherical (r=1μm), (b) ellipsoidal (a=1μm, b=0.5μm) and (c) brick-shaped (a=1μm, b=0.5μm) particles positioned in the near-field $(y = 10\mu m)$ region of the interdigitated electrode geometry (of specifications given in figure 6.2) with three different combinations of electrode width w and spacing g: $w < g$ $(w = 10\mu m, g = 30\mu m), w = g$ $(w = 20\mu m, g = 20\mu m), w > g$ $(w = 30\mu m, g = 10\mu m)$. Legend and vertical axis labels in part (a) apply to all figure parts.

It is clearly observed that particle geometry does not have any effect on the trends with which the moments vary with position x along the horizontal axis. Variation patterns with x of the effective dipole and quadrupole moments are found to be similar to those of the electric field magnitude and first-order gradient, respectively. As with field curvatures, the effective moments are seen to be notably affected by variations in electrode dimensions. Changing electrode width by 50% is seen to give rise to order-of-magnitude changes in the effective quadrupole moments of spherical and non-spherical particles. Values of the effective dipole and quadrupole moments of a given particle shape at a given position within the near-field region are seen to be of about the same order of magnitude.

6.3.1.2. The mid-field region

Results obtained for the effective dipole and quadrupole moments of spherical, ellipsoidal and brick-shaper particles positioned in the mid-field region of the interdigitated electrode geometry are shown in figure 6.9. It can be seen that as in the near-field region, particle geometry is of no effect on the trends with which the moments vary with position x along the horizontal axis. Instead, variation patterns with x of first- and second-order effective moments are seen to be similar to those of the electric field magnitude and first-order gradient, respectively.

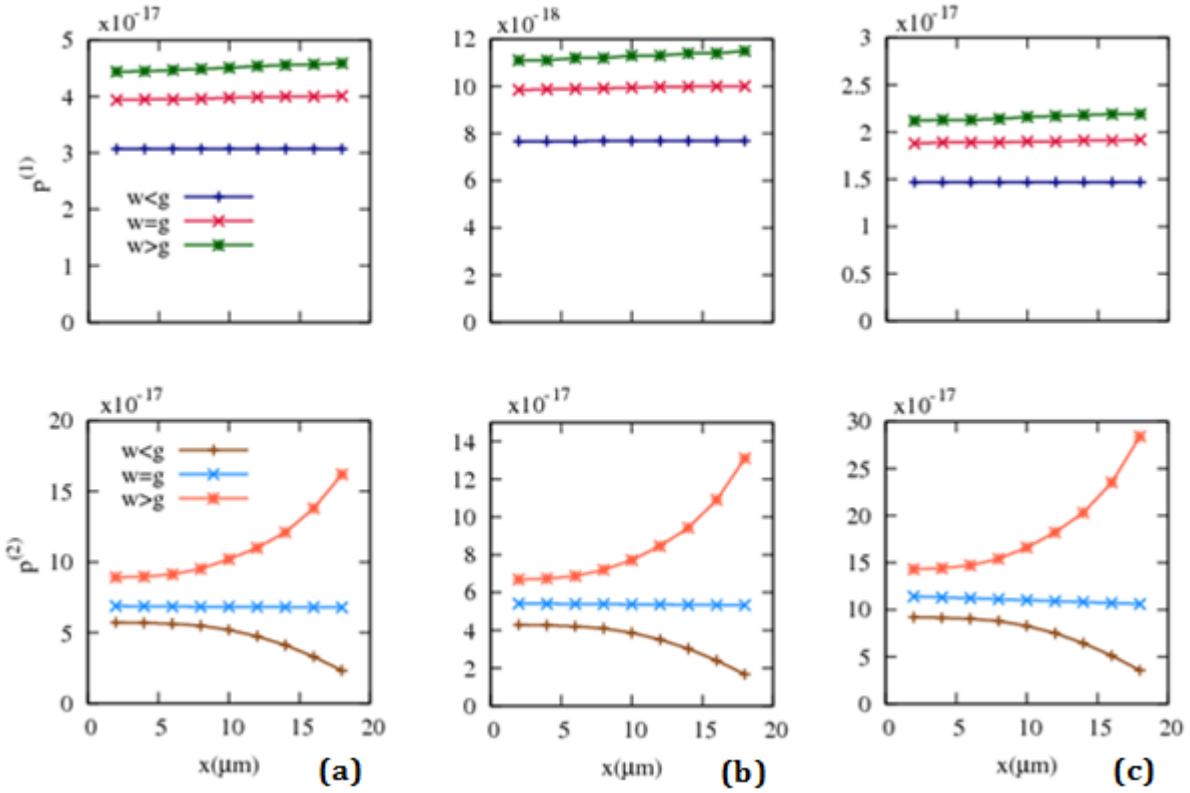

Figure 6.9. General effective moments in the mid-field region of the interdigitated electrode geometry – Variations with particle position x along the horizontal axis of the effective dipole ($p^{(1)}$) and quadrupole ($p^{(2)}$) moments of (a) spherical (r=1μm), (b) ellipsoidal (a=1μm, b=0.5μm) and (c) brick-shaped (a=1μm, b=0.5μm) particles positioned in the mid-field ($y = 30\mu m$) region of the interdigitated electrode geometry (of specifications given in figure 6.2) with three different combinations of electrode width w and spacing g: $w < g$ $(w = 10\mu m, g = 30\mu m)$, $w = g$ $(w = 20\mu m, g = 20\mu m)$, $w > g$ $(w = 30\mu m, g = 10\mu m)$. Legend and vertical axis labels in part (a) apply to all figure parts.

As with the electric field magnitude, the effective dipole moment is seen to be almost constant – for a given set of electrode dimensions w and g – throughout the mid-field region. Increasing the width/spacing ratio of the interdigitated electrodes is seen to give rise to larger effective dipole moments for a given particle shape. The effective quadrupole moment

is also seen to be larger with wider electrodes. It may be noticed that although variation patterns with x of the second-order moment are similar to those of the first-order field gradient, changes in the former are much more pronounced than those of the latter as x is varied from 2μm to 18μm. The effective quadrupole moment is seen to increase, decrease or remain almost constant upon increases in x, depending on whether the width w of the interdigitated electrodes is larger than, smaller than or equal to inter-electrode spacing, respectively.

6.3.1.3. The far-field region

Results obtained for the first two effective moments of spherical, ellipsoidal and brick-shaped particles positioned in the far-field region of the interdigitated electrode geometry, near the insulating lid, are shown in figure 6.10.

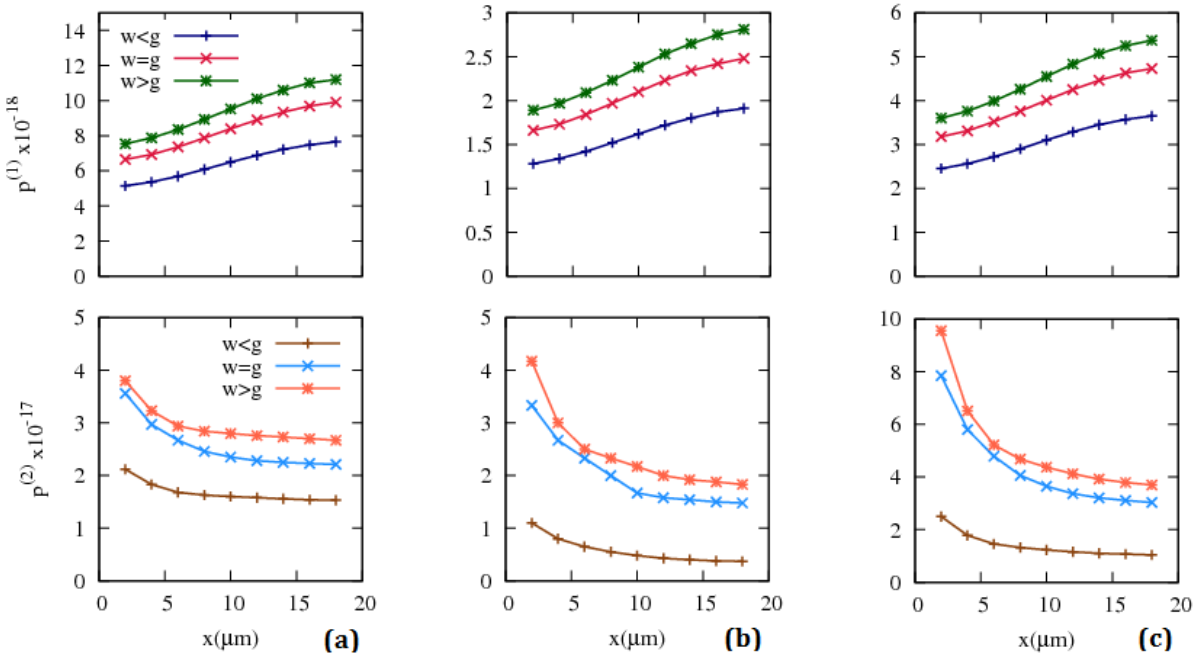

Figure 6.10. General effective moments in the far-field region of the interdigitated electrode geometry – Variations with particle position x along the horizontal axis of the effective dipole ($p^{(1)}$) and quadrupole ($p^{(2)}$) moments of (a) spherical (r=1μm), (b) ellipsoidal (a=1μm, b=0.5μm) and (c) brick-shaped (a=1μm, b=0.5μm) particles positioned in the far-field ($y = 50\mu m$) region of the interdigitated electrode geometry (of specifications given in figure 6.2) with three different combinations of electrode width w and spacing g: $w < g$ ($w = 10\mu m, g = 30\mu m$), $w = g$ ($w = 20\mu m, g = 20\mu m$), $w > g$ ($w = 30\mu m, g = 10\mu m$). Legend and vertical axis labels in part (a) apply to all figure parts.

It can be seen that as in near- and mid-field regions, variation patterns with x of the effective dipole and quadrupole moments are similar to those of the field magnitude and first-order

gradient, respectively, and independent of particle shape. The effect of the field curvature caused by the nearby insulating lid is seen to be first-order moments that increase and second-order moments that decrease with increasing x, for all three particle shapes. As in the mid-field region, increasing the width/spacing ratio of the interdigitated electrodes is seen to give rise to larger effective dipole and quadrupole moments for spherical and non-spherical particles.

6.3.2. Discussion

This section discusses the results presented in the previous section on the general effective moments of spherical and non-spherical particles at different positions within an interdigitated electrode configuration by analysing the effects of electric field and particle geometry on first- and higher-order moments.

6.3.2.1. Effect of electric field geometry

The effect of electric field geometry on first- and second-order moments can be analysed by observing the effects of two sets of parameters: particle position within the electrode geometry (horizontal and vertical), and electrode dimensions (width and spacing). The effects of electrode dimensions and particle position along the horizontal axis were shown through the plots in the previous section. This section is aimed at investigating the effect of particle distance from electrode surface, i.e. vertical particle position, on the general effective moments and, importantly, on the significance of the quadrupole moment.

Figure 6.11 compares the effective dipole moments of an ellipsoidal particle (as an example particle shape) positioned at three different distances above the interdigitated electrode array, within the insulator-capped channel. It can be seen that for all three combinations of electrode width and spacing, the effective dipole moment increases by about an order of magnitude as the particle is brought from the far-field to the mid-field or from the mid-field to the near-field region of the interdigitated electrode geometry. The figure also demonstrates that as observed earlier, and as expected from proximity with the electrode array, the effect of electrode dimensions on the effective dipole moments is most significant in the near-field region of the electrode geometry, where the trend with which the dipole moment varies with position along the horizontal axis is seen to be determined by the width/spacing ratio of the interdigitated electrodes.

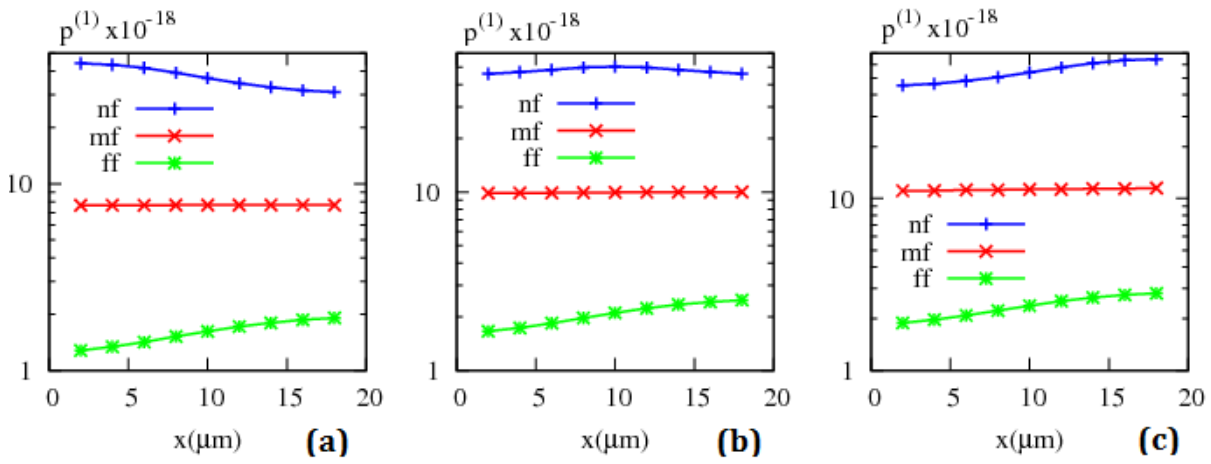

Figure 6.11. Effect of distance from electrode surface on general effective dipole moments in the interdigitated electrode geometry – Variations with position x along the horizontal axis of the effective dipole moment ($p^{(1)}$) of an ellipsoidal (a=1μm, b=0.5μm) particle positioned in three different regions within the interdigitated electrode geometry (of specifications given in figure 6.2), corresponding to three different heights above the electrode array; near-field (nf), mid-field (mf) and far-field regions correspond to particle centre heights of 10μm, 30μm and 50μm, respectively, above the electrode surface. The results are obtained with three different combinations of electrode width w and spacing g: (a) $w < g$ $(w = 10\mu m, g = 30\mu m)$, (b) $w = g$ $(w = 20\mu m, g = 20\mu m)$, and (c) $w > g$ $(w = 30\mu m, g = 10\mu m)$.

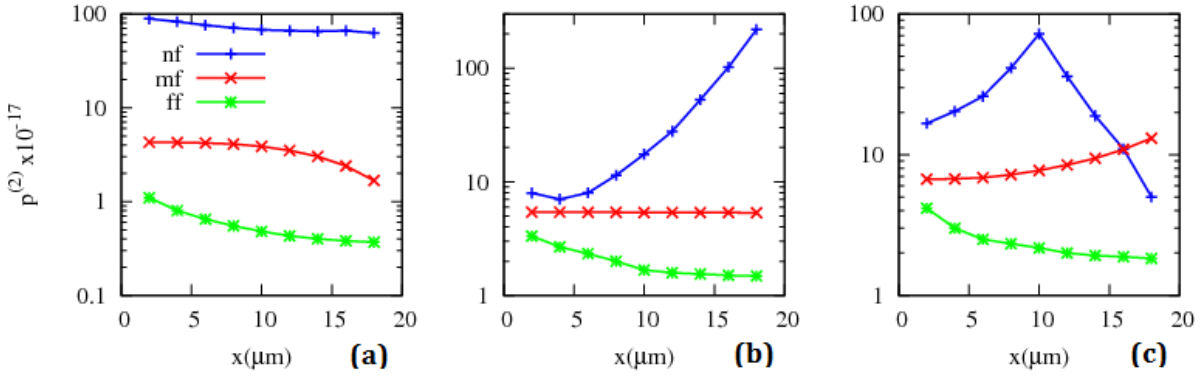

Figure 6.12. Effect of distance from electrode surface on general effective quadrupole moments in the interdigitated electrode geometry – Variations with position x along the horizontal axis of the effective quadrupole moment ($p^{(2)}$) of an ellipsoidal (a=1μm, b=0.5μm) particle positioned in three different regions within the interdigitated electrode geometry (of specifications given in figure 6.2), corresponding to three different particle centre heights above the electrode array; near-field (nf), mid-field (mf) and far-field regions correspond to particle centre heights of 10μm, 30μm and 50μm, respectively, above the electrode surface. The results are obtained with three different combinations of electrode width w and spacing g: (a) $w < g$ $(w = 10\mu m, g = 30\mu m)$, (b) $w = g$ $(w = 20\mu m, g = 20\mu m)$, and (c) $w > g$ $(w = 30\mu m, g = 10\mu m)$. Legend and vertical axis label in part (a) apply to all figure parts.

The effective quadrupole moments of the same ellipsoidal particle are compared in figure 6.12 for when the particle is positioned at three different heights above the interdigitated

electrode array. It can be seen that for all three combinations of electrode width and spacing, and at almost all positions x along the horizontal axis, the effective quadrupole moment is largest in the near-field region of the interdigitated geometry. The extent by which the quadrupole moments in the three regions of the electrode geometry differ is seen to depend on the width/spacing ratio of the interdigitated electrodes and also on position along the horizontal axis. Quadrupole moments in mid- and far-field regions of the interdigitated geometry are seen to be on about the same order of magnitude.

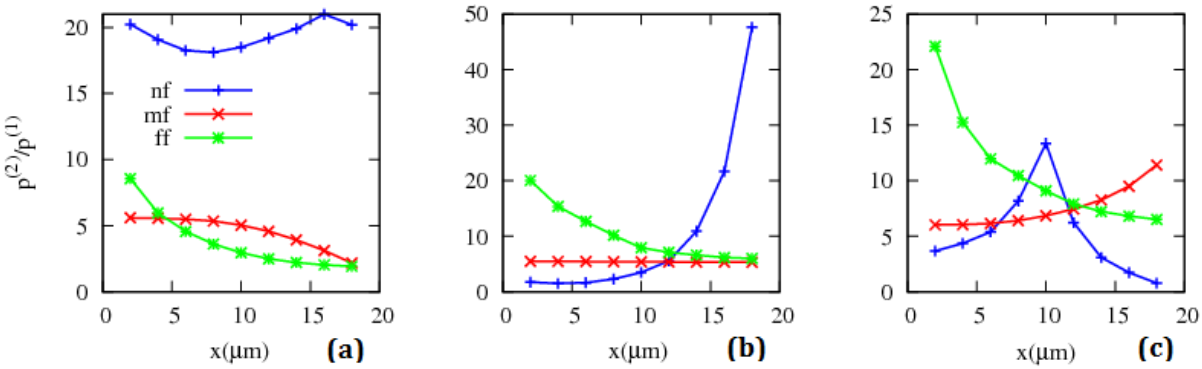

Figure 6.13. Effect of distance from electrode surface on the significance of the general effective quadrupole moment in the interdigitated electrode geometry – Variations with position x along the horizontal axis of the ratio of second- over first-order moments of an ellipsoidal (a=1μm, b=0.5μm) particle positioned in three different regions within the interdigitated electrode geometry (of specifications given in figure 6.2), corresponding to three different heights above the electrode array; near-field (nf), mid-field (mf) and far-field regions correspond to particle centre heights of 10μm, 30μm and 50μm, respectively, above the electrode surface. The results are obtained with three different combinations of electrode width w and spacing g: (a) $w < g$ $(w = 10\mu m, g = 30\mu m)$, (b) $w = g$ $(w = 20\mu m, g = 20\mu m)$, and (c) $w > g$ $(w = 30\mu m, g = 10\mu m)$. Legend and vertical axis label in part (a) apply to all figure parts.

The significance of the effective quadrupole moment at different distances from the interdigitated electrode array is shown in figure 6.13, where the ratio of second- over first-order moments of an ellipsoidal particle at three different regions within the interdigitated geometry are compared, for three different combinations of electrode width and spacing. It can be seen that in most instances the effective quadrupole moment is comparable to, and in many cases larger than, the effective dipole moment.

The relationship between effective moment ratios at different distances from the electrode array is seen to heavily depend on the width/spacing ratio of the interdigitated electrodes. When electrode width is smaller than inter-electrode spacing, the effective quadrupole moment is seen to be most significant in the near-field region of the interdigitated geometry.

When $w > g$, the effective moment ratio is seen to be largest in the far-field region, near the insulating lid. Even in the mid-field region, away from the field curvatures due to the electrode array or the glass lid, the quadrupole moment is found to be comparable to the first-order moment. The observations imply that invoking the dipole approximation for particle characterisation will be subject to considerable error at all but very few positions within the interdigitated electrode geometry.

6.3.2.2. Effect of particle geometry

The effect of electric field geometry on general effective moments in the interdigitated electrode geometry was discussed in the previous section by analysing an ellipsoid as an example particle shape. This section is aimed at investigating the effect of particle geometry on first- and higher-order moments by comparing the results obtained with spherical, ellipsoidal and brick-shaped particles of similar dimensions at different positions within an interdigitated electrode configuration.

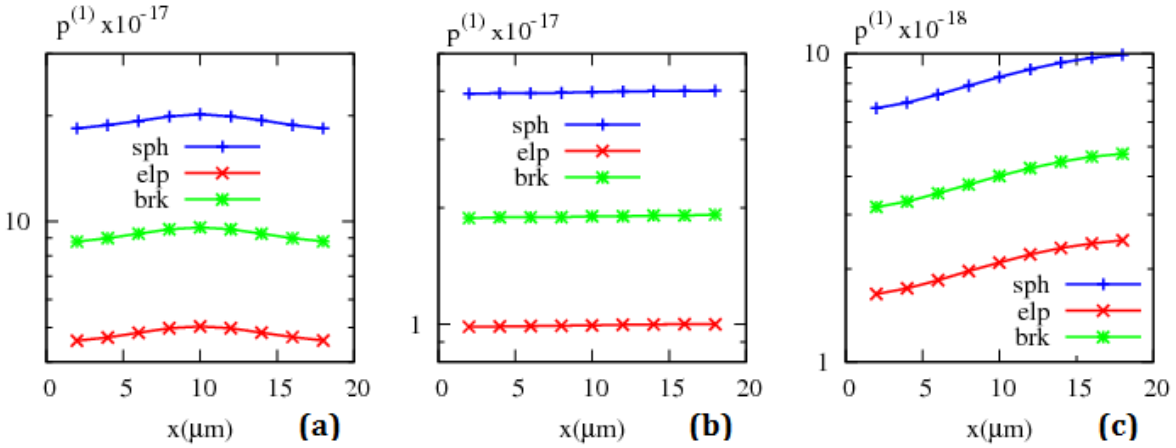

Figure 6.14. Effect of particle shape on general effective dipole moments in the interdigitated electrode geometry – Variations with position x along the horizontal axis of the effective dipole moments of spherical (sph) (r=1μm), (b) ellipsoidal (elp) (a=1μm, b=0.5μm) and (c) brick-shaped (brk) (a=1μm, b=0.5μm) particles positioned in (a) near-field $(y = 10\mu m)$, (b) mid-field $(y = 30\mu m)$, and (c) far-field $(y = 50\mu m)$ regions of the interdigitated electrode geometry (of specifications given in figure 6.2) with equal electrode width and spacing: $w = g = 20\mu m$.

Figure 6.14 compares the effective dipole moments of spherical, ellipsoidal and brick-shaped particles positioned in each of the three regions within the interdigitated electrode geometry (as specified in figure 6.4) with a sample combination of electrode width and spacing ($w = g = 20\mu m$). It is understood from the data in the plots that the effective dipole moment is directly proportional to particle volume, being largest for the spherical and smallest for the ellipsoidal particle. The same observation is made with other electrode width/spacing ratios.

The results imply that if particle characterisation is to be made based on the dipole approximation, i.e. ignoring higher-order moments, non-spherical particles of arbitrary shape can be modelled as spheres of equal volume, with zero error incurred.

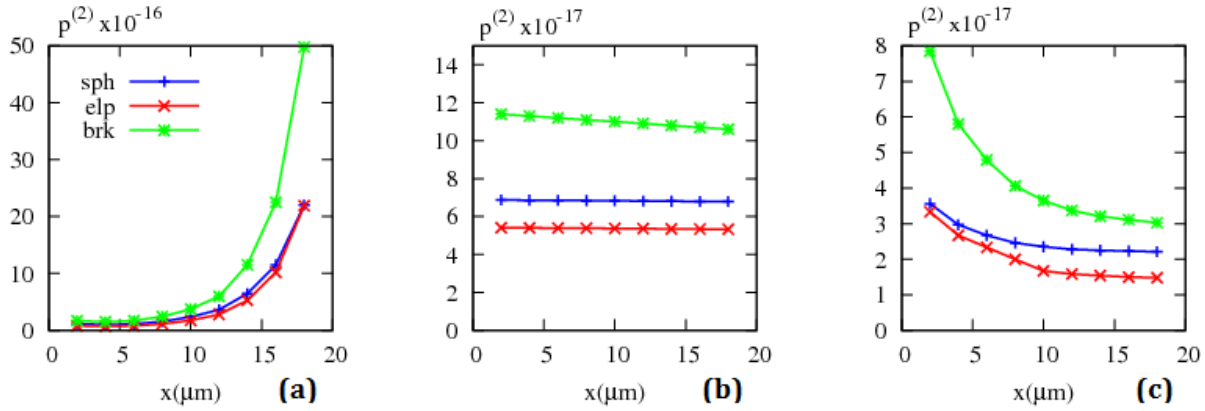

Figure 6.15. Effect of particle shape on general effective quadrupole moments in the interdigitated electrode geometry – Variations with position x along the horizontal axis of the effective quadrupole moments of spherical (sph) (r=1μm), (b) ellipsoidal (elp) (a=1μm, b=0.5μm) and (c) brick-shaped (brk) (a=1μm, b=0.5μm) particles positioned in (a) near-field $(y = 10\mu m)$, (b) mid-field $(y = 30\mu m)$, and (c) far-field $(y = 50\mu m)$ regions of the interdigitated electrode geometry (of specifications given in figure 6.2) with equal electrode width and spacing: $w = g = 20\mu m$. Legend in part (a) applies to all figure parts.

The effective quadrupole moments of the same particles positioned in near-, mid- and far-field regions of the interdigitated electrode geometry are compared in figure 6.15. The second-order moment is clearly not proportional to particle volume. In all of the three regions within the interdigitated electrode geometry, the effective quadrupole moment is seen to be largest for the brick-shaped and smallest for the ellipsoidal particle. Due to the quadrupole moment not being proportional to particle volume, approximation of non-spherical particles with spheres, albeit of equal volume, will be subject to considerable error.

Figure 6.16 shows the significance of the effective quadrupole moment for particles of different shapes through plots of variations with particle position along the horizontal axis of the ratio of second- over first-order moments of spherical, ellipsoidal and brick-shaped particles in near-, mid- and far-field regions of the interdigitated electrode geometry.

It can be seen that non-spherical particles possess notably more significant higher-order moments than a spherical particle of similar dimension. The second- over first-order effective moment ratio is seen to range from values no smaller than ~0.5 to as larger as ~50 depending on particle position within the interdigitated geometry. It can be noticed that the effective quadrupole moment of the spherical particle, although less significant than that of

non-spherical particles, can reach values notably (~10 times) larger than its effective dipole moment. It may therefore be concluded that invoking the dipole approximation for characterisation of particles (spherical *or* non-spherical) incurs significant error. The error is notably larger if the particle being characterised is non-spherical in shape, in which case approximation with a sphere will not reduce the error to negligible values.

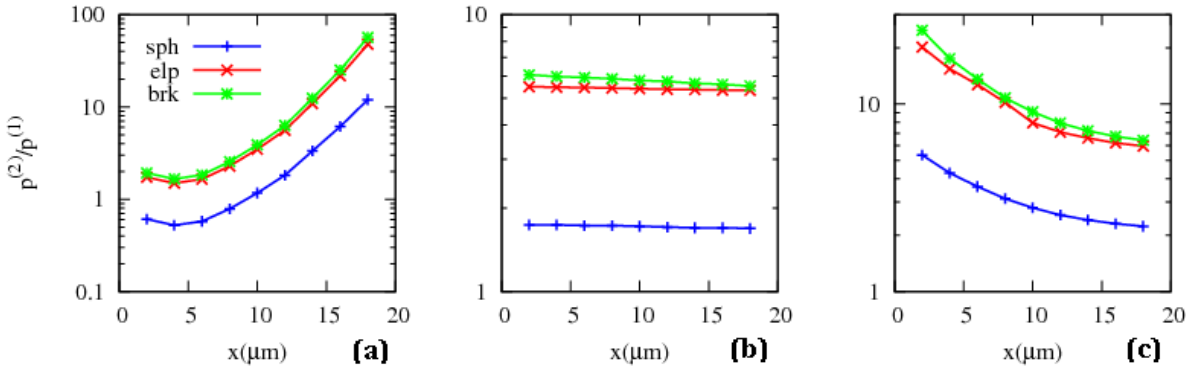

Figure 6.16. Effect of particle shape on the significance of the general effective quadrupole moment in the interdigitated electrode geometry – Variations with position x along the horizontal axis of the ratio of second- over first-order moments of an ellipsoidal (a=1μm, b=0.5μm) particle positioned in three different regions within the interdigitated electrode geometry (of specifications given in figure 6.2), corresponding to three different heights above the electrode array; near-field (nf), mid-field (mf) and far-field regions correspond to particle centre heights of 10μm, 30μm and 50μm, respectively, above the electrode surface. The results are obtained with three different combinations of electrode width w and spacing g: (a) $w < g$ $(w = 10\mu m, g = 30\mu m)$, (b) $w = g$ $(w = 20\mu m, g = 20\mu m)$, and (c) $w > g$ $(w = 30\mu m, g = 10\mu m)$. Legend and vertical axis label in part (a) apply to all figure parts.

Table 6.1. Errors incurred in values of effective dipole and quadrupole moments of non-spherical particles upon approximation with simpler shapes of similar dimensions – List of ratios of the effective dipole and quadrupole moments of model particles (spheres or ellipsoids) over those of original particles (ellipsoids or brick-shaped particles) positioned in near- (nf), mid- (mf) and far-field (ff) regions of the interdigitated electrode geometry (of specifications given in figures 6.2 and 6.4) with $w = g = 20\mu m$. Different ratios are obtained at different positions within each of the three regions in the electrode geometry. Values in the table represent averages of ratios at different particle positions in each region.

Original particle	**Model particle**	**$p^{(1)}$ ratio**			**$p^{(2)}$ ratio**		
		nf	**mf**	**ff**	**nf**	**mf**	**ff**
Ellipsoid (a=1μm,b=0.5μm)	Sphere (r=1μm)	4.0	4.0	4.0	1.3	1.3	2.0
Brick-shaped (a=1μm,b=0.5μm)	Sphere (r=1μm)	2.1	2.1	2.1	0.6	0.6	0.9
Brick-shaped (a=1μm,b=0.5μm)	Ellipsoid (a=1μm,b=0.5μm)	0.5	0.5	0.5	0.5	0.5	0.8

Errors incurred in the values of the effective dipole and quadrupole moments of ellipsoidal and brick-shaped particles when they are modelled with simpler shapes (spheres/ellipsoids) of similar dimensions is listed in Table 6.1 for when the particles are positioned in near-, mid- and far-field regions of the interdigitated electrode geometry with $w = g = 20\mu m$. For the first-order effective moment, the ratios represent the volume ratio of original and model particles – as expected from the direct proportionality of the effective dipole moment with particle volume. When dimensions of the model particle are adjusted for volumes to equate, the effective dipole moments are also seen to equate, bringing the approximation error down to 0. The observation confirms that, as in axial symmetry, if the dipole approximation is to be invoked for effective moment-based particle characterisation, particles of any shape can be modelled as spheres of equal volume with no error incurred in the value of the effective dipole moment.

The effective quadrupole moment is not proportional to particle volume and, as a result, the ratios of the second-order effective moments of model and original particles are seen not to reduce to negligible values even when dimensions of the model particle are adjusted for equal volumes. It can be concluded, given the increased significance of higher order moments for non-spherical particles (evident from figure 6.16), that effective moment-based characterisation of non-spherical particles can be erroneous if the dipole approximation is invoked and/or if the particle is modelled with a simpler shape, albeit of equal volume.

6.3.3. Summary and conclusions

A novel method for the determination of general effective moments has been exploited to derive the effective dipole and quadrupole moments of spherical, ellipsoidal and brick-shaped particles at different positions within an interdigitated electrode configuration. It has been shown that the trends with which the first- and second-order moments vary with horizontal particle position at a given height above the electrode array are determined solely by those of the electric field magnitude and first-order gradient, and are hence independent of particle geometry. As with the field curvature, electrode geometry – through width and spacing of the interdigitated electrodes – is seen to have a significant effect on variation patterns with particle position of first- and higher-order moments.

Effective dipole and quadrupole moments of spherical and non-spherical particles have been seen to decrease in magnitude as particles distance from the electrode array. The significance of the effective quadrupole moment, defined as its ratio over the first-order moment, has been observed to bear a more complicated dependency on particle distance from the electrode surface. It has been shown that, depending on the width/spacing ratio of the

interdigitated electrodes, the effective quadrupole moment can be most significant near the insulating lid that caps the channel above the electrode array.

It has been shown that the effective dipole moment is directly proportional to particle volume. Consequently, if particle characterisation is to be made using the dipole approximation, non-spherical particles can be modelled as spheres of equal volume with zero error incurred. However, it has been shown that the effective quadrupole moment is comparable to, and in most instances larger than, the effective dipole moment for spherical and non-spherical particles – with non-spherical particles possessing notably more significant higher-order moments. As a result, any characterisation of spherical or non-spherical particles (albeit modelled as spheres of equal volume) will be subject to significant error if the effective quadrupole moment is not accounted for.

6.4. The dielectrophoretic force terms

This section presents and discusses calculations, using the effective moment method, of first- and second-order terms of the dielectrophoretic force on spherical, ellipsoidal and brick-shaped particles at different positions within an interdigitated electrode configuration. The results will be presented in three different sections, one for each of the three regions in the interdigitated electrode geometry (as specified in figure 6.4). Units for the DEP force terms will be pico-Newtons (pN).

6.4.1. Results and discussion

6.4.1.1. The near-field region

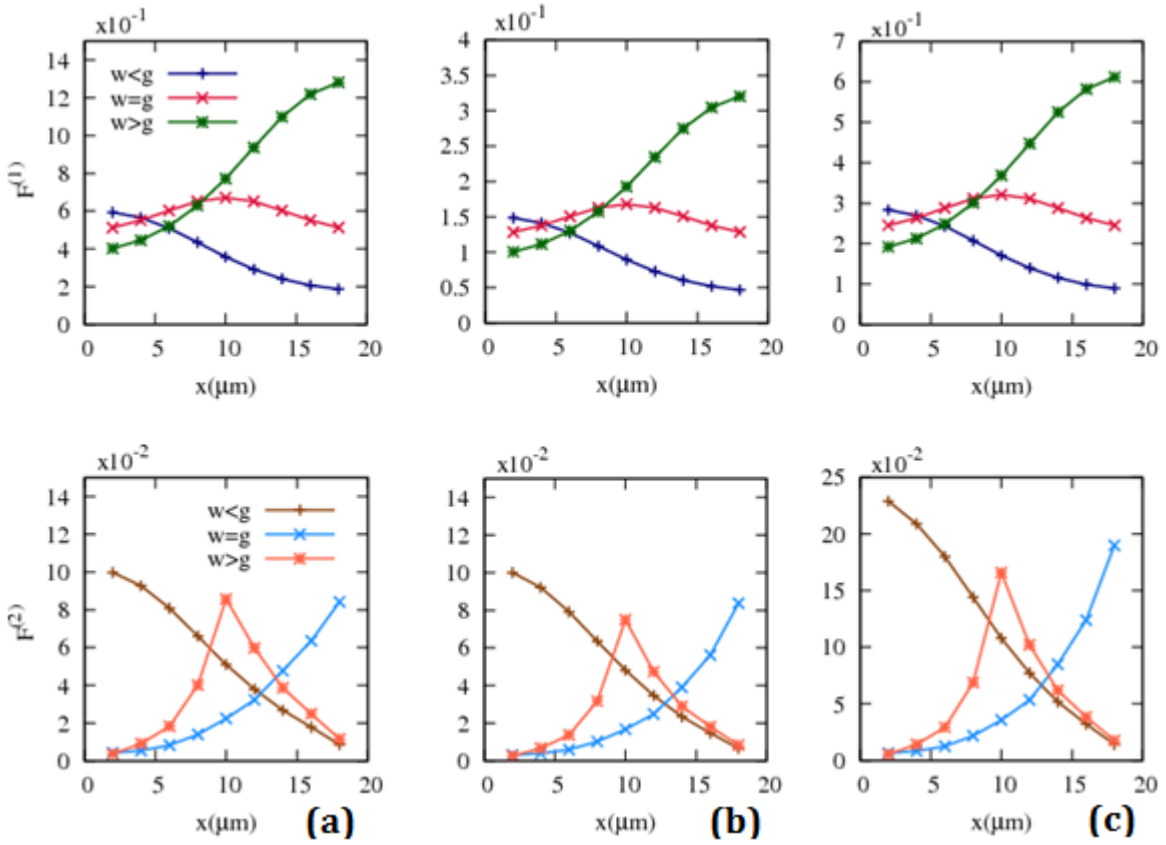

Figure 6.17. Dielectrophoretic force terms in the near-field region of the interdigitated electrode geometry – Variations with particle position x along the horizontal axis of first- ($F^{(1)}$) and second-order ($F^{(2)}$) terms of the dielectrophoretic force on (a) spherical (r=1μm), (b) ellipsoidal (a=1μm, b=0.5μm) and (c) brick-shaped (a=1μm, b=0.5μm) particles positioned in the near-field ($y = 10\mu m$) region of the interdigitated electrode geometry (of specifications given in figure 6.2) with three different combinations of electrode width w and spacing g: $w < g$ ($w = 10\mu m, g = 30\mu m$), $w = g$ ($w = 20\mu m, g = 20\mu m$), $w > g$ ($w = 30\mu m, g = 10\mu m$). Legend and vertical axis labels in part (a) apply to all figure parts.

Figure 6.17 shows the results obtained for dipolar and quadrupolar DEP forces on spherical, ellipsoidal and brick-shaped particles positioned in the near-field region of the interdigitated electrode geometry with three different combinations of electrode width w and spacing g: $w < g$ $(w = 10\mu m, g = 30\mu m), w = g$ $(w = 20\mu m, g = 20\mu m), w > g$ $(w = 30\mu m, g = 10\mu m)$. It can be seen that as with field curvatures and effective moments, variation patterns with x of the DEP force terms are independent of particle geometry. On the contrary, electrode geometry – through width and spacing of the interdigitated electrodes – is seen to have a significant effect on the DEP force terms: magnitudes of the force terms and the trends with which they vary with particle position within the near-field region are seen to be significantly affected by changes in the width/spacing ratio of the interdigitated electrodes.

Particle geometry, of no effect on the trends with which DEP force terms vary with positions within the near-field region, is seen to affect the strength of dipolar and quadrupolar forces. The first-order DEP force term is found to be directly proportional to particle volume, as expected from a similar observation made for the effective dipole moment. The spherical particle therefore experiences the strongest dipolar force among the three particle shapes. The quadrupolar DEP forces experienced by spherical and ellipsoidal particles are seen to be almost equal throughout the near-field region, while the brick-shaped particle is found to experience a notably stronger (more than twice in magnitude) quadrupolar force.

6.4.1.2. The mid-field region

Results obtained for first- and second-order terms of the dielectrophoretic force experienced by spherical, ellipsoidal and brick-shaped particles positioned within the mid-field region of the interdigitated electrode geometry are shown in figure 6.18 for three different combinations of electrode width and spacing. Variation patterns with x of dipolar and quadrupolar forces are seen to be similar to those of first- and second-order moments, respectively, as expected from the field gradients – which are multiplied by the moments to yield the DEP force terms – being almost independent of x throughout the mid-field region. It can be found, from a comparison of the plots in figures 6.17 and 6.18, that dipolar and quadrupolar forces on a particle in the mid-field region are smaller than those in the near-field region by one to two orders of magnitude.

The dipolar DEP force is seen to be almost constant, for a given width/spacing ratio of the interdigitated electrodes, and directly proportional to particle volume – as in the near-field region. The quadrupolar DEP force is seen to increase, decrease, or remain constant with increasing x, depending on whether electrode width w is larger than, smaller than, or equal to inter-electrode spacing g, respectively. Unlike the dipolar force, the quadrupolar term does

not show proportionality with particle volume and is found to be largest for the brick-shaped and smallest for the ellipsoidal particle – in agreement with, and indeed due to, similar observations for the effective quadrupole moment (figure 6.15).

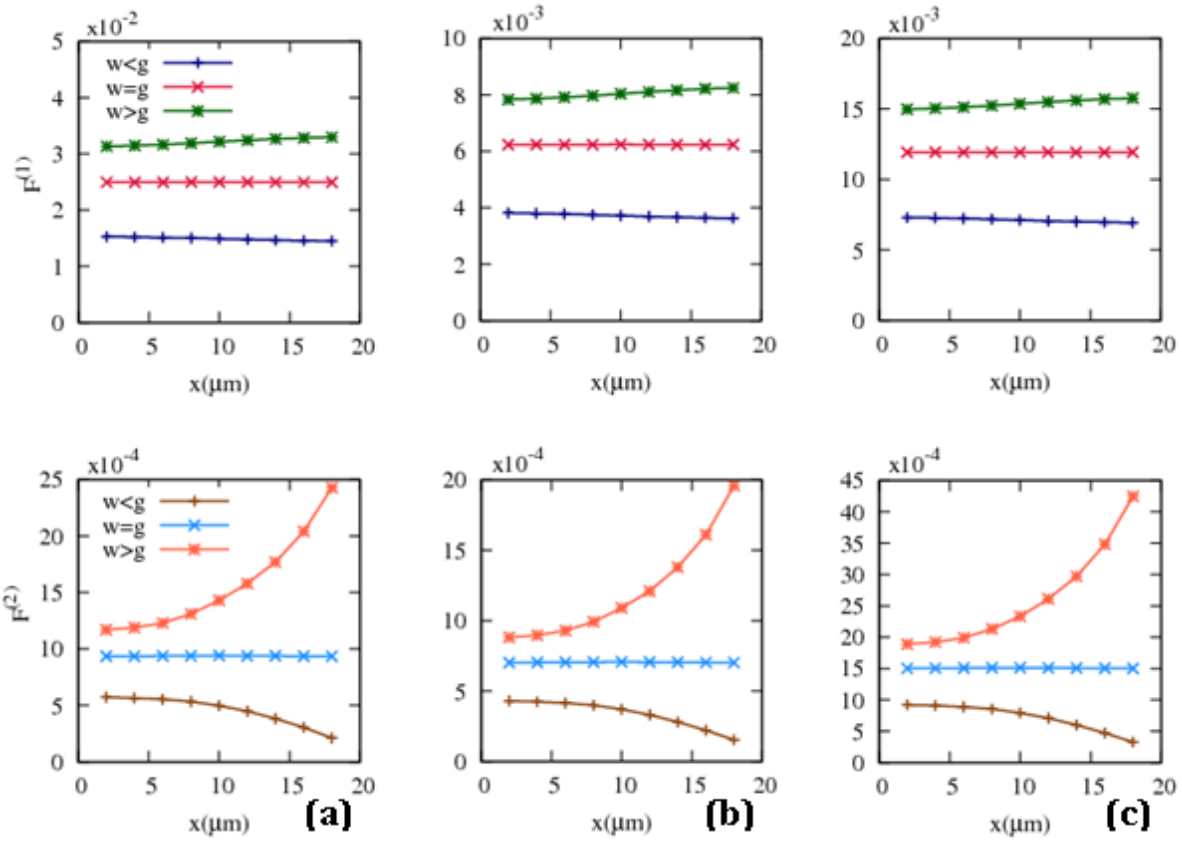

Figure 6.18. Dielectrophoretic force terms in the near-field region of the interdigitated electrode geometry – Variations with particle position x along the horizontal axis of first- ($F^{(1)}$) and second-order ($F^{(2)}$) terms of the dielectrophoretic force on (a) spherical (r=1μm), (b) ellipsoidal (a=1μm, b=0.5μm) and (c) brick-shaped (a=1μm, b=0.5μm) particles positioned in the mid-field ($y = 30\mu m$) region of the interdigitated electrode geometry (of specifications given in figure 6.2) with three different combinations of electrode width w and spacing g: $w < g$ ($w = 10\mu m, g = 30\mu m$), $w = g$ ($w = 20\mu m, g = 20\mu m$), $w > g$ ($w = 30\mu m, g = 10\mu m$). Legend and vertical axis labels in part (a) apply to all figure parts.

6.4.1.3. The far-field region

Variations with position x along the horizontal axis of the first- and second-order terms of the dielectrophoretic force on spherical, ellipsoidal and brick-shaped particles positioned in the far-field region of the interdigitated electrode geometry are shown in figure 6.19 for three different combinations of electrode width and spacing. It can be seen that as in near- and mid-field regions, the trends with which the DEP force terms vary with position along the horizontal axis are independent of particle geometry and determined by those of electric field

curvatures. Dipolar and quadrupolar forces are seen to attain values symmetrical around a maximum at the midpoint $x = 10\mu m$.

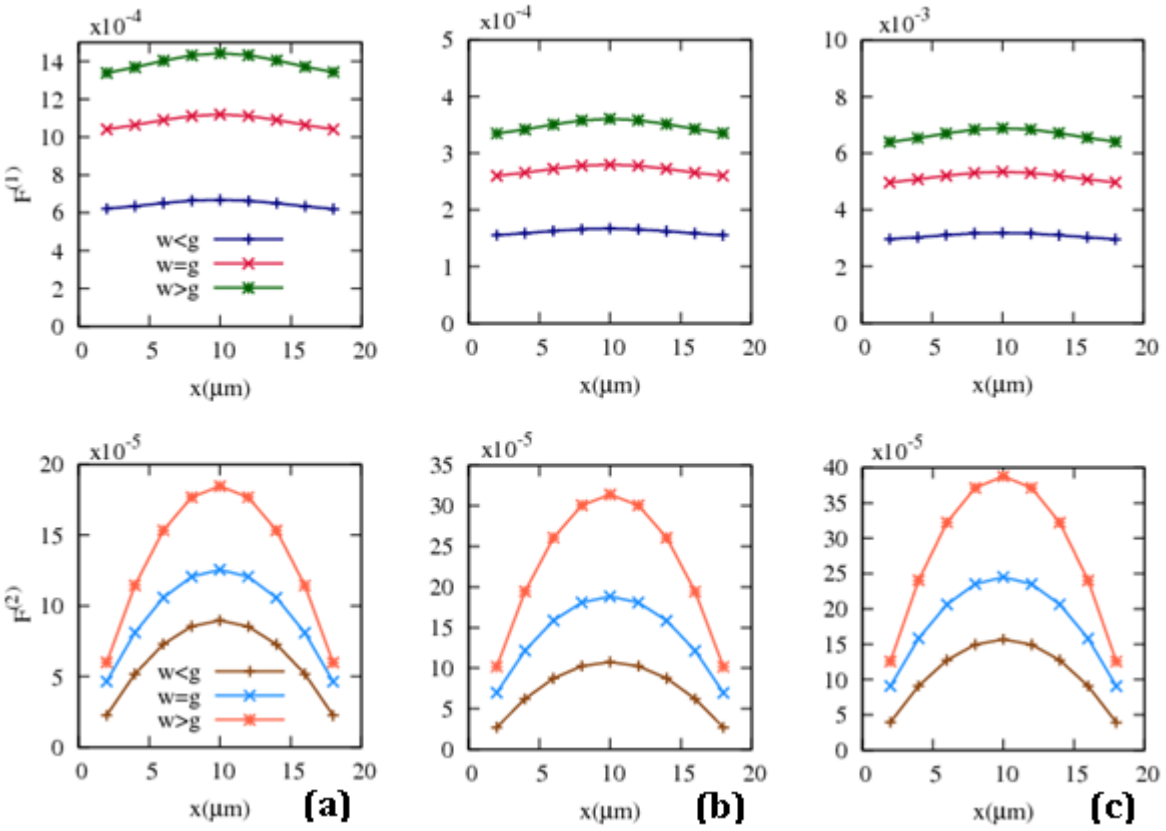

Figure 6.19. Dielectrophoretic force terms in the far-field region of the interdigitated electrode geometry – Variations with particle position x along the horizontal axis of first- ($F^{(1)}$) and second-order ($F^{(2)}$) terms of the dielectrophoretic force on (a) spherical (r=1μm), (b) ellipsoidal (a=1μm, b=0.5μm) and (c) brick-shaped (a=1μm, b=0.5μm) particles positioned in the far-field $(y = 50\mu m)$ region of the interdigitated electrode geometry (of specifications given in figure 6.2) with three different combinations of electrode width w and spacing g: $w < g$ $(w = 10\mu m, g = 30\mu m), w = g$ $(w = 20\mu m, g = 20\mu m), w > g$ $(w = 30\mu m, g = 10\mu m)$. Legend and vertical axis labels in part (a) apply to all figure parts.

Particle and electrode geometry, of no effect on the trends with which the force terms vary with position within the far-field region, are seen to notably affect the magnitudes of dipolar and quadrupolar forces. Greater width/spacing ratio for the interdigitated electrodes is seen to give rise to stronger first- and second-order DEP forces on spherical and non-spherical particles. At a given position within the far-field region, the quadrupolar force is seen to be strongest on the brick-shaped particle. As in near- and mid-field regions, the dipolar force is found to be directly proportional to particle volume. Dipolar and quadrupolar forces in the far-field region are seen to be weaker than those in the mid-field region of the interdigitated electrode geometry by about an order of magnitude.

6.4.2. Summary and conclusions

Results have been presented for first- and second-order terms of the dielectrophoretic force on spherical, ellipsoidal and brick-shaped particles at different positions within an interdigitated electrode configuration, corresponding to electric fields with varying curvature. The DEP force terms have been calculated from the effective moment method, by combining previously presented results for electric field gradients and effective moments. It is essentially the weighted, by a constant factor, multiplication of effective moments and field gradients that yields the DEP force terms. As a result, and as confirmed by the results just presented, the trends with which DEP force terms vary with position within the electrode geometry can be predicted from those of the electric field magnitude and its gradients.

Particle geometry has been shown to have no effect on variation patterns with position along the horizontal axis of the DEP force terms. However, particle shape has been shown to have a strong effect on the magnitudes of dipolar and quadrupolar forces at a given position within the electrode geometry. Due to the formulation of the effective moment method, discussions regarding the effects of particle and electrode geometry on effective dipole and quadrupole moments are identically valid for dipolar and quadrupolar DEP forces. The dipolar force has been confirmed to be directly proportional to particle volume. Discussions regarding the significance of the second-order DEP force term will be presented in the next section where Maxwell stress tensor calculations of the dielectrophoretic force are compared against DEP force term results obtained using the effective moment method to derive quadrupolar contributions to the total force.

6.5. The total dielectrophoretic force

This section presents and discusses calculations of the total dielectrophoretic force on spherical, ellipsoidal and brick-shaped particles at different positions within an interdigitated electrode configuration. The total DEP force is calculated using the Maxwell stress tensor (MST) method, which is known for its mathematical rigorousness in accounting for all elements of electrical force on a dielectric. MST calculations of the dielectrophoretic force will be compared against DEP force term results presented in the previous section to derive the quadrupolar contribution in different circumstances regarding particle and electric field geometry. In the results that will be presented, units for the DEP force will be pico-Newtons (pN).

6.5.1. Maxwell stress tensor calculations of the dielectrophoretic force

6.5.1.1. Results and discussion

Results obtained for the total dielectrophoretic force on spherical, ellipsoidal and brick-shaped particles positioned in the near-field region of the interdigitated electrode geometry, with three different combinations of electrode width and spacing, are shown in figure 6.20. Trends with which the DEP forces vary with position within the near-field region are seen not to be identical for particles of different shapes, as was shown to be the case for DEP force terms. The observation reflects on quadrupolar forces of differing significance for particles of different shapes.

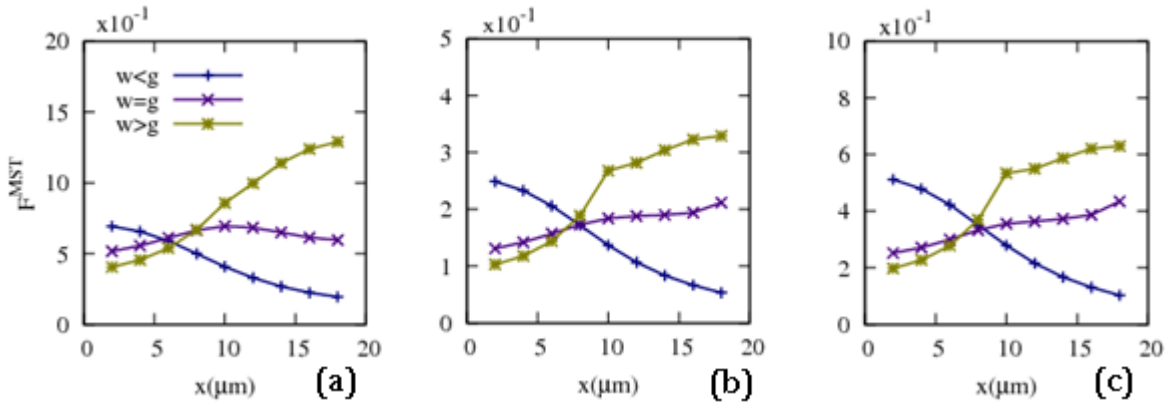

Figure 6.20. Total dielectrophoretic force in the near-field region of the interdigitated electrode geometry – Variations with particle position x along the horizontal axis of the total DEP force, calculated using the Maxwell stress tensor (MST) method, on (a) spherical (r=1μm), (b) ellipsoidal (a=1μm, b=0.5μm) and (c) brick-shaped (a=1μm, b=0.5μm) particles positioned in the near-field $(y = 10\mu m)$ region of the interdigitated electrode geometry (of specifications given in figure 6.2) with three different combinations of electrode width w and spacing g: $w < g$ $(w = 10\mu m, g = 30\mu m), w = g$ $(w = 20\mu m, g = 20\mu m), w > g$ $(w = 30\mu m, g = 10\mu m)$. Legend and vertical axis labels in part (a) apply to all figure parts.

As with DEP force terms, the total dielectrophoretic force in the near-field region is seen to be affected, in trends and magnitude, by variations in electrode width and spacing. Depending on particle position within the near-field region, increasing the width/spacing ratio of the interdigitated electrodes can give rise to an increase or decrease in the DEP force exerted on particles. At all positions within the near-field region, the DEP force is seen to be stronger on particles of larger volume although, due to the quadrupolar contribution, no direct proportionality with particle volume is observed.

Figure 6.21 shows variations with position within the mid-field region of the total dielectrophoretic force on spherical, ellipsoidal and brick-shaped particles. Due to the dipolar force being almost independent of particle position within the mid-field region (figure 6.18), the DEP force is seen to vary less notably in the mid-field region than in the near-field region of the interdigitated geometry.

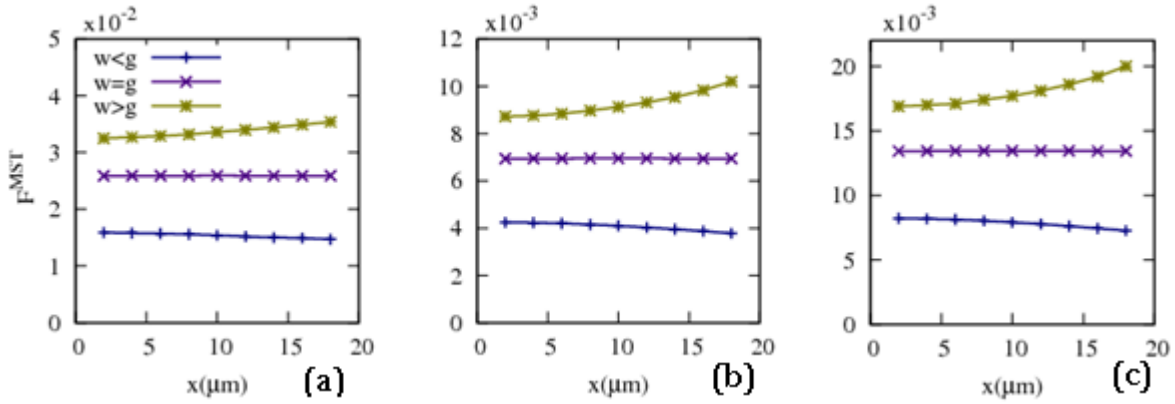

Figure 6.21. Total dielectrophoretic force in the mid-field region of the interdigitated electrode geometry – Variations with particle position x along the horizontal axis of the total DEP force, calculated using the Maxwell stress tensor (MST) method, on (a) spherical (r=1μm), (b) ellipsoidal (a=1μm, b=0.5μm) and (c) brick-shaped (a=1μm, b=0.5μm) particles positioned in the mid-field $(y = 30\mu m)$ region of the interdigitated electrode geometry (of specifications given in figure 6.2) with three different combinations of electrode width w and spacing g: $w < g$ $(w = 10\mu m, g = 30\mu m), w = g$ $(w = 20\mu m, g = 20\mu m), w > g$ $(w = 30\mu m, g = 10\mu m)$. Legend and vertical axis labels in part (a) apply to all figure parts.

For spherical and non-spherical particles, the DEP force is seen to increase, decrease or remain almost constant with increasing x, depending on whether electrode width is larger than, smaller than or equal to inter-electrode spacing, respectively. At any given position within the mid-field region, wider electrodes are found to give rise to stronger DEP forces on all particle shapes. As in the near-field region, the DEP force is seen to be stronger on particles of larger volume. As a particle moves vertically from the near-field to the mid-field

region of the interdigitated geometry, the DEP force it experiences is found to decrease by about an order of magnitude.

Results obtained for the total dielectrophoretic force on spherical, ellipsoidal and brick-shaped particles in the far-field region of the interdigitated electrode geometry, near the insulating lid, are shown in figure 6.22 for three different combinations of electrode width and spacing. As with first- and second-order force terms, the total DEP force on any of the three particle shapes is seen to attain values symmetrical around a maximum at the midpoint $x = 10\mu m$. Particle and electrode geometry are seen to affect the magnitude, and not variation patterns with position, of the dielectrophoretic force. As in near- and mid-field regions, the DEP force is found to be stronger on particles of larger volume. Increasing the width/spacing ratio of the interdigitated electrodes is seen to give rise to stronger DEP forces on spherical and non-spherical particles.

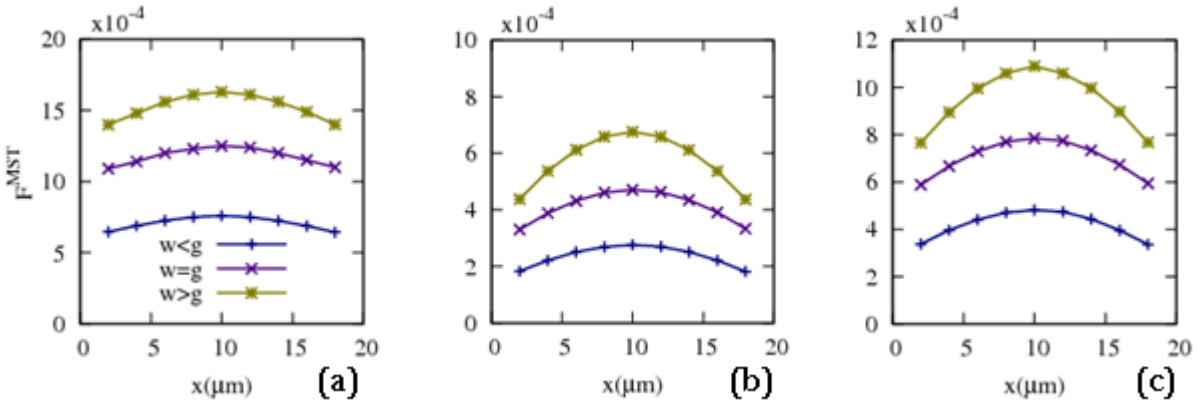

Figure 6.22. Total dielectrophoretic force in the far-field region of the interdigitated electrode geometry – Variations with particle position x along the horizontal axis of the total DEP force, calculated using the Maxwell stress tensor (MST) method, on (a) spherical (r=1μm), (b) ellipsoidal (a=1μm, b=0.5μm) and (c) brick-shaped (a=1μm, b=0.5μm) particles positioned in the far-field $(y = 50\mu m)$ region of the interdigitated electrode geometry (of specifications given in figure 6.2) with three different combinations of electrode width w and spacing g: $w < g$ $(w = 10\mu m, g = 30\mu m), w = g$ $(w = 20\mu m, g = 20\mu m), w > g$ $(w = 30\mu m, g = 10\mu m)$. Legend and vertical axis labels in part (a) apply to all figure parts.

6.5.1.2. Summary and conclusions

Calculations, using the Maxwell stress tensor method, of the total dielectrophoretic force on spherical, ellipsoidal and brick-shaped particles at different positions within an interdigitated electrode configuration have been presented. It has been shown that as with first- and second-order force terms, the total dielectrophoretic force is stronger on particles of larger volume. In what can be attributed to the significance of the quadrupolar term, the direct

proportionality with particle volume – observed previously for the dipolar force – has been found not to hold valid for the total DEP force. Electrode geometry, through the width/spacing ratio of the interdigitated electrodes, has been shown to have a significant effect on the magnitude of the DEP force on spherical and non-spherical particles. Near the electrode surface, variation patterns with position of the DEP force have also been seen to be affected notably by variations in electrode dimensions.

6.5.2. The significance of higher-order dielectrophoretic forces

This section is aimed at what forms the principal goal of this chapter and indeed the whole body of work: quantified evaluation of the significance of higher-order DEP forces in different circumstances regarding particle and electric field geometry. Results will be presented for quadrupolar contributions to the DEP force on spherical, ellipsoidal and brick-shaped particles at different positions within an interdigitated electrode configuration. Total force and force term results, calculated using completely different methods (Maxwell stress tensor and effective moment method, respectively), have been compared against each other to yield the second-order contribution to the DEP force: $F^{(2)}/F^{MST}$. In all of the wide-ranging positions within the interdigitated electrode geometry (as specified in figure 6.4) and for all three particle shapes, the sum of first- and second-order forces has been seen to equal the total DEP force (as obtained using the MST method) to within an error margin of no more than 1%. The observation importantly serves as verification for the results and allows for accurate determination of the quadrupolar contribution to the dielectrophoretic force.

6.5.2.1. Results and discussion

Quadrupolar contributions to the dielectrophoretic force on spherical, ellipsoidal and brick-shaped particles positioned in the near-field region of the interdigitated electrode geometry are shown in figure 6.23 for three different combinations of electrode width and spacing: $w < g$ $(w = 10\mu m, g = 30\mu m), w = g$ $(w = 20\mu m, g = 20\mu m), w > g$ $(w = 30\mu m, g = 10\mu m)$. It can be seen that, as expected from total force and force term results, the trends with which the second-order contributions, presented as percentage values, vary with position x along the horizontal axis are independent of particle geometry. Particle shape is, however, seen to have a notable effect on the actual magnitude of quadrupolar contributions: non-spherical particles are found to be subject to considerably more significant second-order forces compared to the spherical particle of similar dimensions. Maximum contribution from the quadrupolar term is seen to be ~14% for the spherical particle, whereas for ellipsoidal and brick-shaped particles, second-order contributions as high as ~40% and ~45% are

observed. The results show that near the electrode surface, the dipole approximation is particularly unreliable in predicting the DEP force on non-spherical particles.

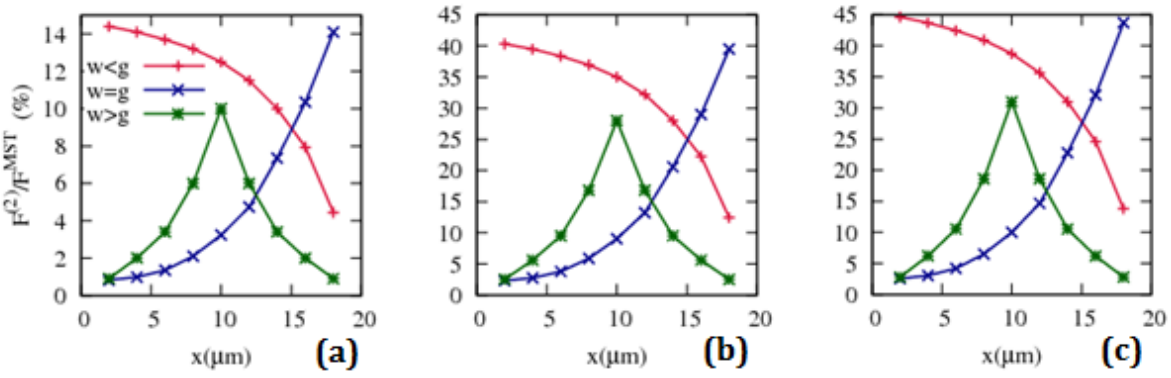

Figure 6.23. The significance of the second-order contribution to the dielectrophoretic force in the near-field region of the interdigitated electrode geometry – Variations with position x along the horizontal axis of the second-order contributions to the total DEP force on (a) spherical (r=1μm), (b) ellipsoidal (a=1μm, b=0.5μm) and (c) brick-shaped (a=1μm, b=0.5μm) particles positioned in the near-field $(y = 10\mu m)$ region of the interdigitated electrode geometry (of specifications given in figure 6.2) with three different combinations of electrode width w and spacing g: $w < g$ $(w = 10\mu m, g = 30\mu m), w = g$ $(w = 20\mu m, g = 20\mu m), w > g$ $(w = 30\mu m, g = 10\mu m)$. Legend and vertical axis labels in part (a) apply to all figure parts.

As with field curvature and, accordingly, effective moment, force term and total force results, electric field geometry is seen to have a significant effect on the significance of the quadrupolar DEP force on spherical and non-spherical particles positioned in the near-field region of the interdigitated geometry. The effect of electric field geometry is reflected through two parameters: the width/spacing ratio of the interdigitated electrodes and position x along the horizontal axis. The quadrupolar contribution profile is seen to be monotonically decreasing, monotonically increasing, or symmetrical around a maximum at the midpoint, depending on whether the width of the interdigitated electrodes is smaller than, equal to, or larger than inter-electrode spacing, respectively. At a given position within the near-field region, changing the width of interdigitated electrodes by 50% is seen to give rise to a notable change – from negligible to very significant, or vice versa – in the quadrupolar contribution to the DEP force on particles. For a given set of electrode dimensions, a given particle experiences a quadrupolar force of varying significance as it moves within the near-field region. As an example, for an ellipsoidal particle subjected to the electric field generated by evenly-spaced electrodes $(w = g)$, the quadrupolar contribution is seen to increase from $\sim$3% to $\sim$40% as the particle moves from one end of the near-field region $(x = 2\mu m)$ to another $(x = 18\mu m)$.

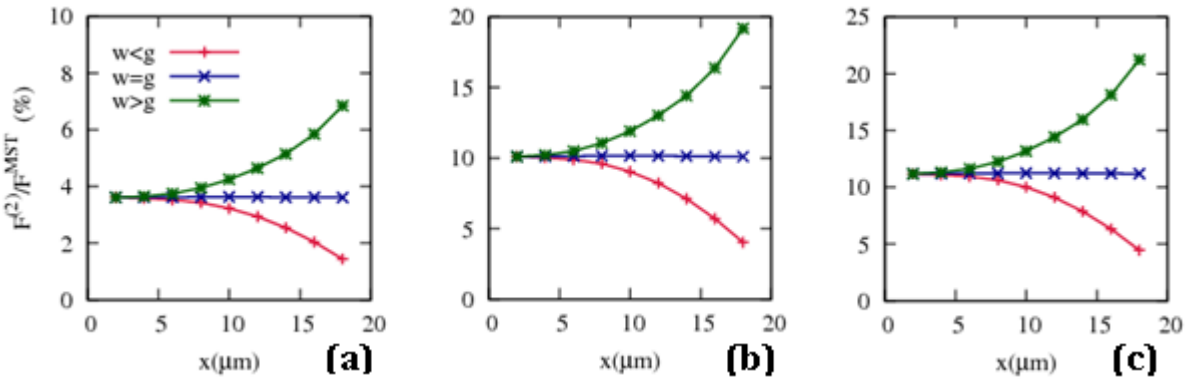

Figure 6.24. The significance of the second-order contribution to the dielectrophoretic force in the mid-field region of the interdigitated electrode geometry – Variations with position x along the horizontal axis of the second-order contributions to the total DEP force on (a) spherical (r=1μm), (b) ellipsoidal (a=1μm, b=0.5μm) and (c) brick-shaped (a=1μm, b=0.5μm) particles positioned in the mid-field $(y = 30\mu m)$ region of the interdigitated electrode geometry (of specifications given in figure 6.2) with three different combinations of electrode width w and spacing g: $w < g$ $(w = 10\mu m, g = 30\mu m), w = g$ $(w = 20\mu m, g = 20\mu m), w > g$ $(w = 30\mu m, g = 10\mu m)$. Legend and vertical axis labels in part (a) apply to all figure parts.

Results obtained for second-order contributions to the DEP force on spherical, ellipsoidal and brick-shaped particles positioned in the mid-field region of the interdigitated electrode configuration are shown in figure 6.24. As in the near-field region, electrode geometry is seen to be a determining factor in the significance of the quadrupolar force term. The second-order contribution to the total force is seen to increase, decrease, or remain almost constant with increasing x, depending on whether electrode width w is larger than, smaller than, or equal to inter-electrode spacing, respectively.

Variation patterns with x of the quadrupolar contribution are seen not to be affected by particle geometry. Particle shape is, however, seen to notably affect the magnitudes of percentage contributions from the quadrupolar term. As in the near-field region, non-spherical particles are found to be subject to considerably more significant second-order forces, with the brick-shaped particle experiencing a (slightly) less predominantly dipolar force than the ellipsoidal particle. In general, quadrupolar contributions are seen to be considerably smaller than those in the near-field region of the interdigitated geometry. Maximum second-order contributions for spherical, ellipsoidal and brick-shaped particles are seen to be ~7%, ~20% and ~21%, respectively, compared to ~14%, ~40% and ~45%, respectively, in the near-field region of the electrode geometry. The difference in significance of quadrupolar contributions in near- and mid-field regions of the interdigitated geometry can be attributed to the electric field bearing notably larger curvature near the electrode array (figures 6.5 and 6.6). From an initial inspection, the observation can be regarded as evidence for the commonly-stated qualitative criterion for the reliability of the dipole

approximation: that the field varies inconsiderably across particle dimensions. However, closer examination of the field gradient profile in near- and mid-field regions of the interdigitated geometry suggests that the criterion is by no means general. When $w = g$, for example, the electric field gradient in the near-field region was seen to be maximum at the midpoint $x = 10\mu m$, whereas the quadrupolar contribution is found to be largest at $x = 18\mu m$. The observation underlines the importance of *quantified* assessment of the reliability of the dipole approximation and of the significance of higher-order forces/moments.

Second-order contributions to the DEP force on spherical, ellipsoidal and brick-shaped particles positioned in the far-field region of the interdigitated electrode geometry, near the insulating lid, are plotted in figure 6.25. It can be seen that regardless of particle and electrode geometry, percentage contributions from the quadrupolar term bear symmetry around a maximum at the midpoint $x = 10\mu m$. The far-field region appears distant enough from the electrode surface for changes in electrode dimensions to only slightly alter quadrupolar contributions to the DEP force.

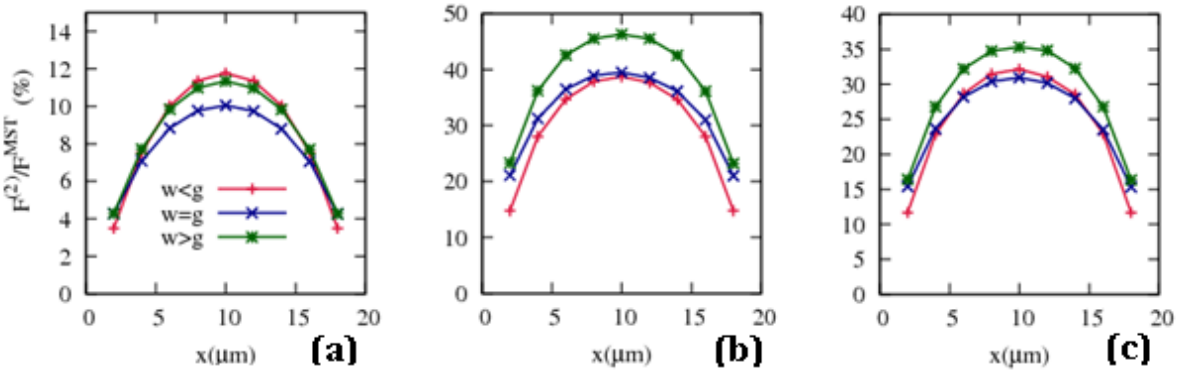

Figure 6.25. The significance of the second-order contribution to the dielectrophoretic force in the far-field region of the interdigitated electrode geometry – Variations with position x along the horizontal axis of the second-order contributions to the total DEP force on (a) spherical (r=1μm), (b) ellipsoidal (a=1μm, b=0.5μm) and (c) brick-shaped (a=1μm, b=0.5μm) particles positioned in the far-field $(y = 50\mu m)$ region of the interdigitated electrode geometry (of specifications given in figure 6.2) with three different combinations of electrode width w and spacing g: $w < g$ $(w = 10\mu m, g = 30\mu m), w = g$ $(w = 20\mu m, g = 20\mu m), w > g$ $(w = 30\mu m, g = 10\mu m)$. Legend and vertical axis labels in part (a) apply to all figure parts.

As in near- and mid-field regions, non-spherical particles are found to be subject to considerably more significant quadrupolar forces. Second-order contributions to the total force are seen to be comparable to those in the near-field region of the electrode geometry, with percentage values reaching maxima of ~12%, ~48% and ~35% for spherical, ellipsoidal and brick-shaped particles, respectively. Unlike near- and mid-field regions, the ellipsoidal

particle is seen to be subject to less predominantly dipolar forces than the brick-shaped particle. The increased significance of higher-order forces in the far-field region can be attributed to the large field curvatures caused by the presence of the nearby insulating lid (figure 6.7), although it is important to note that positions within the far-field region where higher-order forces are more significant are *not* necessarily those where the field gradient is maximum.

6.5.2.2. Summary and conclusions

Results have been presented for second-order contributions to the total dielectrophoretic force on spherical, ellipsoidal and brick-shaped particles at different positions within an interdigitated electrode configuration. The quadrupolar contributions have been calculated by comparing Maxwell stress tensor (MST) calculations of the total DEP force and DEP force term calculations using the effective moment method. In all instances regarding particle and electric field geometry, the sum of first- and second-order force terms has been seen to equal the DEP force calculated from the MST method to within an error margin of <1%, hence the validation of numerical calculations.

It has been shown that in near- and mid-field regions of the interdigitated geometry, and particularly in the former, electrode dimensions have a significant effect on quadrupolar contributions to the dielectrophoretic force on spherical and non-spherical particles. A 50% change in electrode width (and inter-electrode spacing) has been shown to change the quadrupolar contribution from negligible to very significant. Electric field geometry has also been seen to affect the quadrupolar contribution through particle position along the horizontal axis. As a particle moves within any of the designated regions in the interdigitated geometry, the quadrupolar force it experiences has been seen to vary considerably in significance.

Non-spherical particles have been shown to be subject to considerably more significant higher-order forces as compared to a sphere of similar dimensions. At any given position within the interdigitated electrode geometry, quadrupolar contributions to the DEP force on ellipsoidal and brick-shaped particles have been seen to be almost three times as large those on a most closely fitting sphere. The observations indicate the important effect of shape-dependent polarisation on the reliability of the dipole approximation. At positions within the interdigitated geometry, one-third, and at other positions nearly a half of the DEP force on ellipsoidal and brick-shaped particles has been shown to be constituted by the quadrupolar term. For accurate determination of the DEP force, the second-order term of the force on the spherical particle cannot be underestimated. It has been shown that at most positions within

the interdigitated electrode geometry, the quadrupolar contribution to the DEP force on the spherical particle is more than 5%, and at certain positions above 10%. It must be noted that the examined particles are very modest in size, compared to electrode dimensions.

Higher-order forces have been shown to be most significant in near- and far-field regions of the interdigitated geometry. The increased significance of the quadrupolar contribution can be attributed to the large field curvatures due to the presence of nearby electrodes/insulating lid. However, it has been seen from a comparison of field curvature and quadrupolar contribution results that although the two are closely correlated, "the extent of field non-uniformity compared to particle dimensions" cannot be regarded as a general criterion for the reliability of the dipole approximation. Calculations of the second-order contribution have shown that the dipole approximation can be *more* reliable where the field varies *more* notably across particle dimensions. The observations emphasise the importance of making quantitative assessment of the significance of higher-order forces, accounting for effects such as shape-dependent polarisation.

Conclusions

- A novel method has been presented with which the first three general effective moments of any particle shape subjected to an electric field of arbitrary geometry can be determined.
- The method has been used to determine the effective moments of spherical, ellipsoidal and brick-shaped particles at different positions within an interdigitated electrode configuration. It has been shown that at any given height above the electrode array, the trends with which the effective moments vary with particle position are similar to those of field gradients of preceding order and independent of particle geometry. Same observations were reported on previously in axially symmetric geometries.
- Shape-dependent polarisation has been shown to result in particles of different shapes possessing first- and second-order moments that differ largely in magnitude.
- The effective dipole moment has been shown to be directly proportional with particle volume. Therefore, if the dipole approximation is to be invoked for non-spherical particle characterisation, the particles can be modelled as spheres of equal volume for which the effective dipole moment can be calculated analytically.
- No proportionality has been observed between the second-order effective moment and particle volume. Also, non-spherical particles have been shown to possess notably more significant higher-order moments. As a result, non-spherical particle characterisation based on the dipole approximation will be subject to significant error. The dipole approximation has been shown to be more reliable in characterisation of spherical particles, but significant error can be incurred depending on electric field geometry.
- Electric field geometry, through electrode dimensions and particle position within the electrode geometry, has been shown to be a determining factor in the significance of higher-order moments, even at positions distant from the electrode surface.
- First- and second-order terms of the dielectrophoretic force on spherical, ellipsoidal and brick-shaped particles at different positions within the interdigitated electrode geometry have been calculated using the effective moment method. The results have been compared against total force calculations using the Maxwell stress tensor method. It has been shown that in all instances regarding particle and electric field geometry, the sum of dipolar and quadrupolar forces equals the total force to within an error margin of no more than 1%, hence the validation of the numerical results.
- It has been shown that the quadrupolar DEP force is considerably more significant on non-spherical particles, with contributions to the total force reaching values as high as ~45% for ~50% for brick-shaped and ellipsoidal particles, respectively. For the spherical

particle, contributions as large as ~15% from the second-order term have been observed. It has been shown that the DEP force is most significantly constituted by the higher-order term in near- and far-field regions of the interdigitated electrode geometry, where electric field curvatures are largest.

- It has been shown that contrary to the commonly stated criterion for the reliability of the dipole approximation, higher-order moments/forces are not necessarily more significant where the electric field magnitude varies more notably across particle dimensions.

References

[1] Stratton, J. A.: Electromagnetic Theory. McGraw-Hill, New York (1941).

[2] Sun, T., Morgan, H., Green, N. G.: Analytical solutions of AC electrokinetics in interdigitated electrode arrays: Electric field, dielectrophoretic and traveling-wave dielectrophoretic forces. Phys. Rev. E 76, 046610 (2007).

Chapter Seven

Summary, Conclusions and Further Work

7.1. Summary

Higher order moments and dielectrophoretic forces are commonly ignored. In analysis of electric field interactions with dielectrics, higher order effects are commonly ignored. Based on the dipole approximation, the potential due to polarised dielectrics is represented through the effective dipole moment alone. When invoked for determination of the dielectrophoretic force on dielectric particles in suspension, the dipole approximation ignores contribution from multipolar force terms. The principal goal of this work was to assess the reliability of the dipole approximation in its two 'versions'.

This work analysed the significance of multipolar effects by focussing attention on field and particle geometry as determining factors. As higher-order effective moments are representatives of the electrical energy stored in subject dielectric(s) and higher-order DEP forces result from interactions of field gradients with effective moments of succeeding order, it was a simple matter to expect electric field geometry to be a determining factor in the significance of higher-order moments/forces. The shape-dependent nature of dielectric polarisation suggests particle geometry can affect the significance of higher-order moments/forces. The focus of analysis in this work was therefore directed towards the effects of field and particle geometry as control parameters for the reliability of the dipole approximation. As a result, basic assumptions were made on other particle/field specifications: the electric field was assumed to be DC, not AC as it conveniently is in most dielectrophoresis applications, and the particles and their suspending media were assumed to be ideal dielectrics with zero conductivity.

In axial symmetry: multipole moments were derived using an available method, and results on multipolar forces on non-spherical particles were presented for the first time. The starting point for analysis was particle and electrode geometries that lend themselves to axial symmetry. Primary reason for the choice was the simplicity of analysis: effective moments become scalar, rather than tensor, quantities and even then a method was readily available in the literature for determination of effective moments up to any order for particles of arbitrary shape, given axial symmetry holds. Despite the availability of this method, no analysis has been done to date towards higher-order electrical forces in axial symmetry (and, needless to say, otherwise). The major obstacles in not doing so appear to have been the unavailability of analytic derivations for higher-order moments of non-spherical particles, the reluctance to use numerical methods due to successive differentiation (of the electric potential, required for calculation of DEP force terms) being highly susceptible

to error in finite element method (FEM)-based solvers, and finally the deemed negligence of multipolar contributions to the dielectrophoretic force.

A wide range of particle geometries and field curvature strengths were examined. This work applied the readily available method for determination of linear effective moments to spherical, ellipsoidal and cylindrical particles positioned on the symmetry axes of two electrode geometries, point-plane and disc-plane, to calculate the first three effective moments of the particles. The effect of electric field geometry was analysed by studying the two different electrode geometries, which give rise to vastly different field curvature profiles along their axes of symmetry, different electrode dimensions within each geometry, and different positions along the symmetry axis of either geometry. The effect of particle geometry was analysed by comparing the results obtained for different particle shapes and sizes: two different radii for the spherical and two different aspect ratios for each of the non-spherical particles were examined.

First three terms of the dielectrophoretic force were derived without involving numerical differentiation. The effective moment method was invoked to determine the first three terms of the dielectrophoretic force experienced by the particles by combining numerical calculations of the effective moments and analytic derivations of the field gradients. The susceptibility to error of numerical differentiation was avoided by studying electrode structures along the symmetry axis of which the electric field has been derived analytically; FEM calculation of the effective moments required integration of the electric potential due to particles, thus no numerical differentiation was involved. The significance of higher-order moments was analysed by determining their ratio over the first-order moment in different circumstances regarding particle and field geometry.

A novel method was presented for determination of the first three general effective moments with no restrictions on particle or electric field geometry. For non-axisymmetric cases, which comprise the vast majority of instances in DEP applications, a novel method was developed for determining the first three (as many as can be realised in three-dimensional space) general effective moments of particles of arbitrary shape subjected to electric fields of arbitrary geometry. The method was applied to spherical, ellipsoidal and brick-shaped particles in a widely-used electrode structure for dielectrophoretic applications: an interdigitated electrode configuration, consisting of an insulator-capped channel, within which particles flow, above the array of electrodes. The first two effective moments of the particles were determined numerically from a weighted integration of the

electric potential, thereby avoiding numerical differentiation. The third-order effective moment was shown to equal zero based on axis attributions.

The method was applied to calculate the effective moments of particles of different geometry subjected to electric fields of varying curvature in the interdigitated electrode structure. As in axial symmetry, the significance of the higher-order moment was analysed by examining its ratio over the effective dipole moment for different field and particle geometries. The effect of electric field geometry was studied by considering different electrode width/spacing ratios. The change in width and spacing of the interdigitated electrodes moves the position of the field maximum at the electrode tip and resulting field curvatures. Different particle positions within the interdigitated geometry, corresponding to field magnitudes and gradients of varying strength were examined to broaden analysis regarding the effect of electric field geometry. Results obtained with three different particle shapes were compared to observe the effect of particle geometry.

Higher order moments and forces were analysed in a non-axisymmetric setting for the first time. First- and second-order terms of the DEP force on spherical and non-spherical particles positioned within the interdigitated electrode geometry were calculated by incorporating the effective moment method. Numerical calculations of the effective moments, which (as in axial symmetry) do not involve any differentiation, were combined with analytic calculations of electric field gradients, based on a readily-available derivation for the electric field vector inside the interdigitated geometry, to obtain the first two terms of the dielectrophoretic force experienced by the particles.

Force term calculations using the effective moment method were verified by comparison against total force calculations using the Maxwell stress tensor method. In axial symmetry and otherwise, the total DEP force was calculated using the mathematically rigorous Maxwell stress tensor method for verification of numerical results and for obtaining multipolar contributions to the dielectrophoretic force for different field/particle geometries, hence assessing the reliability of the dipole approximation in its second version, i.e. in predicting the DEP force on dielectrics.

7.2. Conclusions

As explained in the Summary section, this work presented quantified evaluation of higher-order interaction between electric fields and subject dielectric(s) by addressing two versions of the dipole approximation: one used for dielectric characterisation, ignoring higher-order effective moments, and another used for prediction of the dielectrophoretic force, ignoring higher-order terms of the DEP force. The significance of higher-order moments was studied through their ratio over the effective dipole moment, and the significance of higher-order force terms was studied through their contribution to the total DEP force – as determined by the Maxwell stress tensor method. The conclusions will accordingly be presented in two separate subsections.

7.2.1. Higher-order moments

Particle geometry has a significant effect on the values of first- and higher-order moments. In axial symmetry and otherwise, it was shown that particle geometry has significant effect on the values of first- and higher-order moments. However, trends with which effective moments of any given order vary with particle position within a given electrode structure were found to be determined by that of the field gradient of preceding order, and independent of particle geometry. The observation is compatible with the definition of effective moments as representatives of the electrical energy stored in subject dielectric(s) by the field gradient of preceding order.

Only the first-order of effective moments is proportional to particle volume. In axially symmetric and non-axisymmetric settings, the effective dipole moment was shown to be directly proportional to particle volume. Higher-order *linear* moments were also shown to be larger for particles of larger volume, although no direct proportionality with particle volume was observed. In the interdigitated geometry, where axial symmetry does not hold, the second-order effective moment of the brick-shaped particle was seen to be considerably larger than that of the smaller-in-volume spherical particle at all positions within the electrode structure.

Modelling non-spherical particles with simpler shapes, albeit of equal volume, can incur significant error in effective moment-based dielectric characterisation. Assessment was made on effective moment-based characterisation of non-spherical dielectrics approximated as simpler shapes of similar dimensions or equal volume. Errors incurred upon approximation of ellipsoidal and cylindrical particles as spheres, and ellipsoids in the case of the cylindrical particle, were assessed by comparing first- and higher-order

moments of modelled and model particles. It was shown that in the case of the dipole moment, the difference reflects the volume ratio of the two particles and can be reduced to zero if particles are of equal volume – as expected from the direct proportionality of the first-order moment with particle volume. Errors incurred in values of higher-order moments were found to be significant: as an example, the second- and third-order moments of a 1μm sphere have been found to be larger than those of a (1μm, 0.5μm, 0.5μm) ellipsoid by factors of ~3 and ~1.5, respectively. Due to higher-order moments not being proportional to particle volume, errors were seen not to reduce to insignificant values when dimensions of the model particles were adjusted for equal volumes.

Higher-order moments are notably more significant for non-spherical particles. Yet, spherical particles of modest dimensions compared to the electrodes were also seen to possess multipole moments comparable to, and in many instances larger than, their effective dipole moment. It has been shown that higher-order moments of spherical and non-spherical particles are comparable to the first-order moment at all positions along the symmetry axis of either of the two axisymmetric electrode structures examined in this work, i.e. the point-plane and the disc-plane. Higher-order moments of non-spherical particles have been shown to be of increased significance. Second- and third-order moments of ellipsoidal and cylindrical particles subjected to the axisymmetric fields of point-plane and disc-plane geometries have been shown to sum up to values more than 10 times larger than their effective dipole moment when the particles are positioned on the symmetry axis of either of the two electrode geometries. **Choice of electrode structure has been seen to have a considerable effect on the reliability of the dipole approximation**, as it has been shown that multipole moments are notably more significant in the point-plane (as compared to the disc-plane) geometry.

At all examined positions within the interdigitated electrode geometry, where axial symmetry does not hold, the second-order moment has been shown to attain values comparable to that of the effective dipole moment – for spherical and non-spherical particles. Ellipsoidal and brick-shaped particles have been seen to possess notably more significant higher-order moments than the spherical particle of similar dimensions.

In axial symmetry and otherwise, the higher-order moments of spherical and non-spherical particles have been found to be more significant nearer the electrodes. The observation has been attributed to increased field curvature, which may not necessarily arise from proximity with electrodes. In the interdigitated electrode geometry, particles near the insulating lid

have been shown to possess more significant higher-order moments compared to when they are positioned in the mid-field region, nearer the electrode array.

The commonly stated criterion for the reliability of the dipole approximation cannot be used as a measure for the significance of higher order moments. A general criterion stated in the literature for the reliability of the dipole approximation posits that higher-order moments find significance when particle dimensions become comparable to the scale of electric field non-uniformity, i.e. when the field varies notably across particle dimensions. It was shown in this work that the criterion may by no means be used as a measure for the significance of higher-order moments. As a counter-example, higher-order moments of spherical and non-spherical particles positioned on the symmetry axis of the disc-plane electrode geometry were found to be least significant at a point where electric field non-uniformity, defined conventionally as its first-order gradient, is strongest.

Larger particles are subject to higher order moments of increased significance. In agreement with observations by other research groups, particle size was found to be a determining factor in the significance of higher-order moments. Doubling the radius of a 1μm sphere positioned on the symmetry axis of the disc-plane electrode geometry, for example, was seen to result in a tripling of the ratio over the effective dipole moment of the sum of second- and third-order moments.

7.2.2. Higher-order dielectrophoretic forces

As the dielectrophoretic force terms were derived, using the effective moment method formulation, from weighted multiplication of effective moments and field gradients of corresponding order, statements regarding the effects of particle and electric field geometry on first- and higher-order moments are identically valid for first- and higher-order DEP force terms. However, based on the measures used in this work for the *significance* of higher-order moments and forces, statements regarding the former may not be equally valid for the latter.

Multipolar contributions to the dielectrophoretic force are notably larger for non-spherical particles. The significance of higher-order DEP forces was assessed by deriving their contribution to the total dielectrophoretic experienced by particles, as obtained using the Maxwell stress tensor method. In axial symmetry and otherwise, it was shown that non-spherical particles are subject to multipolar forces of notably increased significance compared to spheres of similar dimensions. Higher-order contributions up to ~50% were observed with non-spherical particles of modest dimensions – compared to those of surrounding electrodes.

In axial symmetry, second- and third-order terms have been shown to constitute up to ~40% and ~50% of the DEP force on ellipsoidal and cylindrical particles positioned on the symmetry axis of the disc-plane electrode geometry. Maximum multipolar contribution to the DEP force on a spherical particle of similar dimensions has been shown to be lower, but still a significant ~20%. At most positions along the symmetry axis of the disc-plane geometry, multipolar contributions to the DEP force on spherical and non-spherical particles have been shown to be larger than 10%. In contrast, and signifying the importance of the choice of electrode structure on the reliability of the dipole approximation, higher-order forces have been found to contribute negligibly to the total force on spherical and non-spherical particles positioned on the symmetry axis of the point-plane at all but the nearest of positions to the point electrode.

The dipole approximation may be reliable in one version but not another: multipolar contributions to the DEP force by an applied electric field on a particle may be negligible, while higher order moments of the particle are comparable in value to the effective dipole moment. The case of the point-plane geometry is a good example in that it reflects on the distinction between the two versions of the dipole approximation: while higher-order moments attain significant values, compared to that of the dipole moment, corresponding DEP forces are of negligible contribution to the DEP force at almost all positions along the symmetry axis of the point-plane configuration, regardless of particle geometry. The dipole approximation may be safely applied for calculation of the DEP force, while effective moment-based dielectric characterisation based on the dipole approximation will be erroneous.

In axial symmetry: for a given particle shape, it is the dimension along the axis of electric field symmetry that determines the significance of higher order contributions to the dielectrophoretic force. Changing the aspect ratio of a given non-spherical particle alters individual contributions from higher order terms, but the overall contribution from multipolar terms remains constant. An interesting observation in the axisymmetric case pertains to multipolar forces of equal overall significance for particles of a given shape with different aspect ratios. It has been shown that 'thinning' ellipsoidal and cylindrical particles of a fixed dimension along the axis of electric field symmetry gives rise to larger octupolar and smaller quadrupolar contributions to the DEP force in a manner that the sum of second- and third-order contributions remains independent of particle aspect ratio and specific to the given particle shape.

Increased field curvature, not necessarily arising from nearby electrodes, gives rise to higher order forces of increased significance. Yet, how particle dimensions compare to the scale of field non-uniformity cannot be used as a measure for the significance of multipolar forces. In the non-axisymmetric case of the interdigitated electrode geometry, higher-order contributions to the DEP force have been found to be largest near the electrode array and the insulating lid. Multipolar contributions of ~14%, ~40% and ~45% in the near-field and ~12%, ~48% and ~35% in the far-field region have been observed for spherical, ellipsoidal and brick-shaped particles, respectively. The notable significance of higher-order contributions to the DEP force on non-spherical particles is such that even in the mid-field region, distant from the field curvatures due to the electrode array and the insulating lid, the second-order term constitutes ~20% of the DEP force on ellipsoidal and brick-shaped particles.

Particle size has very significant effect on multipolar contributions to the dielectrophoretic force. Doubling the radius of a spherical particle has been shown to give rise to notable increase in higher-order contributions to the DEP force. Maximum quadrupolar and octupolar contributions of ~35% and ~15%, respectively, have been observed to the DEP force on a 2μm sphere up from ~15% and ~5% for a sphere of half the radius.

7.2.3. Relevance of key conclusions

It has been shown that depending on electric field and particle geometry, the error incurred upon invoking the dipole approximation, either for dielectric characterisation or prediction of the dielectrophoretic force, can range from very negligible to very significant. The results presented in this work are specific to the circumstances of particle and field geometry. In other electrode structures and for particles of other geometry, the dipole approximation may be found to be more or less reliable. Changing non-geometrical parameters of the electric field and subject dielectric(s) may also affect the significance of higher-order moments/forces. The importance of this work is that is has provided, for the first times, the tools and techniques for accurate determination of higher-order moments and dielectrophoretic forces for arbitrary particle and field geometry. The results may be regarded as bearing secondary importance as they only present examples, designed to cover as broad a range of situation as possible but inevitably specific to the circumstances, of how significant higher-order interactions between electric fields and dielectric particles can be and how erroneous the commonly invoked dipole approximation can get.

Based on the method presented in this work, the significance of higher-order moments can be determined using a numerical method that requires weighted integration of the electric potential due to the particles for yielding results. In relying on the variable originally given by the FEM package from its solution of Poisson's equation, and not involving error-prone numerical differentiation, the method presented in this work is not computationally expensive. Extra computational effort will be required to yield the DEP force terms from the effective moment method if analytic derivation of the field within an electrode structure is not available. Maxwell stress tensor calculation of the total electric field can always be used for checking the validity of force term calculations. With the current trend toward micro- and nano-electrode structures used for analysis of single particles, large field curvatures at the position of particles are expected to become predominant, in which case the method presented in this work can be applied for determination of higher-order moments/forces. An important conclusion of this work is that 'by inspection' judgements regarding the significance of higher-order moments – based on how the field varies across particle dimensions, for example – can be erroneous. An important motive for conducting the research summarised in this work, reflected in the title of the thesis, has been for quantitative evaluation to replace qualitative judgements regarding the reliability of the dipole approximation.

Referring to the results, it has been shown that the dipole approximation is particularly unreliable for effective moment-based dielectric characterisation of, or predicting the dielectrophoretic force on non-spherical particles. Higher-order force terms have been shown to constitute up to more than half the total DEP force on ellipsoidal, cylindrical and brick-shaped particles, some of them of modest dimensions compared to those of the electrodes. The effect of shape-dependent polarisation is even more notably reflected through the substantial effect of particle size on the significance of higher-order moments and DEP force terms. In axial symmetry, it has been shown that particle dimension along the axis of electric field symmetry that determines the reliability of the dipole approximation for a given particle shape; changing aspect ratio has been shown to alter individual, but not overall contributions to the DEP force on a non-spherical particle of given shape.

Approximating non-spherical particles with spheres of similar dimensions has been seen to incur significant error on values of first- and higher-order moments. If dimensions of the model particle are adjusted to equate volumes, the dipole moments have been shown to also equate, while higher-order moments have been seen to remain vastly different. Consequently, if multipolar analysis of non-spherical particles is performed by approximation with a sphere – as has been done in almost all studies of the type to date – significant error may result from

the assumption of equal multipole moments for particles of different shapes. The method presented in this work poses no restriction on particle geometry and thereby removes the need for approximation with simpler shapes.

7.3. Further work

In the analysis presented in this work on the significance of higher-order moments and dielectrophoretic forces, attention has been focussed on the effects of electric field and particle geometry as control parameters or determining factors for the significance of multipolar effects. The results have shown that the factors are indeed of notable effect on the reliability of the first-order approximation. However, fuller analysis of higher-order interactions between electric fields and dielectrics should consider the effects of other field and particle characteristics.

The assumptions made in this work regarding the non-geometric specifications of electric fields and particles do not comply with at least a large variety of experimental conditions, and at times are unrealistic. Most dielectrophoretic applications involve the use of AC, rather than DC, electric fields as the frequency can be used as an easily-accessible control parameter for dielectric particle manipulation, particularly for separation purposes. The usefulness of AC dielectrophoresis arises from the frequency-dependent nature of dielectric polarisation. As mentioned in Chapter Two, the permittivity of real dielectrics is a complex quantity, determined by its real permittivity, finite conductivity and frequency. This work has assumed DC fields and ideal dielectrics throughout the analysis. Early results using real dielectrics with AC fields suggests that frequency does not independently affect the significance of higher-order moments, but does so through the effect it has on field curvatures at a given particle position. One room for further work is to develop such observations and present analysis on the significance of higher-order moments for an experimental setting involving AC electric fields and conducting dielectrics.

An important particle characteristic not addressed in this work, and of possible significance in the analysis of higher-order moments, is particle orientation within the electric field. The assumption of axial symmetry sets a limit on particle orientation, but the method presented in Chapter Six does not and can be applied for the various orientations a non-spherical particle can exhibit as it moves within an electrode structure. This work assumed 'upright' positioning of all non-spherical particles, but it would be an enlightening task to observe how higher-order moments/forces (possibly) change in significance as a particle changes orientation within the electric field.

The summarised desire of the author for 'further work', following from the motivation behind undertaking this task, is for the methods presented in the work to be applied in current and future settings where discrepancy is observed between experimental results and theoretical models based on the first-order approximation.

An important, application-oriented extension of this work would be to determine higher-order torques on non-spherical particles subjected to uniform or non-uniform electric fields. The formulation for calculating higher-order torque terms has been developed, which requires the determination of higher-order moments of corresponding order – derivable from the method presented in this work. The author observed huge discrepancy between electro-rotational behaviour of brick-shaped particles with theoretical predictions based on the effective dipole moment of an ellipsoid of similar dimensions. The results presented in this work provide an indication of why the two sets of results may vastly differ, but correct analysis of the particle response would require the calculation of higher-order electric torque terms. The status of electro-rotation as a means of dielectric characterisation adds to the necessity of accurate analysis accounting for higher-order torque terms.

Appendix A

Tensor Notation

Definition and representation

The notion of tensors is central to the formulation for higher order interaction between an applied electric field and subject dielectric(s). The effective moments representing polarisation at dielectric discontinuities are conveniently represented as tensors of ranks equal to the order of the effective moment. The 0-th order moment, the charge of a monopole, is represented as a tensor of rank 0, i.e. a scalar. The 1-st order effective moment, also called the effective dipole moment, is a vector, or a tensor of rank 1.

Tensors of ranks higher than 1 can be thought of as generalisations of vectors, or vectors along multiple dimensions. In the same way that a vector is represented through its components along $x-$, $y-$ and $z-$axes (in a Cartesian coordinate system, as an example), a rank-n tensor is represented through its components along n-element permutations of axes. This work uses superscripts in brackets to denote the ranks of tensors. A tensor $\boldsymbol{A}^{(2)}$ (of rank 2) can be represented through its components (in a Cartesian coordinate system) as:

$$\boldsymbol{A}^{(2)} = a_{xx}\hat{x}\hat{x} + a_{xy}\hat{x}\hat{y} + a_{xz}\hat{x}\hat{z} + \cdots + a_{zz}\hat{z}\hat{z} \tag{A.1}$$

As can be understood from equation (A.1), the elements of a rank-2 tensor can be arranged in a 2×2 matrix:

$$\boldsymbol{A}^{(2)}: \begin{bmatrix} a_{xx} & a_{xy} & a_{xz} \\ a_{yx} & a_{yy} & a_{yz} \\ a_{zx} & a_{zy} & a_{zz} \end{bmatrix} \tag{A.2}$$

A unit tensor of rank 2, denoted as $\boldsymbol{U}^{(2)}$, is one whose representative 2×2 matrix is an identity matrix with diagonal elements equal to 1 and off-diagonal elements equal to 0.

The Maxwell stress tensor, which represents the force by an electric field $\boldsymbol{E}$ per unit area of a subject dielectric, is a tensor of rank 2 given by:

$$\boldsymbol{T}^{(2)} = \epsilon_m[\boldsymbol{EE} - \tfrac{1}{2}E\boldsymbol{U}^{(2)}] \tag{A.3}$$

where ϵ_m is the (real part of the) permittivity of the medium in which the subject dielectric body sits, $\boldsymbol{U}^{(2)}$ is the unit tensor of rank 2, and $\boldsymbol{EE}$ denotes the so-called *dyadic product* of the

electric field vector with itself. The dyadic product, alongside other forms of tensor multiplication will be discussed in the next section.

Tensor products

Dyadic product of tensors

One way that a tensor may be produced is through the so-called *dyadic product* of two or more vectors. The notation $\boldsymbol{AB}$ with $\boldsymbol{A}$ and $\boldsymbol{B}$ both vectors denotes the dyadic product of two vectors. The dyadic product of n vectors produces a tensor of rank n. The components of the tensor $\boldsymbol{T}^{(n)}$ resulting from the dyadic product of n vectors $\boldsymbol{V}_1$, $\boldsymbol{V}_2$,... and $\boldsymbol{V}_n$ are defined as:

$$T^{(n)}_{a_1 a_2 \dots a_n} = \sum_{a_1=1}^{3} \sum_{a_2=1}^{3} \cdots \sum_{a_n=1}^{3} (\boldsymbol{V}_1)_{a_1} (\boldsymbol{V}_2)_{a_2} \cdots (\boldsymbol{V}_n)_{a_n} \tag{A.4}$$

where $T^{(n)}_{a_1 a_2 \dots a_n}$ denotes the $(a_1 a_2 \dots a_n)^{th}$ component of $\boldsymbol{T}^{(n)}$, $(V_m)_{a_j}$ represents the $\left(a_j\right)^{th}$ component of vector $\boldsymbol{V}_m$ and values 1, 2, 3 for a_1, a_2, ..., a_n correspond, in a Cartesian coordinate system, to the $x-$, $y-$ and $z-$axes, respectively.

Multipole moments, including the effective moments which represent polarisation at the interface with an electrolyte of a dielectric particle subjected to an electric field, are conveniently represented as dyadic products of the displacement vectors that constitute the multipoles – as described in Chapter Two (equation 2.11). Tensors produced through the dyadic product of two or more vectors, like the effective moments, are called *dyadic tensors*. It is important to note that not all tensors are dyadic. One important example of a non-dyadic 'stand-alone' tensor is the Maxwell stress tensor – defined through equation (A.3).

Dot product of tensors

The definition of the dot product has been generalised to allow for the n-th order dot product $[\cdot]^{(n)}$ of two tensors of rank n, resulting in a scalar:

$$\boldsymbol{T}_1^{(n)} [\cdot]^{(n)} \boldsymbol{T}_2^{(n)} = \sum_{a_1=1}^{3} \sum_{a_2=1}^{3} \cdots \sum_{a_n=1}^{3} \left(\boldsymbol{T}_1^{(n)}\right)_{a_1 a_2 \dots a_n} \left(\boldsymbol{T}_2^{(n)}\right)_{a_n a_{n-1} \dots a_1} \tag{A.5}$$

In equation (A.5), the indices 1, 2 and 3 for a_1, a_2, ..., a_n correspond, in a Cartesian coordinate system, to the $x-$, $y-$ and $z-$axes, respectively.

The n-th order dot product may also be applied to tensors of unequal ranks: the n-th order dot product of a tensor of rank n and one of rank $(n+1)$ generates – regardless of n – a vector whose elements are given by:

$$V_m = \sum_{a_1=1}^{3} \sum_{a_2=1}^{3} \cdots \sum_{a_n=1}^{3} \left(\boldsymbol{T}_1^{(n)}\right)_{a_1 a_2 \ldots a_n} \left(\boldsymbol{T}_2^{(n)}\right)_{a_1 a_2 \ldots a_m} \quad \text{(A.6)}$$

where indices 1, 2 and 3 for a_1, a_2, …, a_n or m correspond, in a Cartesian coordinate system, to the $x-$, $y-$ and $z-$axes, respectively.

Through the formulation of the effective moment method, the terms of the dielectrophoretic force exerted by a non-uniform electric field on a dielectric particle in suspension are defined as the dot product of the effective moment and field gradient of corresponding order:

$$\boldsymbol{F}_{DEP}^{(n)} = \frac{1}{n!} \boldsymbol{p}^{(n)} [\cdot]^{(n)} \nabla^{(n)} \boldsymbol{E} \quad \text{(A.7)}$$

in which the dot product is operated on $\boldsymbol{p}^{(n)}$, a dyadic tensor of rank n resulting from the dyadic product of n vectors, and $\nabla^{(n)}\boldsymbol{E}$, the n-th order gradient of the electric field, which is a tensor of rank $(n+1)$, resulting in a vector that is the n-th order term of the dielectrophoretic force. The next section explains how the del (∇) operator can be generalised to not only act on scalars to produce a vector, but also operate on tensors of an arbitrary rank n to generate a tensor of rank $(n+1)$.

Gradient of tensors

The vector $\boldsymbol{V}$ resulting from applying the del operator to a scalar variable c, referred to as the gradient of c has elements given by:

$$V_m = \frac{\partial}{\partial m} c(x, y, z); \quad m = 1,2,3 \quad \text{(A.8)}$$

where values 1,2,3 for m correspond, in a Cartesian coordinate system, to the $x-$, $y-$ and $z-$axes, respectively.

As well as scalars, the del operator can be applied to vectors, and in general to tensors of all ranks. Just as the gradient of a scalar (tensor of rank 0) produces a vector (a tensor of rank 1), the gradient of a tensor of rank n produces a tensor of rank $(n+1)$.

The elements of the tensor $\boldsymbol{T}_2^{(n+1)}$ that results from applying the generalised del operator $\nabla^{(n)}$ on a tensor $\boldsymbol{T}_1^{(n)}$ are given by:

$$\left(\boldsymbol{T}_2^{(n)}\right)_{a_1 a_2 \ldots a_{n+1}} = \nabla_{a_1} \left(\boldsymbol{T}_1^{(n)}\right)_{a_2 a_3 \ldots a_{n+1}} \quad \text{(A.9)}$$

where indices 1, 2 and 3 for a_1, a_2, …, a_n, a_{n+1} correspond, in a Cartesian coordinate system, to the $x-$, $y-$ and $z-$axes, respectively, and the symbol ∇_m is an operator defined as:

$$\nabla_m \equiv \begin{cases} \frac{\partial}{\partial x}, & m = 1 \\ \frac{\partial}{\partial y}, & m = 2 \\ \frac{\partial}{\partial z}, & m = 3 \end{cases} \tag{A.10}$$

References

[1] Byrd, P. F., Friedman, M. D.: Handbook of Elliptic Integrals for Engineers and Physicists. Springer-Verlag, Berlin (1954).

[2] Lovelock, D., Rund, H.: Tensors, Differential Forms and Vriational Principles. Dover, New York (1989).

Appendix B

Electric field along the symmetry axis of the disc-plane electrode geometry

In Chapter Four, the disc-plane electrode geometry shown in figure B.1 is one of the two axisymmetric electrode structures studied for examining the significance of higher order effective moments and dielectrophoretic forces. An important reason why this electrode structure was studied has been the availability of an analytic derivation for the electric field along the symmetry axis of the disc-plane electrode geometry, so that the successive differentiation required for obtaining the field gradients of first, second and third orders can be done analytically without resorting to error-prone numerical differentiation.

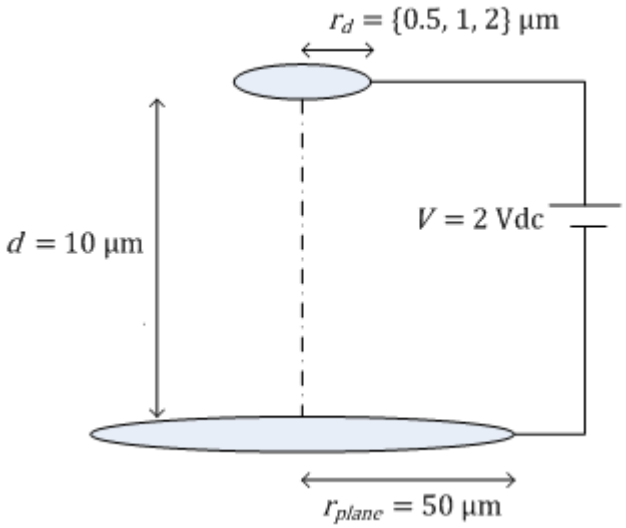

Figure B.1. Structure of the disc-plane electrode geometry studied in this work for investigating the significance of higher order effective moments and dielectrophoretic forces in axial symmetry. Figure shows structural parameters and the voltage applied across the disc and plane electrodes for generation of a non-uniform axially symmetric electric field.

The analytic derivation used in this work is that of Sloggett and co-workers using the Schwarz-Christoffel mapping method [1, 2]. Figure B.2 shows the structure of the disc-plane electrode geometry, as viewed by Sloggett et al, in a cylindrical coordinate system. The disc electrode is represented with A, the plane electrode with B, and the image of the disc electrode with C. The separation between the two electrodes is *d*, and a voltage *V* is applied to the disc electrode while the plane electrode is grounded.

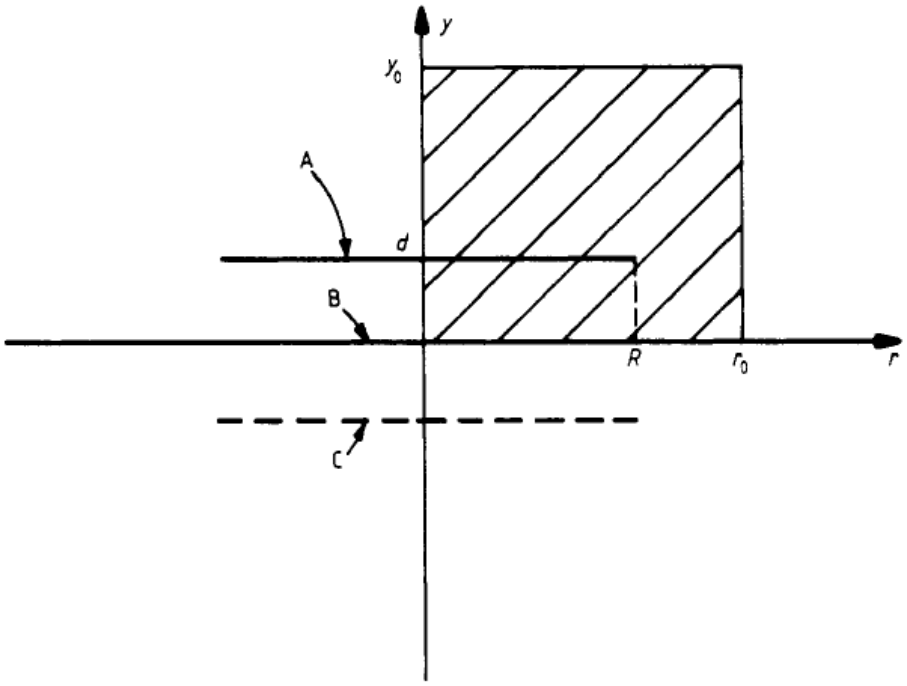

Figure B.2. Geometry of the disc-plane electrode configuration in a cylindrical coordinate system, as viewed by Sloggett et al [1]. The disc electrode is represented with A ($\varphi = V$), the plane electrode with B ($\varphi = 0$), and the image of the disc electrode with C ($\varphi = -V$). Figure copied from [1].

The axisymmetric electric potential must satisfy Laplace's equation in cylindrical coordinates:

$$\frac{\partial^2 \varphi}{\partial r^2} + \frac{1}{r}\frac{\partial \varphi}{\partial r} + \frac{\partial^2 \varphi}{\partial y^2} = 0 \quad \text{(B.1)}$$

The equation has been solved for $y \geq 0$ and $r \geq 0$ with the boundary conditions:

$$\varphi = V \quad \text{for } y = d \text{ and } r \leq R \quad \text{(B.2a)}$$

$$\varphi = 0 \quad \text{for } y = 0 \quad \text{(B.2b)}$$

and

$$\frac{\partial \varphi}{\partial r} = 0 \quad \text{for } r = 0 \quad \text{(B.2c)}$$

with the last condition resulting from axial symmetry.

Laplace's equation has been solved by mapping the electrode arrangement in the $x - y$ plane (also called the z −plane), using the conformal mapping method – also known as Schwarz-Christoffel mapping (SCM), to the $u - v$ plane (also called the w −plane) as shown in figure B.3.

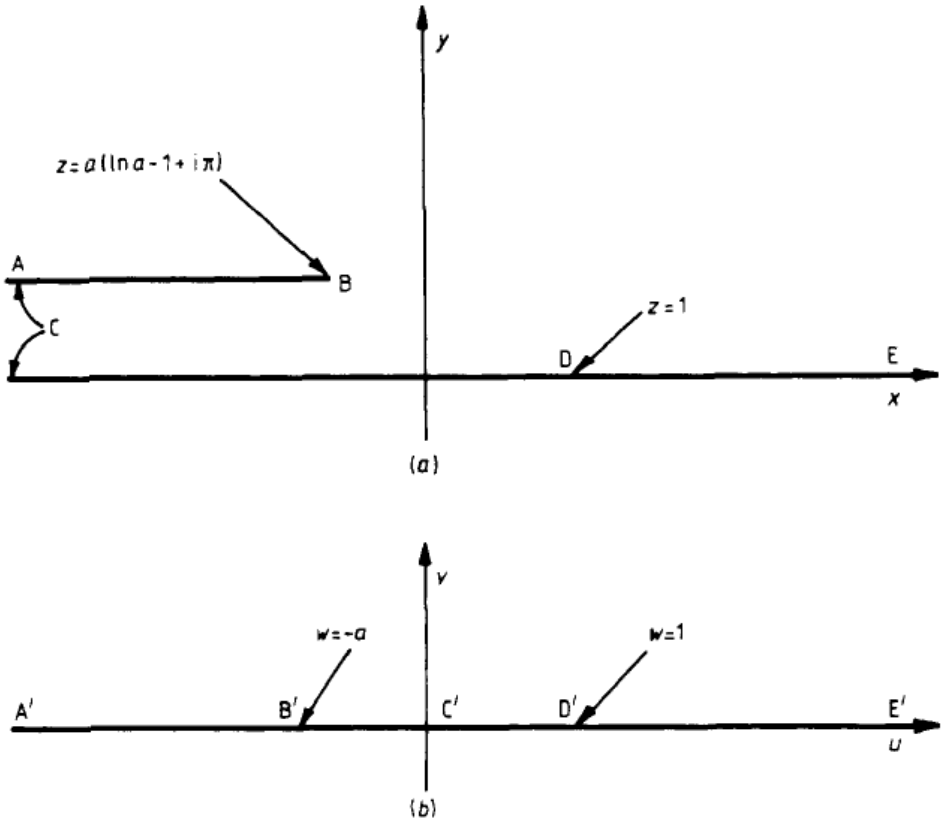

Figure B.3. Schwarz-Christoffel mapping method applied to the disc-plane electrode geometry for easier solution of Laplace's equation: (a) the z −plane, $z = x + iy$, and (b) the w −plane, $w = u + iv$. Figure copied from [1].

The mapping of the upper half of the complex z −plane ($z = x + iy$) to the upper half of the complex w −plane ($w = u + iv$) is defined by:

$$z = w + a \ln w \tag{B.3}$$

where $a = d/\pi$. The electrode system ABCDE in the z −plane maps to the points A'B'C'D'E' on the real axis of the w −plane (figure B.3(b)). In the w −plane, the upper half-plane problem is to solve Laplace's equation subject to boundary conditions:

$$\varphi(u, 0) = V \quad \text{for } u < 0 \tag{B.4a}$$

$$\varphi(u, 0) = 0 \quad \text{for } u > 0 \tag{B.4b}$$

and, by standard arguments [3], the solution is:

$$\varphi(u, v) = \frac{1}{\pi} \int_{-\infty}^{\infty} \frac{\varphi(s,0)}{(u-s)^2 + v^2} ds \tag{B.5}$$

or:

$$\varphi(u, v) = \frac{V}{\pi} \tan^{-1} \frac{v}{u} = \frac{V}{\pi} Im(\ln w) \tag{B.6}$$

Now the electric field components are given by evaluating $\partial\varphi/\partial x$ and $\partial\varphi/\partial y$ as follows. By defining $G = (V/\pi)\ln w$, we have:

$$\frac{\partial\varphi}{\partial x} = Im\left(\frac{\partial G}{\partial x}\right) = Im\left(\frac{dG}{dz}\right) = Re\left(\frac{dG}{dz}\right) = Im\left(\frac{dG}{dw}\left(\frac{dz}{dw}\right)^{-1}\right) \tag{B.7a}$$

$$\frac{\partial\varphi}{\partial y} = Im\left(\frac{\partial G}{\partial y}\right) = Im\left(i\frac{dG}{dz}\right) = Re\left(\frac{dG}{dz}\right) = Re\left(\frac{dG}{dw}\left(\frac{dz}{dw}\right)^{-1}\right) \tag{B.7b}$$

Since $dz/dw = (w + a)/w$, we have:

$$E_x = \frac{\partial\varphi}{\partial x} = \frac{V}{\pi}Im\left(\frac{1}{w+a}\right) \tag{B.8a}$$

$$E_y = \frac{\partial\varphi}{\partial y} = \frac{V}{\pi}Re\left(\frac{1}{w+a}\right) \tag{B.8b}$$

In the case of points on the electrodes we have $v = 0$, from which it follows that E_x vanishes, as expected, and:

$$E_y = \frac{V}{\pi(u+a)} \tag{B.9}$$

The results can now be interpreted in terms of the original (x, y) coordinate system. For points on the underside of the upper electrode and near to its edge B, we may write:

$$z = a(\ln a - 1 - i\pi) - t \tag{B.10}$$

and:

$$w = u = -a + s \tag{B.11}$$

where s and t are real and positive and t measures distance from the edge of the electrode. Substituting in equation (B.3) and expanding the ln term, we find that, for small s and t,

$$s = (2at)^{1/2} \tag{B.12}$$

And, from equation (B.9):

$$E_y = \frac{V}{\pi}(2at)^{-1/2} = V(2\pi dt)^{-1/2} \tag{B.13}$$

This equation describes the singular behaviour of E_y near the edge of a disc of large radius.

Points which are between the electrodes and remote from the edge correspond to w near 0 in figure B.3(b). For $|w|$ sufficiently small, equation (B.3) gives:

$$w \approx e^{z/a} = e^{x/a}\left(\cos\frac{y}{a} + i\sin\frac{y}{a}\right) \tag{B.14}$$

and equations (B.8a) and (B.8b) therefore give:

$$E_x \approx \frac{V}{\pi a} Im\left(1 - \frac{w}{a}\right) \approx -\frac{V}{\pi a^2} e^{x/a} \sin\frac{y}{a} \tag{B.15a}$$

$$E_y \approx \frac{V}{\pi a} Im\left(1 - \frac{w}{a}\right) \approx \frac{V}{\pi a}\left(1 - \frac{1}{a} e^{x/a} \cos\frac{y}{a}\right) \tag{B.15b}$$

The approximations are valid for when the disc electrode radius is not smaller than, as a rule of thumb, 5% of the plane electrode radius. The equations are applicable to the cases studied in this work as the smallest of examined disc electrode radii is 0.5μm, which is 10% the radius of the plane electrode (50μm). To obtain the electric field magnitude along the symmetry axis of the disc plane electrode geometry at a point of height h above the plane electrode, x must be set to 0 in equation (B.15b):

$$E(h) = \frac{V}{\pi a}\left(1 - \frac{1}{a}\cos\frac{y}{a}\right) \tag{B.16}$$

Substituting $a = d/\pi$ in equation (B.16) gives:

$$E(h) = \frac{V}{d}\left[1 - \frac{\pi}{d}\cos\left(\frac{\pi h}{d}\right)\right] \tag{B.17}$$

Which is the equation used for obtaining the field magnitude along the symmetry axis of the disc-plane geometry in Chapter Four (equation 4.6) and for obtaining the field gradients by analytical differentiation of the equation in MATLAB.

References

[1] Sloggett, G. J., Barton, N. G., Spencer, S. J.: Fringing fields in disc capacitors. J. Phys. A: Math. Gen., 19, 2725-2736 (1986).

[2] Schizinger, R., Laurra, P. A. A.: Conformal Mapping: Methods and Applications. Dover Publications, Inc., Mineola, NY (2003).

[3] Carrier, G. F., Krook, M., Pearson, C. E.: Functions of a Complex Variable. McGraw-Hill, London (1966).

Appendix C

Electric field along the symmetry axis of the point-plane electrode geometry

The point-plane electrode geometry in figure C.1 is one of the two electrode structures studied in this work (Chapters Four and Five) for the analysis of higher order effective moments and dielectrophoretic forces in axial symmetry. An important reason for choosing this electrode geometry has been the availability of an analytic derivation for the electric field along the symmetry axis of the point-plane configuration, so that resort need not be made to numerical means of differentiation which are highly susceptible to error, particularly given the requirement for successive differentiation to obtain higher order dielectrophoretic force terms.

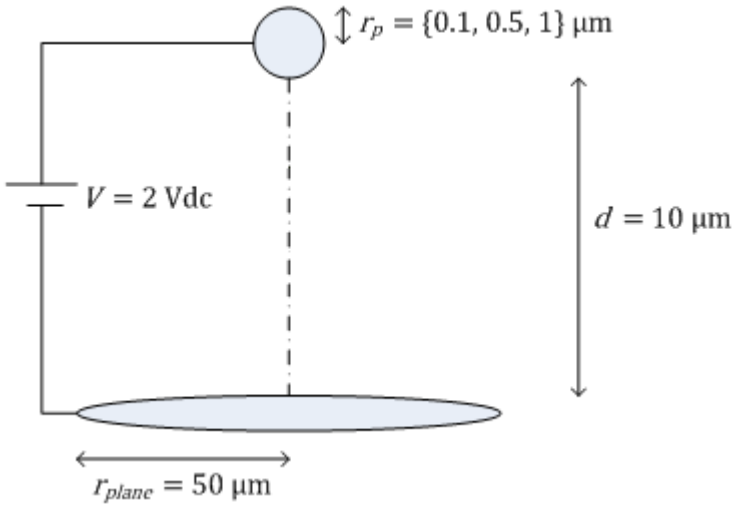

Figure C.1. The structure of the point-plane electrode geometry studied in this work for the analysis of higher order effective moments and dielectrophoretic forces in axial symmetry. Figure shows the structural parameters and the voltage applied across the point and plane electrodes for generation of a non-uniform electric field along the axis of field symmetry.

The analytic derivation used in this work is based on a hyperbolic approximation to the point electrode [1]. Other geometric approximations have also been incorporated for obtaining the electric field within a point-plane electrode configuration; these include a parabolic approximation [2] which has the issue of actual points not fitting the shape of a paraboloid, unless the radius of the point electrode is rather large, and the approximation of the point

electrode with a half sphere on a truncated cone [3]. The latter approximation is likely to fit actual point electrode shapes better, since two independent parameters, namely the point electrode radius and the shaft angle, are involved. However, it does not provide a straightforward formulation for the electric field within the electrode geometry. The advantage of the hyperbolic approximation is that it is simple and has been validated using experimental results [1].

Figure B.2 shows a representation of the point-plane electrode configuration, alongside the parameters involved for a hyperbolic approximation to the point electrode. Using this approximation, the point electrode is generated by hyperbola of equations:

$$x = a\sin\xi\cosh\eta \tag{C.1a}$$

$$y = a\cos\xi\sinh\eta \tag{C.1b}$$

rotating around the x −axis.

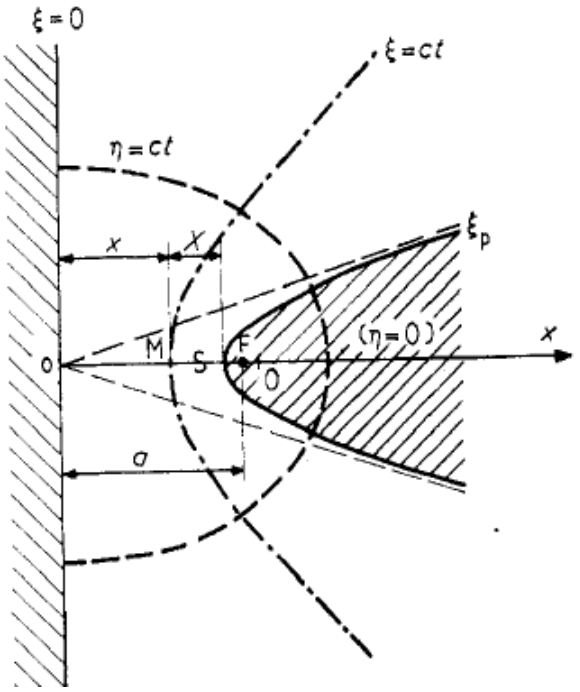

Figure C.2. Representation of the point-plane electrode configuration when a hyperbolic approximation is used for the shape of the point electrode. Figure copied from [1].

Equations (C.1) define two orthogonal confocal sets of ellipses and hyperbolas. Since we consider the hyperbolas only, ξ must be regarded as the parameter defining the hyperbola. Particular values of ξ are:

$\xi = 0 \quad (x = 0) \quad Oy$ axis generating the plane

$\xi = \frac{\pi}{2} \quad (y = 0) \quad Ox$ axis generating an infinitely sharp hyperbola

η is the parameter defining a particular point on the hyperbola defined by ξ.

It has been shown [4] that if two of the hyperbolas are equipotential surfaces, all of the hyperbolas of the set are also equipotentials and, furthermore, that if the origin of the potential is taken at the plane $x = 0$ ($\xi = 0$), the potential $V(\xi)$ of the hyperbola of parameter ξ is:

$$V(\xi) = Cln \tan(\xi/2 + \pi/4) \tag{C.2}$$

where C is a constant depending on the applied voltage. The flux lines of the field generate a family of ellipsoids of revolution orthogonal to the hyperboloids, and the values of the electric field at point (ξ, η) is:

$$E(\xi, \eta) = \frac{C}{a \cos \xi (\cosh^2 \eta - \sin^2 \xi)^{1/2}} \tag{C.3}$$

The constant C is calculated as follows: under the assumption that the point electrode is sharp, the corresponding value of ξ is close to $\pi/2$. If V is the potential of the point electrode, we have $V(\pi/2 - \epsilon) = V$ with $\epsilon \ll 1$, so that, using (C.2):

$$V = Cln \tan\left(\frac{\pi}{2} - \frac{\epsilon}{2}\right) = Cln \cot\frac{\epsilon}{2} \tag{C.4a}$$

or:

$$V = Cln \left(\frac{2}{\epsilon} - \frac{\epsilon}{6} + \cdots\right) \cong Cln \frac{2}{\epsilon} \tag{C.4b}$$

Using equation (C.4), equation (C.2) becomes:

$$V(\xi) \cong V \frac{\ln \tan(\xi/2+\pi/4)}{ln(2/\epsilon)} \tag{C.5}$$

To obtain the field at any point M along the symmetry axis of the point-plane electrode geometry, we let η be zero in equation (C.3), which now reads:

$$E(\xi, 0) = \frac{C}{a \cos^2 \xi} \tag{C.6}$$

and, since $x = a \sin \xi$ if $\eta = 0$,

$$E(x) = \frac{aC}{a^2 - x^2} \tag{C.7}$$

We now consider figure C.2. The abscissa of the point electrode apex S is:

$$x_S = a\sin\xi_S = a\cos\epsilon \cong a\left(1-\frac{\epsilon^2}{2}\right) \tag{C.8}$$

And the distance X between point M and the point electrode apex is:

$$X = x_S - x \cong a\left(1-\frac{\epsilon^2}{2}\right) - x \tag{C.9}$$

Therefore:

$$E(X) = \frac{aC}{(X+a\epsilon^2/2)(2a-X-a\epsilon^2/2)} \tag{C.10}$$

Expanding the denominator to the second power in ϵ, $E(X)$ reduces to:

$$E(X) \cong \frac{aC}{X(2a-X)+(a-X)a\epsilon^2} \tag{C.11}$$

Now it can be seen, by expanding the equations of the hyperbola and that of a circle of radius r around the common apex $x = x_S = a\cos\epsilon$ and identifying both expansions, that the radius of curvature of the hyperbola is:

$$r = \frac{a\,\cos^2\xi}{\sin\xi} = a\frac{\sin^2\epsilon}{\cos\epsilon} = a\epsilon^2\left(1+\frac{\epsilon^2}{6}+\cdots\right) \tag{C.12}$$

On the other hand, some algebraic manipulation shows that:

$$C = V/ln\left\{2\left(a/r_p\right)^{1/2}\left(1+\alpha\frac{{r_p}^2}{a^2}-\cdots\right)\right\} \tag{C.13}$$

where r_p is the radius of the point electrode and α is a numerical coefficient much smaller than unity. Therefore, to a very good approximation, even if the point electrode is not very sharp:

$$E(X) = \frac{aC}{X(2a-X)+(a-X)r_p} \tag{C.14}$$

with:

$$C = \frac{V}{\ln[2\left(\frac{a}{r_p}\right)^{\frac{1}{2}}]} \tag{C.15}$$

As from figure C.2, $x + X + \frac{r_p}{2} = a$, equation (C.14) can be re-written to give the electric field magnitude at a point of height h above the plane electrode along the symmetry axis of the point-plane electrode geometry as:

$$E(h) = \frac{aC}{(d-h)(2a-d+h)+(a-d+h)r_p} \qquad \text{(C.16)}$$

where d is the separation between point and plane electrodes. Equation (C.16) is the analytic expression used in this work (equation 4.7) for derivation of the electric field along the symmetry axis of the point-plane electrode geometry. Electric field gradients of first, second and third orders have been derived by analytic differentiation of equation (C.16) in MATLAB.

References

[1] Coelho, R., Debeau, J.: Properties of the tip-plane configuration. J. Phys. D: Appl. Phys. 4, 1266-1280 (1971).

[2] Nikolopoulos, P.: Impulse breakdown of insulating oil. Elektrotech. Z. A. 87, 239-245 (1966).

[3] Dreschsler, M., Henkel, O.: Field Electron Emission. Z. Angew. Phys. 61, 341 (1954).

[4] Durand, E.: Electrostatics. Masson, Paris (1966).

Appendix D

Electric field within the interdigitated electrode geometry

In Chapter Six, the interdigitated electrode geometry has been studied for analysing the significance of higher order effective moments and dielectrophoretic forces. An important reason for the choice of electrode geometry, alongside its widespread use in DEP applications – particularly for particle separation, is the availability of an analytical derivation for the electric field vector within the electrode structure, so that resort need not be made to error-prone numerical means of differentiation for obtaining the electric field and its gradient to derive DEP force terms. This appendix presents the analytical derivation used in this work for the electric field vector inside the interdigitated electrode geometry. Electric field gradients have been calculated by analytic differentiation in MATLAB of the expression that shall be presented in this appendix.

The Schwarz-Christoffel mapping method

The analytic derivation of the electric field within an interdigitated electrode configuration, consisting – as shown in Chapter Six – of an interdigitated array of electrodes beneath a channel capped by an insulating lid – is based on the Schwarz-Christoffel (SCM; also known as conformal) mapping method. The SCM method maps the upper half of a complex plane (T-plane) into the interior of a given polygon in another complex plane (Z-plane). The Z-plane represents the real system in our case. Complex numbers in this plane represent vectors in the real system, with the real component representing the horizontal direction (x-axis) and the imaginary component the vertical direction (y-axis). Detailed mathematical description of the SCM method can be found in [1].

For the electric field analysis, a non-uniform two-dimensional electric field polygonal region is transformed into an equivalent rectangular region (a parallel plate capacitor), where the electric field distribution is uniform, as follows.

(a) Select a basic cell for the physical two-dimensional geometry using symmetrical axes in the physical plane (Z-plane). Determine the boundary conditions (i.e., Neumann or Dirichlet condition) along each boundary of the cell.
(b) Apply SCM method to map the basic cell from the Z-plane to the upper half of an auxiliary plane (T-plane).

(c) Apply a second SCM method to transform the upper half of the *T*-plane into a closed parallel plate capacitor region in the model plane (*W*-plane).

The original non-uniform field problem in the *Z*-plane can then be easily solved in the *W*-plane. The details of the transformation procedure along with the analysis of the electric field are described in the following sections

Boundary conditions for DEP electrode arrays

(a) Before performing the electric field analysis, the boundary conditions in the corresponding system must be determined.
(b) Since the electrodes transform the upper half of the *T*-plane into a closed parallel plate capacitor region in the model plane (*W*-plane).
(c) The electrodes are much thinner than the electrode width and the gap, so that the electrodes can be represented by a thin section of the bottom boundary at a fixed potential. Since the normal component of the total current passing through the electrolyte-lid and electrolyte-substrate interfaces must be continuous and the lid and the substrate are made from glass, which has a much smaller permittivity and conductivity than the electrolyte _water_ in the channel, the normal component of the electric field in the electrolyte at the interface is negligible compared to that of the glass [2]. Therefore, we assume that Neumann boundary condition (insulating) holds for the potential at the electrolyte-lid and electrolyte-substrate interfaces, $\frac{\partial \tilde{\varphi}}{\partial n} = 0$, where *n* is the normal to the boundary). The maximum error due to the assumption of Neumann boundary condition at the water-glass interface is found to be less than 1% of the applied voltage which occurs at the top lid.

The SCM method allows analysis of systems with or without an insulating lid. Therefore in order to demonstrate the effect of the lid on the electric field distribution in the DEP array, we first solve the electric field distribution with complete boundary conditions including an insulating lid. Secondly, the same system is solved without the lid, extending the upper surface to infinity. The resulting analytical solutions of the electric field are compared with numerical simulations. The effect of the lid is discussed for the near and far field regions, equivalent to a shallow and deep channel. The dielectrophoretic force is then calculated from the field solutions and compared with Fourier series analytical solutions.

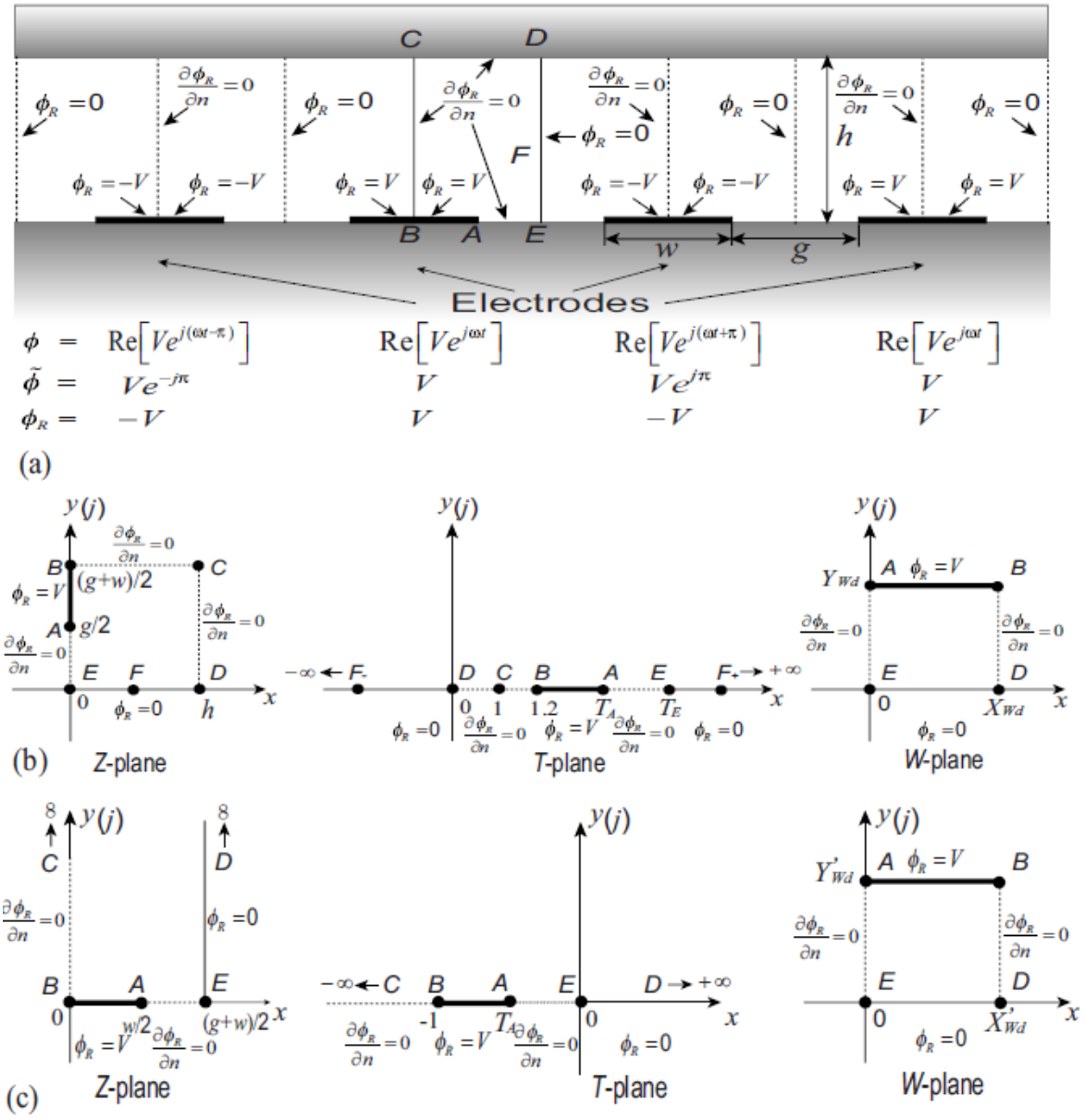

Figure D.1. Schematic of a 2D section of the DEP electrode showing the potentials. The vertical lines mark the period over which the system repeats. The rectangle *ABCDE* is the basic cell for analysis. Also shown is the potential φ, the potential phasor $\tilde{\varphi}$, and the value of the real part of the potential phasor φ_R on each electrode. The imaginary part of the potential phasor φ_I is zero everywhere. (b) Diagram showing three complex planes used for Schwarz-Christoffel mapping (SCM) taking into account the lid. (c) Diagram showing the three complex planes used for the Schwarz-Christoffel mapping (SCM) procedure for array without the lid. Figure copied from [3].

The values for the real and imaginary parts of the potential phasor at each electrode, together with the boundary conditions are shown in figure D.2(a). Since the two signals of phases 0° and 180° are alternately connected to the electrodes, the boundary conditions are equivalent to two in-phase signals with opposite sign and the imaginary part of the potential phasor is zero ($\varphi_I = 0$) and only the real part φ_R needs to be solved. From symmetry, the basic cell (*ABCDE*) is chosen for the electric field analysis. For a detailed description of the boundary conditions in the DEP array, see [2]. Figure D.2(b) shows the three complex planes used for

the mapping procedure. The selected cell *ABCDE* is rotated 90° and set in the *Z*-plane with the boundary conditions for φ_R as shown: $\frac{\partial \varphi_R}{\partial n} = 0$, along the insulating walls *AE* and *CD* and the boundary for the axis of even symmetry (*BC*). Dirichlet boundary conditions define the fixed potential $\varphi_R = V$ along the electrode (*AB*) and the boundary for the axis of odd symmetry, $\varphi_R = 0$ (*DE*). The complex coordinates for each point in the physical plane (according to the geometrical parameters of the system) are $Z_A = jg/2, Z_B = j(w+g)/2, Z_C = h + j(w+g)/2, Z_D = h$, and $Z_E = 0$.

The SCM procedure

The interior of the polygon *ABCDE* in the *Z*-plane is mapped into the upper half of the *T*-plane using the SCM method. The polygon *ABCDE* is opened at point *F* and the boundaries of the polygon mapped to the real axis of the *T*-plane. The coordinates of the corresponding points Z_A to Z_E in the *T*-plane are T_A to T_E, respectively. The point *F* is mapped to positive and negative infinity. The four interior angles of polygon *ABCDE* at points *E, B, C, D* are all $\pi/2$. The SCM integral from *T*-plane to *Z*-plane is given by:

$$Z = C_1 \int (T - T_E)^{-1/2} (T - T_B)^{-1/2} (T - T_C)^{-1/2} (T - T_D)^{-1/2} dT + C_2 \qquad \text{(D.1)}$$

where $Z = Z_x + jZ_y$ refers to the complex coordinate of any point in the interior of polygon *ABCDE* in the *Z*-plane. $T = T_x + jT_y$ refers to the complex coordinate of any point in the upper half of the *T*-plane.

Since the SCM method allows up to three points to be arbitrarily chosen along the real axis of the *T*-plane, we fix the coordinates of $T_D = 0, T_C = 1$ and $T_B = 1.2$ as shown in figure D.2(b). For $T > T_E > T_B > T_C > T_D$, the solution of equation (D.1) is an elliptic integral [3]:

$$Z = C_3 F\left(\widetilde{\omega}_{d_1}, k_{d_1}\right) + C_2 = C_3 \int_0^{\lambda_{d_1}} \frac{d\lambda_{d_1}}{\left(1-\lambda_{d_1}^2\right)\left(1-k_{d_1}^2 \lambda_{d_1}^2\right)} + C_2 \qquad \text{(D.2)}$$

where $F\left(\widetilde{\omega}_{d_1}, k_{d_1}\right)$ is the elliptic integral of the first kind and k_{d_1} is the modulus of the elliptic function.

Equation (D.2) links the *T*-plane to the *Z*-plane. The values of the coefficients C_2 and C_3 can be solved by a mapping relationship between the coordinates of the corresponding points in the two planes [3]:

$$C_2 = 0, \quad C_3 = \frac{h}{K(k_{d_1})} = \frac{w+g}{2K\left(k'_{d_1}\right)} \qquad \text{(D.3)}$$

where $K(k_{d_1})$ is the complete elliptic integral of the first kind and $k'_{d_1} = \sqrt{(1-k_{d_1}^2)}$. The expression for C_3 also provides the relationship between the complete elliptic integral and the geometrical parameters of the system:

$$\frac{K(k_{d_1})}{K(k'_{d_1})} = \frac{2h}{w+g} \tag{D.4}$$

The value of the modulus k_{d_1} can be calculated by inputting arbitrary geometrical parameters using Hilberg's approximation [4].

The inverse function of equation (D.2) enables us to express T in terms of Z:

$$T = \frac{T_E T_B cn^2\left(\frac{Z}{C_3}, k_{d_1}\right)}{T_B - T_E sn^2\left(\frac{Z}{C_3}, k_{d_1}\right)} \tag{D.5}$$

where *sn* and *cn* are the Jacobian elliptic functions.

The second SCM is used to transform the upper half of the T-plane into a rectangle in the model plane (W-plane). The electric field is uniformly distributed in the interior of the rectangle, due to the restriction from the transformed boundaries in the W-plane. The corresponding points are $W_A = jY_{W_d}$, $W_B = X_{W_d} + jY_{W_d}$, $W_D = X_{W_d}$, and $W_E = 0$, where X_{W_d} and Y_{W_d} are the size of the rectangle along the real and imaginary axis, respectively. Similarly, the transformation from the T-plane to the W-plane is given by:

$$W = D_1 \int (T - T_E)^{-1/2} (T - T_A)^{-1/2} (T - T_B)^{-1/2} (T - T_D)^{-1/2} dT + D_2 \tag{D.6}$$

It should be noted that, compared to equation (D.1), in this transformation point A replaces C to become an angle of the rectangle.

Analytical electric field solution in the interdigitated electrode geometry

Since Laplace's equation remains invariant under conformal mapping, the potential gradients in the physical plane, $\nabla\varphi_Z$, and the model plane, $\nabla\varphi_W$, are related by:

$$\nabla\varphi_Z = \nabla\varphi_W \overline{f'(Z)} = \nabla\varphi_W \frac{\overline{dW}}{dZ} \tag{D.7}$$

where $\overline{f'(Z)}$ is the conjugate of the derivative of $f(Z)$, which is the linking transformation equation between the Z- and W-planes. Using this relationship and combining equation (D.1) and (D.7), the non-uniform electric field distribution in the Z-plane, $\boldsymbol{E}_{Z_d}$, can be derived as:

$$\boldsymbol{E}_{Z_d} = -\nabla\varphi_{Z_d} = -\nabla\varphi_{W_d}\left(\overline{\frac{dW}{dT}\frac{dT}{dZ}}\right) = \overline{J\frac{V}{h}\frac{K(k_{d_1})}{K\left(k'_{d_2}\right)}\left[\frac{T_A(T_E-T_B)(T-T_C)}{T_B(T_E-T_C)(T-T_A)}\right]} \tag{D.8}$$

Where φ_{Z_d} and φ_{W_d} are the potentials in the *Z*- and *W*-planes, respectively, and V is the potential difference between the electrode *AB* and the axis of odd symmetry, *DE*.

Equation (D.8) is the analytical solution for the electric field in the basic cell for the interdigitated DEP array. The features of the electric field distribution that are governed by the geometry of the device are clearly identified. The electric field magnitude approaches zero at point *C* and infinity at point *A*, the edge of the electrode. Substituting equation (D.5) into (D.8), we obtain the electric field expression as a function of position in the interior of polygon *ABCDE* in the *Z*-plane:

$$\boldsymbol{E}_{Z_d} = \overline{J\frac{V}{h}\frac{K(k_{d_1})}{K\left(k'_{d_2}\right)}\left\{\frac{T_A(T_E-T_B)\left[\frac{T_ET_Bcn^2\left(\frac{Z_x+JZ_y}{C_3},k_{d_1}\right)}{T_B-T_Esn^2\left(\frac{Z_x+JZ_y}{C_3},k_{d_1}\right)}-T_C\right]}{T_B(T_E-T_C)\left[\frac{T_ET_Bcn^2\left(\frac{Z_x+JZ_y}{C_3},k_{d_1}\right)}{T_B-T_Esn^2\left(\frac{Z_x+JZ_y}{C_3},k_{d_1}\right)}-T_A\right]}\right\}^{1/2}} \tag{D.9}$$

Equation (D.9) has been used as the basis for obtaining the electric field magnitude and gradients at near-, mid- and far-field regions of the interdigitated electrode geometry in Chapter Six.

References

[1] Schizinger, R., Laurra, P. A. A.: Conformal Mapping: Methods and Applications. Dover Publications, Inc., Mineola, NY (2003).

[2] Green, N. G., Ramos, A., Morgan, H.: Numerical solution of the dielectrophoretic and traveling wave forces for interdigitated electrode arrays using the finite element method. J. Electrostat. 56, 235-254 (2002).

[3] Sun, T., Morgan, H., Green, N. G.: Analytical solutions of AC electrokinetics in interdigitated electrode arrays: Electric field, dielectrophoretic and traveling-wave dielectrophoretic forces. Phys. Rev. E 76, 046610 (2007).

[4] Hilberg, W.: From approximations to exact relations for characteristic impedances. IEEE Trans. Microwave Theory Tech. 259-265 (1969).